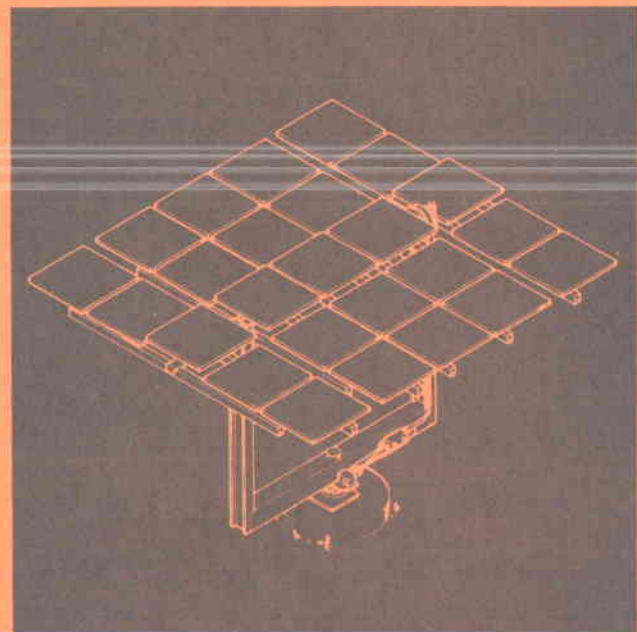


Volume I

Technical
Proposal

December 1975

Heliostat Array and Control System for 5-MW Solar Thermal Test Facility



MARTIN MARIETTA

Volume I

Technical
Proposal

Heliostat Array and Control System for 5-MW Solar Thermal Test Facility

MARTIN MARIETTA

P75-48341-1

Volume I

Technical
Proposal

December 1975

**HELIOSTAT ARRAY
AND CONTROL
SYSTEM FOR 5-MW
SOLAR THERMAL
TEST FACILITY**

~~#####~~
WHY IN LINE SENSOR DELETED?

Approved

George W. Morgenthaler

Dr. George W. Morgenthaler
Vice President
Technical Operations

MARTIN MARIETTA CORPORATION
DENVER DIVISION
Denver, Colorado 80201

MARTIN MARIETTA AEROSPACE

DENVER DIVISION
POST OFFICE BOX 179
DENVER, COLORADO 80201
TELEPHONE (303) 794-5211

our new number is:
(303) 979-7000

21 November 1975

TO: Sandia Laboratories

The Martin Marietta Corporation is pleased to submit this proposal to Sandia Laboratories for the Heliostat Array and Control System to be used in the 5-MW Solar Test Facility. The Denver Division of Martin Marietta has been designated as the segment of our Corporation responsible for applying our aerospace developed capability to the terrestrial use of Solar Energy. All of the energy work in the Division, both research and applied technology, is performed within my organization, Technical Operations.

In our Technical Proposal we have defined our proposed design, the design rationale, and our plan for verification. We are convinced that we have a sound design which will meet your specified requirements. As you know, however, the Heliostat Array and Control System program is more than hardware design and fabrication -- it also is a site activation/field installation and checkout job to be accomplished within a tight schedule. Martin Marietta offers Sandia and ERDA a project team and organizational arrangement which will assure technical performance, on time, and within proposed contract costs.

Mr. M. Marx Hintze has been selected as Program Manager. Marx was chosen because of his technical experience and demonstrated program leadership in the design and fabrication of electronic controls hardware. Marx has been responsible for Titan III Launch Vehicle autopilots, the electronics for operating the Skylab Viewfinder Tracker, and critical Viking Mars Lander electronics interfacing with a computer and controlling the descent engines and vehicle attitude. He has also been Unit Head of our Guidance and Controls Laboratory supervising 40 people. Marx will report to Mr. Lester J. Lippy on this program. Les was the Martin Marietta Titan II Intercontinental Ballistic Missile Site Activation Director at Davis Monthan Air Force Base near Tucson, Arizona. He played the key role in the field installation and checkout program which we believe is unmatched by any other contractor in terms of achieving technical quality, meeting difficult schedules, and under-running a CPFF contract.

Mr. Floyd Blake, who is our Program Director for the Central Receiver Solar Thermal Power System, which we are performing for ERDA, participated in the preparation of this proposal and has approved it. He will stay involved in this program for Sandia in the manner described in our proposal which will ensure the continued application of his expertise on collectors and other elements of the system without perturbing his other contractual obligations.

Bechtel is our proposed subcontractor for the A&E work required on the Heliostat Array and Control System program. We selected Bechtel because of their international superb reputation in the design of power stations and the excellent working relationships we have established with them on our other terrestrial solar power programs.

You may be assured of my personal interest in the Heliostat Array and Control System program and I commit all the resources required to ensure its success.

George W. Morgenthau
George W. Morgenthau
Vice President
Technical Operations

FOREWORD

Submitted in response to Sandia Laboratories, Albuquerque, New Mexico request for quotation (RFQ) 03-3731, this document outlines Martin Marietta's plan for design, test, manufacture, installation, focusing, alignment, and calibration of a Helio-stat Array and Control System for ERDA's 5-Megawatt Solar Thermal Test Facility.

Our proposal is submitted in four volumes:

Volume I - Technical Proposal;

Volume II - Program Plans;

Volume III - Cost Proposal;

Volume IV - Addenda for P75-48341.

CONTENTS

	<u>Page</u>
I. INTRODUCTION	I-1 thru I-9
II. CONCEPTUAL DESIGN AND DESIGN RATIONALE	II-1 and II-2
A. Heliostat Array and Control System Description	II-A-1 thru II-A-5
B. Heliostat Array Subsystem (HASS)	II-B-1 thru II-B-91
C. Heliostat Array Control Subsystem	II-C-1 thru II-C-38
D. Focusing and Alignment Subsystem	II-D-1 thru II-D-26
E. Calibration Subsystem	II-E-1 thru II-E-42
F. Installation and Maintenance Equipment	II-F-1 thru II-F-3
G. Key System-Level Considerations	II-G-1 thru II-G-10
H. Maintenance Requirements	II-H-1 thru II-H-7
I. Verification Program	II-I-1 thru II-I-17
APPENDIX A	
WIND TUNNEL TESTS FROM CRSTPS	A-1 thru A-13
APPENDIX B	
SUBSYSTEM RESEARCH EXPERIMENT TRADEOFF STUDIES	B-1 thru B-30

Figure

I-1	Artist's Concept, CRSTPS	I-3
I-2	Heliostat Array and Control System Functional Schematic	I-7
II-1	Control Loop and Data Transmission Breadboard Simulation	II-2
II-A-1	Heliostat Array and Control System Functional Schematic	II-A-2
II-A-2	Heliostat Zone Layout	II-A-3
II-B-1	Test Facility Zone Layout	II-B-1
II-B-2	Heliostat Baseline Configuration	II-B-5
II-B-3	CNRS Solar Furnace Facility	II-B-7
II-B-4	Heliostat-Modular Concept	II-B-10
II-B-5	Mirror Wind Loading	II-B-13
II-B-6	Out-of-Plane Deflections of 25-Mirror Assembly	II-B-16
II-B-7	Mirror Support Scheme	II-B-19
II-B-8	Mirror Assembly and Support Scheme	II-B-20
II-B-9	Mirror Alignment	II-B-21
II-B-10	Azimuth Drive Unit	II-B-28
II-B-11	Elevation Drive Unit	II-B-29
II-B-12	Tangential Load vs Torque	II-B-30
II-B-13	Backlash vs Pitch Radius	II-B-31
II-B-14	Deflections of Bearings & Associated Structure	II-B-32
II-B-15	Drive Train Schematic	II-B-34
II-B-16	Drive Mechanism and Controls Breadboard	II-B-35
II-B-17	Direct Gear Drive	II-B-37
II-B-18	Sun-Present Sensor	II-B-39
II-B-19	Functional Diagram of Sun-Present Sensor System	II-B-39
II-B-20	Heliostat Control Electronics Block Diagram	II-B-43
II-B-21	Heliostat Control Electronics	II-B-44
II-B-22	Typical Triac Motor Controller	II-B-46
II-B-23	Heliostat Interface Command (HIC)	II-B-48
II-B-24	Power Turn-On Initialization	II-B-49
II-B-25	Portable Controller for Heliostat Manual Positioning	II-B-50
II-B-26	Heliostat Control Electronics Electrical Interface	II-B-52
II-B-27	Heliostat Electrical Installation	II-B-54
II-B-28	Fine and Coarse Tracking Coordinate System	II-B-63
II-B-29	Heliostat Control Loop	II-B-65
II-B-31	Peak Azimuth Rates vs Distance from Node	II-B-70
II-B-32	Heliostat Manufacturing/Site Installation Flow Sequence	II-B-80
II-B-33	Mirror Rack Weld Assembly Fixture	II-B-82
II-B-34	Mirror Adjustment Tab Welding Fixture	II-B-82
II-B-35	Mirror Handling Dolly	II-B-83
II-B-36	Mirror Module Transporter	II-B-84

II-B-37	Heliostat Control Electronics Manufacturing Flow	II-B-85
II-B-38	Fabrication of Manual Control Box	II-B-86
II-B-39	Typical Interface Between Heliostat Interface Module and Heliostat Control Electronics Assemblies	II-B-87
II-B-40	Heliostat/Foundation Electrical Interface	II-B-90
II-B-41	Outlet Center at Heliostat Foundation	II-B-91
II-C-1	MCS-HACSS Functional Schematic	II-C-2
II-C-2	Heliostat Array Control Subsystem	II-C-4
II-C-3	Heliostat Control System Block Diagram	II-C-5
II-C-4	Control Loop Breadboard Demonstration Setup	II-C-7
II-C-5	Block Diagram of Breadboard Data Transmission and Control System	II-C-7
II-C-6	Software Planning Guide	II-C-17
II-C-7	Hardware/Software Event Relationship	II-C-18
II-C-8	System Data Flow	II-C-24
II-C-9	Heliostat Interface Command Definition	II-C-26
II-C-10	Heliostat Attribute Table	II-C-27
II-C-11	HAC/MCS Alarm Message	II-C-29
II-C-12	Fabrication of the Heliostat Interface Module	II-C-31
II-C-13	Typical Interface between Heliostat Interface Module and Heliostat Control Electronics	II-C-35
II-D-1	Solar Simulation Focusing and Alignment Geometry	II-D-2
II-D-2	Heliostat Workstand	II-D-3
II-D-3	Alignment Target/Calibration Target Interface	II-D-4
II-D-4	Sample Alignment Target Configuration	II-D-6
II-D-5	Bridge Crane Concept	II-D-9
II-D-6	Mobile Tower Concept	II-D-10
II-D-7	Alignment Light And Alignment Target on the Receiver Tower Geometry	II-D-20
II-D-8	Computer Ray Trace of Focus Offset Positions for Light and Target on Receiver Tower Concept - Sample 1	II-D-22
II-D-9	Computer Ray Trace of Focus Offset Positions for Light and Target on Receiver Tower Concept - Sample 2	II-D-23
II-D-10	Off-Site Heliostat Focusing Using Off-Axis Angle Simulation	II-D-24
II-D-11	Parabolic 2F Focusing and Alignment Geometry	II-D-26
II-E-1	Optical Target Photograph and Overlay of Test Observation Images on Computer Pattern between 9 and 11 am MDT, May 29, 1974	II-E-5
II-E-2	Optical Target Photograph and Overlay of Test Observation Images on Computer Pattern between Noon and 1 pm, May 29, 1974	II-E-7
II-E-3	Calibration Target on the Calibration Ring	II-E-11
II-E-4	Calibration Target on the Elevation Module	II-E-11
II-E-5	Calibration Target below the Receiver	II-E-11
II-E-6	Pyrheliometer	II-E-14

II-E-7	Prototype Calorimeter Being Used for Heliostat Tests at Martin Marietta	II-E-18
II-E-8	Calibration Subsystem Block Diagram	II-E-22
II-E-9	Calibration Subsystem Module	II-E-23
II-E-10	Calibration Target Assembly	II-E-25
II-E-11	Solar Cell Sensor Assembly	II-E-27
II-E-12	Calorimeter Subsystem	II-E-30
II-E-13	Calibration Subsystem Electronics Block Diagram	II-E-35
II-F-1	Mirror Cleaning Equipment	II-F-1
II-F-2	Heliostat Workstand	II-F-2
II-F-3	Mirror Module Transporter	II-F-3
II-G-1	Power and Control Wiring Block Diagram	II-G-7
II-G-2	HACSS Electrical Interfaces	II-G-7
II-I-1	Specular Reflectivity Test Rig Using Normal-Incidence Pyrheliometers, Profile View	II-I-6
II-I-2	Specular Reflectivity Test Rig Using Normal-Incidence Pyrheliometers, Front View	II-I-6

Table

II-B-1	HASS Major Requirements	II-B-3
II-B-2	Fine-Tracking Error Budget	II-B-15
II-B-3	Heliostat Power Budget	II-B-56
II-B-4	Total Power Budget	II-B-56
II-B-5	Zone A (1-MWt) Field Performance, Martin Marietta Receiver	II-B-57
II-B-6	Zone A and B (5.5 MWt) Field Performance, Martin Marietta and McDonnell Douglas Receivers	II-B-58
II-B-7	Zones A, C, D, and E (5 MWt) Field Performance - Honeywell Receiver	II-B-58
II-B-8	Collector Array Power Requirements	II-B-59
II-B-9	Average Heliostat Tracking Motor Velocities, Duty Cycles	II-B-69
II-B-10	Tracking Time Loss Per Day Due to High Azimuth Rates	II-B-70
II-B-11	Heliostat Manufacturing Requirements	II-B-76
II-B-12	Heliostat Manufacturing and Assembly Site Selection Rationale	II-B-78
II-C-1	Heliostat Array Control Subsystem Major Requirements and Proposed Approach	II-C-3
II-C-2	Successful Software Systems	II-C-12
II-C-3	Computer Timing Comparison	II-C-13
II-C-4	Computer Availability Comparison	II-C-15
II-C-5	MCS/HACSS Interface Formats	II-C-33
II-C-6	HACSS/HASS Interfaces	II-C-34
II-D-1	Focusing and Alignment Subsystem Requirements and Approach	II-D-2

II-E-1	Summary of Major Calibration Subsystem Requirements and Approach	II-E-2
II-E-2	Comparison of Three Approaches for the CSS Target Location	II-E-12
II-G-1	Power Quality	II-G-8
II-B-2	Total HACSS Power Budget	II-G-8
II-G-3	Total Power Budget	II-G-9
II-H-1	Calibration Subsystem Maintenance Requirements	II-H-7
II-I-1	Heliostat Array and Control System Verification Requirements Matrix	II-I-2
II-I-2	Component Design Verification Test Matrix	II-I-3
II-I-3	Acceptance Test Program Matrix	II-I-8
II-I-4	Software Verification and Validation	II-I-15

I. Introduction

I. INTRODUCTION

This proposal is completely responsive to the requirements of Sandia Laboratories request for quotation (RFQ) 03-3731 dated October 10, 1975. Martin Marietta understands the technical performance required of the Heliostat Array and Control System (HAACS) for the ERDA 5-Megawatt Solar Thermal Test Facility. We offer a design and an implementation plan we believe will produce a superior system on schedule and within proposed costs.

The Martin Marietta Corporation has made a strong commitment to the terrestrial solar energy field as evidenced by our performance on the following contracts:

- Central Receiver Solar Thermal Power System (CRSTPS) Phase I, ERDA Contract E(04-3)1110.
- Solar Power System and Component Research Program, National Science Foundation Contract AER 75-07570.
- 1-Megawatt Thermal Bench Model Cavity Receiver Steam Generator, ERDA Contract E(04-3)1068.
- Preliminary Insolation Investigation and Solar Power Feasibility Study for St. Croix, U.S. Virgin Islands, Contract VIWAP 07700.

We have adapted Martin Marietta's basic concept for heliostat design now being applied to the CRSTPS Subsystem Research Experiment. An artist's conception of the CRSTPS is shown in Figure I-1. Our heliostat design incorporated the following features:

- 1) A 25 mirror array in a 5x5 matrix of easily focusable mirror assemblies;
- 2) Each mirror assembly constructed of commercially available, stock-size material;
- 3) Mirrors store in "face-down" position for protection from the elements, resulting in longer life, and minimizing and assuring less atmosphere particulate contamination;
- 4) Safety features such as limited travel, fail-safe control, and laminated safety glass mirrors.

Our calibration subsystem design incorporates the following capabilities:

- 1) Calorimetric determination of reflected energy from each heliostat using a unique, straightforward scientific and proven approach;
- 2) Heliostat reflected-beam quality characterization by using a ~~single vertical array of solar cells to affect economy~~ on numbers of solar cells required (64 vs 4096);
- 3) Heliostat gimbal encoder offset determination to remove pointing error using software to correct encoder offset, eliminating the need for costly manual alignment adjustment;
- 4) Heliostat pointing capability determination.

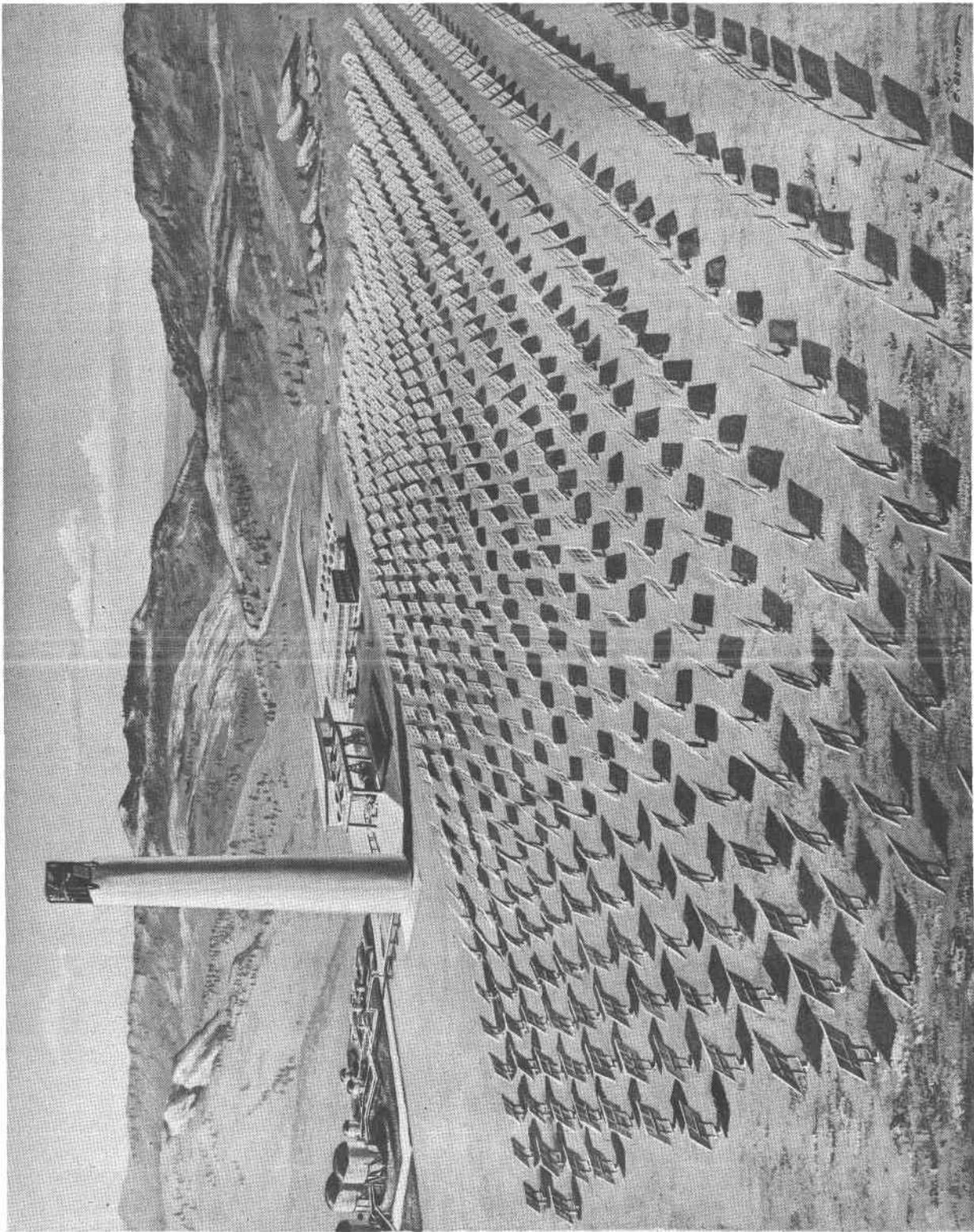


Figure I-1

Figure I-1 Artist's Concept, CRSTPS

The heliostat control system is state-of-the-art in design and has the following features:

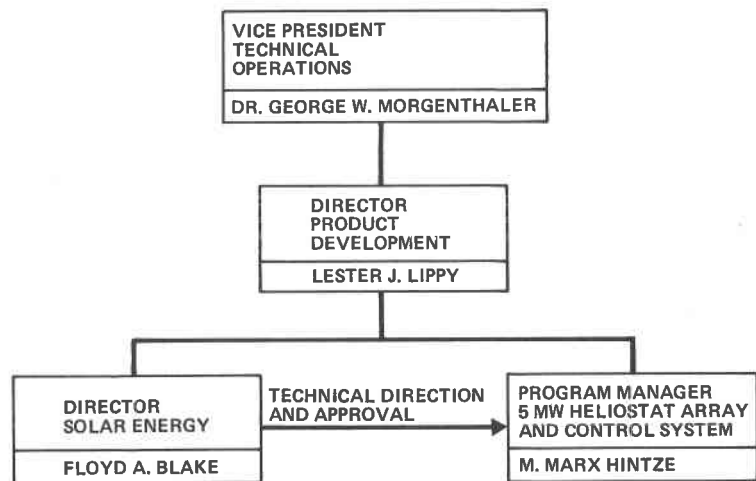
- 1) One controller for up to 128 heliostats, four data bus lines with up to 32 heliostats per line, and multiplexed communication scheme expandable to 256 heliostats;
- 2) Pointing control assured by feedback from 14-bit absolute encoder;
- 3) Meets 1.5-milliradian aiming requirement in fine-tracking mode;
- 4) [REDACTED] features such as [REDACTED] electronics in case of power failure, and emergency stowage from independent power bypass circuit;
- 5) Independent checkout capability at each heliostat.

Martin Marietta's focusing alignment subsystem will provide ease of initial adjustment as well as rapid refocusing. Our system incorporates:

- 1) Heliostat astigmatic off-axis correction for equinox solar noon by a straightforward simulation of this condition with a 0.5-degree collimated white light source;
- 2) A basic, accurate approach for mirror focusing by using the entire mirror surface, eliminating focusing and alignment errors due to local surface irregularities that are known to exist in focusable mirrors (this phenomenon is discussed in Chapter II.D.7);
- 3) Direct image viewing during focusing to minimize focusing time and electronic interface requirements;

- 4) Alignment and focusing of each heliostat in its installed field position to assure installed optical integrity;
- 5) A target near the receiver aperture to properly define the image at the aperture with negligible defocusing rather than a target separated from the receiver that would result in unacceptable defocusing at the receiver aperture;
- 6) Focusing and alignment target attached to the calibration target module, thereby minimizing interface requirements and maximizing focusing efficiency.

We have established a special program team to accomplish the heliostat array and control system program and have placed it in our Denver Division organization to provide the maximum benefits to this program. As shown, our Program Manager, Marx Hintze, reports to Les Lippy our Director for Product Development.



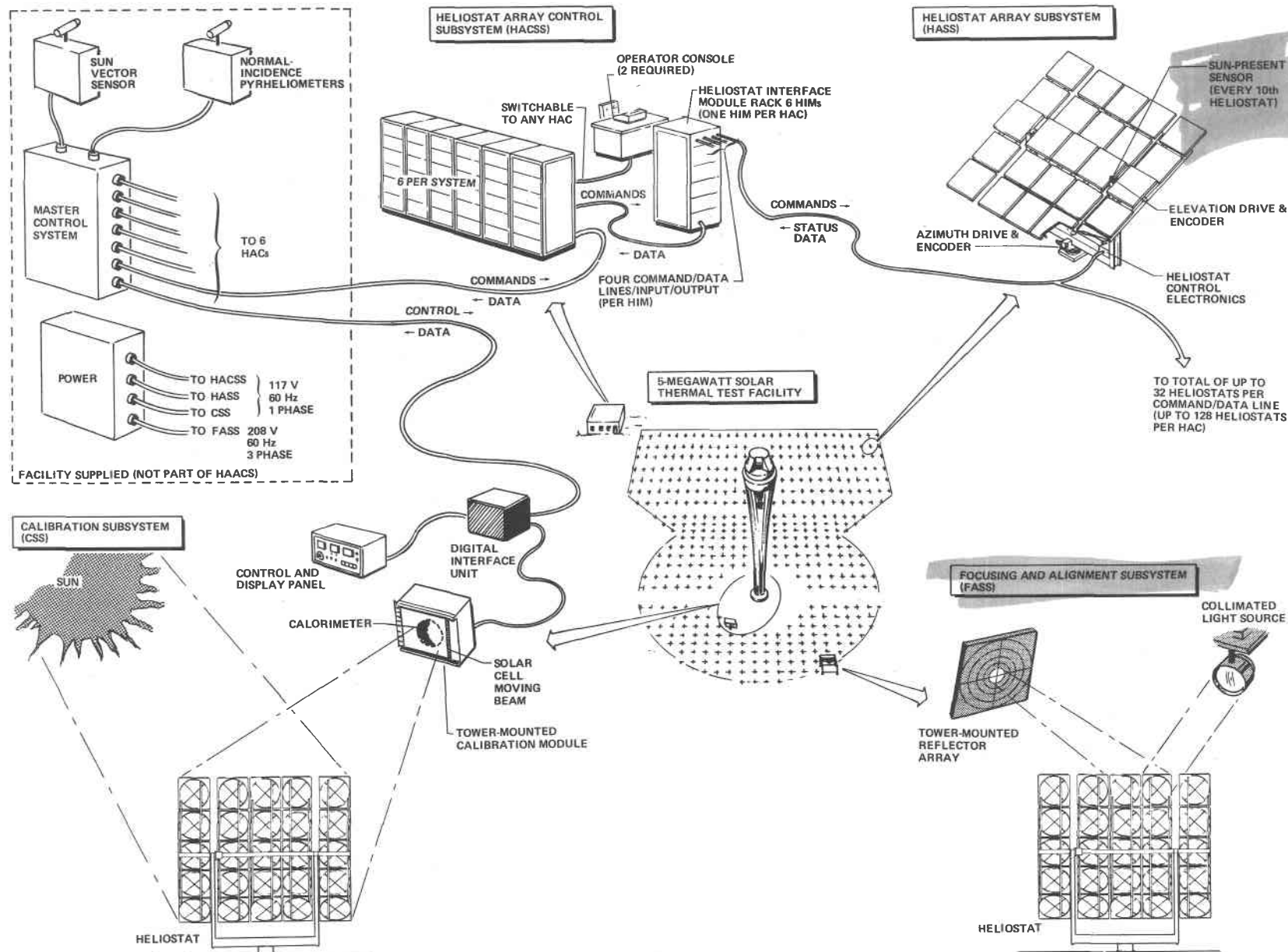
Les Lippy was our Site Activation Director for the Titan II ICBM base near Tucson, Arizona. Les' experience in accomplishing the Titan II site activation on schedule and *below* contract target cost will be invaluable in assisting Marx Hintze in detailed planning and performance of the field installation and checkout

portion of HAACS. Another feature of our organization arrangement is the relationship between Marx Hintze and Floyd Blake, who is in charge of our Central Receiver Solar Power System program for ERDA. Floyd will provide technical direction and approval for all designs as they are being prepared by Marx' engineers. The Blake and Hintze teams will be located immediately adjacent to each other in Denver to assure good continuous technical interchange.

The baseline design depicted in Figure I-2 has evolved from a complete analysis of the RFQ system requirements document K93681, and the application of our work in the CRSTPS Subsystem Research Experiment now under development at our Denver Division. Table I-1 summarizes key requirements from K93681 and the capability of our baseline design to meet them. The aspects of our proposal that we consider key to Sandia Laboratories and to the ERDA 5-Megawatt Solar Thermal Test Facility are defined below.

- Optimized heliostat zone arrangement. The rectangular arrangement provides more efficient utilization of space and results in a minimum of shading and blocking of one heliostat by another.
- Modular system approach. The major elements of our design, namely the heliostats, the controllers, and the software, are designed on a modular basis for versatility, ease of assembly, maintenance, and replacement, and for selection of additional numbers of facility expansion.

Figure I-2



I-7

Figure I-2
HelioStat Array and Control System (HAACS) Functional Schematic

Table I-1 Key System Requirements Conformance

K93681 PARAGRAPH	SUMMARY OF REQUIREMENT	MARTIN MARIETTA'S DESIGN
3.1.3.2	CONTROL OF UP TO 128 HELIOSTATS PER HELIOSTAT ARRAY CONTROLLER.	SOFTWARE CONTROL CAPABILITY TO EXPAND TO CONTROL OF 256 HELIOSTATS.
3.1.3.2b	INTERFACE WITH MASTER CONTROL SYSTEM OVER 9600 BAUD LINE USING UNIVERSAL ASYNCHRONOUS RECEIVER/ TRANSMITTER (UAR/T).	UAR/T AT 9600 BAUD IS USED TO INTERFACE WITH MCS. THE SAME TECHNIQUE IS APPLIED TO OUTPUT OF HELIOSTAT ARRAY CONTROLLERS FOR HELIOSTAT DATA LINE INTERFACE.
3.1.4.1 AND TABLE 2	MINIMUM POWER LEVEL TO FOUR RECEIVERS TO BE TESTED IS 1.0, 5.5, 4.4 AND 5.0 MWt.	POWER LEVEL IS MET WITH MARGINS OF GREATER THAN 4% IN EVERY CASE.
3.1.4.3.a	FINE-TRACKING CAPABILITY SHALL BE WITHIN ± 1.5 mrad, 1σ FOR EACH AXIS AT 20-mph SUSTAINED WIND; ± 3.0 mrad 1σ FOR EACH AXIS AT 30-mph SUSTAINED WIND.	FINE-TRACKING CAPABILITY OF ± 1.48 mrad, 1σ IS MET WITH MARGIN AT 20-mph SUSTAINED WIND AND 2.74 mrad, 1σ AT 30-mph SUSTAINED WIND.
3.1.4.4.g	FAILURE OF HELIOSTATS, CONTROLS, OR COMMERCIAL ELECTRIC POWER SHALL NOT RESULT IN AN UNSAFE CONDITION.	OUR FAIL-SAFE SCHEME MEETS THIS REQUIREMENT IN ALL RESPECTS. SOFTWARE AND HARDWARE MONITORS WITH AUTOMATIC REMEDIAL ACTION ASSURES FAIL-SAFE OPERATION.
3.2	CALIBRATION SUBSYSTEM SHALL BE CAPABLE OF CHARACTERIZING POWER DISTRIBUTION IN REFLECTED BEAM AND OF MEASURING ENERGY IN CIRCULAR TARGET OF 0.012 TIMES SLANT RANGE OF HELIOSTAT TO TARGET.	CALIBRATION SUBSYSTEM WILL DEFINE BEAM SIZE SHAPE AND RELATIVE ENERGY DISTRIBUTION AS WELL AS PERFORM ABSOLUTE ENERGY MEASUREMENT.

- Software control credentials. Martin Marietta has extensive, up-to-date experience in the application of software to control systems. Examples of this capability are:
 - Our current work in the Central Valley Project in which software control will be applied to several power substations and other facilities;
 - Viking ground test program in which a master computer was used to command a spacecraft computer and to monitor all responses of onboard sensors continually on a real-time basis. The system had the capability to input over 1000 discrete stimulus commands, nearly 100 million (5×2^{24}) digital commands, and to monitor over 4500 responses with a sampling rate that allowed each analog measurement to be sampled 20 times per second.
- Off-the-shelf hardware. During our design studies for the National Science Foundation and CRSTPS, Phase I Contracts, as well as in our studies to respond to this request for proposals,

we have designed a system that is low in cost, easy to maintain and repair, and that will produce efficient, long-life operation.

II. Conceptual Design and Design Rationale

A. HELIOSTAT ARRAY AND CONTROL SYSTEM DESCRIPTION

The system Martin Marietta has selected is based on the work accomplished thus far in the CRSTPS contract, particularly in the area of heliostat design. In the area of heliostat control the requirements of RFQ specification K93681 indicate the need for a departure from the in-line sun sensor approach of the CRSTPS design. In this area we have selected a quasi-closed-loop system that depends on knowledge of the sun's position from the facility master control system (MCS) and heliostat azimuth and elevation angle data from encoders mounted on their respective axes.

The HAACS will comprise four subsystems plus installation and maintenance equipment. The relationship between the four subsystems and the facility is depicted in Figure II-A-1. The heliostat array control subsystem will be located in the facility control room and will interface with the MCS by a 9600-baud line coupled to the HACSS with a universal asynchronous receiver/transmitter. A separate heliostat array controller will be allocated for each heliostat zone having up to 128 heliostats; for the zone having more than 128 heliostats (zone B), two HACs will be required (Fig. II-A-2). Each HAC will have an output of four duplex data buses, each capable of communicating by digital commands to and from, the heliostats for up to 32 heliostats (making the maximum 128 heliostats per HAC).

Figure II-A-1

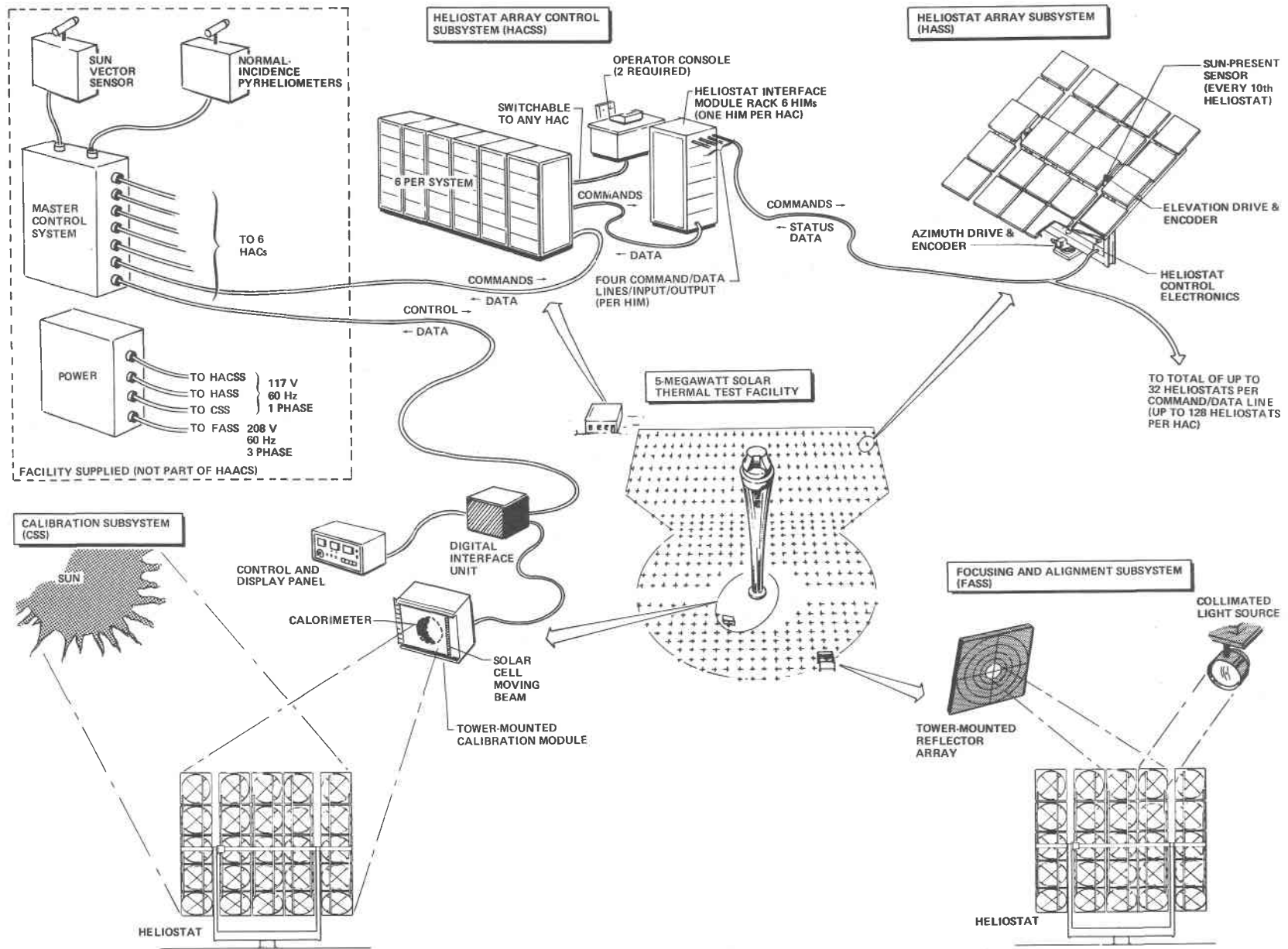


Figure II-A-1 Heliostat Array and Control System (HAACS) Functional Schematic

The HAC software will be

responsive to MCS com-

mands and queries and

will service each of the

assigned heliostats

every second, insuring

reliable fail-safe

heliostat operation.

The HACSS will include

the peripheral equip-

ment necessary for pro-

gramming, such as tele-

type, magnetic tape,

and on-line disc stor-

age. The HACSS will

require 117-Vac 60-Hz

power from the facil-

ity.

The heliostat array subsystem (HASS) will include, collectively, all of the individual heliostats located in the heliostat zones as shown in Figure II-A-2. The heliostats will comprise focusable mirrors mounted on a gimbaled structure with drive mechanisms, absolute position encoders, and the control and data circuitry needed to direct them from the HACSS and to return mode and position data to the HACSS. The array of heliostats will collect the sun's energy and direct it to the

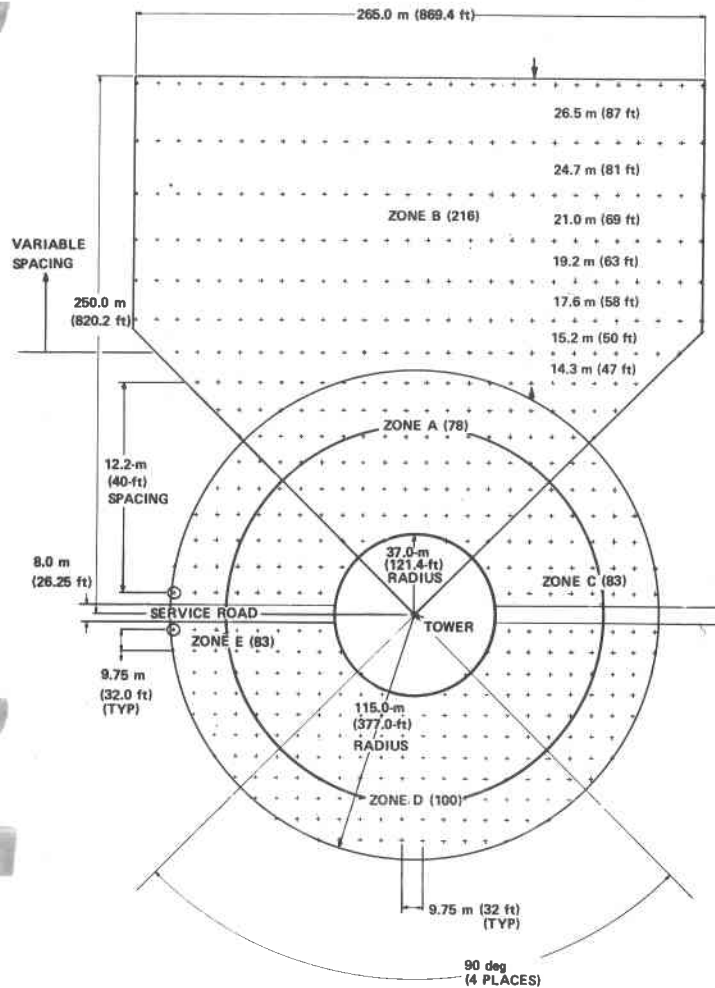


Figure II-A-2 Heliostat Zone Layout

experiment located on the tower for the on-target mode or to a point off-target for the standby mode. A sun-present sensor (SPS) will be mounted on at least one of every 10 heliostats.

The focusing and alignment subsystem (FASS) will adjust the heliostat mirrors so they will focus at least 90% of the reflected sun's energy (at equinox solar noon) at the target in an area no larger than 0.012 times the slant range from heliostat to target. The FASS will consist of a mobile bridge crane on which is mounted a directable collimated white-light source, and a reflector array mounted on the facility tower. The crane will be moved to a location, for each heliostat, that will allow the light source to be placed at a position that simulates the sun's location at noon of the solar equinox. The 25 mirrors will be individually adjusted, using the reflective array, to focus the reflected image near the experiment aperture plane and to align the mirrors so all 25 images converge at the same location.

The calibration subsystem (CAS) will consist of four major components--solar cell beam, a calorimeter panel, a digital interface unit, and a control unit. The CAS will interface with a group of facility normal-incidence pyrhelimeters (NIPs). The solar cell beam, the calorimeter panel, the digital interface unit, and the control unit will be located on the tower. The NIPs will be located at any convenient location in the facility, e.g., on the roof of the administration and control building. The panel will be mounted on the elevation module as near the receiver aperture plane as possible.

The vertically oriented solar cell beam will be mechanized to traverse horizontally across the calorimeter panel, and solar cell voltages will be sampled at regular intervals. The data from this operation will be converted by the digital interface unit. The digital interface unit will receive signals from the calorimeter and the solar cell beam and multiplex them for transmission to the facility MCS. The CSS will provide the functions of beam quality evaluation, beam size and energy distribution assessment, and heliostat encoder offset correction data.

The installation and maintenance equipment will consist of such items as work platforms, mirror cleaning equipment, yoke module and mirror module transporters, and heliostat manual control units. Although equipment of a commercial nature normally available in a maintenance shop, e.g., oscilloscopes, meters, and hand tools, are not included in this category, these items will be identified in the maintenance instructions to be delivered per paragraph 3.1.2.j of K93681.

CONCEPTUAL DESIGN AND DESIGN RATIONALE

Successful implementation of the heliostat array and control system (HAACS) within the required timetable can be achieved by a contractor that has conducted significant development work prior to contract award. Martin Marietta is able to use immediately the results of a three-year development effort in the solar thermal power field. We have drawn heavily from the work being performed in the Central Receiver Solar Thermal Power System (CRSTPS) contract [ERDA E(04-3)1110] awarded to us in June of this year. The tradeoff studies required to arrive at a viable system have already been performed (ref Appendix B). We have also built and tested a breadboard encompassing all the electronics between the heliostat array controller (HAC), universal asynchronous receiver/transmitter (UAR/T) and the heliostat shaft encoder and are therefore able to propose a system based on actual test results. A photograph of the laboratory test setup is shown in Figure II-1.

The 10-year operational life requirement played a large part in arriving at our design. Our design features "standard" parts available from multiple sources, conservative design margins, and modularity for ease of maintenance.

We have addressed personnel and hardware safety thoroughly, considering it through all phases from manufacturing and assembly to installation, checkout, and normal operations.

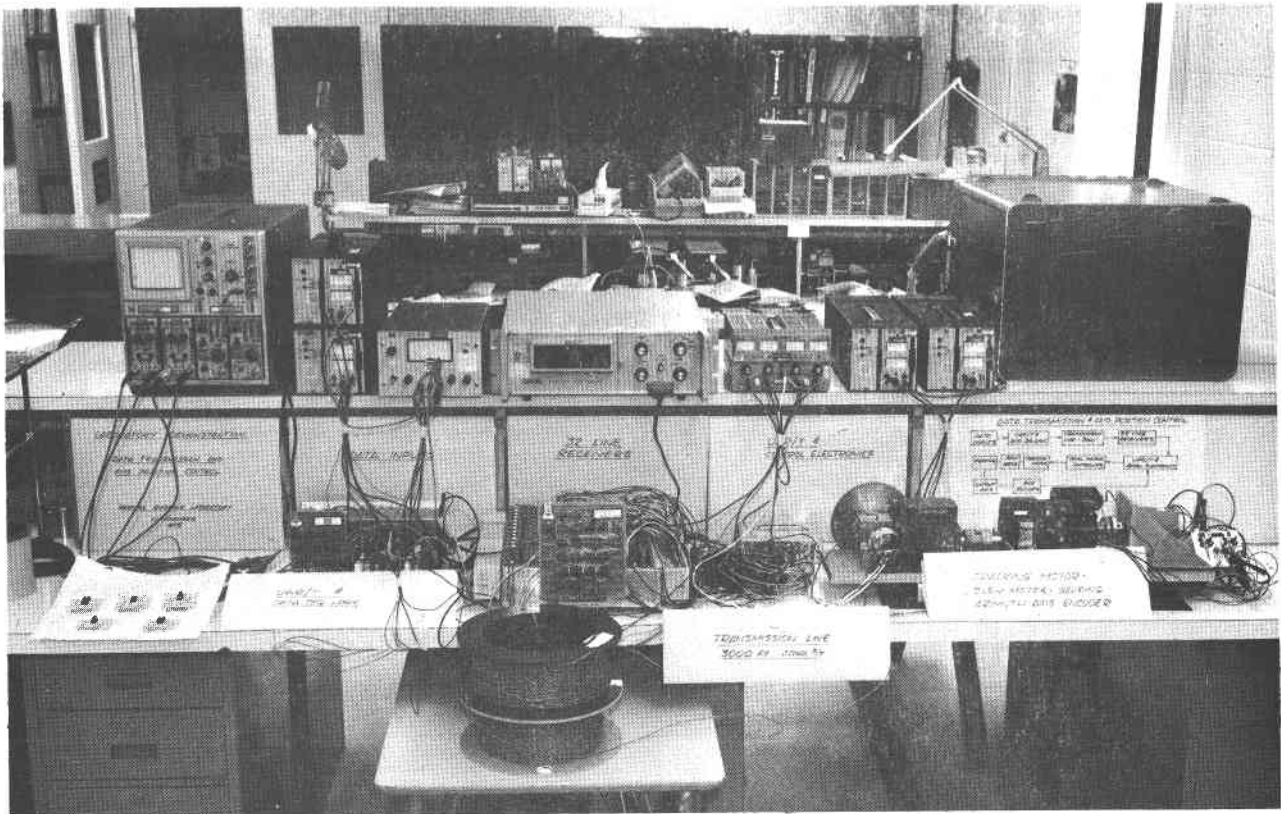


*Figure II-1
Control Loop and Data Transmission Breadboard Simulation*

Section A gives an overall view of our proposed design. Sections B, C, D, E, and F give detailed design information for each of the subsystems comprising the HAACS.

A. Heliostat Array and
Control System
Description

**B. Heliostat Array
Subsystem (HASS)**

B. HELIOSTAT ARRAY SUBSYSTEM (HASS)

The heliostat array subsystem comprises all of the heliostats located in the five zones of the test facility, either in part or in total. The allocation of heliostats to the zones is depicted in Figure II-B-1. The zones are configured to provide adequate solar energy from a single zone (zone A) for operation of the 1-MWt receiver, energy from zones A and B for operation of the Martin Marietta 5.5-MWt and McDonnell Douglas 4.4-MWt receivers, or energy from zones A, C, D, and E for the 5-MWt Honeywell receiver.

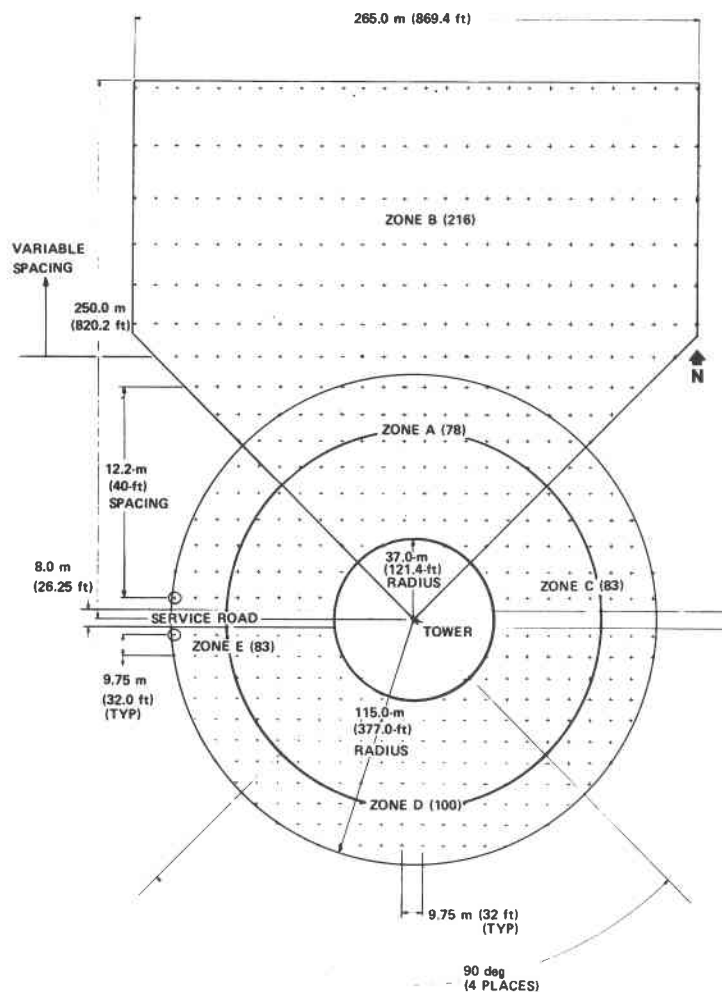


Figure II-B-1 Test Facility Zone Layout

Design of the collector fields for a central receiver solar power plant has continuously moved toward the maximum simulation of parabolic mirror performance through the use of heliostats. The key to accomplishment of efficient simulation has been the combining of both collection and concentration functions into the heliostat surface. The Martin Marietta heliostat design uses individually warped and pointed mirrors to achieve this effect.

The field configuration proposed by Martin Marietta to satisfy the HAACS specifications, as shown in Figure II-B-1, reflects a total collector area less than that specified in the RFQ. The radius for zones A, C, D, and E has been decreased from 125 m (410 ft) to 114.9 m (377 ft). This proposed reduction in collector area is the result of using a high-efficiency collector surface--a second-surface, silvered white glass mirror. In our arrangements we have oriented the heliostats in a rectangular configuration. This arrangement allows us to optimize the field area for heliostat placement and economize in zone conduit installation.

Designated heliostat locations, in conjunction with the facility-provided interconnecting wiring for power and control, afford an optimum approach through the use of common installation trenches/conduits for the wiring, along with sufficient clearance between heliostat locations, permitting ease of installation and maintenance. The plan for on-site final assembly of each heliostat further enhances the ease of heliostat installation.

The HASS comprise 79 heliostats capable of providing 1.65 MWe, 294 heliostats in zones A and B capable of providing 6.70 MWt, and 344 heliostats in zones A, C, D, and E capable of providing 7.06 MWt (all MWt values are referenced to 1200 hr solar time on the spring equinox).

Table II-B-1 summarizes the major RFQ requirements and our approach to meeting them. Addendum II of Volume IV is a preliminary heliostat subsystem requirements specification. The physical configuration and functional capabilities of our heliostat are discussed in the following subsections.

Table II-B-1 HASS Major Requirements

ITEM	RFP REQUIREMENTS	RFP PARAGRAPH	PROPOSED APPROACH
1	PROVIDE: <ul style="list-style-type: none"> • 1.0 MWt TO RECEIVER FROM ZONE A • 5.5 MWt TO RECEIVER FROM ZONES A + B • 4.4 MWt TO RECEIVER FROM ZONES A + B • 5.0 MWt TO RECEIVER FROM ZONES A + C + D + E 	3.1.4.1	<ul style="list-style-type: none"> • HIGH EFFICIENCY OF HELIOSTATS • SUFFICIENT QUANTITY OF HELIOSTATS IN EACH ZONE TO PROVIDE PERFORMANCE MARGINS • INDIVIDUAL MIRROR FOCUSING AND ALIGNMENT • INDIVIDUAL AIMING CONTROL OF EACH HELIOSTAT BY THE HACSS • HIGH SPECTRAL REFLECTIVITY OF MIRRORS
2	EACH HELIOSTAT MUST BE CAPABLE OF DIRECTING 90% OF ITS REFLECTING POWER INTO A CIRCULAR TARGET OF DIAMETER 0.012 SR FROM ITS LOCATION IN THE FIELD AT SOLAR NOON ON THE EQUINOXES	3.1.4.2	<ul style="list-style-type: none"> • INDIVIDUAL MIRROR ALIGNMENT AND FOCUSING • HIGH-EFFICIENCY HELIOSTAT • WARPING TECHNIQUE FOR MIRROR FOCUSING • HELIOSTAT CONFIGURATION OF 25 MIRRORS (5x5 MATRIX)
3	EACH HELIOSTAT MUST BE CAPABLE OF DIRECTING THE SUN'S RAYS AT A SPOT IN AN IMAGINARY THREE-DIMENSIONAL GRID SYSTEM	3.1.4.3	<ul style="list-style-type: none"> • ACCEPTANCE TEST OF EACH HELIOSTAT USING THE FOCUSING AND ALIGNMENT SUBSYSTEM AND THE HELIOSTAT ARRAY CONTROLLER WILL DEMONSTRATE COMPLIANCE • INDIVIDUAL MIRROR FOCUSING AND ALIGNMENT

1. Physical Description - Heliostat

The baseline heliostat configuration is illustrated in Figure II-B-2. This concept features an array of 25 warped mirrors rigidly mounted in a 5x5 symmetrical pattern on gimbaled frames. Each 1.22x1.22-m² (4.0x4.0-ft) square mirror can be individually focused and aligned on its supporting framework. The entire mirror array provides 37.2 m² (400 ft²) of reflective surface and is capable of focusing an aberrated image of the sun on a fixed target. Attainment of measured component reflectivity in fully assembled heliostat has been verified by extensive Martin Marietta testing. The focal length of the heliostat is fixed after installation at the time of the focusing and alignment adjustment.

The selected configuration evolved from numerous tradeoff studies and experimental work conducted at Martin Marietta's Denver facility over the past three years. Lessons learned and experience gained in the central receiver solar thermal power system (CRSTPS) phase 1 program (ERDA contract E(04-3)1110] have been extensively applied in our design approach to the components comprising the heliostat (See Appendices A and B). Long life is assured through the utilization of commercially available hardware in the design, plus the maintainability features described in subsection 4 of this section. Concepts conceived and verified by testing in our CRSTPS program, such as mirror arrangement, drive system, component error allocations, and focusing and alignment features, have been advantageously applied to our designs with updating

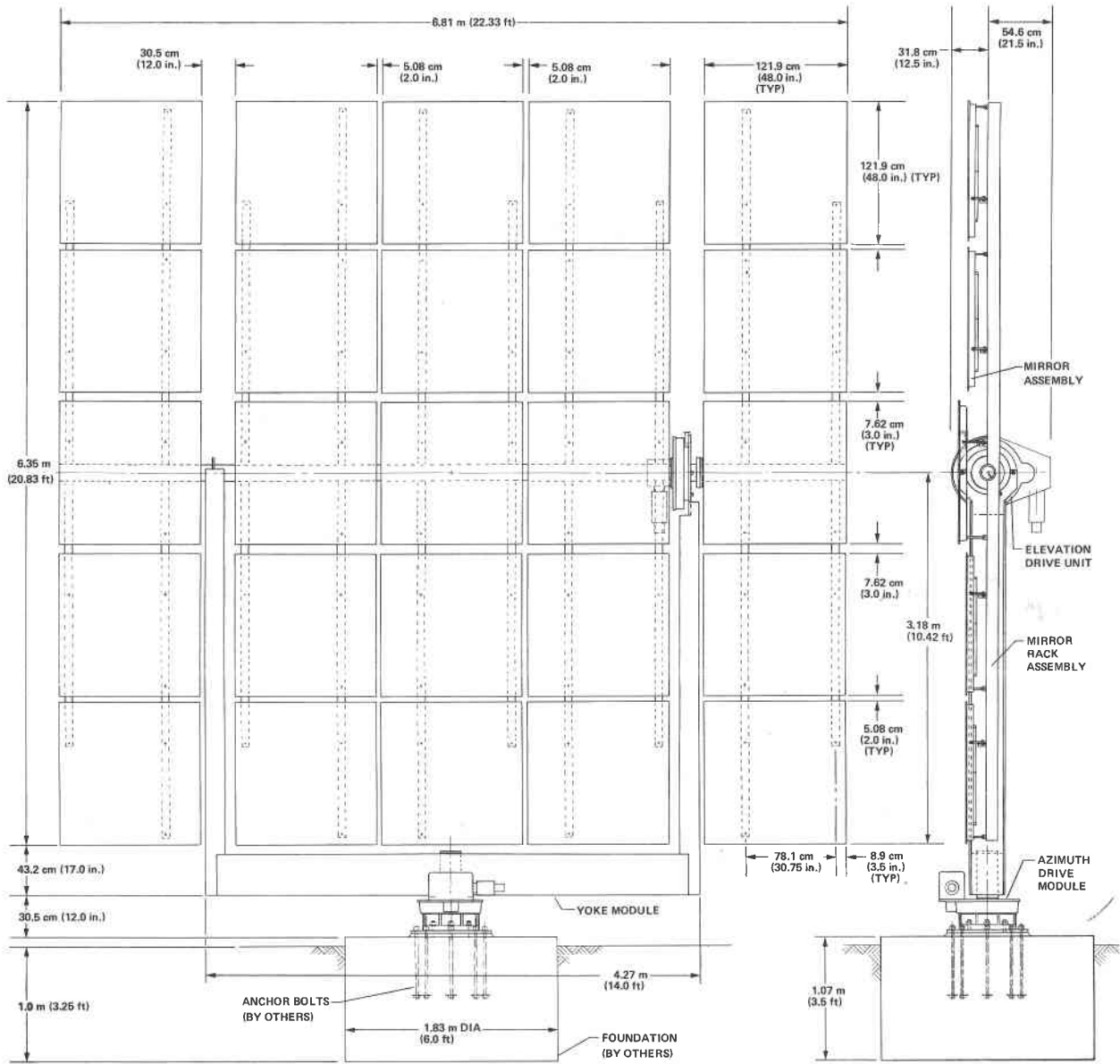


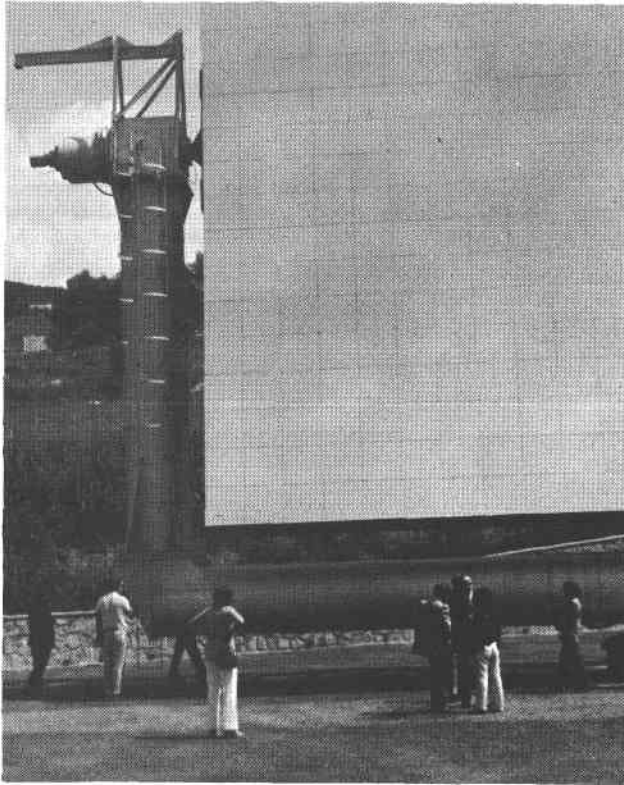
Figure II-B-2 Heliostat Baseline Configuration

incorporated where required. Operating criteria are virtually identical although some modification, mainly in regard to the sensitivity of the feedback encoders, will be necessary because of the quasi-closed-loop mode of heliostat control.

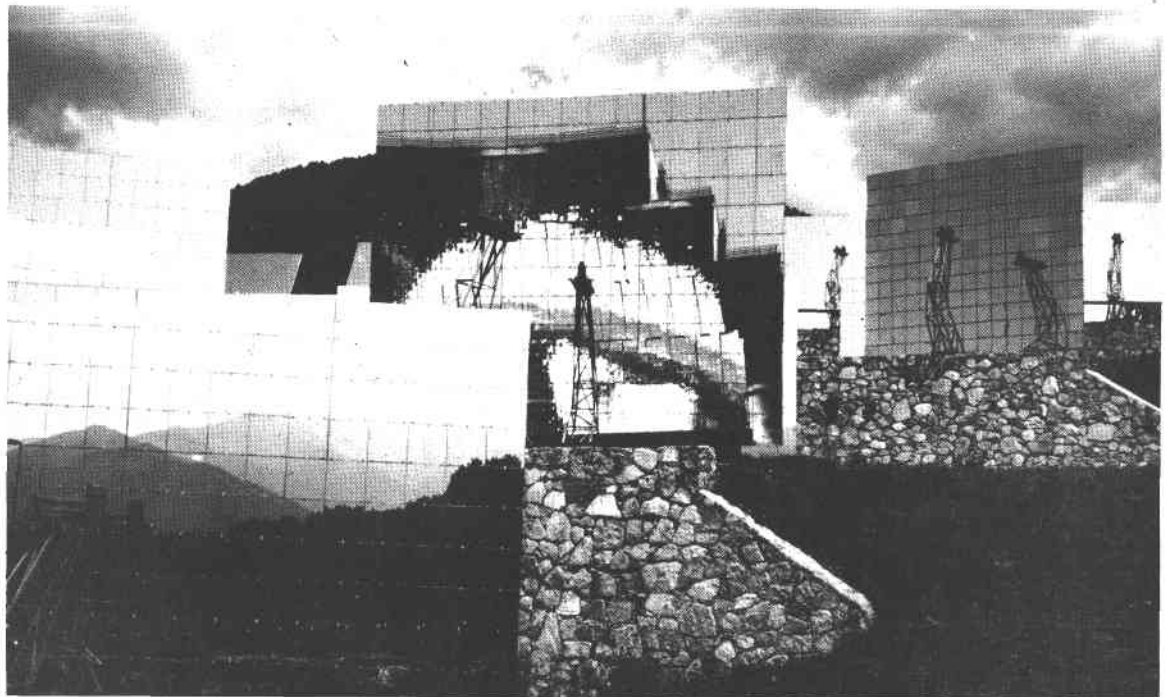
Heliostats as large as 17.0x13.5 m (55.8x44.3 ft) that have been used at the CNRS solar furnace facility in France were reviewed during our proposal phase. These heliostats, shown in Figure II-B-3, require massive and expensive support structures. A structural analysis indicated that a 17.0x13.5-m (55.8x44.3-ft) heliostat increased in weight by a factor of six over the 6.1x6.1-m (20x20-ft) heliostat shown in Figure II-B-2, while its reflective surface increased only by a factor of five. The 6.1x6.1-m (20x20-ft) design was selected because it provided an optimum combination of cost, size, and structural support to meet the environmental and performance requirements.

The operating and nonoperating environmental conditions specified in K93681 precluded the direct transfer of technology from the CRSTPS program. Modifications of the mirror support structures and the drive systems were incorporated because of the wind loads and pointing and tracking accuracies specified in K93681.

The heliostats of the HASS employ components and subassemblies that are completely interchangeable. No special hardware requirements exist because of the utilization of commercially available equipment.



(a) 13.5x17.0 m (44.3x55.8-ft) HELIOSTATS AT CNRS FACILITY SHOWING MASSIVE STRUCTURAL REQUIREMENTS



(b) 6.1x6.1-m (20x20-ft) HELIOSTATS AT CNRS FACILITY

Figure II-B-3 CNRS Solar Furnace Facility

The heliostat, in its normal tracking mode, will be capable of continuously tracking the sun while maintaining pointing control to ± 1.48 mrad when subjected to wind velocities up to 9.0 m/s (20 mph) and 2.47 mrad at 13.5 m/s (30 mph). At wind velocities exceeding 13.5 m/s (30 mph), the heliostat will be returned to the "face-down" stowed position. Structurally, the heliostat is capable of surviving the effects of sustained wind velocities of 32 m/s (71.6 mph) with gusts up to 44.7 m/s (100 mph) without permanent deformation or mechanical degradation. All load analyses are based on results gained from comprehensive wind tunnel tests (see Appendix A) that were conducted on 1/10 scale models of the selected heliostat configuration.

Special precautions have been taken to protect moving parts and sensitive electronic assemblies from environmental conditions. The wiring and cables are specially wrapped and the heliostat control electronics is sealed. The drive system employs seals on the gear drives and bearings as well as employing sealed drive motors.

The heliostat drive systems are capable of maneuvering the heliostat as follows:

- 1) Azimuth, $\pm 2.40 \pm 0.044$ rad ($\pm 137.5 \pm 2.5$ deg)
- 2) Elevation, $-4.71 \begin{smallmatrix} +0.00 \\ -0.09 \end{smallmatrix}$ rad ($-270 \begin{smallmatrix} +0 \\ -5 \end{smallmatrix}$ deg);
- 3) Azimuth slew rate, 13.4 rad/hr (755 deg/hr);
- 4) Azimuth tracking rate, 1.5 rad/hr (89 deg/hr);
- 5) Elevation slew rate, 17.82 rad/hr (1133 deg/hr);
- 6) Elevation tracking rate, 0.84 rad/hr (48 deg/hr).

The physical characteristics of the components used in the heliostat are discussed in the following paragraphs.

a. Structure - The heliostat consists of the azimuth drive module, yoke module, and the mirror module. The mirror module includes the elevation drive unit as an integral part of the assembly. Figure II-B-4 depicts this modular concept. The modular approach for the baseline design greatly simplifies field installation, assembly, and maintenance and permits interchangeability of entire assemblies as well as major components or subassemblies. Use of standard, commercially available structural steel sections, tubes, and accessories throughout minimizes procurement and fabrication time.

Strength Criteria - Conservative strength criteria have been established for use in design of the collector structure to preclude the need for in-depth structural integrity testing. The criteria are in the form of safety factors applied to limit loads and the interpretation of wind loading. The safety factors are 2.0 for allowable stress (yield) and 4.0 for allowable stress (ultimate). Wind gusts were treated as steady-state loads.

Because of the precise pointing accuracy required of the collector assembly, the heliostat supporting structure has been designed primarily for stiffness rather than stress considerations and the above safety factors have little effect on the design. The only areas they may affect are local bolted joints and connections. Even in these cases, however, deflection criteria tend to dominate.

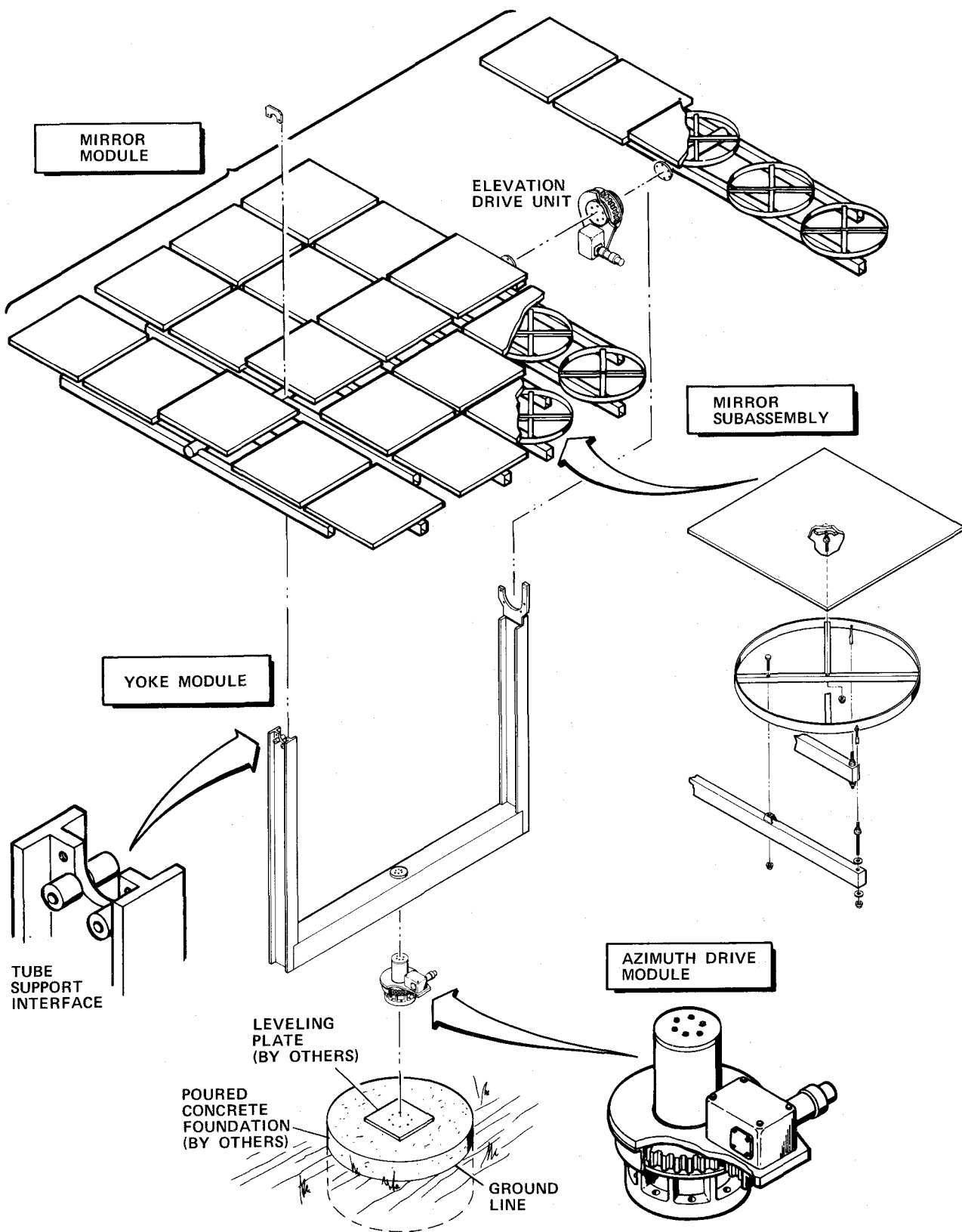


Figure II-B-4 Heliostat-Modular Concept

The symmetrical arrangement of the baseline configuration has proved to be very beneficial in minimizing the effects of elastic deformation. Most of the structural deformation contributing to pointing error is in the yoke structure, accounting for the relatively large and heavy sections. In standard practice, where deflection requirements are critical and govern the structural design, deep built-up sections or truss-type structures are generally indicated. This results in the highest strength-to-weight ratios for given applications. However, due to increased fabrication and assembly time, this approach is more expensive and thus not appropriate for low unit cost mass-produced items.

Structural Distortion Analysis - Mechanical or structural distortion results from two environmental conditions, i.e., thermal deformation and deformation resulting from wind loading. Thermal deformation is relatively small in comparison to that caused by wind loading and has not been fully evaluated for our baseline design. In the contractual design phase, a transient thermal analysis of the finalized design will be conducted to determine structural temperatures and temperature differentials. Temperature differentials will be translated to thermal deformations to determine overall distortion.

Structural deformations due to wind loading are a function of wind direction and velocity. Wind direction is important in determining whether the resulting deformation has any effect on mirror aiming accuracy. For example, a side wind will cause a

sideward deflection of the vertical arms and vertical yoke members but will not significantly affect mirror aim.

The worst-case condition is a wind normal to the plane of the mirrors. The baseline was designed for a nonuniform wind velocity of 9.0 m/s (20 mph) at 10 meters above the ground normal to the plane of the mirrors. The wind profile assumed was $V_z = 30 (z/30)^{0.233}$.

The wind tunnel tests (see Appendix A) indicated that loads should be calculated using an integrated average wind velocity over the height of the collector. The integrated average is represented by the expression

$$V = \left(\frac{V_R}{(X_R)^E} \right) \left(\frac{(X_2)^{E+1} - (X_1)^{E+1}}{(E+1)(X_2 - X_1)} \right)$$

where

V_R = velocity at reference height,

X_R = reference height,

X_1 = height to bottom of mirror array,

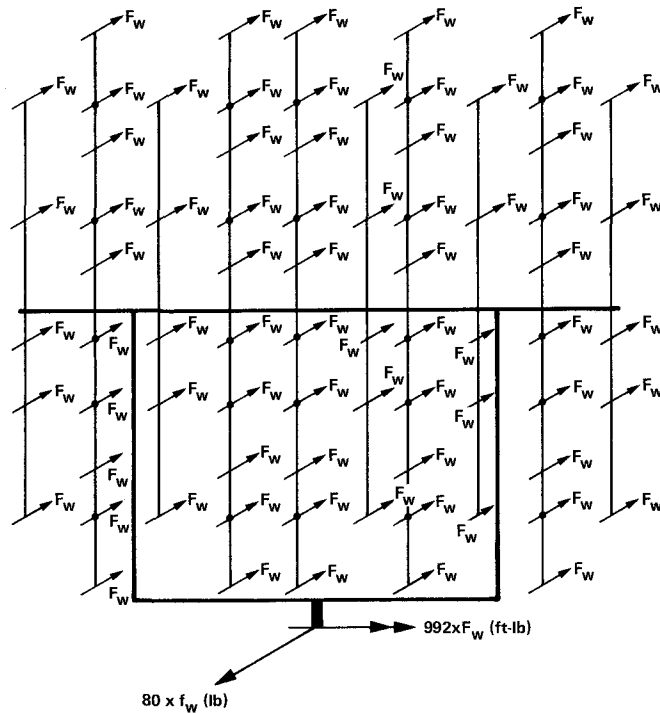
X_2 = height to top of mirror array,

$E = 0.233$.

Our design uses a reference height of 10 m (32.8 ft). The integrated average velocity is 6.47 m/s (23.3 mph) for $V_R = 30$ mph, $X_R = 32.8$ ft, $X_1 = 2$ ft, and $X_2 = 23$ ft.

The loads result from wind forces on all the frontal area including the mirrors and the exposed supporting structure. Wind loading varies as the velocity squared and the loadings on an

individual mirror for velocities of interest are tabulated in Figure II-B-5. The base loads reflect the additional loads due to wind forces on the supporting structure.



WIND VELOCITY		MIRROR LOAD, F_w	
m/s	MPH	N	lb
8.94	20	17.21	3.87
13.41	30	38.70	8.70
17.88	40	68.81	15.47
22.35	50	107.51	24.17

Figure II-B-5 Mirror Wind Loading

The distortion or deflection analysis may be divided into two parts--deflection up to the reference point of the elevation axis encoder, and deflection within the mirror rack about the elevation axis. The first part amounts to a pointing error and includes deflection in the foundation, azimuth drive mechanisms, yoke structure, and elevation axis structure. Also included are errors

introduced by gear backlash in the drive mechanisms. Gear backlash in the elevation drive mechanism is eliminated by an intentional structural unbalance in addition to wind torques as the mirrors rotate from a vertical to horizontal plane; thus the backlash will only be realized when the collector is being moved to the stowed position. The second part of the distortion analysis considers a defocusing because of out-of-plane deflection of the mirror support arms and elevation axis shaft.

Gear backlash in the azimuth drive mechanism adds vectorially to the primary deflection (rotation) of the elevation encoder. Although the effect is small, azimuth gear backlash must be included in the analysis as an additional error.

Detailed analysis of deformations, involving all the above contributors, and proper selection of cross-sectional geometries and sizes for the various members will assure adequacy of the final design.

Our preliminary distortion analysis illustrates the type and magnitude of mirror rotations that may be realized in a practical collector configuration. Contributions to the pointing error on the center mirror may be broken into the various contribution components as tabulated.

COMPONENT	ERROR CONTRIBUTION, mrad (arc-min)
COLLECTOR FOUNDATION	0.17 (0.60)
AZIMUTH DRIVE MECHANISM	0.50 (1.71)
YOKE STRUCTURE	<u>0.46 (1.58)</u>
	1.13 (3.89)

The tabulated errors are for a 13.4-m/s (30-mph) wind condition at 10 meters above the ground and are a rotation about the elevation axis. The azimuth drive gear backlash must be added vectorially to the above error (Table II-B-2).

Table II-B-2 Fine-Tracking Error Budget

ERROR SOURCE (FOR EACH HELIOSTAT AXIS)	1 σ ERROR BUDGET, mrad	
FINAL BEAM POINTING CALIBRATION	0.083	
TRACKING MOTOR SERVOLOOP		
ENCODER RESOLUTION (14 Bits)	0.064	
ENCODER ACCURACY	0.067	
DRIVE MECHANISM ACCURACY	0.062	
DRIVE MECHANISM BACKLASH	0.194	
DELATED SUN UPDATING	0.030	
TOTAL MIRROR POINTING ERROR DUE TO RANDOM SOURCES (rss)	0.241	
WIND SPEED	8.94 m/s (20 mph)	13.41 m/s (30 mph)
MIRROR POINTING ERROR DUE TO WIND SPEED	0.50	1.13
TOTAL MIRROR POINTING ERROR DUE TO RANDOM SOURCES PLUS WIND	0.741	1.37
REFLECTED BEAM ERROR = TWICE MIRROR POINTING ERROR	1.48	2.74

In addition to the above pointing error, the wind loading caused a racking and therefore defocusing of the entire mirror support assembly. Each mirror rotates, to some degree, about the azimuth (θ_y) and elevation (θ_x) axes. The magnitudes of rotation realized in this preliminary analysis are given in Figure II-B-6. These rotations are easily reduced by stiffening the mirror assembly.

Azimuth Drive Module - The azimuth drive module incorporates the azimuth drive mechanism, azimuth bearing system, and a mounting flange for securing the entire heliostat assembly to the foundation. This module is the first component of the heliostat assembly to be installed in the field (Fig. II-B-4). The unit is lowered over a ring of 3.175-cm (1.25-in.) diameter threaded anchor studs imbedded in the reinforced concrete foundation. These studs protrude through a leveling plate that provides a stable mounting

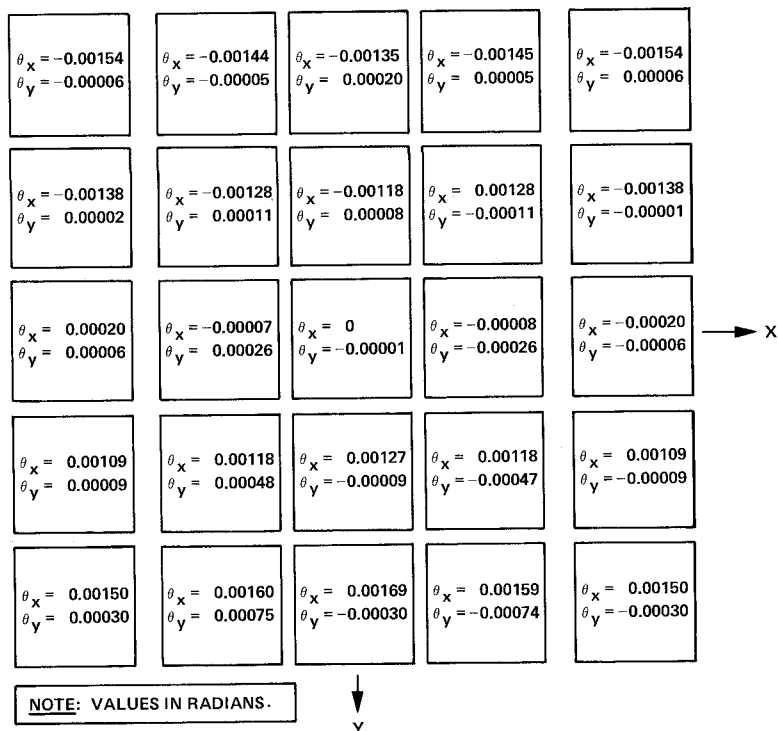


Figure II-B-6 Out-of-Plane Deflections of 25-Mirror Assembly

base. The yoke module is then lowered by crane and attached to the azimuth drive module. The last item to be installed is the mirror module.

Yoke Module Assembly - The yoke module comprises the major structural element in the heliostat assembly and transfers wind-induced loads directly to the azimuth bearings. The vertical members of the yoke module are fabricated from wide flange sections (W14x38) welded to a horizontal member fabricated from (14-in.) square commercial tubing (TS14x14x0.500). At the center of the square tube section, corresponding to the azimuth center of rotation, a steel tube section (TS7.75 OD x 3.5) is welded in place. The lower end of the tube bore is chamfered to provide for centering registration of the yoke module on the stub

shaft of the azimuth drive module. A 1.27-cm (1/2-in.) thick steel plate welded to the top of the tube has chamfered holes to accommodate threaded studs and cone nuts. After the yoke module has been lowered into position, centered, and properly seated on the azimuth module, the cone nuts are installed and torqued to provide a rigid, self-centering connection to the azimuth drive unit.

Materials - The proper selection of materials for heliostat design is important, considering the severe environmental requirements and duration of exposure. Components sensitive to sand, dust, humidity and corrosion shall be protected by environmental enclosures or sealed cavities.

In addition to a moderate thermal environment, components will be exposed to ultraviolet radiation. At the geographical location of the proposed test site, the annual number of usable sun hours varies from 2500 to 3100 hours per year. Therefore, during the 10-year lifetime of the facility, materials will experience UV exposure of between 25,000 and 31,000 hours of radiation. Plastics, rubbers, and some elastomeric compounds deteriorate under long exposure of UV radiation. The use of these materials has been limited.

Mirror Module - The mirror module consists of the 25 individual mirror assemblies, the horizontal tube assembly, the elevation drive mechanism, and the parallel pairs of vertical support tubes for each of the five rows of mirrors.

The selected heliostat design places the horizontal tube assembly approximately 3.96 m (13.0 ft) above the ground. This approach, with the horizontal pivot arm located at the center of the total area of reflective surfaces, tends to balance the torsional effects of wind load distributions. Another advantage of this approach is that the mirror surfaces are elevated above the zone where blowing sand and dirt are most dense.

The elevation drive tube assembly is supported near each end by the vertical members of the yoke module assembly as shown in Figure II-B-4. To minimize the bending moments and midspan deflections due to weight unbalance, the horizontal tube is supported inboard from each end of the tube so the vertical members of the yoke module occur in the first interior mirror space. The elevation drive module is integrated directly into the elevation drive tube as shown in Figure II-B-4.

The ring gear portion of the elevation drive mechanism assembly is attached to the web of the vertical yoke strut by three 19-mm (3/4-in. dia) high-strength bolts that are installed during field assembly. The horizontal tube is fabricated from a standard steel tube section (TS5.56 OD x 0.258). To facilitate assembly and accommodate the elevation drive module, the tube is fabricated in two sections and attached by flange connections to the double-ended output shaft of the elevation drive module. The other end of the tube is cradled by a cutout in the web of the vertical support member where two pairs of cam rollers provide the bearing interface. A separate plate attached to the web slightly above

the horizontal tube retains the tube without introducing any additional friction to the rotating tube. This comes into play whenever aerodynamic lift forces exceed mirror module weight for high wind velocities when a heliostat is in the stowed position.

Pairs of parallel mirror support tubes are attached to the elevation drive tube at 78.1-cm (30.75-in.) spacing as shown in Figure II-B-7. These pairs of tubes are circular notched at their centerline or point of intersection with the drive tube and welded in place. These mirror support tubes are fabricated from rectangular steel tube sections (TS 2x4x0.120) and cantilever symmetrically off of the elevation drive tube.

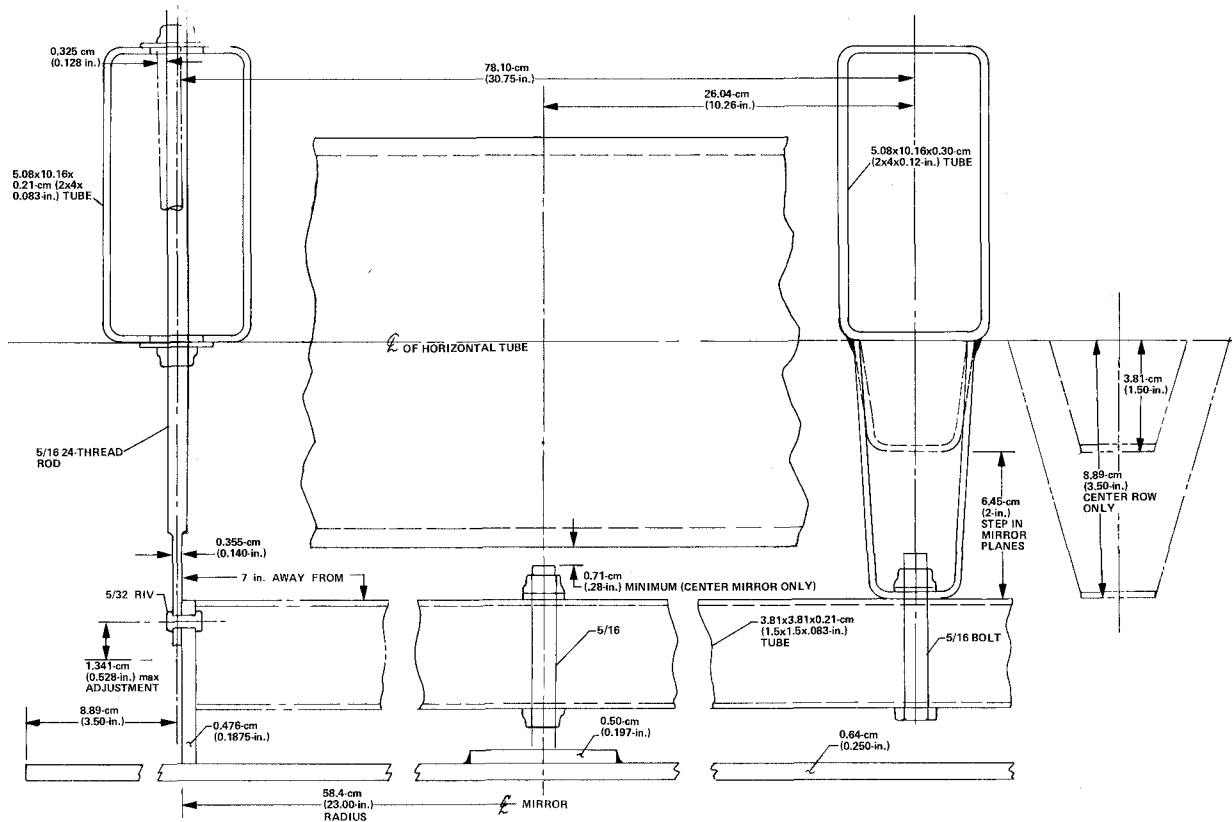


Figure II-B-7 Mirror Support Scheme

An individual mirror assembly shown in Figure II-B-8 consists of a 1.2 m (4 ft) square mirror, support ring, stabilizer struts, and attachment accessories.

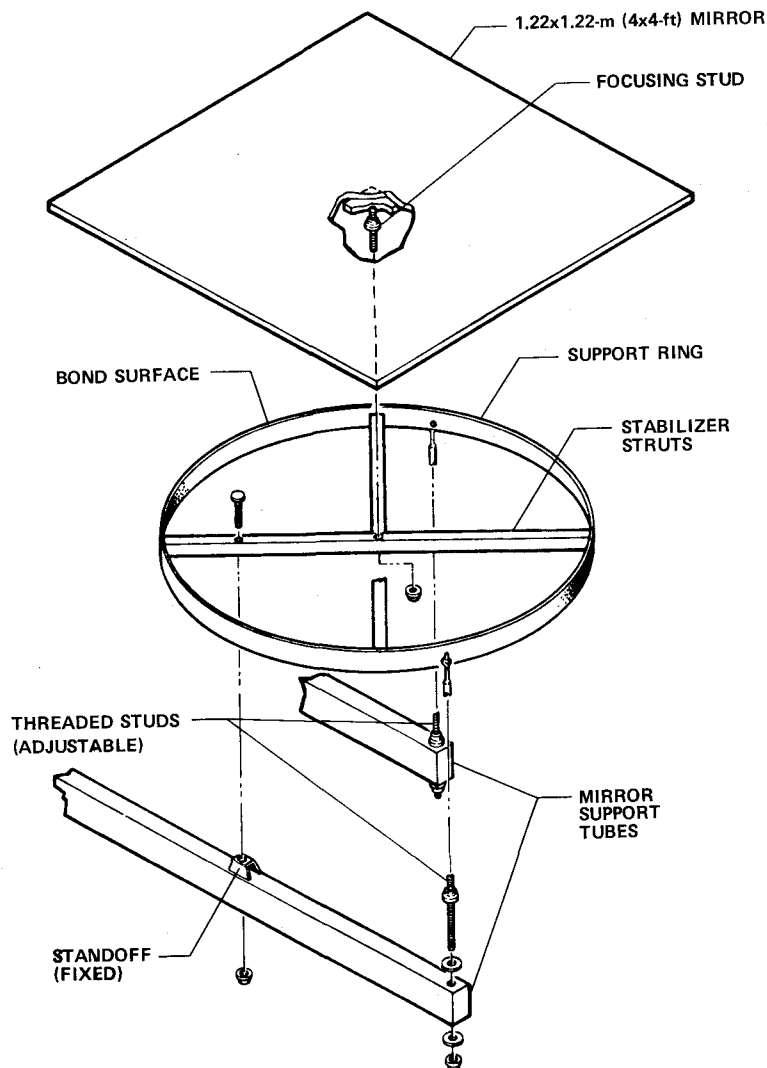


Figure II-B-8 Mirror Assembly and Support Scheme

Each mirror requires a separate warping structure to achieve proper focusing. Our technique, which is the result of several iterations, has been tested and evaluated for simplicity and cost effectiveness. This scheme is based on providing local stiffening

to the back of the mirror about a 1.17-m (46-in.) diameter circle centered on the mirror substrate. The stiffener is a 0.48-cm (3/16-in.) thick by 5.71-cm (2¼-in.) deep steel hoop with a 1.17-m (46-in.) outside diameter. This ring is securely bonded to the back of the mirror with RTV, a stable yet elastic bonding agent that remains flexible over wide extremes in temperature. This ring is reinforced by a planar strut assembly composed of two 3.81-cm (1½-in.) square tubes 3.81x3.81x0.210 cm (TS1.5x1.5x0.083) welded to the ring and provides pickup and attachment points for the mirror. These two tubes intersect at the ring/mirror centerline to form a "cross" structure oriented along the mirror diagonals. Pads with integral threaded studs are bonded to the mirror at the centerline. The "cross" structure, in conjunction with the ring stiffener, provide the reaction structure about which the mirror can be warped. The ring frame becomes the edge support, which allows the mirror to rotate as a simply supported plate free to rotate in circular symmetry. The warping forces are applied at the mirror centerline through the threaded stud fastener and jamb nuts. The mirrors would be focused in the field under controlled conditions.

Each mirror assembly can be individually aligned by a simple, economic method depicted in Figure II-B-7 and II-B-9. This method features a three-point attachment scheme in which a fixed attachment point in concert with two adjustable attachments provides two degrees of rotation about orthogonal pivot axes. The fixed point involves a fabricated standoff welded to one of the 5.08x10.16-cm

(2x4-in.) tubes in the rack to which is bolted the square stabilizer tube of the mirror module. The two adjustable points consist of threaded rods attached to the ring frame by a single rivet. The threaded rod extends through oversized holes in the rack tube and a pair of jamb nuts are installed on each

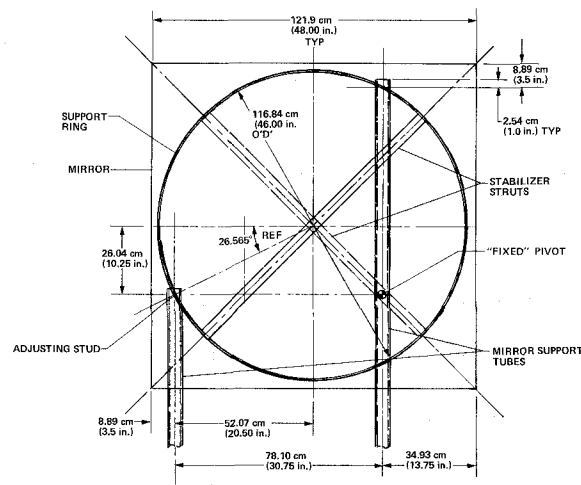


Figure II-B-9 Mirror Alignment

side after the adjustment procedure is complete. The locations of the three pickup points is such that each point is equally loaded under the action of wind loads normal to the plane of the mirror. In addition, by using no more than three points of attachment to secure the mirror module to the rack, a statically determinate system is assured whereby unequal distortion in the supporting structure due to temperature gradients or unsymmetric loads does not induce strains back to the mirror module. The wide 78.1-cm (30.75-in.) spacing of the adjusting points provides a very precise method of mirror pointing adjustment.

b. *Foundation Design and Plot Plan* - The foundation design for each heliostat installation will be accomplished in accordance with standard engineering practice for installations of this nature. Due to the unique constraints imposed by the heliostat tracking and pointing requirements, foundation tilt is limited to 1 arc-minute under the action of (30-mph) winds. Load criteria

for foundation design are summarized below for a (50 mph) uniform wind load:

- 1) Base bending moment, 53,709 N-m (39,600 lb-ft);
- 2) Base shear, 14,280 N (3210 lb);
- 3) Torque, 6,917 N-m (5100 lb-ft);
- 4) Dead load (axial), 26,690 N (6000 lb).

It is therefore imperative that a comprehensive subsurface exploration program be implemented early in the program, and a detailed laboratory test of core samples be conducted. Only methods of penetrating overburden soils that offer the opportunity for core sampling and subsequent laboratory testing will be used. For economic reasons it is not recommended that core drilling for samples be done for each heliostat installation but rather in zones covered by a grid net enveloping the affected project area. This approach establishes geological and engineering properties of soils in quantitative form, which to a certain degree involves the risk of data not being totally representative but that can be offset somewhat by adequate margins and safety factors.

The governing factors applied to the design process include:

- 1) Magnitude and cyclical nature of the heliostat loads directed to the foundation by the heliostat assembly;
- 2) Mechanical and elastic properties of the subsurface soils;
- 3) Stability of bearing soils under all conditions of applied loads and fluctuating moisture content;
- 4) Depth below surface of the selected bearing strata;

- 5) Local anomalies requiring special attention or revised design criteria.

The foundation design will be performed by the Bechtel Corporation, San Francisco, California under separate contract. A detailed statement of work will be issued outlining the design constraints and requirements imposed on the foundation by the heliostat.

A detailed plot plan of the collector will be prepared showing overall size of field and zone boundaries. Precise location coordinates and elevations of each heliostat installation will be depicted (after completion of heliostat installation, all location coordinates and critical elevations will be determined and correlated with the receiver tower coordinate system). Soil bore logs and locations of test holes will be included on the plot plan.

The selected foundation for the baseline heliostat is shown in Figure II-B-2. Since very little data are available regarding actual soil conditions at the proposal test facility, the foundation shown is representative of that developed for the subsystem research experiment foundation in the CRSTPS contract. Approximately 3.5 to 4.0 cubic yards of concrete will be required for each poured-in-place heliostat foundation. Considering the large amount of construction, a concrete batch plant will be required on site; it is assumed that a batch plant will be available for construction of the entire facility.

c. *Mirrors* - Comparison of the characteristics of all candidate surfaces shows that second-surface silvered white glass mirrors are the logical choice at this time in all respects, including cost effectiveness. Glass mirrors combine high spectral reflectivity with long life under UV exposure, as well as other severe environments.

Future development of either second-surface silvered plastic mirrors or front-surface plastic mirrors with a coating may allow further considerations of these materials. Currently, plastic mirrors are not available in large quantities, have relatively low reflectivities, and will not survive the severe environmental conditions as well as glass. Additionally, the current cost of these materials is approximately that of low-reflectivity glass.

In the design of a cost-competitive solar thermal plant, the objective is to obtain high optical efficiency. One of the most critical factors is that of mirror reflectivity. The reflectivity parameter of concern to the designer of a concentrating power system is the specular reflectivity rather than the reflectivity normally obtained with spectrophotometers. The reflectivity also needs to be referenced to a terrestrial solar spectrum in the geographical zone where the installation is to be located.

The design specular reflectivity necessary to be consistent with the design sizing is 85%. With specular reflectivities less than 85%, the size of the heliostat field becomes too large to achieve cost effectiveness. Based on the results

from samples tested (see Appendix B), it was shown that a reflectivity of 85% is obtainable with only two of the candidates--a first-surface aluminized teflon or laminated second-surface mirror. The second-surface silvered white glass laminated mirrors were chosen because they exhibit the highest spectral reflectivity of all samples tested, has less tendency toward degradation in the presence of ultraviolet radiation, and is easily cleaned. The size is 1.2x1.2 m (4x4 ft) and they are available from a commercial supplier. The weight of 18.1 kg (40 lb) per mirror permits handling in the field, without special equipment, by a two-man crew. This configuration, in conjunction with the proposed mirror mount, readily adapts to focusing and maintenance operations.

d. Drive Mechanisms - Separate positioning systems for the azimuth and elevation axes of rotation are provided by direct gear mechanisms designed to minimize the tracking error associated with gear backlash and bearing deformation. Wind and gravity-induced torques are prevented from backdriving the mechanism by introducing a worm gear reducer in the final stage of gear reduction. The principal factor governing drive mechanism design is the nonuniform distribution of wind-induced forces across the heliostat surface areas.

Since appropriate values of the aerodynamically induced torques could not be satisfactorily ascertained by analysis due to the absence of test data pertaining to the particular "slotted" configuration of the mirror assembly, we conducted wind tunnel tests

(see Appendix A) that yielded the tabulated load criteria for the drive mechanism.

MAXIMUM SLEW TORQUE AT 22.35 m/s (50 mph) WIND VELOCITY	= 6,598 N-m (58,400 in.-lb)
MAXIMUM TRACKING TORQUE AT 13.5 m/s (30 mph) WIND VELOCITY	= 2,373 N-m (21,000 in.-lb)
BASE BENDING MOMENT AT 22.35 m/s (50 mph) WIND VELOCITY	= 53,698 N-m (39,600 ft-lb)
BASE SHEAR AT 22.35 m/s (50-mph) WIND VELOCITY	= 14,280 N (3,210 lb)

The drive mechanisms for both azimuth and elevation positioning are basically identical with respect to motor and gearing requirements. Some minor differences exist in the ring gear configuration due to mounting constraints.

Figures II-B-10 and II-B-11 show the direct gear drive concept developed to meet the requirements of this proposal. Appendix B summarizes the tradeoff studies that led to this concept.

The design was mostly influenced by the azimuth drive since, in addition to operating against the aerodynamic torques previously defined, it must resist a large base bending moment with negligible deflection and anchor to the foundation. A further criterion, was that both elevation and azimuth drive mechanisms use the same components to the greatest extent possible to facilitate maintenance and spare parts planning. Also, only simple foundations and site preparations should be necessary.

Another requirement is drive irreversibility--demanding a worm or similar reducer in the gear train as close to the azimuth axis as possible. In the azimuth axis, gear backlash is important since it induces errors whenever veering winds cause torque reversals. This does not occur in the elevation axis because aerodynamic and unbalance torques eliminate backlash errors. Backlash will not exceed 2 arc-minutes.

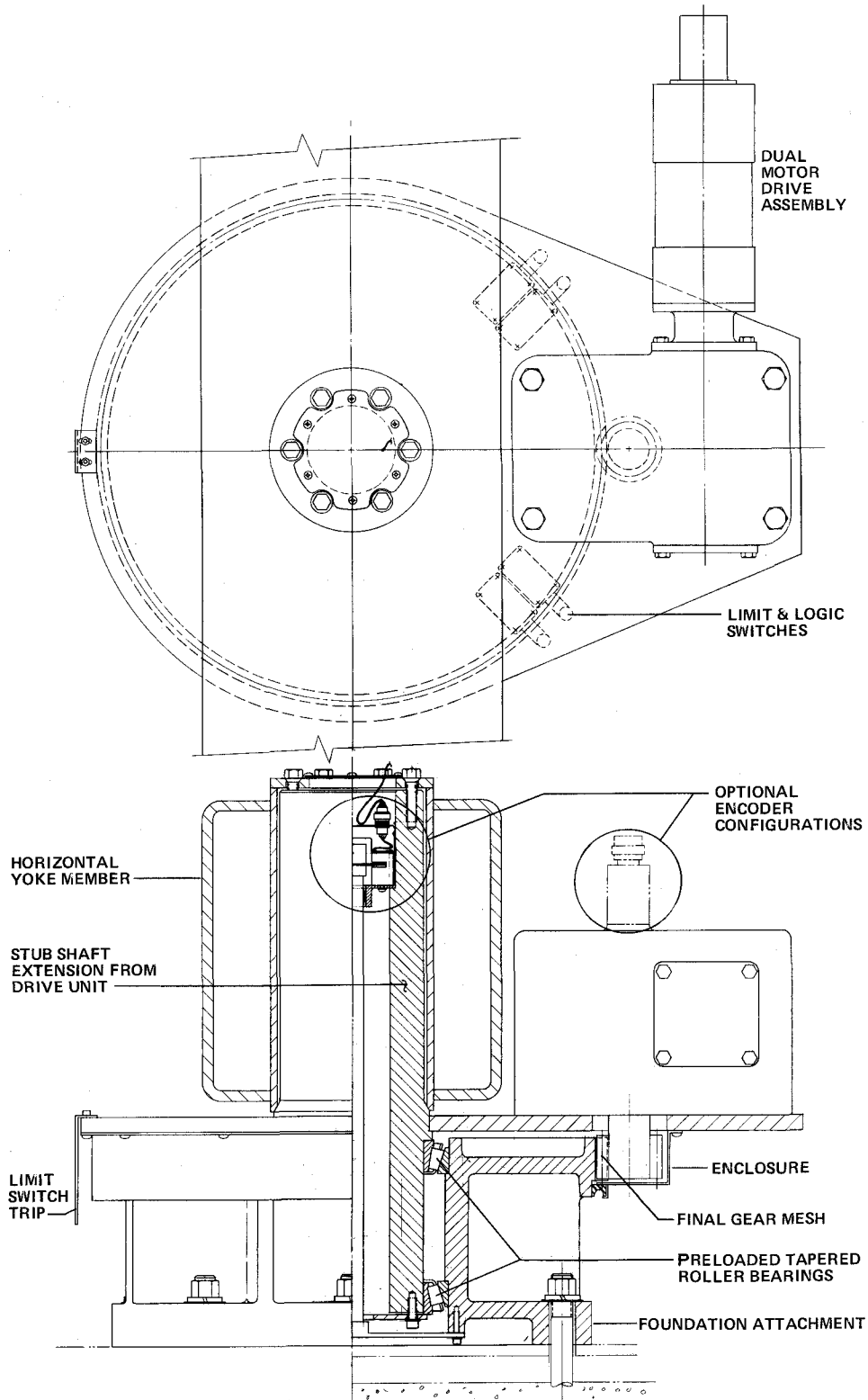


Figure II-B-10 Azimuth Drive Unit

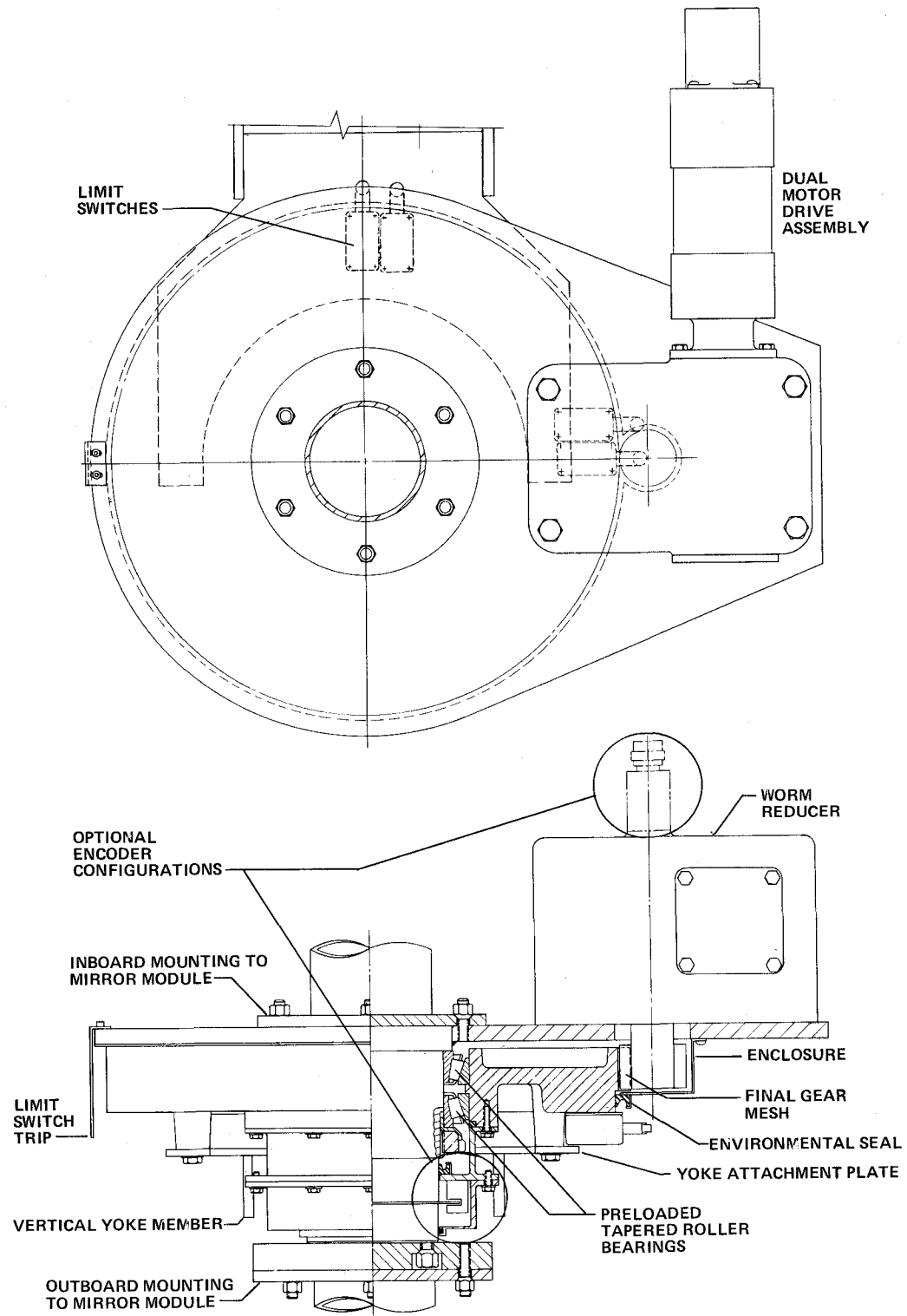


Figure II-B-11 Elevation Drive Unit

The design illustrated in Figures II-B-10 and II-B-11 satisfies all the requirements.

The diameter was determined by the gear tooth strength, and by cost requirements. This diameter provides a satisfactory foundation stud circle diameter of 50.8 cm (20 in.) adequate for eight 3.17 cm (1.25-in.) diameter high-strength studs. The relationships between tooth load, gear diameter, backlash, mesh clearance, worm reducer size and cost are given in Figures II-B-12 and II-B-13.

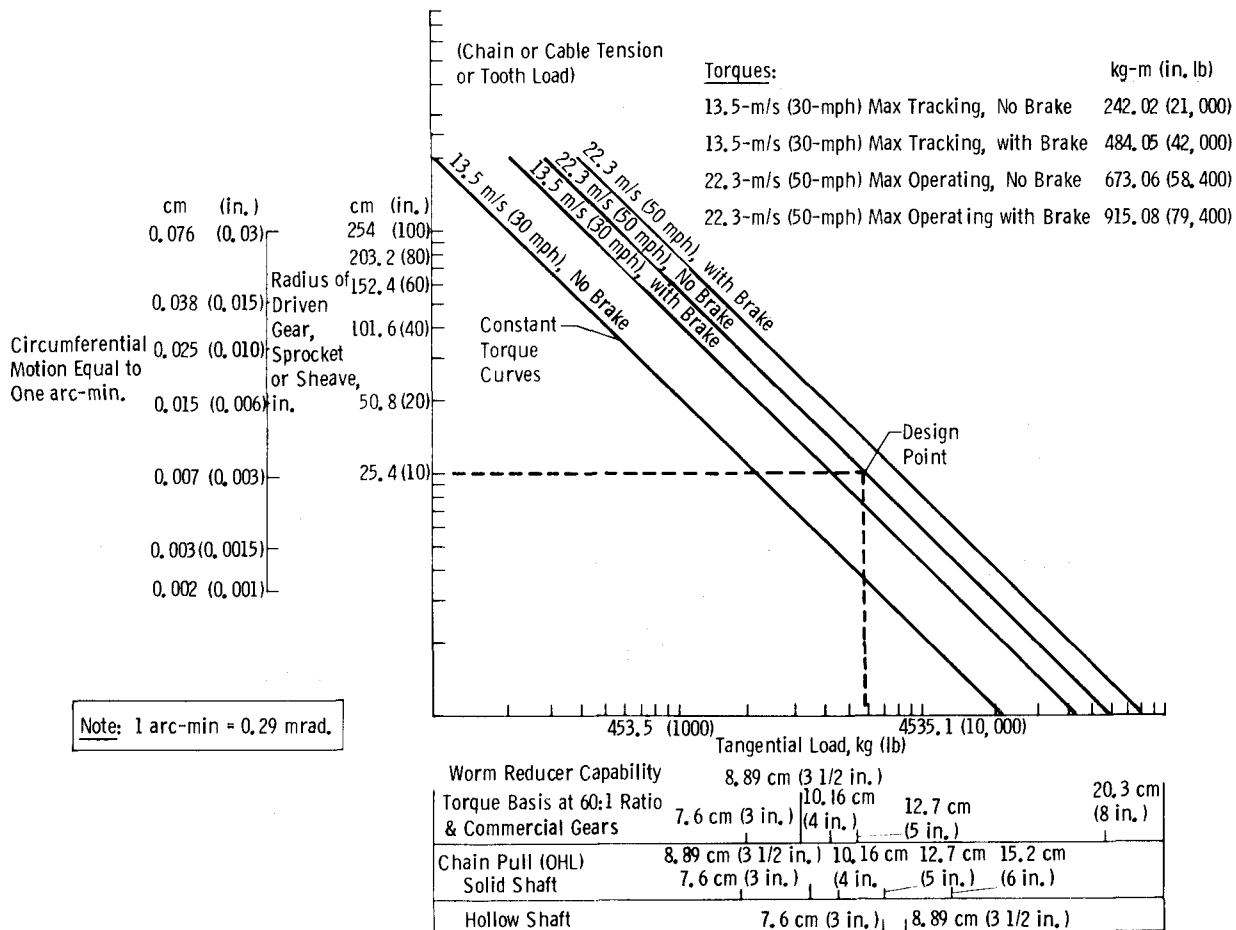


Figure II-B-12 Tangential Load vs Torque

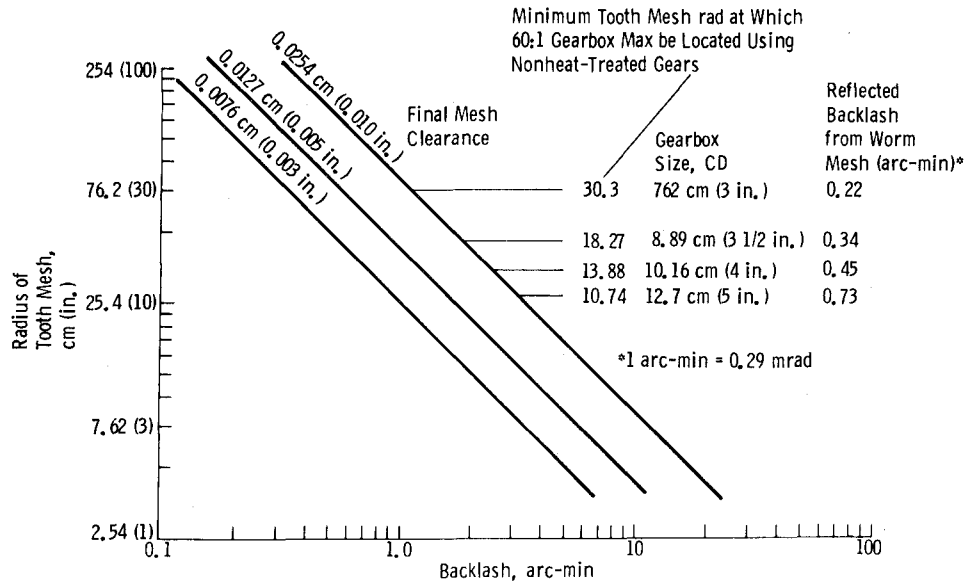


Figure II-B-13 Backlash vs Pitch Radius

Figure II-B-10 shows a nodular (ductile) iron casting to American Gear Manufacturers Association (AGMA) specification NI5 that will be used to provide not only the gear but also the foundation mounting flange and bearing mounting in one component. The casting will be simple; the webbed and recessed areas may be formed by a single ring core.

This gear casting, heat-treated to 255 BHN, will be readily machinable and will mate with a steel pinion of 300 BHN hardness, thus providing an optimum hardness difference between the tooth surfaces. Structural deflections that would significantly affect the tracking accuracy of the heliostat will be held to an acceptable level.

The compactness of this design is largely due to the few tooth stress cycles throughout the required life, allowing a maximum tooth bending stress of approximately 65% of the yield stress

of the gear material rather than the fatigue stress level that is the normal situation. Using this stress level in AGMA strength formula leads to a 5 DP tooth size.

Figure II-B-14 illustrates three designs comparing bearing and associated structural deflections. Small, less costly, and more widely spaced bearings provide the lowest bearing deflection but shaft deflections are excessive. A larger short shaft and larger bearings provide satisfactory deflections and can resist the same bending moment at much closer centers.

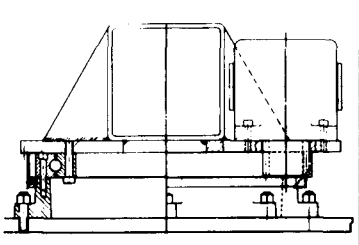
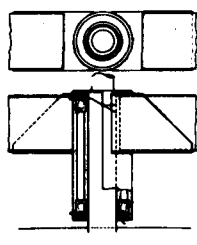
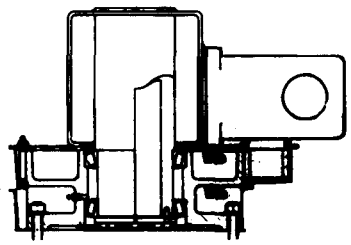
Bearing Arrangement				
		arc-min	arc-min	arc-min
6.70 m/s (15 mph)	Bearing Deflection Only	0.47	0.28	0.6
	Bearing & Structure Deflection	0.48	1.29	0.61
13.41 m/s (30 mph)	Bearing Deflection Only	13.0	0.66	1.6
	Bearing & Structure Deflection	13.4	4.71	1.7

Figure II-B-14 Deflections of Bearings & Associated Structure

The bearings will be tapered single row, straight bore, roller bearings of 170 mm ID and 254 mm OD. This selection is based on a computer analysis conducted by the Timken Company optimizing bearing capability and cost for a given deflection. These bearings will be operating at 50% of their ultimate capacity at wind

velocities of 22.35 m/s (50 mph) on a heliostat normal to that wind. This is the maximum load condition they will experience since at greater wind velocities the heliostat will be in the stowed condition. At the maximum tracking wind velocity of 13.5 m/s (30 mph) they operate at 20% of ultimate capacity.

The bearings will be preloaded in the azimuth drive by torquing the retaining plate screws to predetermined levels. A subsequent test of the "load friction" torque of the bearing will provide an accurate verification of preload. Bolts will be lockwired to preserve this setting. Preloading is essential for gear mesh accuracy and elimination of bearing play.

Plain (sleeve) bearings either of teflon or bronze were also investigated but they suffer from the clearances normal to such bearings that result in intolerable pointing errors. Preloading could overcome this problem but is more expensive than preloaded tapered roller bearings.

The same tapered roller bearings are used in the elevation drive, not because the loads warrant such large bearings, but because they permit a through-shaft sufficiently large to facilitate attachment to the mirror module. These are high-production bearings and the most economical in their size and capacity range.

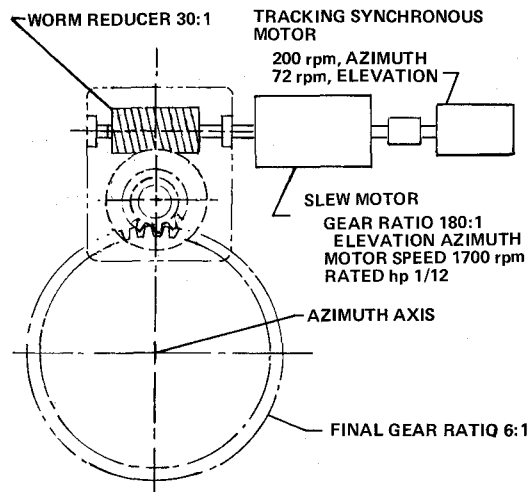
The final gear mesh will be totally enclosed using a sheet metal or cast housing surrounding gear and pinion, and incorporating a peripheral seal as shown in Figure II-B-10 and II-B-11. This seals against a machined diameter provided on the main casting. We propose precisely cut lengths of elastometric seal material

that can be readily inserted into the seal cavity and retained by means of helical garter springs rather than a continuous circular seal that would be difficult to replace.

Grease nipples will be provided for direct access to both bearings and gear mesh. We expect that the initial lubricant charge will suffice for many years of operation. In view of the very low speed of operation we propose to use an EP grease having good oxidation stability and rust prevention qualities.

The dual electric motor drive system is shown in Figure II-B-15. The Slo-Syn tracking motor will drive through the slew motor and will be back-driven to 1700 rpm by the slew motor during slew operation.

Figure II-B-15 provides details of gear ratios and motor speeds, efficiencies, and horsepowers. The fact that the slew motor rating is slightly below the peak requirement means that on the rare occasion when a 50-mph wind coincides with the critical angle of attack of a heliostat, the motor will be slightly overloaded for a brief interval. This is permissible.



EFFICIENCIES, HORSEPOWER AND RUNNING CURRENTS

	TRACKING	SLEW
FINAL GEAR DRIVE	96%	95%
WORM REDUCER	46%	61%
SLEW MOTOR GEAR HEAD AND SEAL	60%	60%
OVERALL EFFICIENCY	26.5%	34.5%
REQUIRED MOTOR HP	0.005	0.09
SELECTED MOTOR HP	0.01	0.083
MOTOR RUNNING CURRENT, A	0.3	1.2

Figure II-B-15 Drive Train Schematic

The lower worm reducer efficiency under tracking conditions is due to the very low speed of operation where friction remains in the "breakaway" regime. This situation, however has been optimized by using a 30:1 ratio worm reducer, which is the minimum ratio offering irreversibility and hence optimum efficiency. Figure II-B-16 shows a mechanical and electronic breadboard of the actual electrical motors and their servocontrol circuits built by Martin Marietta that has satisfactorily demonstrated the proposed method of control.

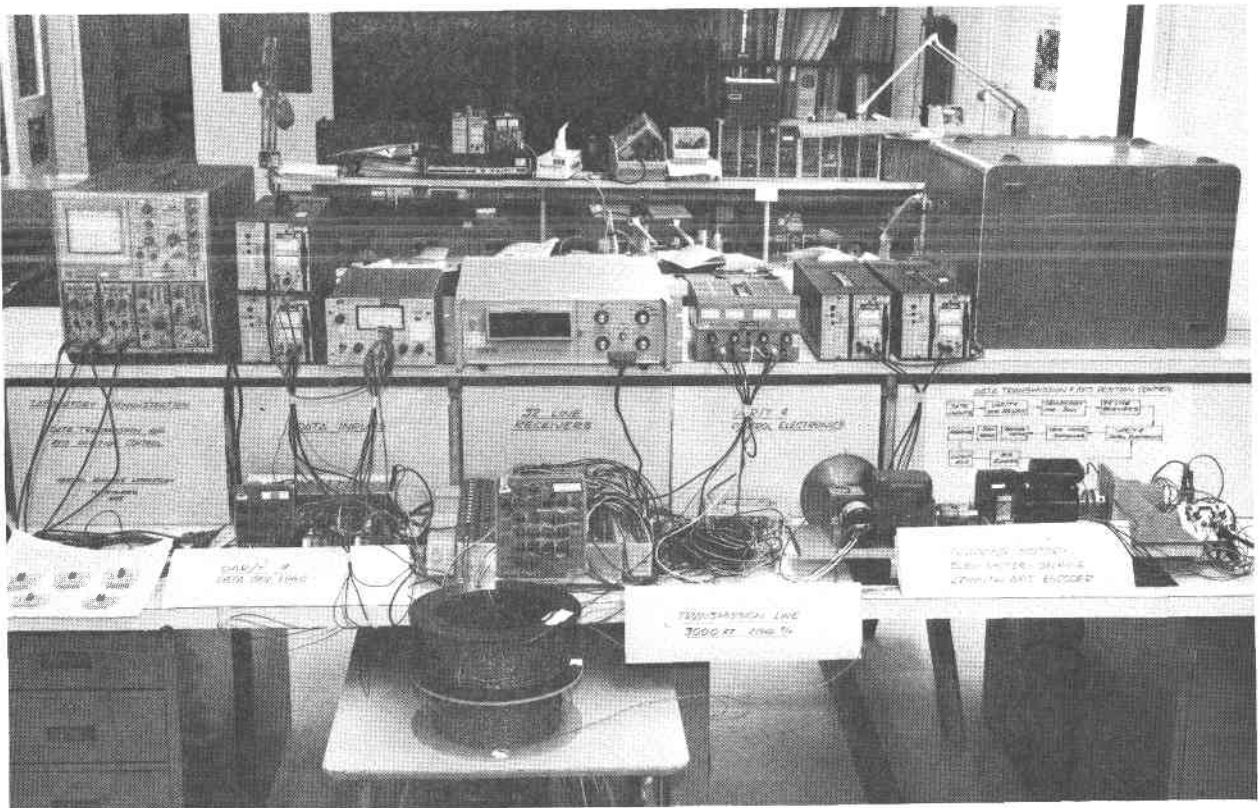


Figure II-B-16 Drive Mechanism and Controls Breadboard

The dual-motor approach is simple and electrically more efficient than a single variable-speed motor and its associated control. Neither motor uses centrifugal starting switches or brushes and both are totally enclosed, off-the-shelf items. The slew motor will be a permanent split capacitor motor. The tracking motor will be a Slo-Syn by Superior Electric. The Slo-Syn has numerous advantages--no inrush or stall currents, no rotor heating, and mechanical simplicity. All these features lead to high reliability and long life.

The ratios and efficiencies in Figure II-B-15 apply to the Martin Marietta designs shown in Figures II-B-10 and II-B-11. These figures will vary somewhat with the vendor. Also, certain vendors may offer proprietary devices such as Spiroid gears and Compudrive elements. Others may prefer to build the worm reducer as an integral part of the design. Martin Marietta regards all these as usable variants of the direct gear drives and will evaluate them on a cost/effectivity basis. In all instances the same dual motor drive system is contemplated.

One direct gear drive, by Milwaukee Gear Corporation, is illustrated in Figure II-B-17. Here the worm reducer is in the base casting and the shaft and hull gear rotate. It utilizes the same bearings and offers the advantages of eliminating the large peripheral seal and the rotating mounting provisions for the reducer. It readily adapts to the elevation drive.

II-B-37

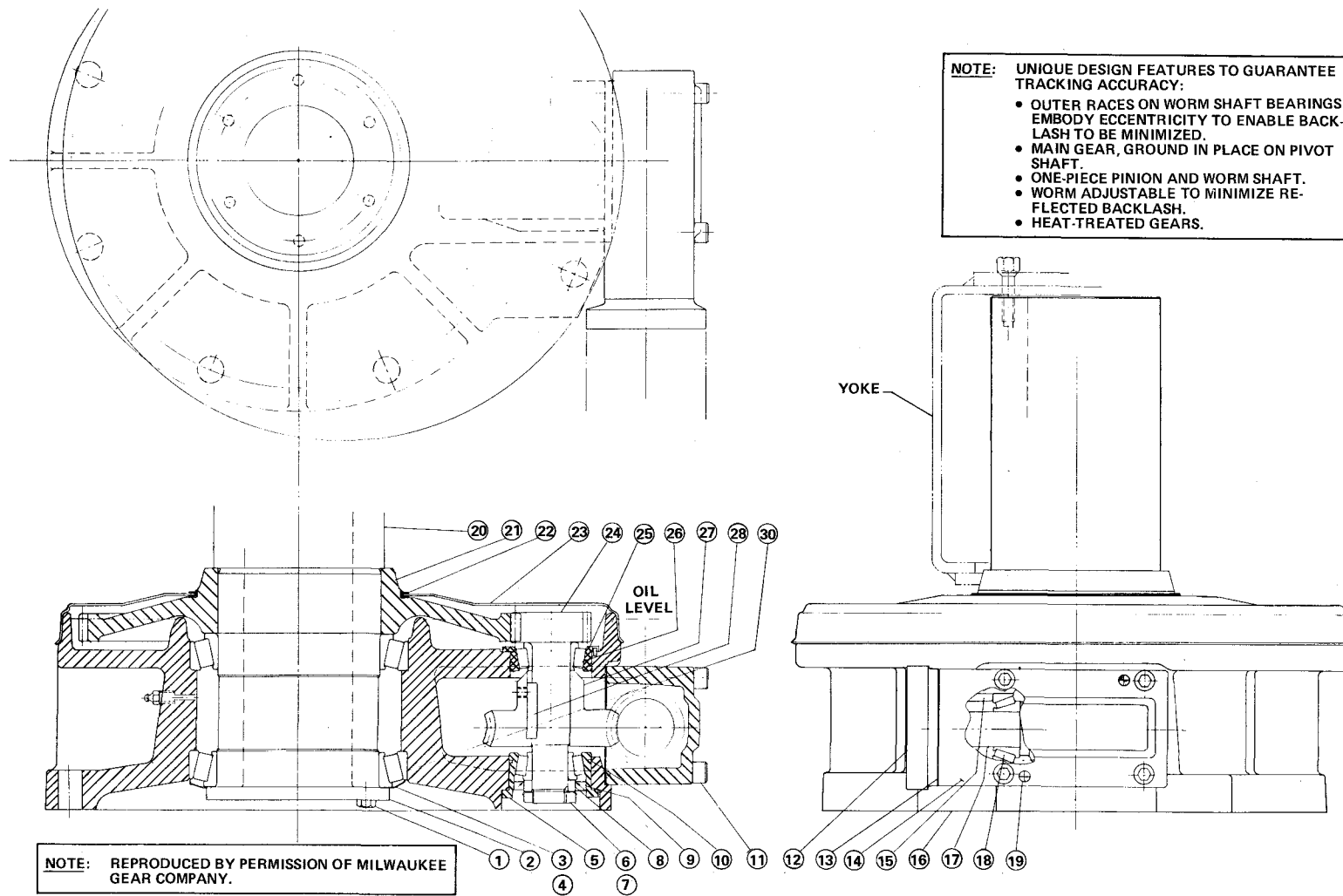


Figure II-B-17 Direct Gear Drive

e. *Encoders* - The exact location and means of mounting the necessary encoders for azimuth and elevation position indication will depend on the final drive mechanism design as discussed earlier. Figures II-B-10 and II-B-11 both show optional location. Those mounted directly on the actual axes need to be of 13-bit resolution and those on the pinion shaft of 14-bit resolution. The former are of the type that incorporate within a mechanism utilizing existing bearings. As a result they are totally enclosed and environmentally protected but less accessible. However, the very low maintenance risk involved justifies the approach. For instance, modern gallium arsenide light sources have a useful life of 100,000 cycles, which exceeds the 10 years (operating) life requirement. The latter are integral (pre-packaged) multiturn encoders and may prove to be the most cost effective.

f. *Limit Switches* - Environmentally sealed limit switches will be installed on the drive unit as shown in Figures II-B-10 and II-B-11 in pairs operable at the limits of rotation by the trip shown. The first switch (normal limit) operates in the electrical control logic. The second switch (emergency limit) is a safety override. Mounting these switches on the drive units minimizes site installation operations.

These switches will be set as follows:

- 1) Azimuth - Normal limit ± 2.27 rad (± 130 deg),
Emergency limit ± 2.36 rad (± 135 deg);

- 2) Elevation - Normal limit -4.71 rad (-270 deg),
 Emergency limit -4.79 rad (-275 deg).

g. *Sun-Present Sensor* - A sensor located on at least every tenth heliostat in each zone will indicate to the master control system (MCS) whether the heliostat is irradiated with direct sunlight. The sensor is located on selected heliostats so that no larger than 10 of the heliostats are represented. The sensor is a planar diffused silicon diode positioned behind a diffuser, as shown in Figure II-B-18. The sensor and diffuser will be mounted on a pedestal-type mount on the heliostat structure near the center of the mirror array and approximately 0.635 cm (0.25 in.) above the mirror face level. This will minimize stray reflected light from the mirrors. The diffuser gives the sensor a π -rad (180 -deg) field of view so all sun angles can be sensed without tracking. A functional diagram of the sun-present sensor system is shown in Figure II-B-19.

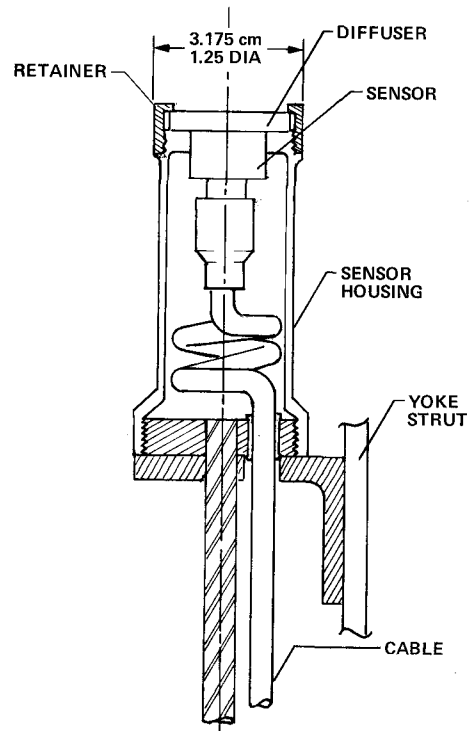


Figure II-B-18 *Sun-Present Sensor*

pedestal-type mount on the heliostat structure near the center of the mirror array and approximately 0.635 cm (0.25 in.) above the mirror face level. This will minimize stray reflected light from the mirrors. The diffuser gives the sensor a π -rad (180 -deg) field of view so all sun angles can be sensed without tracking. A functional diagram of the sun-present sensor system is shown in Figure II-B-19.

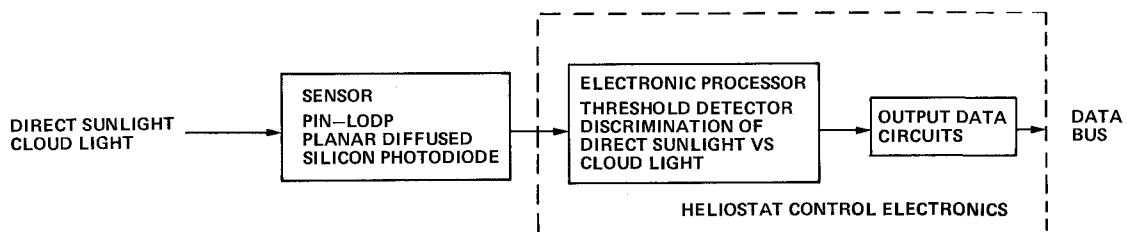


Figure II-B-19 *Functional Diagram of Sun-Present Sensor System*

The incident solar irradiance, whether direct sunlight or cloud light, is sensed by the silicon photodiode sensor after the light passes through the diffuser. As mentioned earlier, this results in a π -rad (180-deg) field of view, which allows all sun angles to be sensed. This eliminates any need for solar tracking with the sensor. The critical requirement of the sensor system is being able to differentiate signal levels from direct sunlight incident on the heliostat/mirror surface from the signal from cloud-shaded conditions. The total sunlight incident on the mirror/sensor face H_S is given by

$$H_S = I \cos \theta + S$$

where I is the normal incident direct sunlight intensity, θ is the incident angle of the direct solar beam to the sensor surface, and S is the diffuse sunlight and/or reflected light from the nearby ground and objects. Under power conditions the normal-incidence direct beam will be a minimum of 0.8 W/m^2 , and under worst-case/maximum incident angle conditions, occurring during winter solstice in the southern fields of heliostats, θ is approximately 64 deg. This gives a direct-incidence sunlight on the sensor of

$$0.8 \text{ W/m}^2 * \cos 64 \text{ deg} = 0.35 \text{ W/m}^2.$$

This flux level is for the 0.3 to $2.8 \text{ }\mu\text{m}$ region. The silicon sensor senses the region from 0.4 to $1.1 \text{ }\mu\text{m}$, which makes up approximately 65% of the flux from 0.3 to $2.8 \text{ }\mu\text{m}$; hence the direct flux actually sensed will be approximately 0.23 W/m^2 . The diffuse/ground reflected skylight component can vary depending

on ground albedo, nearby objects, sun geometry, etc, but we have found that it normally is approximately 10 to 20% of the normal-incident direct beam on clear/partly cloudy days. This gives a skylight component of 0.052 to 0.104 W/m². Therefore if the sensor were shaded by a cloud, the signal level would drop by a minimum of 77 to 38%. This drop is more than adequate, as discussed later, for differentiating the sunlight from shaded conditions.

The sensor signal is transmitted (by cable) to an electronic processing unit located on the heliostat that discriminates the signal in terms of a threshold level. If the signal is above a selected threshold level an "on" condition is then transmitted through the data bus to the MCS. Similarly if the signal is below a selected level, an "off" condition is transmitted to the facility master control. The "on" threshold will correspond to direct-incidence sunlight, and the "off" position will correspond to a cloud-shaded condition.

In the heliostat control electronics threshold adjustment will be accomplished by calibrating with a potentiometer. The ability of the operator to set a threshold will allow maximum flexibility. For example, the threshold can be set for either equinox and solstice and/or for various atmospheric/cloud conditions. The variable threshold level set will also allow any unforeseen reflections from the ground or nearby objects to be accounted for and will assure that each heliostat has a proper threshold setting according to its position in the zone and its

flux conditions. On installation of the heliostats, threshold levels will be set for each sensor/ heliostat for flux conditions existing at that time. Under direct sunlight conditions, this will be done by manually positioning the heliostat/sensor so the maximum-incidence angle, winter solstice, is achieved. The threshold level will then be set to correspond to this solar irradiance level.

h. Heliostat Control Electronics (HCE) - An HCE is located on each heliostat and interfaces with the data bus. It performs all of the functions necessary to control the heliostat gimbals in the slew and track modes. The electronics contains interface isolation, data check circuits, position comparators, motor drivers, and output data formatting and processing logic. A block diagram is shown in Figure II-B-20. The HCE is similar to other units built by Martin Marietta in that it accepts serial digital commands from a central computer, processes these commands for closed-loop control of electromechanical devices, and collects, formats, and delivers data back to the computer. Using experience from past tradeoff studies of data transmission and line drivers and receivers, we have selected a technique that solves the problems of interfacing digital logic with noisy environments such as triac ac motor controller. A detailed description of the HCE follows.

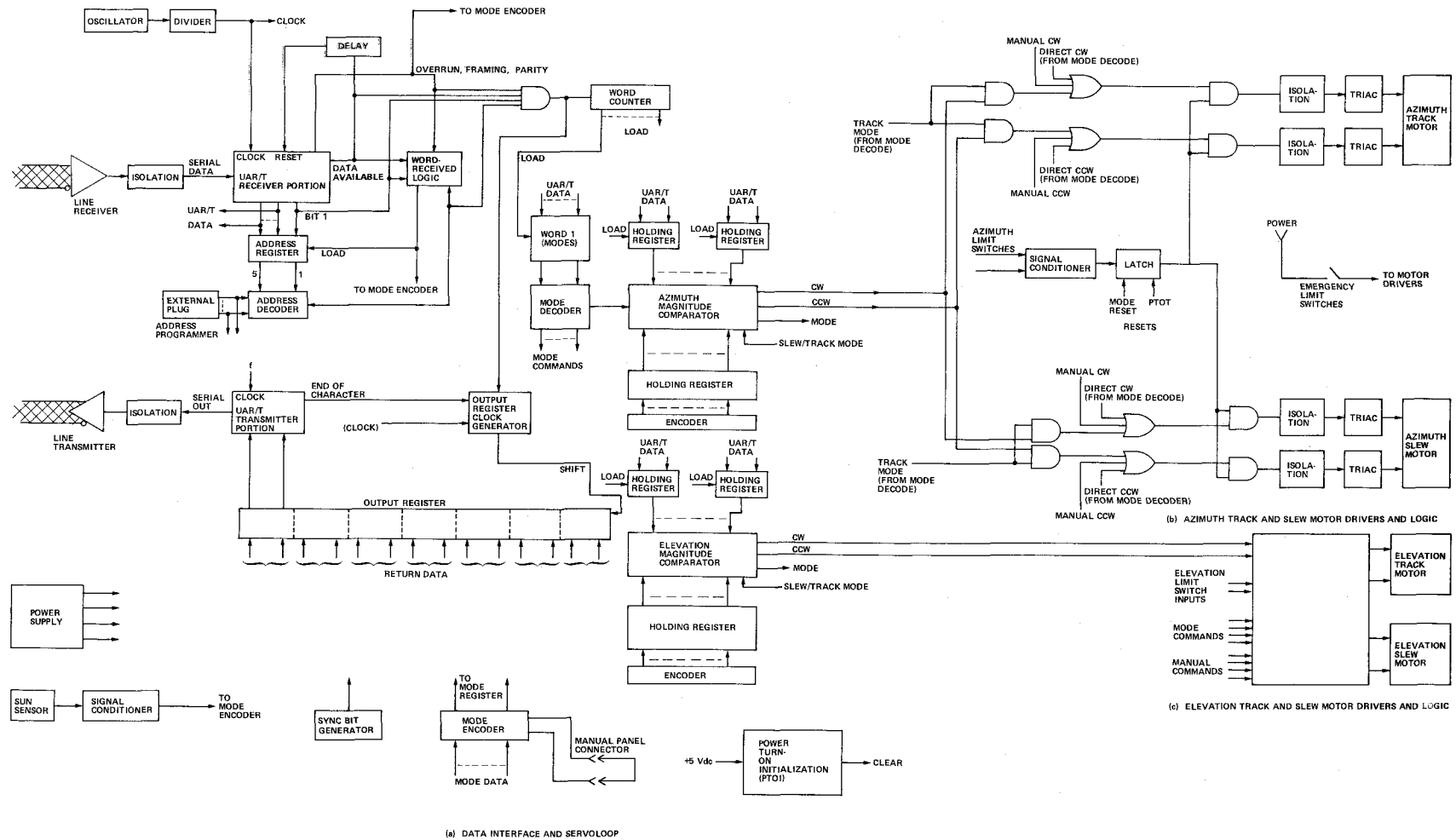


Figure II-B-20 Heliostat Control Electronics Block Diagram

II-B-43

Heliostat Control Electronics Mechanical Description - The HCE is housed in a sealed enclosure located on the lower heliostat yoke (Fig. II-B-21). The control electronics circuits are packaged on a separable subchassis for ease of fabrication, assembly, and maintenance. The subchassis contains power supplies mounted within its lower compartments for direct thermal conduction and structural support. Circuit board-mounted parts are contained on two printed circuit assemblies (in the basic configuration) located along the top surface of the subchassis and interconnected by an internal wiring harness. An alternative configuration required for heliostats equipped with sun-present sensors includes an additional small circuit board assembly for detector processing electronics.

The housing is designed to preclude moisture, sand, or dust intrusion. Access to the electronics is provided by a removable top cover secured with captive fasteners. Sealing washers are used in conjunction with the fasteners to insure a weatherproof seal.

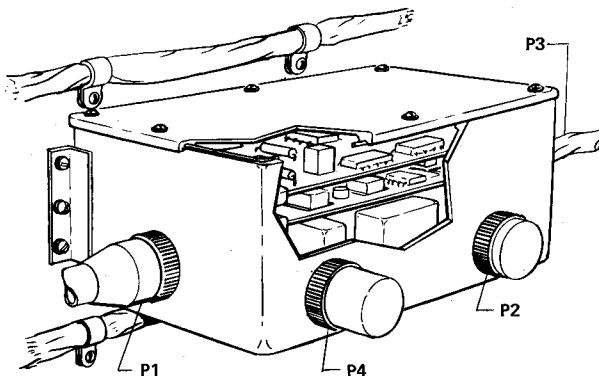


Figure II-B-21 Heliostat Control Electronics

Electronics Description - Serial data sent up to 32 HCEs are received via an isolated line receiver to the UAR/T interface. After the parity error checks are performed, the first character is loaded in the address register. Each string of 32 heliostats has a unique address that is determined by an external plug inserted at the front of the unit. If the decoded address is valid, a gate is enabled that allows the remaining characters of the message to be loaded into data registers. The detection of overrun, framing, or parity error or wrong sync will cause the entire message to be rejected and a flag to be set in the return data. The first word to be received after the address is mode data--track, slew, direct, or data modes. The next characters will be azimuth and elevation position data.

For the track mode a magnitude comparison is made between the command and the position. A difference between the command and the feedback will cause the comparator to output either a "greater than" or "less than" signal that will cause either a clockwise (CW) or counterclockwise (CCW) motor command.

A 14-bit absolute encoder will parallel-interface with the control logic. Each time a bit changes, a delay will be initiated that allows time for the position data bits to settle and prevents encoder data from being clocked into the holding register faster than the natural response of the system.

The CW and CCW outputs of the comparators will interface with the motor drive logic so the mode register status will enable the comparator outputs to feed through the motor drivers in the track mode. A direct input from the mode decoder will override other inputs and cause the motor to drive continuously until the limit switches are activated or a reset command is received.

The motor control signals will be digitally filtered and dc-isolated from the motor driver. A typical motor driver is shown in Figure II-B-22.

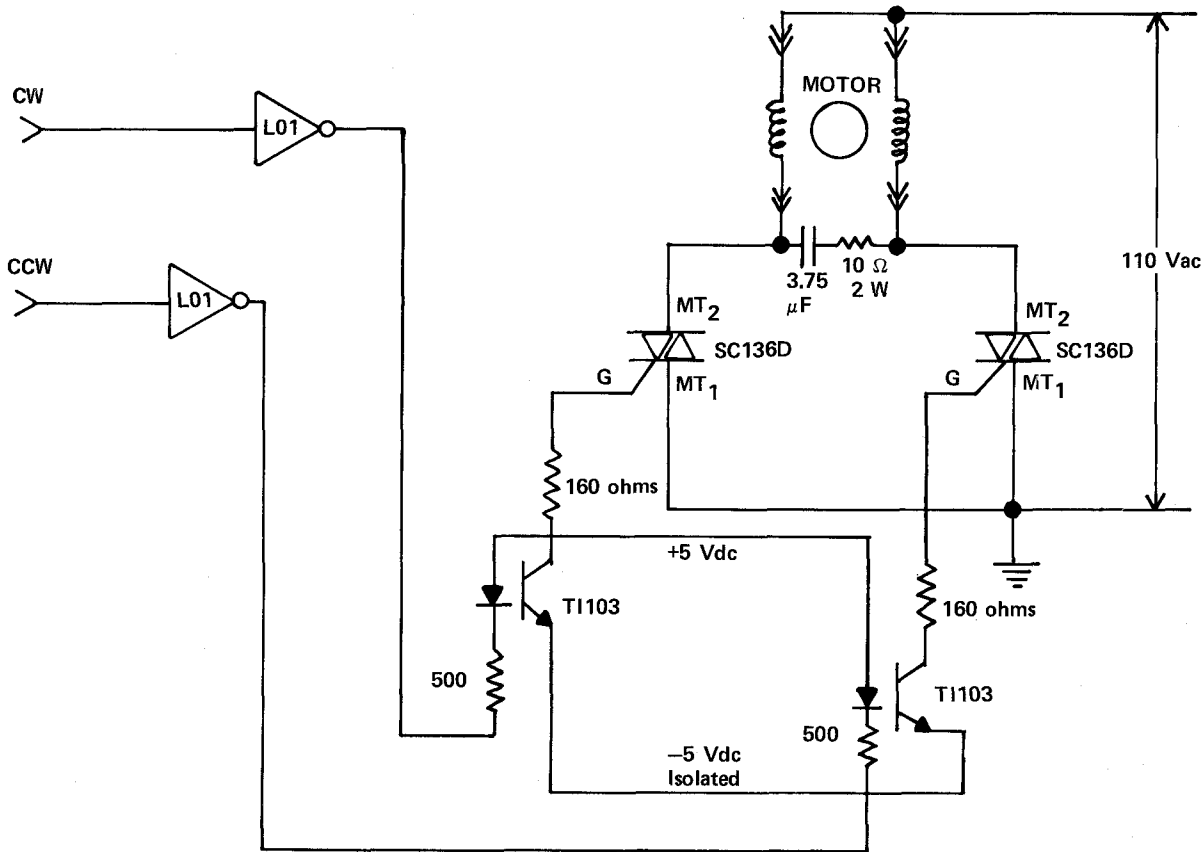
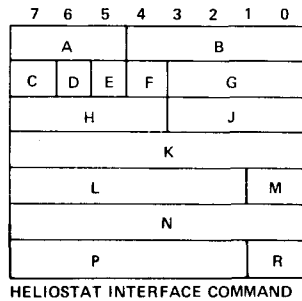


Figure II-B-22 Typical Triac Motor Controller

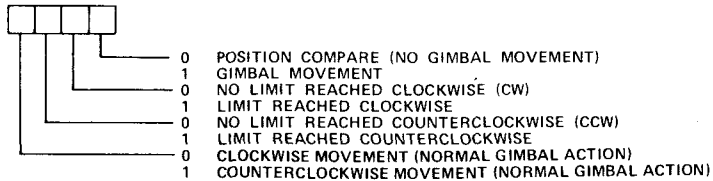
Return data will be assembled in an output register each time a valid address is decoded. The return data will be parallel-transferred to the UAR/T. Since serial transmission of output data to the line transmitter will start at the beginning of the second character received, the return data will always be one character behind the received data. This is a natural requirement since the received word address will initiate the transmission of return data. Each time a character is loaded into the UAR/T, a serial shift will take place in the output register so data will be available for parallel entry at the completion of a character transmittal. The transmitted data rate will be identical to the received data rate.

Since a transmitter is used on a party line, an inhibit signal will disable the transmitter at the end of the message. The data assembled into the output register will consist of two position words, mode data, and 5 bits of address. The sync bits will be added to each word making it a complete character. The mode encoder will take all of the status data shown in Figure II-B-23 and encode them into a mode word.



- A = LINE DESIGNATOR PORTION OF HELIOSTAT ADDRESS
- B = 5-BIT HELIOSTAT ADDRESS (32 DEVICES PER LINE)
- C = 0 SUN AVAILABLE
1 SUN NOT AVAILABLE
- D = 0 HELIOSTAT UNDER MCS CONTROL
1 HELIOSTAT IN MANUAL CONTROL (WILL NOT RESPOND TO ANY COMMAND)
- E = HELIOSTAT ELECTRONICS RECEIVER ERROR CONDITION
0 IS NO ERROR
1 INDICATES ANY OR ALL OF THE FOLLOWING:
 - 1) LOSS OF LINE SYNCHRONIZATION
 - 2) PARITY ERROR
 - 3) FRAMING ERROR (LOSS OF PROPER STOP BIT)
 - 4) OVERRUN (TOO MANY DATA BITS BEFORE STOP BIT)
- F = SPARE (1 BIT ZERO)
- G = HELIOSTAT COMMAND (SEE TABULATION)
- H = AZIMUTH GIMBAL STATUS (SEE BELOW)
- J = ELEVATION GIMBAL STATUS (SEE BELOW)
- K = AZIMUTH POSITION (UPPER 8 BITS)
- L = AZIMUTH POSITION (LOWER 6 BITS)
- M = SPARE (2 BITS-ZERO)
- N = ELEVATION POSITION (UPPER 8 BITS)
- P = ELEVATION POSITION (LOWER 6 BITS)
- R = SPARE (2 BITS-ZERO)

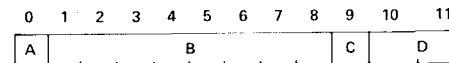
GIMBAL STATUS (FIELDS H AND J)



*HAC WILL ISSUE ALL ZEROES IN THIS FIELD AND HCE WILL INSERT REQUIRED STATUS VALUES
 †HAC WILL ISSUE POSITION COMMAND AND HCE WILL INSERT ACTUAL POSITION

HELIOSTAT COMMAND TABLE

FIELD G OF HIC BINARY VALUE	COMMAND	HELIOSTAT RESPONSE
0000	STATUS	NO PHYSICAL ACTION BY HELIOSTAT. THE ENTIRE CONTENTS OF THE HELIOSTAT CONTROL ELECTRONICS (HCE) REGISTERS ARE RETURNED TO HAC.
0001	CLEAR	ALL HCE MODE REGISTERS ARE CLEARED AND ALL MOTORS ARE STOPPED.
0010 0011	SPARE 1 SPARE 1	RESERVED FOR FUTURE USE.
0100	COARSE-TRACK AZIMUTH	AZIMUTH SLEW MOTOR IS ACTIVATED IN CLOSED-LOOP OPERATION. DEADBAND OF AZIMUTH COMPARATOR IS CHANGED TO 0.012 RADIAN.
0101	COARSE-TRACK ELEVATION	ELEVATION SLEW MOTOR IS ACTIVATED IN CLOSED-LOOP OPERATION. DEADBAND OF ELEVATION COMPARATOR IS CHANGED TO 0.012 RADIAN.
0110	FINE-TRACK AZIMUTH	AZIMUTH TRACK MOTOR IS ACTIVATED IN CLOSED-LOOP OPERATION WITH FULL 14-BIT COMPARATOR.
0111	FINE-TRACK ELEVATION	ELEVATION TRACK MOTOR IS ACTIVATED IN CLOSED-LOOP OPERATION WITH FULL 14 BIT COMPARATOR.
1000	DIRECT SLOW AZIMUTH CW	THESE COMMANDS TURN ON RELATED AXIS TRACK MOTOR. ONLY LIMIT SWITCHES OR CLEAR COMMAND WILL TURN MOTOR OFF.
1001	DIRECT SLOW AZIMUTH CCW	
1010	DIRECT SLOW ELEVATION CW	
1011	DIRECT SLOW ELEVATION CCW	
1100	DIRECT SLEW AZIMUTH CW	THESE COMMANDS TURN ON RELATED AXIS SLEW MOTOR. ONLY LIMIT SWITCHES OR CLEAR COMMAND WILL TURN MOTOR OFF.
1101	DIRECT SLEW AZIMUTH CCW	
1110	DIRECT SLEW ELEVATION CW	
1111	DIRECT SLEW ELEVATION CCW	



1. WORD STRUCTURE
 A = START BIT
 B = DATA BITS (SEE HELIOSTAT INTERFACE COMMAND)
 C = PARITY BIT
 D = TWO STOP BITS
2. COMMAND RATE (7 WORDS):
 1 COMMAND PER SECOND TO EACH HELIOSTAT
3. AZIMUTH AND ELEVATION DATA:
 14 BITS EQUIVALENT TO 2π rad WHERE LSB = 0.3835 mrad.

Figure II-B-23 Heliostat Interface Command (HIC) Definition

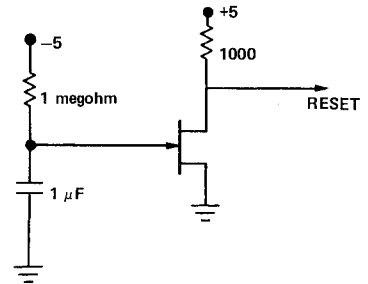
Power turn-on (see Fig. II-B-24 for circuit) will cause reset signals to be issued to appropriate registers and counters.

Manual Controller - A portable control panel is provided for manually controlling heliostat drives in the field. The control panel is housed in a lightweight instrument case affording an environmentally sealed enclosure for the control switches and associated wiring during handling and transportation of the unit. The panel and case configuration are shown in Figure II-B-25. A storage compartment located in the lower portion of the case will be used for stowing the 7.6-m (25-ft) interface cable that interconnects the manual controller and the control electronics assembly on the heliostat yoke.

Control functions, all bidirectional, accommodated by the manual control panel include:

- | | |
|------------------------|--------------------------|
| 1) Azimuth track mode; | 3) Elevation track mode; |
| 2) Azimuth slew mode; | 4) Elevation slew mode |

An on/off switch is used to engage the manual controller, locking out computer control modes. Panel illumination will be provided to facilitate manual control during periods of darkness.



POWER TURN-ON INITIALIZATION

Figure II-B-24 Power Turn-On Initialization

II-B-50

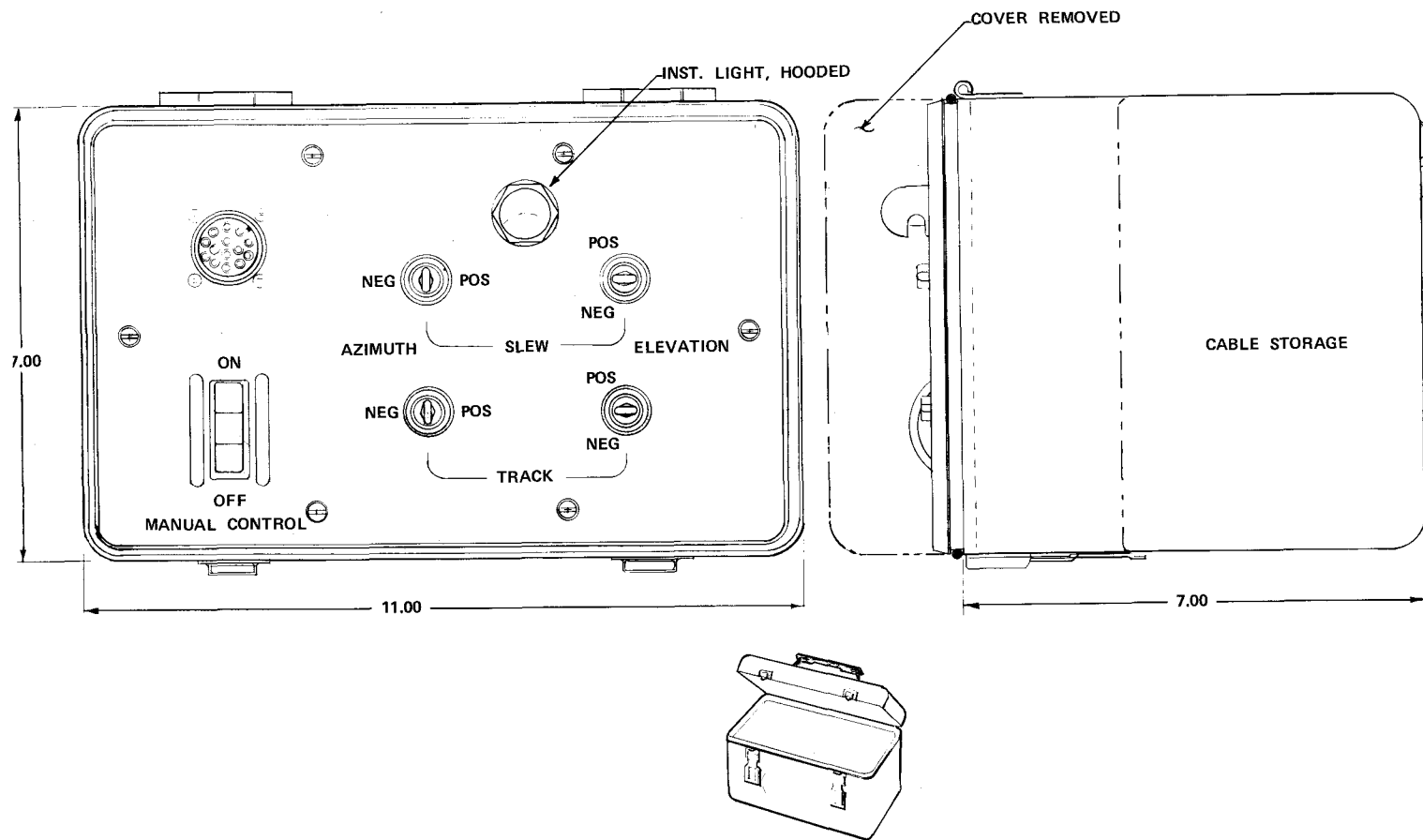


Figure II-B-25 Portable Controller for Heliostat Manual Positioning

Optimizing the manual (local) control interface with each heliostat control electronic unit permits the use of a small quantity of manual units to maintain the heliostats. It also enhances safety because the manual unit can be remotely controlled only when it is interfaced (connectors mated) with a heliostat. A switch on the remote unit front panel is used to lock out the automatic control of the HACSS.

Tradeoff Studies - A basic question requiring an answer in design of the heliostat control electronics and the heliostat interface module was the type of data transmission--manchester or NRZ. Asynchronous NRZ was chosen because it is a proven technique of data transmission at rates of 350 kilobaud or less, whereas manchester is capable of rates greater than 1 MHz, with a significant increase in parts and complexity. The system requirement of 2122 baud shows that NRZ is the preferred approach. By using readily-available MSI and LSI components compatible with UAR/T-type interfaces the task of encoding and decoding the transmitted data is simplified.

Another important tradeoff considered was selection of the type of line drivers and receivers for the HAC/heliostat interface. The major consideration that led to the choice of differential current mode devices was the requirement to have a large number of receivers and transmitters operating in parallel. This requires a high impedance device loading the data bus. Differential operation is a firm requirement due to the long lines and large number of electronic elements loading the line.

A breadboard simulation of the control loop, including all pertinent elements of the HCE, was assembled in our gyro laboratory and tests were conducted. A complete discussion of this subject is contained in Section C.1.

i. Helioostat Electrical Cable Description - The helioostat control electronics is located on the helioostat yoke and is the focal point for all the helioostat cables. This unit has four connectors, as shown in Figure II-B-26. Separate connectors are required to separate the power and control functions to minimize electromagnetic coupling.

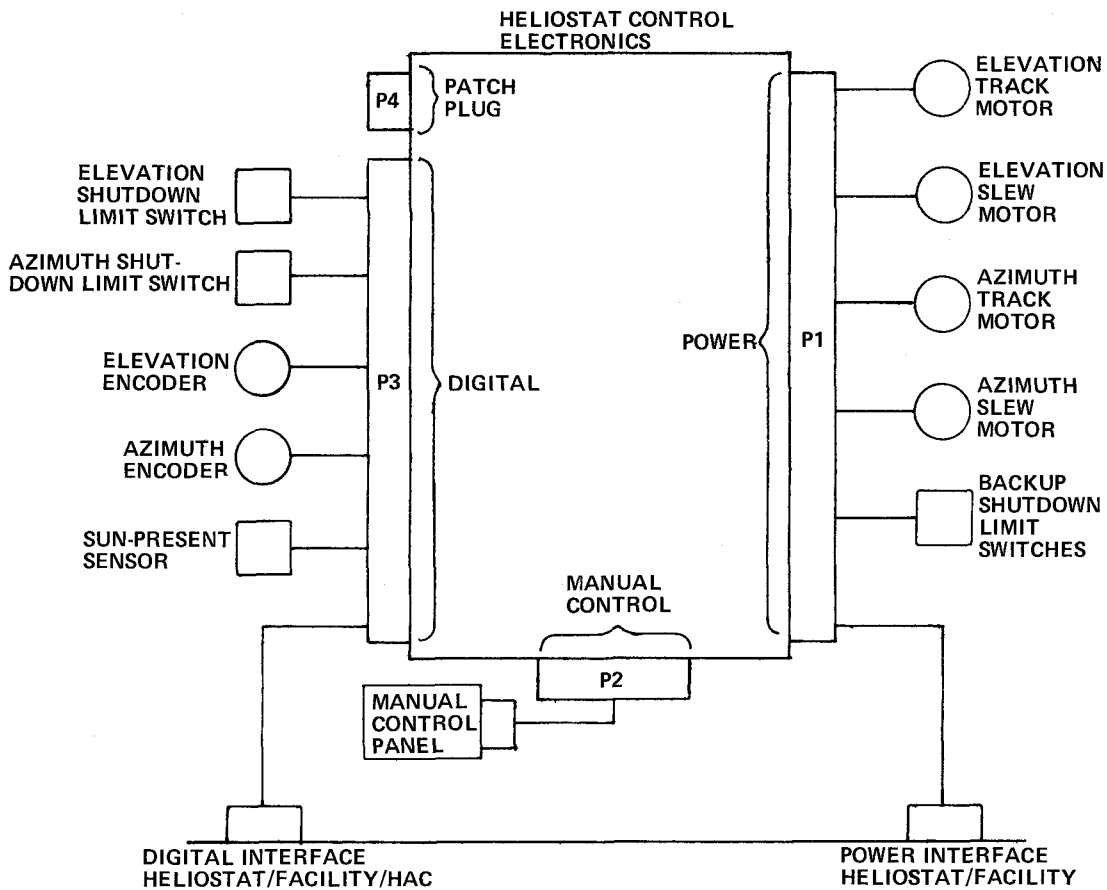


Figure II-B-26 Helioostat Control Electronics Electrical Interface

Connector P1 contains all the 117-Vac power functions from the foundation interface to the heliostat controller and from the controller to the motors and the backup limit switches. A grounding wire is also placed in this connector to ground the heliostat and heliostat controller to the facility ground. This wire serves as a shield return to ground, a ground for lightning strike protection, and for personnel safety. Connector P3 contains all the digital or low-level signal functions from the foundation interface to the heliostat controller and from the sun sensor, encoders, and limit switches to the heliostat controller. Connector P4 performs the function of a patch board to interpret the digital signals from the HAC for this specific heliostat location. The patching is accomplished by terminating jumper wires to the correct connector contacts. Connector P2 mates the manual control box to the heliostat controller and allows manual operation of the heliostat to override control by the HAC. Heliostat operation is obtained by toggle switch control. Normally the manual control box will obtain its power from the heliostat control electronics unit. In case of an emergency, a portable power supply can be used at the heliostat/facility power interfaces.

The location of the heliostat control electronics unit and harness are shown on Figure II-B-27. There are two separate harnesses--one for power and one for control. Each harness has the twisted wires inside a shield covered by an overall jacket. Both the wire insulation material and the jacket material are

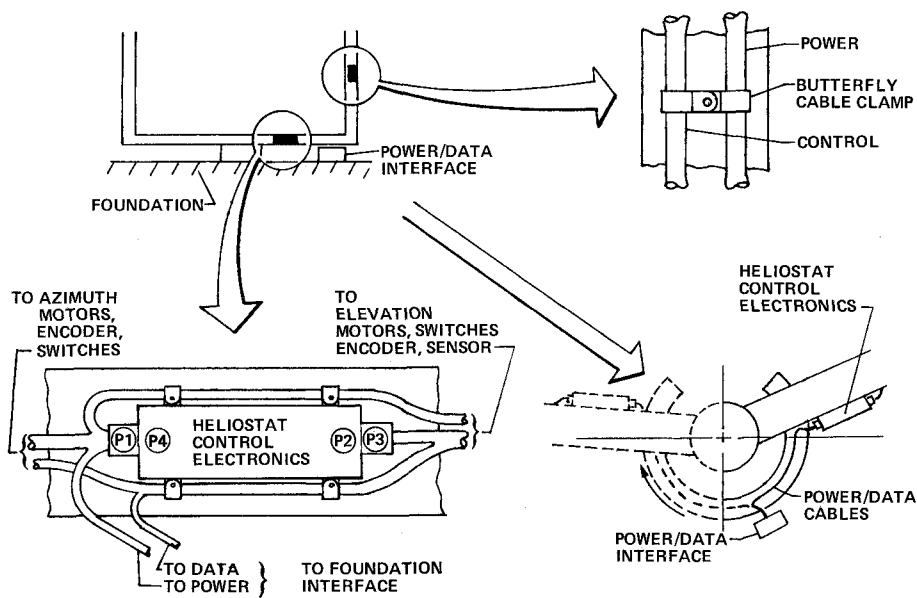


Figure a-2 HELIOSTAT ELECTRICAL INSTALLATION

Figure II-B-27 Heliostat Electrical Installation

polyurethane, which was selected for its ability to withstand 10 years of outdoor use with good resistance to weather, ozone, ultraviolet radiation, and abrasion. The wires are made of tin plated copper strands for good electrical terminations and cable flexibility. Cable clamps keep the bundles separated to further reduce coupling effects. The cables will be installed in accordance with local electrical codes. The 10-year life requirement of paragraph 3.1.f of K93681 will be easily attained with this hardware and design approach.

A number of approaches were investigated for the cabling between the heliostat/facility interface and the heliostat controller. The cables around the heliostat base will fold and unfold almost 360 deg once a day for 10 years or approximately 3000 cycles--a low cycle requirement. The result of the investigations showed that it was unnecessary to go to flat cables (which are flexible

in only one direction) or to special types of insulation like silicon rubber. The round cable with the same insulation and jacket material used on the heliostat yoke has sufficient abrasion resistance, as well as the other outdoor qualities, for this application.

The tracking and slew motors are exposed to all the outdoor environments. The motors selected for these applications are provided with an NEC enclosure within which the motor wires are spliced to the jacketed cable harness from the controller. The encoders and their terminations are enclosed within the heliostat structure.

The electrical interfaces between the heliostat and the foundation are interchangeable for all heliostats. All harnesses are provided with connectors, which allow the heliostat to be easily removed from its foundation to facilitate maintenance and movement in the field. The cable harnesses, motors, limit switches, and the heliostat control electronics can each be readily replaced.

j. Power Budget - The heliostat power budget is summarized in Table II-B-3, along with the ground rules used in deriving this budget. The power budget for the heliostat has been minimized by selecting the smallest feasible motor power size and using solid-state controls. Table II-B-4 reflects the total power by zone and by the entire HAC/heliostat field.

Table II-B-3 Heliostat Power Budget

ITEM	QUANTITY	EQUIPMENT	POWER, W	CYCLE TIME, hr/day	TOTAL, Wh/day
1	1	HELIOSTAT CONTROLLER	10	11.5	115
2	2	ENCODER	---	---	---
3	2	TRACK MOTORS	35.1	1.6	56.2
4	2	SLEW MOTORS	140.4	1.0	140.4
					311.6

NOTE: ELECTRICAL POWER BUDGET ASSUMPTIONS:

- 1) AVERAGE DAY IS 11.5 hours LONG;
- 2) AVERAGE MONTH IS 25 days LONG, 3450 hours OF SUN PER YEAR AT ALBUQUERQUE/11.5 hours/day x 12 months = 25 days/month;
- 3) ENCODERS DERIVE 5 Vdc POWER FROM HELIOSTAT CONTROLLER;
 - a) WINTER SOLSTICE = 7:30 am to 4:30 pm,
 - b) SUMMER SOLSTICE = 5:00 am to 7:00 pm,
 - c) $(9 + 14) 1/2 = 11.5$ hours;
- 4) TRACK MOTORS,
 - a) CURRENT = 0.3 A,
 - b) CYCLE TIME = 14% of 11.5 hours = 1.6 hours;
- 5) SLEW MOTORS,
 - a) CURRENT = 1.2 A,
 - b) CYCLE TIME = 0.25 hours x 4 TIMES A DAY (START, CLOUD SHUTDOWN, AND RESTART, END OF DAY SHUTDOWN) = 1 hour.

Table II-B-4 Total Power Budget

POWER USER	POWER, kW		ENERGY, kWh	
	NOMINAL	MAXIMUM	DAILY REQUIREMENT	MONTHLY REQUIREMENT
ZONE A				
HELIOSTATS (78)	3.5	11.7	24.3	610
HAC (1)	2.0	3.8	42.3	1,057
TOTAL	5.5	15.5	66.6	1,667
ZONES A & B				
HELIOSTATS (294)	13.2	44.0	91.6	2,290
HACs (3)	5.8	9.3	107.5	2,686
TOTAL	19.0	53.3	199.1	4,976
ZONES A, C, D, & E				
HELIOSTATS (344)	15.4	51.4	107.3	2,690
HACs (4)	8.0	15.2	169.2	4,228
TOTAL	23.4	66.6	276.5	6,918
ZONES A, B, C, D, & E				
HELIOSTATS (560)	25.1	83.7	174.6	4,370
HACs (6)	11.8	20.7	234.4	5,857
TOTAL	36.9	104.4	408.0	10,227
ZONE B				
HELIOSTATS (216)	9.7	32.3	67.3	1,680
HACs (2)	3.8	5.5	67.2	1,629
TOTAL	13.5	37.8	132.5	3,309
ZONE C				
HELIOSTATS (83)	3.7	12.4	25.9	650
HAC (1)	2.0	3.8	42.3	1,057
TOTAL	5.7	16.2	68.2	1,707
ZONE D				
HELIOSTATS (100)	4.5	14.9	31.2	780
HAC (1)	2.0	3.8	42.3	1,057
TOTAL	6.5	18.5	73.5	1,837
ZONE E				
HELIOSTATS (83)	3.7	12.4	25.9	650
HAC (1)	2.0	3.8	42.3	1,057
TOTAL	5.7	16.2	68.2	1,707

2. HASS Functional Capability

The functional capabilities of the heliostat array subsystem are presented in this subsection. The ability of the overall subsystem and its components to meet the requirements of K93681 are emphasized.

a. *Aperture Requirements* - Tables II-B-5, II-B-6, and II-B-7 show the winter solstice, equinox, and summer solstice performance for zones A, B, C, D, and E that surround the tower. The RFQ specified that the collector fields shall be sized based on 0.8 kW/m² insolation during the four midday hours and that the power received by an aperture from a given zone or zones shall be as shown in Table II-B-8. The number of heliostats required for each zone is 78 in A, 214 in B, 81 in C and E, and 100 in D. Figure II-B-1 shows 83 heliostats in zones C and E. These additional units provide extra power margin for the field.

Table II-B-5 Zone A (1-MWt) Field Performance, Martin Marietta Receiver

DAY OF YEAR	SOLAR TIME, HR	FIELD AVERAGE COSINE	APERTURE EFFICIENCY*	POWER INTO CAVITY, M Wt
SPRING EQUINOX	1000	0.9219	0.851	1.49
	1200	0.9523	0.912	1.65
SUMMER SOLSTICE	1000	0.8568	0.675	1.13
	1200	0.8868	0.753	1.28
WINTER SOLSTICE	1000	0.9503	0.816	1.46
	1200	0.9782	0.851	1.63
<p>NOTES: MIRROR REFLECTIVITY = 0.85, 78 HELIOSTATS (EACH 400 ft²) IN ZONE A, INSOLATION = 0.8 kW/m².</p> <p>*APERTURE EFFICIENCY = $\frac{\text{POWER REFLECTED TOWARD APERTURE}}{\text{POWER CAPTURED BY APERTURE}}$</p>				

Table II-B-6 Zones A and B (5.5 Mwt) Field Performance, Martin Marietta and McDonnell Douglas Receivers

DAY OF YEAR	SOLAR TIME, hr	FIELD AVERAGE COSINE	APERTURE EFFICIENCY *	POWER INTO MARTIN MARIETTA CAVITY, MWt	POWER ONTO McDONNELL DOUGLAS RECEIVER, MWt
SPRING EQUINOX	1000	0.9143	0.955	6.42	5.42
	1200	0.9437	0.966	6.70	5.70
SUMMER SOLSTICE	1000	0.8440	0.924	5.73	4.87
	1200	0.8734	0.940	6.03	5.13
WINTER SOLSTICE	1000	0.9481	0.965	6.61	5.62
	1200	0.9748	0.970	6.97	5.92

NOTES: MIRROR REFLECTIVITY = 0.85,
NUMBER OF HELIOSTATS: 78 in A, 214 in B,
INSOLATION = 0.8 Kw/m²

*APERTURE EFFICIENCY = $\frac{\text{POWER REFLECTED TOWARD APERTURE}}{\text{POWER CAPTURED BY APERTURE}}$

Table II-B-7 Zones A, C, D, and E (5-Mwt) Field Performance - Honeywell Receiver

DAY OF YEAR	SOLAR TIME, Hr	HELIOSTAT ZONE	FIELD AVERAGE COSINE	APERTURE EFFICIENCY*	POWER INTO CAVITY, MWt
SPRING EQUINOX	1000	A	0.9451	0.997	1.83
		C	0.7396	0.873	1.32
		D	0.7554	0.887	1.69
		E	0.9428	0.995	1.92
		TOTAL	0.8457	0.938	6.76
SUMMER SOLSTICE	1200	A	0.9785	1.000	1.94
		C	0.8673	0.958	1.70
		D	0.7651	0.892	1.72
		E	0.8673	0.958	1.70
		TOTAL	0.8660	0.952	7.06
SUMMER SOLSTICE	1000	A	0.9071	0.980	1.75
		C	0.7896	0.908	1.44
		D	0.8666	0.960	2.10
		E	0.9672	1.000	1.96
		TOTAL	0.8926	0.962	7.25
SUMMER SOLSTICE	1200	A	0.9384	0.994	1.84
		C	0.9008	0.976	1.80
		D	0.8739	0.963	2.13
		E	0.9008	0.976	1.80
		TOTAL	0.9035	0.977	7.57
WINTER SOLSTICE	1000	A	0.9479	1.000	1.84
		C	0.6637	0.824	1.16
		D	0.5964	0.783	1.22
		E	0.8795	0.869	1.75
		TOTAL	0.7719	0.894	5.97
WINTER SOLSTICE	1200	A	0.9783	1.000	1.93
		C	0.8071	0.922	1.52
		D	0.6311	0.792	1.26
		E	0.8071	0.922	1.52
		TOTAL	0.8059	0.909	6.23

NOTES: MIRROR REFLECTIVITY = 0.85,
NO. OF HELIOSTATS: 78 IN A, 81 IN C AND E, 100 IN D.
INSOLATION = 0.8 MW/m².

*APERTURE EFFICIENCY = $\frac{\text{POWER REFLECTED TOWARD APERTURE}}{\text{POWER CAPTURED BY APERTURE}}$

Table II-B-8 Collector Array Power Requirements

ZONE	HEIGHT TO BOTTOM OF APERTURE, m (ft)	APERTURE SIZE AND ORIENTATION	MINIMUM POWER LEVEL, MWt
A	44 (144)	1x1 m (3.3 ft) NORTH FACING, TILTED 0.35 rad (20 deg) DOWNWARD	1.0
A AND B	61 (200)	2.65x2.65 m (8.8 ft) NORTH FACING TILTED 0.35 rad (20 deg) DOWNWARD	5.5
A AND B	61 (200)	2.0 m WIDE BY 17.1 m HIGH, NORTH FACING, TILTED 0.35 rad (20 deg) DOWNWARD	4.4
A, C, D, AND E	70 (230)	AN ANNULAR APERTURE, SLANT HEIGHT 1.65 m (3.3 ft), UPPER DIAMETER 3.66 m (12 ft), LOWER DIAMETER 1.82 m (6.0 ft)	5.0

Calculation Basis - The following energy balance relationships demonstrate the type of calculations entailed in sizing the collector field. The following is a simplified calculation for the sizing of zone A.

Power efficiency of the aperture is

$$\eta_A = \frac{\text{Power reflected toward aperture}}{\text{Power received by aperture}}$$

η_A varies with time of day and time of year. At the equinox noon, $\eta_A = 0.912$ (see Table II-B-5).

The power reflected toward the aperture is a function of the collector efficiency

$$\eta_{col} = N_{area}, N_{refl}, N_{tr}, N_{op}$$

where

N_{area} = average cosine of entire collector field,

N_{refl} = spectral reflectance of mirror,

N_{tr} = error factor due to tracking,

N_{op} = error factor caused by mirror surface irregularities.

For Zone A

$$N_{col} = (0.9219) (0.85) (0.98) (0.98) = 0.7525.$$

The reflectivity of the mirror is shown as 0.85, which is conservative for a second-surface silvered, white glass mirror.

The total power impinging on the collector field yielding 1 MW at the aperture is

$$\begin{aligned} P_T &= \frac{P_A}{N_A N_C} \\ &= \frac{1 \text{ MW}}{(0.7525) (0.912)} \\ &= 1.457 \text{ MW} \end{aligned}$$

where

P_A = power received by aperture,

P_T = total power received by field.

Once the input power is determined, the collector area A can be calculated

$$\begin{aligned} A &= \frac{P_T}{P_2/M^2} \\ &= \frac{1.457 \times 10^3 \text{ KW}}{0.8 \text{ KW/M}^2} \\ &= 1821.25 \text{ M}^2 \end{aligned}$$

where P_2 is the average insolation value of 0.8 kW/m² given for the four midday hours.

The number of heliostats, based on a 6.1x6.1-m (20x20-ft) heliostat is then

$$\begin{aligned} N &= \frac{\text{Total Area, m}^2 \text{ (ft}^2\text{)}}{\text{Area/Heliostat, m}^2 \text{ (ft}^2\text{)}} \\ &= \frac{1821.25 \text{ m}^2}{37.21 \text{ m}^2} \\ &= 48.94 \text{ heliostats.} \end{aligned}$$

Note that this value is considerably smaller than that shown in Table II-B-5 for the same conditions. However, the value given in the table provide a 50% margin. Also, the computerized sizing program that generated Tables II-B-5, II-B-6, and II-B-7 accounts for varying time of year, time of day, and more efficiency factors than could be conveniently shown above. The final field sizing is an optimization of the changing power density received by the aperture.

b. Beam Quality - Specification K93681 states that at solar noon on the equinoxes, each heliostat must be capable of directing 90% of its reflected power onto a circular target of diameter 0.012 SR, SR being distance from the heliostat to the center of the calibration target.

Based on the maximum SR of 291.57 m (956.58 ft) in heliostat zone B, the maximum target diameter (d_{\max}) to satisfy the beam quality requirement at solar noon on the equinoxes is

$$\begin{aligned}d_{\max} &= 0.012 (291.57 \text{ m}) \\ &= 3.5 \text{ m (11.48 ft)}.\end{aligned}$$

To allow for the aberration, a factor of 0.015 was used to determine the maximum diameter of the iris to be designed, which is $(0.015) (291.57 \text{ m}) = 4.37 \text{ m (14.35 ft)}$.

The worst-case solar image size would occur for a heliostat at the most distant point in zone B and when mirror aberrations are at maximum values. The degree of aberration depends on the position of the heliostat in the collector field and the time of day and the day of year. At solar noon on the equinoxes, the

aberrations of the mirrors are at a minimum since the mirrors will be focused onto the target for those times. For the proposed Martin Marietta warped-mirror heliostat, the maximum solar image size d_s , including off-axis aberrations, can be approximated by the relationship

$$d_s = SR \sin \theta + d_a$$

where

θ = angle subtended by the sun's rays on a point on the mirror,

d_a = length of solar image on the target due to optical aberration.

Using the maximum possible aberration of any heliostat, which is 2.44 m (8 ft), the maximum solar image on the target plane for the farthest heliostat is

$$d_s = 291.57 (\sin 0.00931 \text{ rad}) + 2.44$$

$$d_s = 5.15 \text{ m (16.91 ft)}.$$

The approach selected for beam quality verification involves the use of a water calorimeter. Because actual testing will normally be conducted at conditions other than the equinoxes, the exact diameter of the circular target will not be known prior to the test. For this reason, measurements of total power absorbed at the target plane will be repeated at least four times with different circular target areas. The resulting data will then be analyzed to verify the beam quality requirement. This verification requires that the diameter of the circular target corresponding to 0.012 SR at solar noon on the equinoxes be determined via computer analysis.

c. *Aiming and Tracking* - Our design meets all heliostat aiming requirements with margin under the total range of sustained wind conditions specified in the RFQ (see Table II-B-2). All heliostats will track and reflect the sun's rays onto the total target spectrum with minimal solar power loss. On an average day, out of the total field for the total spectrum of targets, the heliostats will effectively maintain accurate tracking 99.68% of the time.

The imaginary three-dimensional grid system comprising the total spectrum of possible targets is illustrated by the volumes S and T on the coordinate system of Figure II-B-28. The target zones and aiming requirements are specified as follow :

- 1) Coarse tracking/standby command - K93681, paragraph 3.1.4.3.a;
- 2) Fine-tracking/on-target command - K93681, paragraph 3.1.4.3.b;
- 3) Environmental conditions - Per requirements of Table II-B-2.

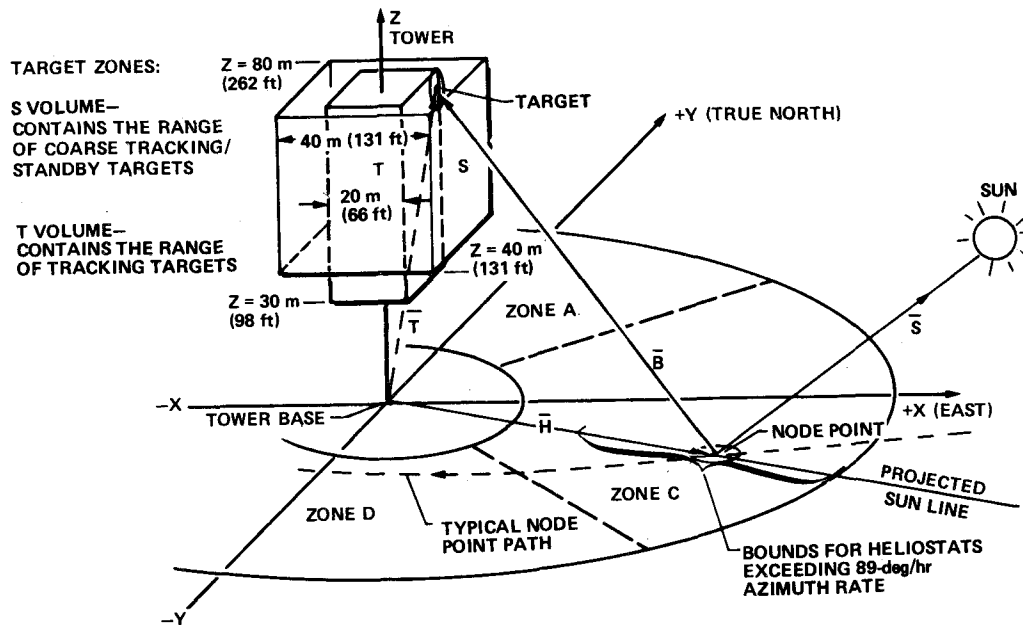


Figure II-B-28 Fine and Coarse Tracking Coordinate System

Figure II-B-29 is a simplified block diagram of a heliostat control loop. Details of the azimuth control loop are not shown because it is equivalent to the elevation loop except operating speed of the tracking motor and gear ratio are different. The elevation and azimuth commands from the HAC are computed based on current sun, target, and mode commands from the MCS. The basic steering algorithm is shown in Figure II-B-30. The azimuth and elevation commands are differenced with the gimbal angles fed back from the encoders and an on or off signal is delivered to the tracking or slewing motor depending on the position of the switch. The slew motors have synchronous speeds of 1700 rpm. The elevation track motor has a synchronous speed of 72 rpm while that of the azimuth track motors is 200 rpm. The motor shaft speeds then pass through a series of gear reduction with an overall ratio of $\left(\frac{1}{48600}\right)$ for azimuth and $\left(\frac{1}{32400}\right)$ for elevation to deliver the final heliostat gimbal speeds, which are then transferred into gimbal angles that are sensed by the encoder for loop feedback.

Heliostat Gimbal Control Law - Our heliostat control loop meets the requirements with a simple and reliable design. The basic azimuth and elevation gimbal commands are obtained as a result of satisfying the constraint imposed by Snell's law, which equates the angles of incidence and reflection of light rays on a planar mirror. The algorithm used for this purpose is illustrated in simplified form by the flow diagram of Figure II-B-30 for one heliostat. Figure II-B-30 shows the vectors \bar{H} , \bar{T} , \bar{B} , and \bar{S} used in the control law. The logic necessary to accommodate all required modes, gimble angle and rate limits is discussed in section II.C.

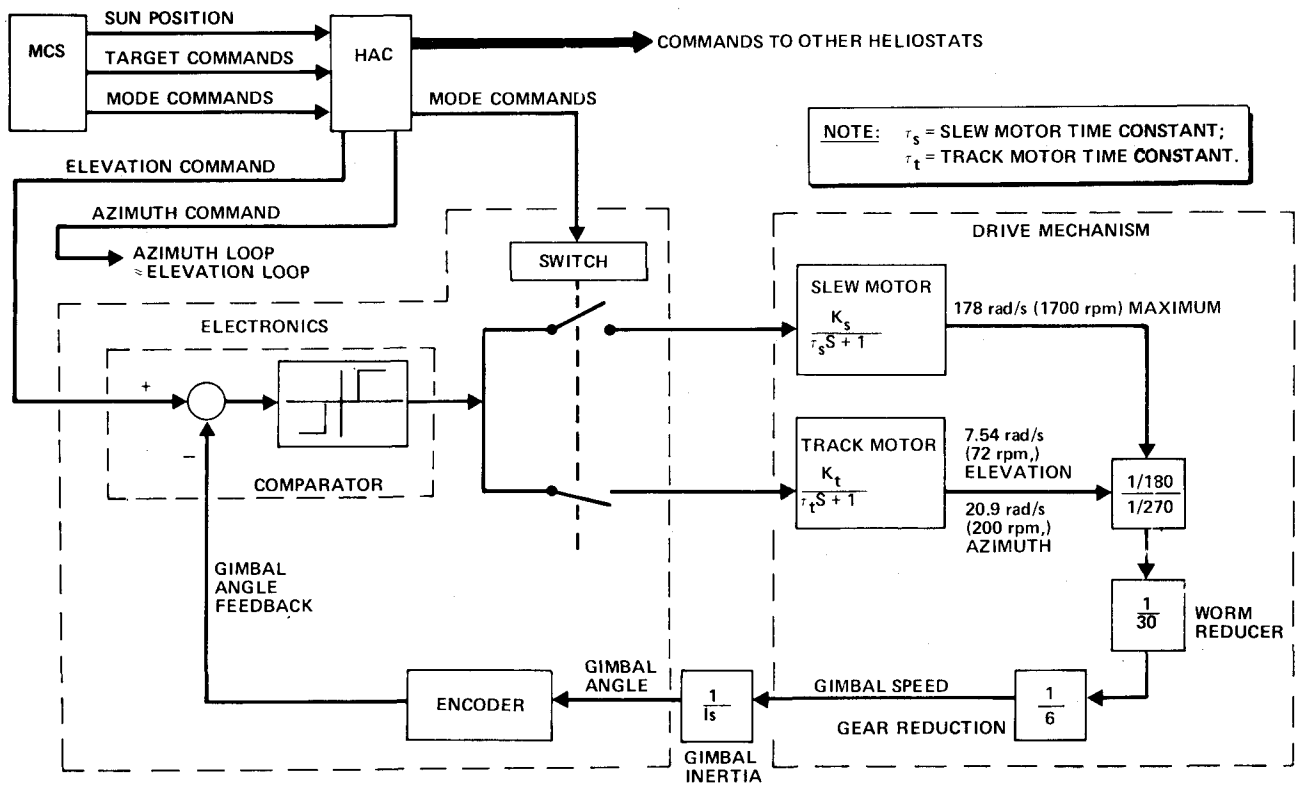


Figure II-B-29 Heliostat Control Loop

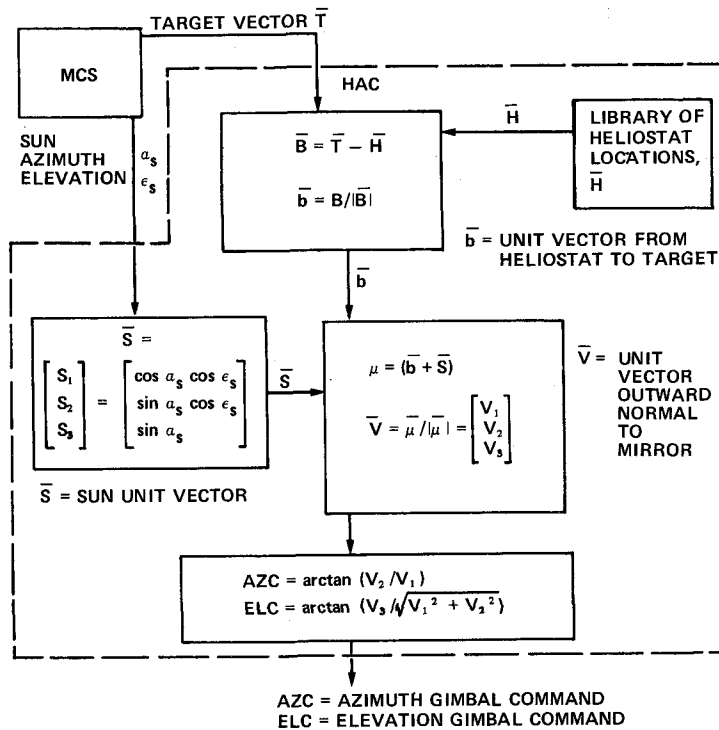


Figure II-B-30 Heliostat Gimbal Control Law

Error Budget for Heliostat Tracking - Table II-B-2 shows that our error budget is within the tracking aiming requirements. The largest source of error is structural deformation due to sustained winds. However, we have used a conservative approach in determining errors due to wind. Wind error, shown in Table II-B-2, is the maximum that would occur when the wind is perfectly normal to the plane of the mirrors. The errors due to wind could be significantly reduced if an "effective" error over an entire day were used instead of the maximum value. Furthermore no heliostat in the entire field would ever be perfectly normal to a horizontal wind since its face would be tilted upward to the sun. The near-normal wind condition can only occur (1) near sunrise or sunset when the sun's rays are almost horizontal, and (2) near noon at winter solstice for several heliostats at a time in the back row of zone B. The chances of a normal wind condition would be further greatly reduced if a limited range of wind velocity directions is assumed. The worst day is at winter solstice when the sun is nearest the southern horizon. This condition gives rise to the largest percentage of heliostats, mostly in the north field, that would, during the day, encounter a sustained wind at angles that would produce significant mirror pointing errors. The worst-case target location is at 30 m (98.4 ft) above the base of the tower. The worst-case wind would be a sustained north wind. When the time history of the heliostat orientation is considered for an entire day of full wind, an "effective"

mirror pointing error is obtained that is approximately 90% of that when perfectly normal to the wind for the entire day.

Wind gusts with a 18-m/s (40.3-mph) rms velocity will not disturb the tracking mode to any significant degree. Any pointing errors due to gusts would quickly damp out with our structural design.

A delay of 1 second in updating the sun position in the HAC will result in a 1 σ mirror pointing error of 0.03 mrad based on a 3 σ required gimbal rate of 19.7 deg/hr.

Several sources of error such as site leveling and encoder alignment are combined under the title "final beam calibration." Final beam calibration of each heliostat will be performed using a reflective beam-sensing target to determine the errors in the heliostat pointing. Once these errors are determined, the azimuth and elevation commands will be biased (in the software) by that amount. A further description of the calibration system is given in Section II.E.

Errors due to motor rundown are considered a bias that can be compensated for in the software and are therefore not a part of the error budget.

Fine Tracking Simulation - A computer program has been written to simulate operation of the heliostat fine-tracking loop. The program includes the equations that define the motion of the beam reflected from the heliostats as the sun and heliostat gimbals move. The program also includes a simplified representation of

the motor, gears, and gimbal inertia. The program is being used to study the fine-tracking loop operation at different times of the day, different times of the year, and different locations of the heliostats in the field.

d. Tracking and Slewing Gimbal Rates and Limits of Travel -

The control and drive system will cause each heliostat to direct its reflected beam to a specified standby position off the experiment and then, on command, to the specified experiment target. Each heliostat will be capable of being pointed at any location in the target zone. The operating modes that require gimbal slewing and tracking are as follows:

- 1) Acquisition - K93681, paragraph 3.1.4.4.a;
- 2) Power - K93681, paragraph 3.1.4.4.b;
- 3) Standby - K93681, paragraph 3.1.4.4.c;
- 4) Stow - K93681, paragraph 3.1.4.4.e;
- 5) Emergency shutdown - K93681, paragraph 3.1.4.4.f;
- 6) Fail-Safe - K93681, paragraph 3.1.4.4.g.

The tracking motors will drive the gimbals at 89 deg/hr maximum in azimuth and 48 deg/hr maximum in elevation. The slew motors will drive the gimbals at 1133.3 deg/hr maximum for elevation and 755.6 deg/hr for azimuth, which is adequate to meet all slew rate requirements.

Table II-B-9 gives average tracking motor velocity requirements and duty cycles based on the tracking motor operating at full range from approximately 4 deg/hr near the tower at the boundary between zones A and C, to 19 deg/hr in the far field of

south zone C near sunrise. The low duty cycle numbers shown in Table II-B-9 mean low power consumption, low wear and tear, and higher reliability of the motors.

Table II-B-9 Average Heliostat Tracking Motor Velocities, Duty Cycles

GIMBAL, LOCATION WITH RESPECT TO TOWER	AVERAGE VELOCITIES, mrad/s (deg/hr)			DUTY CYCLES, (VELOCITY 89 deg/hr) AZIMUTH (VELOCITY 48 deg/hr) ELEVATION					
	ELEVATION	SEPARATE	COMBINATIONS	OVERALL	SEPARATE	COMBINATIONS	OVERALL		
NEAR-FIELD	(4.69) 0.0227	0.0245 (5.05)	0.0576 (11.88)	0.0411 (8.47)*	0.10	0.11	0.12		
	FAR FIELD (5.15) 0.025				0.11				
AZIMUTH									
NEAR-FIELD									
NORTH	(11.91) 0.0577	0.070 (14.43)			0.13	0.16		0.13	
SOUTH	(16.44) 0.0797				0.18				
FAR FIELD									
NORTH	(10.0) 0.049	0.054 (11.14)			0.11	0.13			
SOUTH	(13.73) 0.0666				0.15				

*MEAN VELOCITY IS 0.041 mrad/s (8.47 deg/hr) WITH A STANDARD DEVIATION OF 0.0182 mrad/s (3.75 deg/hr).

A path of "nodes" across the heliostat zones is the locus of all possible heliostats that at one time during the day, theoretically, require infinite azimuth slew rate and a vertical mirror normal to continually track the sun. A typical node path is shown in Figure II-B-28. Figure II-B-31 is a typical plot of azimuth velocities versus distance from a node point along the projected sun line on each side of the node. The plot shows that on this line all heliostats within approximately 31.4 m (103-ft) of a node point will require azimuth slew rates at or above 89 deg/hr. The node path distance from the tower along the north-south line varies north to south depending on target location and day of year. For the fine-tracking target zone specified (zone T in Fig. II-B-28), the node path distance from the tower ranges from approximately 3.87 m (12.69 ft) north of the tower to 140 m (460 ft) south of the tower.

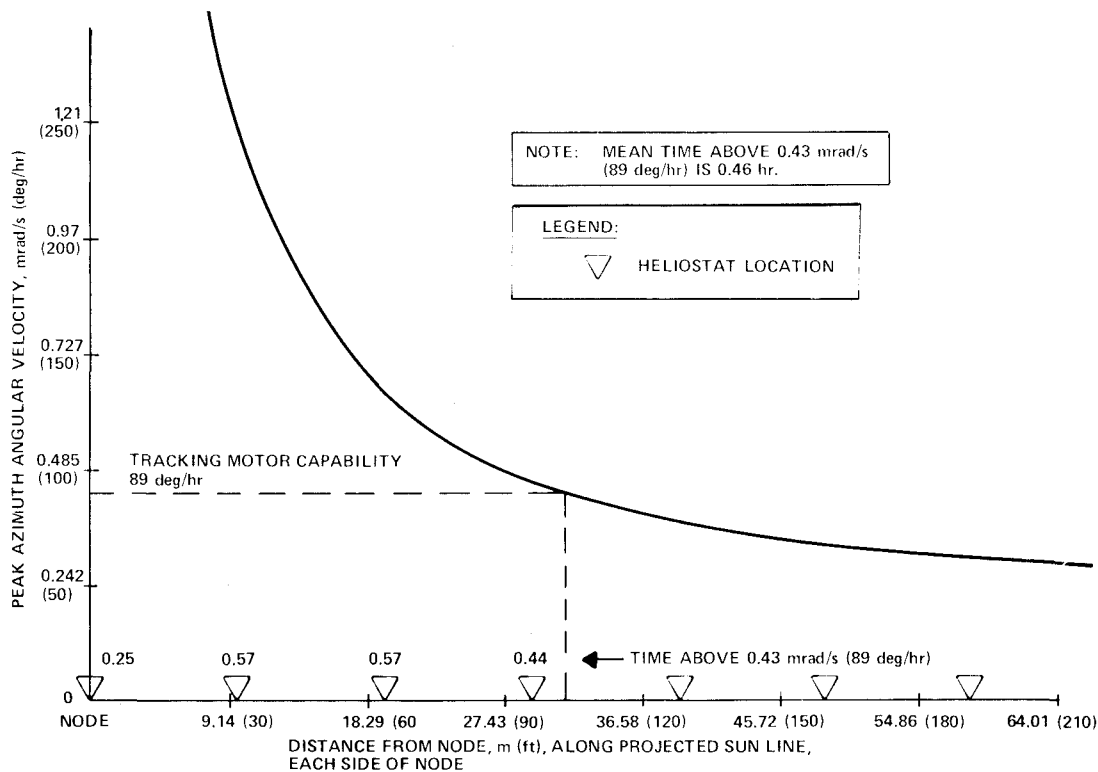


Figure II-B-31 Peak Azimuth Rates vs Distance from Node

Table II-B-10 gives a summary of percentages of tracking time loss (roughly equivalent to percent solar power loss) due to slew rates exceeding the tracking motor

capability. We used a conservative approach to determine tracking time lost because Table II-B-11 combines worst-case day and target conditions. However, since tracking losses heavily depend on the receiver target locations, these losses could be reduced considerably by optimal target locations.

Table II-B-10 Tracking Time Loss Per Day Due to High Azimuth Rates

ZONE	DAY AND TARGET CONDITIONS	PERCENT TRACKING TIME LOSS PER DAY DUE TO HIGH GIMBAL RATES	STRAIGHT AVERAGE, %
TOTAL FIELD	BEST	NO LOSS	0.32
	WORST	0.643	
A + B	ALL	NO LOSS	NO LOSS
C O R E	BEST	NO LOSS	0.79
	WORST	1.58	
D	BEST	NO LOSS	1.07
	WORST	2.14	

e. Operational Modes - The HCE has the capability for 16 operational modes. Currently 14 specific functions are defined. The list below categorizes the functions into 6 classes:

- 1) Status - HCE status returned to HAC;
- 2) Clear - All HCE mode registers are cleared and all motors stopped;
- 3) Coarse track - Slew motor of specified axis is activated in closed-loop operation (one azimuth command, one elevation command);
- 4) Fine-track - Track motor of specified axis is activated (one azimuth command, one elevation command);
- 5) Direct slow - Four commands allow specified axis track motor to be activated in either clockwise or counterclockwise direction. Only limit switches or clear command will turn motor off;
- 6) Direct slew - Four commands allow specified axis slew motors to be activated in either clockwise or counterclockwise direction. Only limit switches or clear command will turn motor off.

The status, clear, coarse, and fine-track modes will be used while the HACSS is under MCS control. These commands as well as direct slow and direct slew will be used for diagnostic purposes and will be commanded from the manual control panel while the heliostat is in "manual" mode or while the heliostat and HACSS are in open-loop control. The "manual" mode will prohibit any external control of the heliostat other than through the manual control panel.

3. Safety Features

To assure safe operation of the heliostats for both personnel and equipment, the following features are incorporated in the design:

- 1) Pointing limits - HAC control programs will preclude pointing the reflected beam of any heliostat at any inhabited structure or personnel area, or toward other locations such as air traffic lanes that could create a hazard;
- 2) Limit switches - There will be a pair of limit switches at each end of azimuth and elevation travel of the heliostat axes. The pair of limit switches will be separated by approximately 0.09 rad (5 deg). The first of the pair will provide an input to the heliostat control electronics to stop movement in that direction and set a limit switch bit in the output data to the HAC. The second will be a backup that will open the power line to the motor to stop movement in that direction. Neither limit switch opened will preclude backing off of the limit by HAC commands to the heliostat control electronics;
- 3) Remote control unit - Local control of the heliostat is possible only when the unit is connected to the heliostat control electronics unit. When it is connected, HAC control of the heliostat can be locked out.

Maintainability Features

Maintainability has been designed in for all components of the heliostat. The following paragraphs discuss these features of the HASS components.

a. *Structure* - Proper selection of material and fabrication processes precludes any maintenance being scheduled or required on the basic heliostat structure except for periodic visual inspections. Rotating components (cams, bearings, etc) will have grease fittings provided for periodic maintenance.

b. *Mirror Assembly* - All maintenance functions required by the mirror assembly are covered by the maintenance equipment capabilities. Cleaning, replacement, alignment, and focusing are all functions encompassed by the equipment.

c. *Sun-Present Sensor* - Other than replacement in case of failure, this sensor requires no maintenance. After initial installation and checkout (threshold sensitivity setting), there is no maintenance requirement except cleaning (accomplished at the same time as mirror cleaning).

d. *Elevation Drive Module* - The elevation drive module is readily replaceable as an entity by removing the end bank of mirrors. The need for such replacement should be extremely remote in view of the simplicity and ruggedness of the final gear train, and the fact that the worm reducer and drive motors can be individually replaced. The bearings, which for standardization are identical to those used in the azimuth drive, are so overrated

for the elevation duty that they should have infinite B10 life. Servicing of the encoder involves dismantling the end bank of mirrors, which entails the removal of only four nuts.

e. Azimuth Drive Module - The need to replace an entire module is extremely remote. Except for the final gear train, all parts are replaceable independently. The process of replacing a drive module requires removal of 14 nuts and the hoisting of the yoke and mirror assembly while interchanging drive modules. It may prove more effective to "block" replace than attempt to service individual portions of the drive.

The azimuth drive encoder is easily replaceable without dismantling any other component.

f. Limit Switches - There is no maintenance required on the travel limit and emergency shutdown switches. The life cycle rating (10×10^6 cycles) will permit the switch to accommodate the 10 years of heliostat operation.

g. Heliostat Control Electronics Assembly - This unit requires no maintenance. In case of a failure, the control panel can be easily replaced with a spare. All cable harnesses can be readily replaced without disassembly of the heliostat.

h. Remote (local Control Unit - Maintenance on this unit will consist only of the replacement of components (switches, lights, etc) in case of failure. No other maintenance is required.

5. Reliability

Reliability lies in the optimized design of the heliostat, the use of commercially available hardware and components, derating of electrical/electronic parts, and the application of adequate safety, design, and operating margins. The basic mirror support structure is of all-steel construction and as such precludes any conditions or problems that would not permit the designated 10 years of operational life to be attained.

To achieve reliability for the remaining heliostat components, i.e., drive mechanisms, heliostat control electronics, etc, we will provide sufficient component spares for components not commercially available to maintain the HASS for five years. The interchangeability and field replacement inherent in our design allows this approach.

6. Manufacturing

The manufacturing effort for the heliostats includes the mirror holding and positioning structure and electrical/electronics control components. The structure includes the mirrors, mirror rack, yoke module, and the mechanical drive systems. The electrical/electronics effort will be the fabrication, test, and delivery of the heliostat control electronics, manual controller unit, and the wiring harnesses associated with the heliostats operation. The heliostat manufacturing requirements are shown in Table II-B-11.

Table II-B-11 Heliostat Manufacturing Requirements

QUANTITY PER HELIOSTAT	QUANTITY PER SUBASSEMBLY	SUBASSEMBLY	DETAILS PER SUBASSEMBLY	OPERATION	FACILITY	EQUIPMENT	TOOLING
1		YOKE MODULE		BUY STRUCTURE	RIO GRANDE STEEL	FORKLIFT CRANE	SPREADER BAR
	1		HORIZONTAL SUPPORT		ALBUQUERQUE, NM		
	2		VERTICAL SUPPORT				
	1		EQUIPMENT COMPARTMENT				
	1		TORQUE TUBE				
	1		CAP				
	2		ROLLER				
	1		RETAINER				
1		MIRROR RACK		WELD, ASSEMBLE AT SITE ASSEMBLY BUILDING	SITE ASSEMBLY BUILDING	300-A WELDER AIR COMPRESSOR	ASSEMBLY FIXTURE
	2		HORIZONTAL TUBE	BUY, CUT TO LENGTH	RIO GRANDE STEEL	PORTABLE A-FRAME	SPREADER BAR
	10		VERTICAL TUBE	BUY, CUT TO LENGTH, NOTCH, DRILL	RIO GRANDE STEEL	STORAGE RACK	
	2		SPLICE PLATE	BUY, CUT, AND DRILL	RIO GRANDE STEEL	SUPPORT STANDS	
	25		MIRROR-ADJUST TAB	BUY, FORM	RIO GRANDE STEEL	PORTABLE DRILL	
25		MIRROR HOLDER		BUY, APPLY PRIMER, RTV AT SITE ASSEMBLY BUILDING	RIO GRANDE STEEL	AIRLESS SPRAY DISPENSER LIGHT STANDARD WORK BENCHES GRINDER DRILL PRESS ACETYLENE TORCH	
	1		RING				
	3		CROSS BRACE				
	2		ADJUSTING SCREW				
	1		FOCUS PAD				
25		MIRROR		BUY MIRROR, APPLY PRIMER, CURE	GLASS MANUFACTURER (PRIME AT SITE ASSY BLDG)	SUCTION GRIPS	MIRROR DOLLY
1		DRIVE UNIT, AZIMUTH		BUY, INSTALL, AND LEVEL AT SITE			
1		DRIVE UNIT, ELEVATION		BUY, INSTALL AT SITE ASSEMBLY BUILDING	DENVER		
1		CONTROL, ELECTRONICS ASSEMBLY		MAKE, & INSTALL AT SITE	DENVER		
1		WIRE HARNESS		MAKE, & INSTALL AT SITE	DENVER		
AS REQUIRED		P CLAMPS		BUY			
AS REQUIRED		PRIMER SS4004		BUY			
AS REQUIRED		ADHESIVE, RTV 560		BUY			

a. *Structure* - Each heliostat of the heliostat array subsystem (HASS) is a welded steel structure consisting of a yoke module, a mirror rack, 25 mirror holders with mirrors, an azimuth drive module, and an elevation drive unit.

Our structural manufacturing tradeoff studies examined product size, quantity, configuration, and transportation, with total cost effectivity being the driver. Our tradeoff analysis is summarized in Table II-B-12. We traded Martin Marietta build versus supplier build and considered existing manufacturing equipment, capability, distance from site, and processing sequence (Table II-B-12). We were particularly critical of costs associated with mirror holder fabrication and mirror assembly costs since 25 are required for each heliostat.

We selected a local Albuquerque supplier for yoke module fabrication because of close proximity to the site and available supplier capability for final alignment of the drive unit torque tube. The same supplier was selected for mirror holder fabrication because of existing hoop rolling and final hoop straightening capability. In both cases, acquisition costs to properly equip the Kirtland AFB (KAFB) assembly building made that selection prohibitive. Fabrication costs at our Denver facility plus transportation costs to the site made that choice more costly than the Albuquerque supplier.

Table II-B-12 Heliostat Manufacturing and Assembly Site Selection Rationale

ITEM	QUANTITY PER HELIOSTAT	DESCRIPTION	ENVELOPE SIZE	UNIT WEIGHT, kg (lb)	MANUFACTURING ALTERNATIVES			RATIONALE FOR SELECTION
					KIRTLAND AFB ASSEMBLY BUILDING	ALBUQUERQUE SUPPLIER	MARTIN MARIETTA DENVER FACILITY	
HELIOSTAT PROTO-TYPE	1 ONLY	STRUCTURAL, ELECTRICAL, ELECTRONICS FABRICATION AND ASSEMBLY	0.46x6.4x7.3 m (1½x21x24 ft)	2722 (6000)			X	ALLOWS FABRICATION, ASSEMBLY, AND CHECKOUT AT EXISTING OPERATING SOLAR FACILITY PRIOR TO PRODUCTION COMMITMENT.
YOKE MODULE	1	WELDED STRUCTURAL STEEL	0.3x4.27x4.27 m (1x14x14 ft)	1089 (2400)		X		SUPPLIER HAS EXISTING CAPABILITY AND CAPITAL EQUIPMENT LOCATED NEAR INSTALLATION FACILITY.
MIRROR RACK	1	WELDED STRUCTURAL STEEL	0.15x6.1x6.9 m (½x20x22½ ft)	680 (1500)	X	X		SUPPLIER WILL CUT AND NOTCH MATERIAL. ASSEMBLY WILL BE PERFORMED AT KAFB TO MINIMIZE TRANSPORTATION PROBLEMS.
MIRROR HOLDER	25	FORMED & WELDED STRUCTURAL STEEL	117 cm x 5 cm (46 in. dia x 2-in. WIDE)	14 (31)		X		SUPPLIER HAS EXISTING CAPABILITY AND CAPITAL EQUIPMENT LOCATED NEAR INSTALLATION FACILITY.
MIRROR HOLDER & MIRROR INSTALLATION WITH RACK	25	MECHANICAL ATTACHMENT OF MIRROR HOLDERS TO RACK—STRUCTURAL BONDING OF MIRRORS TO HOLDERS	0.15x1.2x1.2 m (½x4x4 ft)	1633 (3600)	X			MINIMIZES TRANSPORTATION AND POTENTIAL MIRROR BREAKAGE. MIRROR BONDING TIME AND TOOLING COSTS ARE REDUCED.

Our analysis led to selecting the KAFB assembly building for mirror rack assembly and mirror installation. Structural steel members will be cut to length, drilled and notched by the steel supplier, then weld-assembled at the site. That sequence was chosen to assure control of mirror holder bracket positioning, mirror interchangeability, and total rack assembly cost effectiveness by utilizing the rack as an in-line holding fixture for mirror bonding. A comparison was made of bonding mirrors individually to mirror holders then installing on the rack or with installing holders on the rack and then bonding the mirrors to the installed holders. The latter method was selected since it eliminates at least 37.16 m (400 ft²) of bench work surface and reduces potential mirror breakage.

We have analyzed mirror adhesives and to date have reduced the cure time from 24 to 2 hours. This analysis is continuing to assure selection of an acceptable single component adhesive with comparable two-component adhesive physical properties, thus eliminating weighting, mixing, and deaerating times. Our proposed structural manufacturing flow sequence is shown in Figure II-B-32.

b. *Yoke Module* - The heliostat yoke module consists of a horizontal 35.56x35.56x1.27-cm (14x14x $\frac{1}{2}$ -ft) wall x 4.1-m (13.5-ft) long square steel tube, and two vertical 35.6-cm (14-in.) wide-flange I-beams 3.66-m (12-ft) long. The square tube will be notched at each end and a hole provided for a center support tube. The vertical I-beams will be notched at the top for the rack support tube. The tubes and I-beams will be welded to form the yoke, then attachments will be provided for electrical components. The yoke will be fabricated at a local Albuquerque structural facility then shipped to the 5-MW test facility staging area.

c. *Mirror Holder* - The mirror holder is a 1.67-m (46-in.) diameter steel hoop with a welded tubular X-brace and two adjustment tabs. Twenty-five mirror holders are required for each heliostat. The 1.67-m (46-in.) diameter hoop will be made by roll-forming a 5.71-cm wide x 0.48-cm thick x 365.7-cm long (2 $\frac{1}{4}$ -in. wide x $\frac{3}{16}$ -in. thick x 144-in. long) strip, then butt welding the ends. Square tubing 3.8x3.8x0.21x116.8-cm (1 $\frac{1}{2}$ x1 $\frac{1}{2}$ x0.083x46-in. long) will be welded to form the X-brace, then

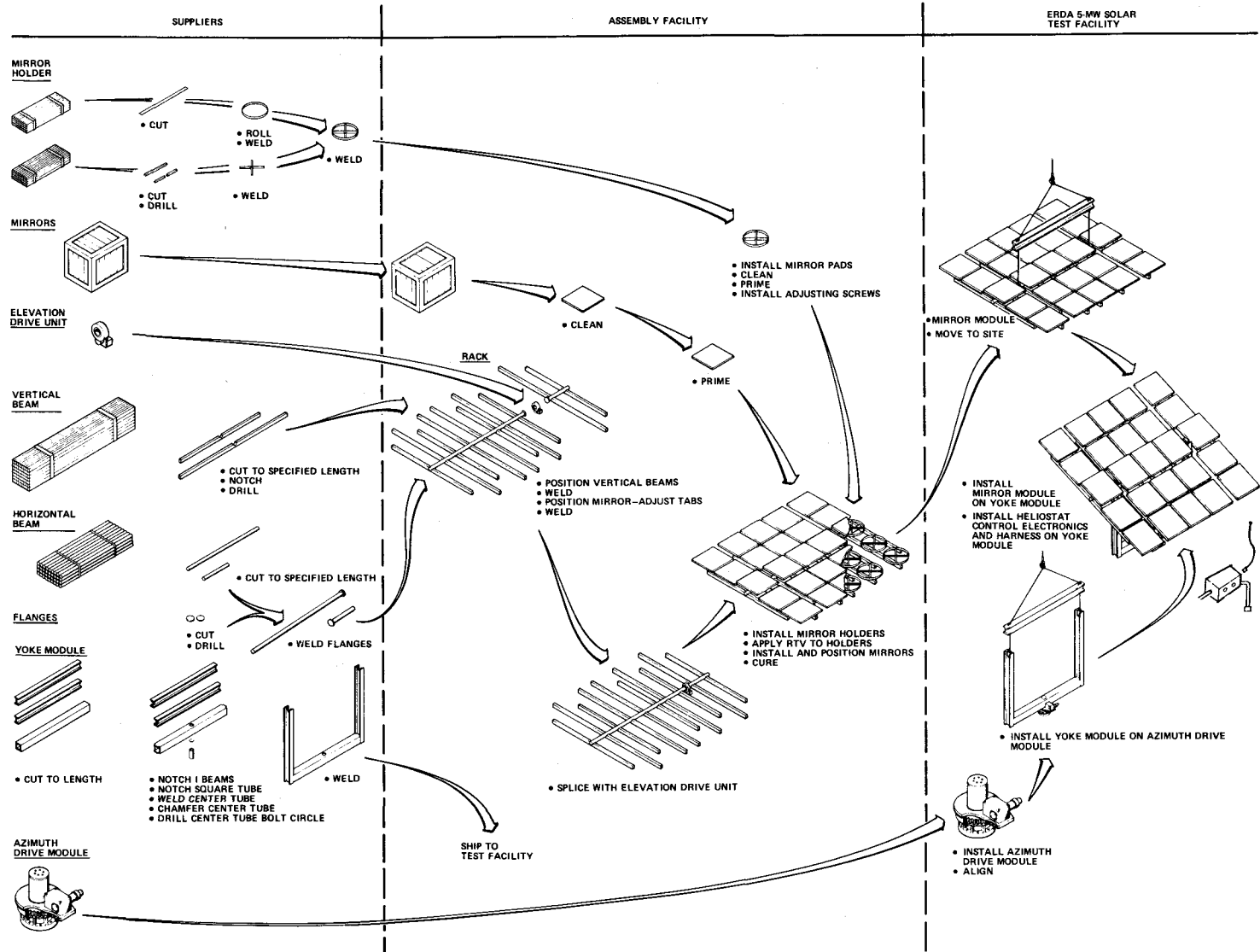


Figure II-B-32 Heliostat Manufacturing/Site Installation Flow Sequence

welded to the hoop. Flatness of the hoop must be verified after welding to provide a continuous interface with the mirror. Mirror holders are to be fabricated at a local Albuquerque structural steel shop, then shipped to the KAFB.

KAFB activities include attaching the mirror focus pad to the cross brace, adjusting the pad to be flush with the mirror attachment surface of the ring, then cleaning and priming the RTV bond surfaces of the ring and pad. The mirror holders are then stored until ready for installation with the mirror rack.

d. Rack - Our plan is to perform the rack final weld assembly in the Kirtland AFB hangar using steel structural members that have been precut, notched, drilled, and attachment flanges welded and aligned by the material supplier.

The first operation will be to bolt the horizontal tubes together using a spacer spool, then position the subassembly in the weld fixture shown in Figure II-B-33. Assembly will continue by placing the 4.71x10.16-cm (2½x4-in.) rectangular tubes one at a time in the fixture, mating with the 14.13-cm (5.562-in.) diameter tubes, then welding. After each pair of rectangular tubes have been welded, mirror adjusting tabs will be welded to the rack using the positioning fixture shown in Figure II-B-34. This procedure will continue until all rectangular tubes have been welded. The weld fixture will position the rack high enough to allow easy welder access to both sides eliminating the need to rotate the rack for final welding. The mirror rack will then be removed from the weld fixture and positioned on the work pedestals.

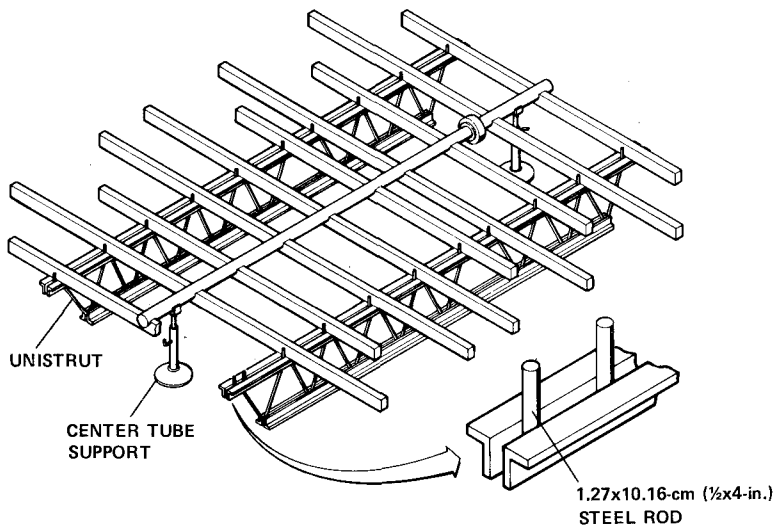


Figure II-B-33 Mirror Rack Weld Assembly Fixture

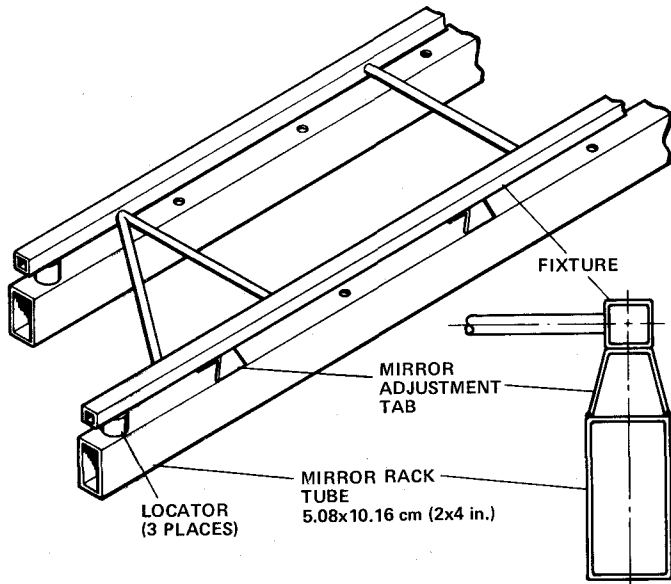
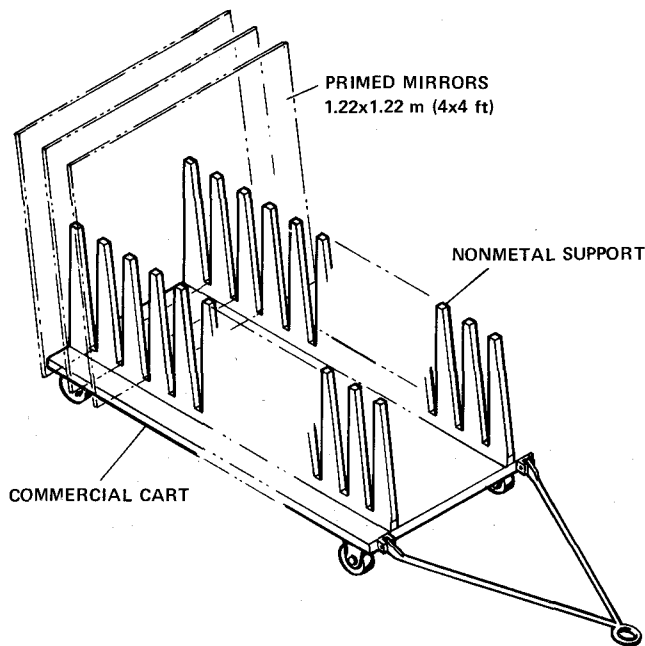


Figure II-B-34 Mirror Adjustment Tab Welding Fixture

The spacer spool will be removed and the elevation drive unit will be mated to the rack. Beginning at the edge of the rack, mirror holders will be attached, one row at a time. RTV will be applied to the ring and center mirror adjusting pad of each holder. Cleaned primed mirrors (Fig. II-B-35) will be positioned on each mirror holder, reflective side up. This procedure will continue



*Figure II-B-35 Mirror Handling Dolly
(Will Transport 25 Primed Mirrors)*

for all five rows, then RTV will be allowed to cure at room temperature until the last mirror installed has been cured.

Using the mirror module spreader bar and the portable crane, completed mirror modules will be loaded into the mirror module transporter (see Figure II-B-36). The trailer has capacity for three completed mirror modules. Surge storage will be provided in the hangar for 10 completed modules.

e. Electrical/Electronic - The heliostat control electronics assemblies for the heliostat will be fabricated, assembled, and tested at one of our electronics manufacturing facilities in Denver.

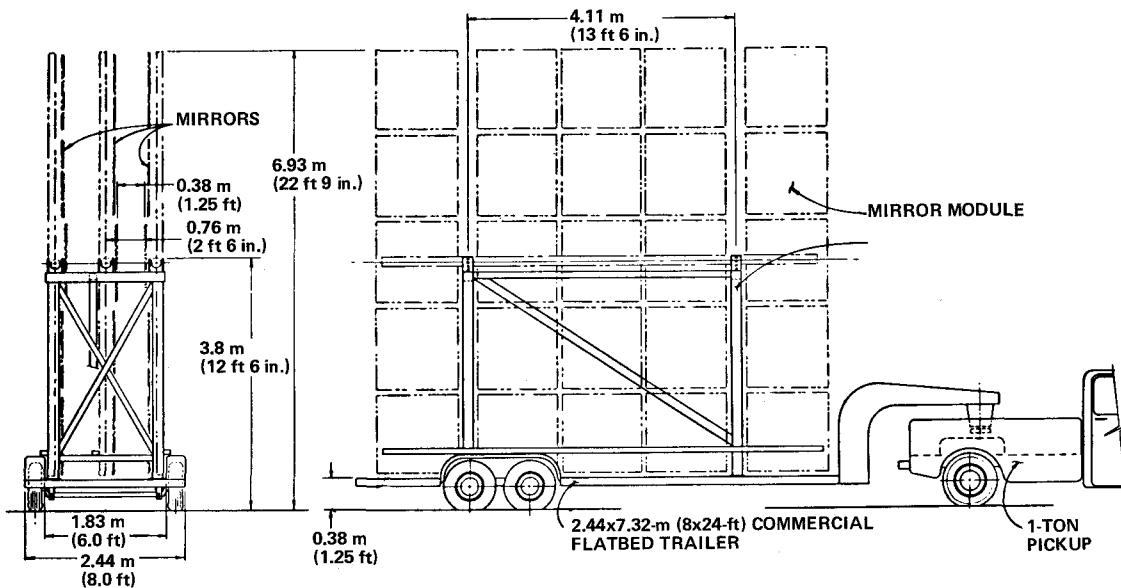


Figure II-B-36 Mirror Module Transporter

The manufacturing objective is to fabricate, assemble, and deliver reliable hardware economically and on schedule. Manufacturing will input concepts and approaches for the unit design during the preliminary design phase. This coordinated effort in the design phase will permit easier fabrication and testing during the actual build of the hardware.

All heliostat control electronics will be delivered to a staging area at the 5-MW test facility. We are retaining the option as to whether the HCE and wire harness will be installed on the heliostat yoke module prior to its delivery to the installation site or at the time of heliostat final installation.

The heliostat harness will be developed and fabricated at our Denver facility. The installation point of this cable will depend on the approach finally selected for the control unit installation.

All design and packaging concepts considered for the control units have been previously used on Martin Marietta hardware, in particular, in commercial and NASA ground support programs.

The fabrication operations will be controlled by manufacturing process plans. This control is used to indicate to manufacturing and inspection personnel the fabrication operations, inspection points, documentation required (engineering drawings, test specifications, etc), special handling requirements, and final acceptance test requirements.

The manufacturing and delivery flow sequence for the heliostat control electronics assembly is presented in Figure II-B-37 and that for the manual control unit in Figure II-B-38.

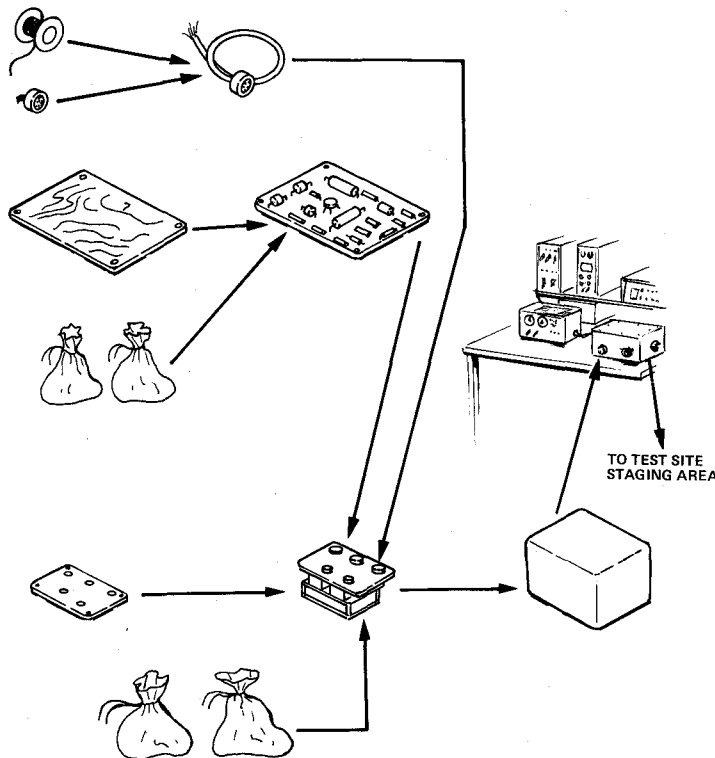


Figure II-B-37 Heliostat Control Electronics Manufacturing Flow

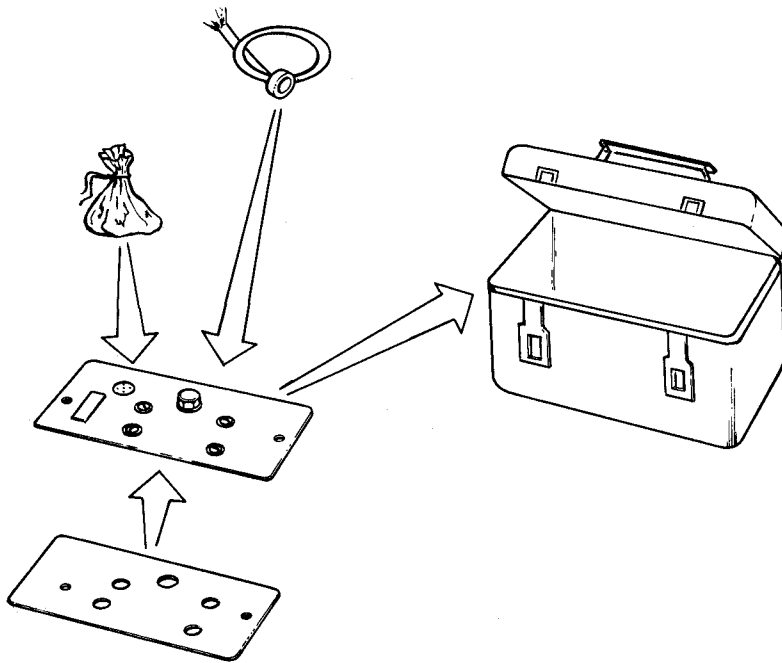


Figure II-B-38 Fabrication of Manual Control Box

7. Interfaces

The HASS must accommodate interfaces that are both physical (HACSS, facility) and functional (focus and alignment, calibration). The compatibility of these interfaces are of prime significance because of the relatively short span time permitted for heliostat installation, checkout, calibration, and acceptance.

a. HACSS/HASS (HIM-HCE) Interfaces - The data interfaces between HACSS and HASS are shown in Figure II-B-39. HAC will output data through an optically coupled isolator to a differential current-mode line driver. The line driver will interface with a twisted shielded pair that runs approximately 600 m (1968.5 ft) maximum to the first of 32 heliostats. Differential line receivers will receive the serial data at each heliostat.

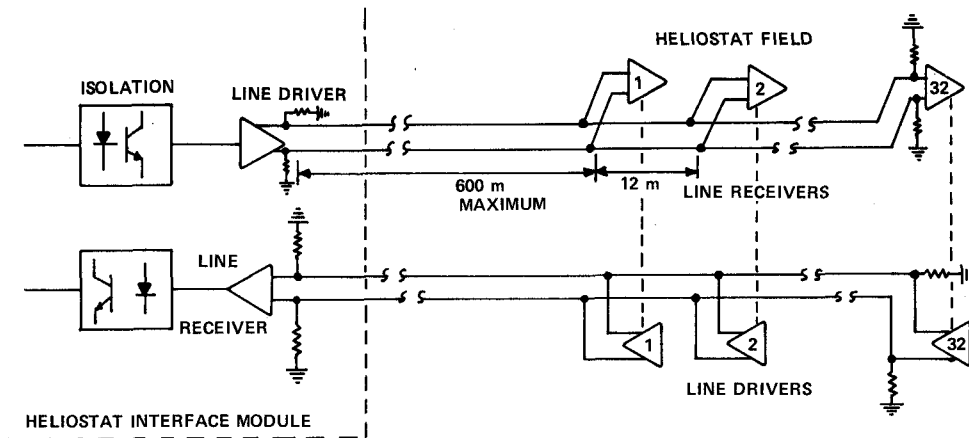


Figure II-B-39 Typical Interface Between Heliostat Interface Module and Heliostat Control Electronics Assemblies

Each receiver will be isolated from the electronics in each heliostat by optical couplers and isolated power supplies.

HAC/HIM output will be messages consisting of 7 characters (a character is the basic word made up of 8 bits). A character format will be used that consists of 8 bits of data, 1 parity bit, 1 start bit, and 2 stop bits (Fig. II-B-23). This scheme is being used on other long-line computer/peripheral interfaces at Martin Marietta with excellent results. The first character of the message will consist of 5 address bits, a sync bit, and 2 spare bits. Every heliostat will receive this character. One of the 32 decoders looking at this character will recognize it and open a gate accepting the next 6 characters. Each of these characters will contain 8 bits of data. The data will be marking one for 10 bit times prior to the start of a block of 32 messages (a message is the group of 7 characters) and for 5 bit times between messages. This will synchronize all 32 receiving heliostats to start looking for an address. If the first

character of the message does not contain the proper sync bit, the character will be rejected until a character with the proper sync is received.

A block of 32 messages will be sent once a second to all four groups of 32 heliostats.

The return data format will be the same as the received data. A separate line for 32 line drivers will be provided. Only one 3-state driver will be active or enabled at one time. Thirty-one drivers will be in a high-impedance output state while one is active. A particular heliostat line driver will go active at acceptance of that heliostat address. It will go inactive at the completion of data transmission from that heliostat. The required data rate between the HAC and the heliostats is computed as follows, assuming an 8-bit data word, 1 start bit, 2 stop bits, and a parity bit:

$$(12 \text{ bits/word}) \times (7 \text{ words/message}) \times (32 \text{ messages}) \\ \div (1 \text{ s} - 170 \text{ bit times}) = 2858 \text{ baud.}$$

The maximum transmission rate capability of the 6-mA current driver in conjunction with our line lengths is calculated by the following:

- 1) 600 m from HAC to field;
- 2) 12 m x 12, spacing between heliostats;
- 3) 3 m x 32, stub lengths;
- 4) 1080 m = total line length.

Capacitance per meter of twisted shielded pair (Belden 8227) is approximately 50 pF. Total line capacitance is $50 \times 1080 = 54000$ pF. Driver output current capability - load = $6.5 \text{ mA} - 32 (0.150) = 1.7 \text{ mA}$:

The time to translate through a 0.025-V receiver sensitivity band is

$$t = \frac{54000 \times 10^{-12} (0.026)}{0.0017} = 0.82 \text{ } \mu\text{s}.$$

Considering that data should be allowed to stabilize for at least 4 times the translation time, this would give an effective data rate of $\frac{1}{4(0.82)10^{-6}}$ or 303 kbaud. This number agrees with both manufacturer's data regarding the capability of this part and our tests results.

In conclusion, the above calculations show the long-line system is capable of data rates far in excess of the 2.858-kbaud requirements.

b. HASS/Facility Interfaces - The overall electrical interfaces of the heliostat are shown in Figure II-B-26. Figure II-B-40 reflects the specific electrical interfaces at the heliostat foundation.

Power - There will be four 117-Vac receptacles at the foundation to provide power of the quality described in Section C. The 117-Vac receptacle outlets are required for (1) direct interface with the controller, (2) maintenance lighting and power tools, (3) focusing and alignment equipment, and (4) spare. In addition, a 208-Vac 3-phase receptacle will be used for the focusing and

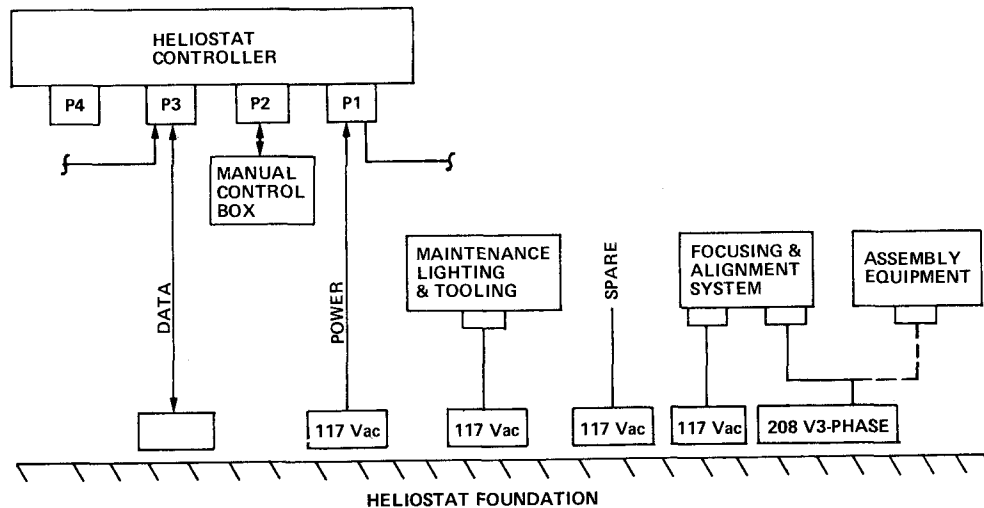


Figure II-B-40 HelioStat/Foundation Electrical Interfaces

alignment subsystem during initial heliostat setup and subsequent focusing and alignment operations. Each of the five power outlets will be protected by appropriately sized circuit breakers. Outlet weatherproofing will be provided at each service entrance by use of Insulprene weatherproof triple seal covers or equivalent, as shown in Figure II-B-41.

Control - The control interface will be in the same location as the power interface between the heliostat and its foundation. This interface will comprise two twisted shielded pairs of wires. The commercial circular multicontact connector will be the same as those used on the heliostat control electronics. It will be protected from the weather environments in the same manner as the power connectors.

6 OUTLETS:
4 117 Vac
1 208 V 3 PHASE
1 DIGITAL

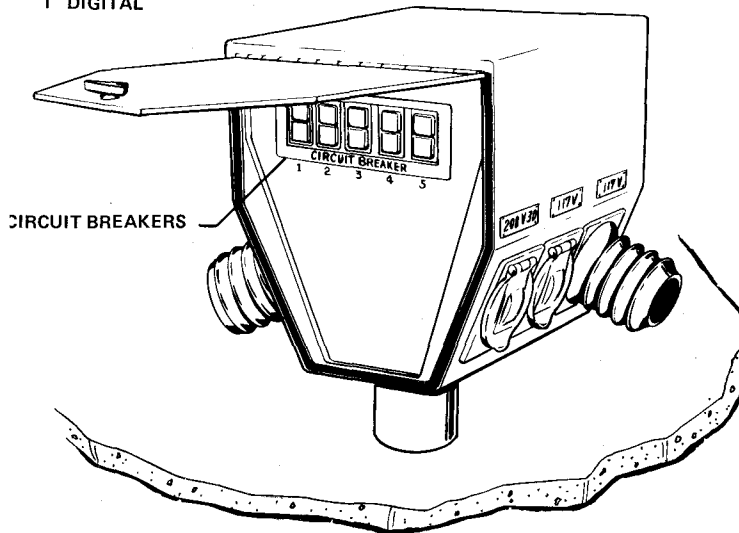


Figure II-B-41 Outlet Center at Heliostat Foundation

c. *HASS/FASS Interfaces* - A functional and a physical interface exists between the HASS and the FASS. The functional interface provides for the mirror focusing and heliostat alignment when utilizing the FASS. The physical interface is accomplished at the heliostat foundation where facility power is provided for the FASS.

d. *HASS/CSS Interface* - The only interface between the HASS and the CSS is functional--the ability to position the mirrors to reflect the sun's ray to the calibration target on the facility tower. This control is exercised through the HACSS, under control of the calibration subsystem.

C. Heliostat Array Control Subsystem

C. HELIOSTAT ARRAY CONTROL SUBSYSTEM (HACSS)

The HACSS will link the master control system (MCS) to the heliostats as shown in Figure II-C-1. Each HACSS may contain up to six heliostat array controllers (HACs) and up to six heliostat interface modules (HIMs). Six HACSS will control five zones of heliostats (one HAC for each of zones A, C, D, and E, and two HACs to allow control of 216 heliostats in zone B). The HACSS will interface with the master control system through one 9600-baud asynchronous line using universal asynchronous receiver/transmitter (UAR/T) couplings. Table II-C-1 presents a compilation of the major requirements the HACSS must satisfy and our approach to meeting these requirements. (See Volume IV, Addendum III for the preliminary HACSS requirements specification.) We will buy the HAC as an off-the-shelf minicomputer and build the HIM unit - as indicated in Figure II-C-2.

The HAC will communicate with individual heliostats through the heliostat array interface module (HIM). HIM will receive heliostat command data from HAC and multiplex and route the data to the appropriate heliostat line and the heliostat control electronics (HCE), which is part of the heliostat array subsystem. HIM will also relay data from HCE to HAC. HIM units that are capable of reliably driving 32 devices over 600- to 1000-m (1968.5- to 3280-ft) lines at the data rates will use are not commercially available at reasonable costs.

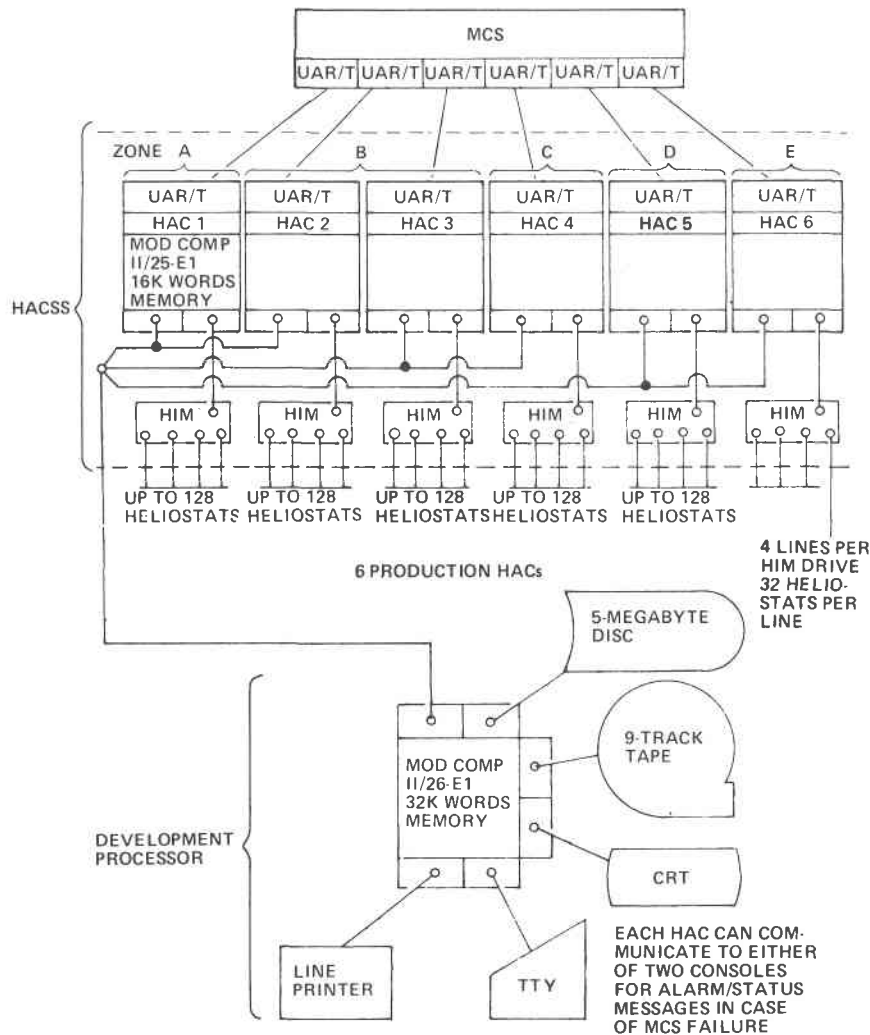


Figure II-C-1 MCS-HACSS Functional Schematic

1. Control Loop

A block diagram of the HACSS is shown in Figure II-C-3. Control mode commands (standby, on-target, etc), sun position, and target position will be transmitted from the facility master control system to the heliostat array controllers. Each HAC will calculate the required azimuth and elevation gimbal angles and transmit the angle and mode commands to the heliostats over serial data buses. The gimbal angles will be calculated as a function of sun position, target position, and heliostat location.

Table II-C-1 Heliostat Array Control Subsystem Major Requirements and Proposed Approach

ITEM	KEY RFQ REQUIREMENTS	K93681 PARA.	PROPOSED APPROACH
1.	HELIOSTAT CONTROLLER TO MAINTAIN REFLECTED RAYS ON SOLAR EXPERIMENTS ON TOWER; INDIVIDUAL CONTROL OF EACH HELIOSTAT	3.1.3.1	COMPUTER/SOFTWARE WILL CONTROL AND MONITOR EACH HELIOSTAT. POINTING PARAMETERS WILL BE PLACED IN COMPUTER MEMORY AT TIME OF HELIOSTAT CALIBRATION.
2.	HAC CAPABILITIES CONTROL POSITION AND MONITOR UP TO 128 HELIOSTATS INTERFACE WITH MCS; RESPOND TO DIGITAL SIGNAL FROM MCS; FULL-DUPLEX COMMUNICATION; 9600-baud DATA RATE STORE STANDBY COORDINATES ELECTRICAL CHARACTERISTICS CONFORM TO EIA RS-232-C	3.1.3.2 3.1.3.2 3.1.3.2b 3.1.3.2 3.1.3.2a	COMPUTER/SOFTWARE WILL CONTROL UP TO 128 HELIOSTATS. WILL PROVIDE COMPATIBLE INTERFACE ELECTRONICS AND SIGNAL LEVELS. DATA WILL BE STORED IN HELIOSTAT ATTRIBUTE TABLE IN COMPUTER MEMORY. UAR/T WITH 9600 baud WILL INTERFACE WITH MCS.
3.	TRANSMIT HELIOSTAT POSITION INFORMATION WITHIN 50 mrad	3.1.4.3c	WILL PROVIDE ENCODER WITH 24.6 mrad ANGULAR RESOLUTION FOR EACH HELIOSTAT AXIS.
4.	MODES OF OPERATION ACQUISITION IN LESS THAN 15 MINUTES; STANDBY POSITION OFF THE EXPERIMENT POWER, INTO EXPERIMENT, OR REDUCTION TO ZERO WITH HELIOSTAT SLEW RATE OF 2 mrad/s OR FASTER STANDBY, WHEN SUN IS OBSCURED AND WHILE IN POWER MODE; PROVIDE SUN SENSOR FOR AT LEAST 10% OF HELIOSTAT ZONE MANUAL FOR MAINTENANCE AND SETUP; ALL OTHER MODES LOCKED OUT STOW IN LESS THAN 15 MINUTES FROM STANDBY POSITION EMERGENCY SHUTDOWN, RESPOND WITHIN 5 sec, THEN TO STOWAGE IN LESS THAN 15 min FAIL-SAFE FROM FACILITY FAILURE AND LOSS OF COMMERCIAL POWER; RETURN TO STOWAGE IN LESS THAN 15 min	3.1.4.4 3.1.4.4.a 3.1.4.4b 3.1.4.4.c 3.1.4.4d 3.1.4.4e 3.1.4.4f 3.1.4.4g	COMPUTER WILL CONTROL OPERATIONAL MODES. HELIOSTAT DRIVE SYSTEMS: AZIMUTH 3.66 mrad/s (755 deg/hr), 135 deg IN 10.73 minutes HELIOSTAT DRIVE SYSTEM: ELEVATION 4.95 mrad/s (1133 deg/hr), 270 deg IN 14.29 minutes WILL PROVIDE ONE SENSOR FOR AT LEAST EACH 10 HELIOSTATS. WILL PROVIDE MANUAL (LOCAL) CONTROL PANEL FOR HELIOSTAT CONTROL. CONTROL PANEL LOCKS OUT COMPUTER CONTROL. WILL PROVIDE HELIOSTAT DRIVE SYSTEMS WITH SLEW RATE CAPABILITY OF 4.95 mrad/s (1133 deg/hr), 270 deg IN 14.29 minutes STOWED POSITION ANGLES WILL BE STORED IN COMPUTER MEMORY FOR CONTROL OF HELIOSTAT POSITION. WILL STORE DATA IN COMPUTER MEMORY FOR HELIOSTAT POSITION CONTROL AND PROVIDE HELIOSTAT DRIVE SYSTEMS CAPABLE OF SLEWING 270 deg IN 14.29 minutes WILL UTILIZE FACILITY BACKUP POWER SOURCE. COMPUTER WILL EMPLOY BATTERY BACKUP SOURCE TO MAINTAIN MEMORY.

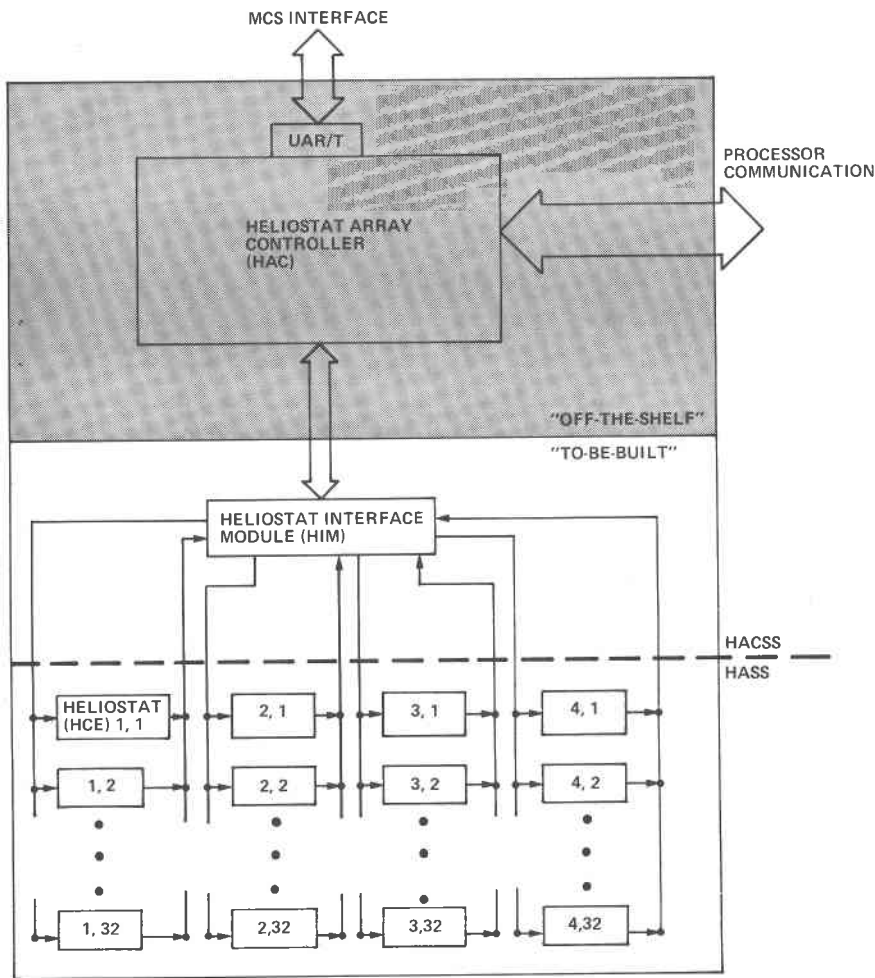


Figure II-C-2 HelioStat Array Control Subsystem (HACSS)

The heliostats will be driven by either fast slew motors or slower tracking motors through gear drives. The slew mode is for acquisition (bringing the heliostat to a standby position) and for moving the heliostat to the stow position either for normal stowage or for emergency shutdown. The tracking motor is for continuous tracking either in the coarse tracking/standby mode of operation or in the fine-tracking/on-target mode.

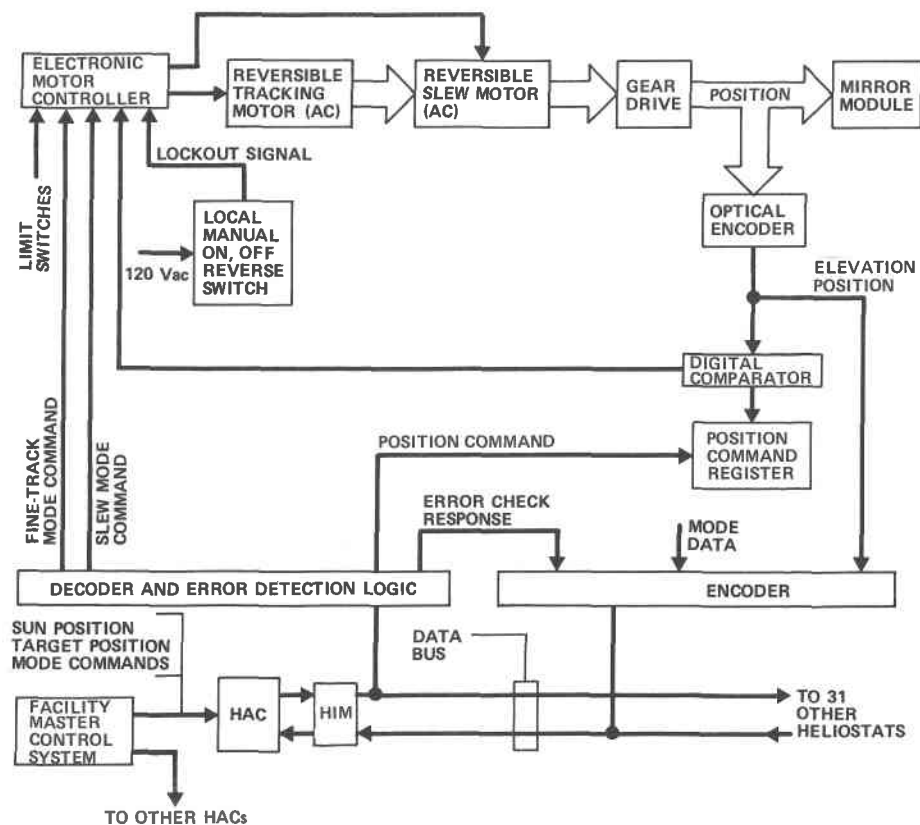


Figure II-C-3 Heliostat Control System Block Diagram (One Axis)

The control loop will use absolute optical encoders to determine actual gimbal positions. The actual gimbal position will be digitally compared to the commanded position; the resulting position error signal will turn on either the tracking motor or the fast slew motor, depending on the mode command, in a direction determined by the sign of the position error. The actual gimbal positions will be transmitted by the data bus to the HAC where they will be available when a status command is received from the MCS.

A manual control panel will connect with any heliostat to allow manual control of azimuth and elevation. Connection of the manual control panel will lock out data bus control yet retain heliostat status feedback. A sun-present sensor (SPS), located on at least every tenth heliostat, will determine sun presence and transmit that information to the HAC and thence to MCS. If sun presence is lost with heliostats in the power mode, the HAC will automatically compute standby positions (offset from the target) and command those positions. When the sun becomes present again, the HAC will continue to transmit standby commands to the heliostat until until commanded on target by the MCS.

We built a laboratory breadboard demonstration system to evaluate the control loop. A photograph of the test setup is shown in Figure II-C-4, and Figure II-C-5 is a block diagram of the setup. Our objectives were to evaluate:

- 1) Long transmission line and transmitter/receiver compatibility;
- 2) Effects of 32 receivers on one line that is long between individual receivers;
- 3) Data rate margin;
- 4) Compatibility of the UAR/T with wiring and data simulating the actual system;
- 5) Data errors possible with various sync and space character arrangements;
- 6) Servo response with actual gear ratios, encoders, ac motor, and drive electronics;

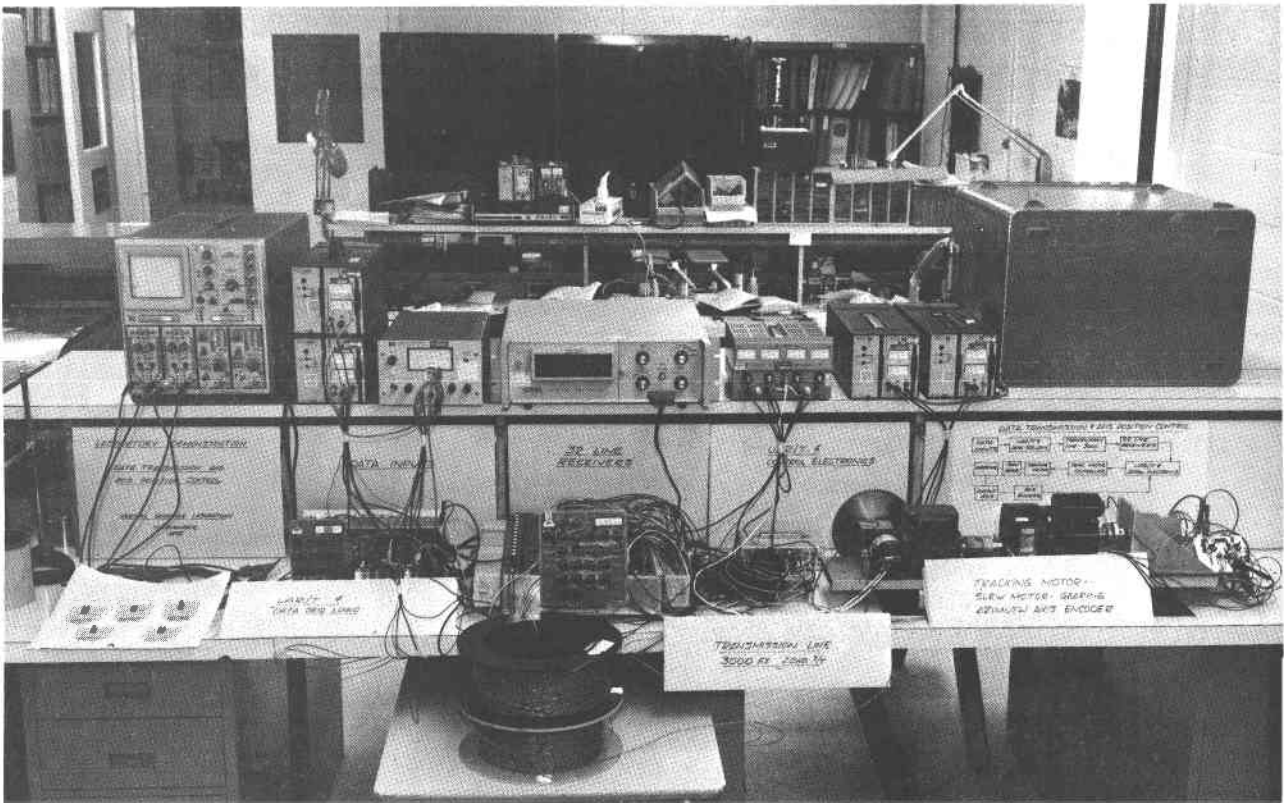


Figure II-C-4 Block Diagram of Breadboard Data Transmission and Control System

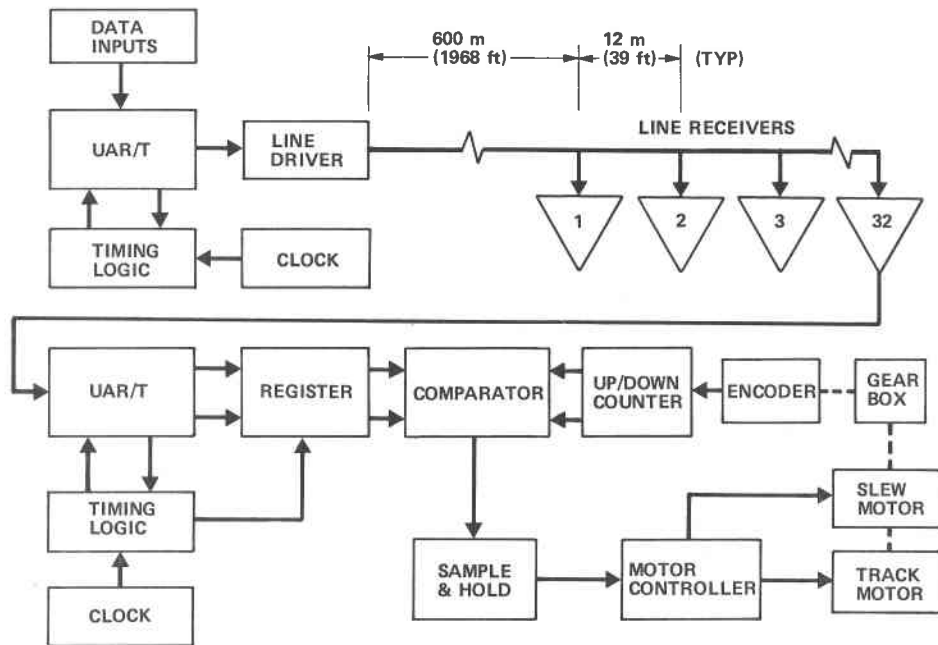


Figure II-C-5 Block Diagram of Breadboard Data Transmission and Control System

- 7) Servoloop and gearing mechanisms' influence on positioning errors;
- 8) AC motor drive techniques;
- 9) Electromagnetic interference effects.

The capability of the breadboard test setup is illustrated in Figure II-C-4 and includes:

- 1) A 12-bit manual data input control unit;
- 2) A UAR/T unit with associated clock and timing logic connected to one line receiver;
- 3) A line driver, 600-m (1985-ft) transmission line using two-conductor shielded/twisted cable, and 32 line receivers spaced apart with 12 m (39.7 ft) of cable;
- 4) A register to hold position command word;
- 5) A digital comparison of the actual and commanded positions;
- 6) Solid-state controllers for both the tracking and slew motors;
- 7) A tracking motor, Superior Electric Slo-syn, with 50-oz.-in. output torque at 200 rpm;
- 8) A Bodine 1/12-hp, 1700-rpm, 180 to 1 gearhead reducer unit;
- 9) An Ohio Gear Co. #8-133 40-to-1 reducer driving a 6-to-1 reduction spur gear stage;
- 10) An output encoder, Sequential Information Systems model #25D10241DZ-MADZ1A driving an up/down counter that provides actual position data to the control system comparator. Since an incremental encoder was the only available sensor, it was used in lieu of an absolute encoder.

Simulation tests using the breadboard have shown that 350 kilobaud can be successfully transmitted over 600 meters to 32 receiving stations, each separated by 12 meters. There have been no data errors as a result of the long lines and receiver loads.

The electronic ac motor drive developed for the breadboard is compatible with both the Slo-Syn tracking motor and the Bodine slew motor.

The gear reduction drive to the output axis and position encoder simulates the azimuth drive ratio and provided closed-loop positioning with the required accuracy (1 mrad).

The encoder output pulse integrated by the up/down counter provides an actual axis position signal of the required accuracy. The physical mounting of the encoder relative to the output axis is critical and must be solid and deflection free.

2. Heliostat Array Controller

The HAC is the nucleus of the subsystem. It is under control of the master control system but must be capable of limited decision-making by itself in case of system failure. The HAC will insure responsive, economical, and fail-safe operation of a heliostat array. It will perform all necessary computations with liberal system growth capability and in addition will provide versatile, unrestricted software development and usage capabilities during the life of the project. The HAC will operate alone or in a combination of six HACs that, under MCS control, can operate up to five zones of heliostats. The HAC production computer must:

- 1) Service nine 11-bit messages (8-bit data word) from MCS over 9600-baud asynchronous RS-232-C line through UAR/T-type interface;
- 2) Execute 34,000 heliostat position control calculation instructions each second;
- 3) Perform 1792 word transactions per second (seven 8-bit commands and seven 8-bit status responses from each heliostat);
- 4) Provide hardware floating-point arithmetic.

These requirements will be satisfied by the production computers.

To prevent development, maintenance, or modification work from interfering with or impeding normal heliostat array testing, our system includes a development processor that will serve multiple purposes;

- 1) Control interprocessor communication including HAC loading;
- 2) Support source input, compiling, assembling, testing, and editing;
- 3) Allow easy input of vendor-supplied system software (by magnetic tape);
- 4) Provide fast hardcopy output;
- 5) Support software development;
- 6) Provide off-line processing/storage (primary storage on disc and backup storage on magnetic tape);
- 7) Be capable of supporting HAC operations.

Advantages to be gained through this configuration are:

- 1) Reduced costs through elimination of low-usage peripheral devices such as secondary storage units and separate interface consoles;
- 2) Reduced operator requirements (one operator can easily handle operation of all five zones through one console);
- 3) Reduced maintenance costs (less devices).

a. Growth Capability - The HAC will have sufficient capability for normal software growth. Our experience in projects like those listed in Table II-C-2 indicates that software requirements for core storage and functions to be executed generally increase or "grow" during development. Therefore, we have allowed processor storage and timing margins for growth. At the start of software development:

- 1) Projected software storage space requirements should be approximately 50% of the available processor memory;
- 2) Projected timing requirement for execution of software functions should be approximately 60% of available processor timing cycle capacity.

Table II-C-2 Successful Software Systems

SYSTEM	CONTROLLER	TEST LANGUAGE AND/OR SOFTWARE SYSTEM
VIKING LANDER CAPSULE SYSTEM TEST EQUIPMENT	HONEYWELL 632	VIKING TEST LANGUAGE (VTL) INCLUDED AS PART OF THE SYSTEMS TEST EQUIPMENT SOFTWARE.
SKYLAB MEDICAL DATA ACQUISITION SYSTEM	VARIAN 620 F/I	SKYLAB MEDICAL DATA ACQUISITION SOFTWARE SYSTEM.*
SKYLAB MOBILE MEDICAL DATA ACQUISITION SYSTEM	VARIAN 620R (RUGGEDIZED 620I)	SKYLAB MOBILE MEDICAL DATA ACQUISITION SOFTWARE SYSTEM.*
DIGITAL DATA ACQUISITION AND TEST SYSTEM	XDS SIGMA 5	TEST INPUT LANGUAGE TRANSLATOR (TILT) INCLUDED AS PART OF THE DIGITAL DATA ACQUISITION AND TEST SYSTEM SOFTWARE.
TITAN III DATA RECORDING AND QUICK-LOOK DATA SYSTEM	VARIAN 620L	TITAN III DATA RECORDING AND QUICK-LOOK DATA SYSTEM SOFTWARE.*
ONBOARD CHECKOUT SYSTEM	IBM 4 PI-EP	TEST-ORIENTED ONBOARD LANGUAGE (TOOL) INCLUDED AS PART OF THE ONBOARD CHECKOUT SYSTEM SOFTWARE.
MARTRON® 1200/12000 AVIONICS LRU TEST SETS	HONEYWELL H316	ATLAS LANGUAGE COMPILERS USED TO GENERATE TESTS TO RUN ON THE MARTRON® 1200/12000 SOFTWARE SYSTEMS.
MARTRON® 12 JET ENGINE FUEL CONTROLLER TEST SET	DEC-PDP11	MARTRON® TEST TRANSLATION SYSTEM (MTTS) INCLUDED AS PART OF THE MARTRON® 12 SOFTWARE SYSTEM.
TITAN III MOL COMPUTERIZED AGE	TWO SDS SIGMA 7s	CAGE TEST LANGUAGE (CTL) INCLUDED AS PART OF THE COMPUTERIZED AGE SYSTEM SOFTWARE.
TITAN III SPACE LAUNCH VEHICLE AGE	TAPE PROGRAMMER	VEHICLE CHECKOUT SET SOFTWARE SYSTEM (VECOS).

*TEST PROGRAMS--IN ASSEMBLY LANGUAGE ONLY.

b. *Instruction Cycle Requirements* - We estimate 34,000 instruction cycles per second to position 128 heliostats in both axes. This is a worst case, but our analysis indicates that for 20% of the time during midday hours this is realistic, especially for south zone heliostats. Using the projected requirements, several alternative computer configurations were evaluated for their ability to meet timing requirements. The results shown in Table II-C-3 are discussed in the following paragraphs.

c. *Computer Interrupt Levels* - For immediate MCS response such as an emergency shutdown command, multiple-level interrupts will be provided with the following priority levels:

- 1) MCS commands;
- 2) Heliostat return status messages;

- 3) Control algorithm calculations;
- 4) Interprocessor communication.

To minimize possible interference from interrupts, we will use direct memory access (DMA) for heliostat communication.

d. Floating-Point Arithmetic - There is a slight cost penalty for hardware floating-point arithmetic. An alternative is software floating point. As seen in Table II-C-3 for computer configurations F, software floating-point requires a 77% duty ratio. Considering normal software growth, this initial margin is insufficient. The floating-point hardware in this case allows an average 35% duty ratio, which is acceptable. This is the average of computers B and H for the floating-point estimates of Table II-C-3.

Table II-C-3 Computer Timing Comparison

COMPUTER MANUFACTURER	MODULAR COMPUTER SYSTEMS INCORPORATED		DATA GENERAL CORPORATION		DIGITAL EQUIPMENT CORPORATION			
	A	B	C	D	E	F	G	H
COMPUTER CONFIGURATION	11/25-E1	11/25-E1 HARDWARE FLOATING POINT	NOVA 3-12	NOVA 2-10	PDP 11-04	PDP 11-04 SOFTWARE FLOATING POINT	PDP 11-35	PDP11-35 HARDWARE FLOATING POINT
COMPUTER MODEL								
CONTROL ALGORITHM INSTRUCTION MIX								
47% LOAD/STORE	6.2	6.2	2.4	2.5	15.3	15.3	7.9	7.9
23% ARITHMETIC	12.4	18.6	2.6	2.8	7.5	52.5	3.9	22.0
13% SHIFT	1.9		1.4	1.4	2.9		2.9	
17% REGISTER-TO-REGISTER	2.5	2.5	0.4	0.46	1.7	1.7	0.5	0.5
% DUTY RATIO FOR } CONTROL ALGORITHM INSTRUCTION/sec	23.0	27.3	6.8	7.2	27.3	69.5	15.2	30.4
% DUTY RATIO FOR } /sec FOR OPERATING SYSTEM	5.6	5.6	6.3	6.3	7.2	7.2	7.2	7.2
% DUTY RATIO FOR } /sec TOTAL CYCLES REQUIRED	28.6	32.9	13.1	13.5	34.5	76.7	22.4	37.6
% DUTY RATIO FOR } MARGIN (100 MINUS TOTAL ABOVE)	71.4	67.1	86.9	86.5	65.5	23.3	77.6	62.4

e. *Memory Estimate* - The memory estimate is 5K of algorithm program, 1.5K words of operating system, and 2K words of buffer table area for a HAC software total of 8.5K words of memory; therefore we recommend at least 16K-word memory.

f. *Selection of HAC Processor* - The HAC processor we will use is the Modcomp II/25-E1. This selection is based on the results of an extensive study of available and applicable minicomputers. This study involved evaluation of system requirements and software requirements, development of generalized computer specifications, solicitation of responses from interested vendors, elimination of nonapplicable systems, and several conferences with the top three vendors to develop the best configurations. The top three responses were from Modular Computer Systems, Inc. (Modcomp), Data General Corporation (Nova), and Digital Equipment Corporation (PDP). All three responses were essentially the same configuration. The final ratings resulted from delivery availability, machine characteristics, and computer availability over the projected lifetime of the project. Since the machine characteristics are essentially the same, Table II-C-4 tabulates delivery dates, and computer availability. Configurations B, C, and H have floating-point hardware.

Computer availability, as shown in Table II-C-4, during the lifetime of the project will reduce maintenance costs and allow easy configuration expansion and/or modification. Only configurations B and C can really offer any continuity at this time. In order to insure schedule performance, we must be able to start

using the computer within 50 days from award-of-contract. Only configuration B offers 45-day delivery. Configuration B represents the Modcomp computer as shown in Table II-C-3.

Table II-C-4 Computer Availability Comparison

COMPUTER CONFIGURATION	A	B	C	D	E	F	G	H
COMPUTER DELIVERY DATE IN DAYS FROM RECEIPT OF ORDER	45	45	60	80	90	90	90	90
COMPUTER MODEL AVAILABILITY DURING PROJECT LIFE	CURRENT MODEL	CURRENT MODEL	NEW MODEL	MODEL BEING REPLACED IN 1976	MODEL BEING REPLACED IN 1976	MODEL BEING REPLACED IN 1976	MODEL BEING REPLACED IN 1976	MODEL BEING REPLACED IN 1976

The Modcomp model II/25-E1 computer to be used in the production units offers the following capabilities:

- 1) Arithmetic unit;
- 2) Read-only control memory;
- 3) Modular bus control interface;
- 4) 16,384-word core memory (800 ns);
- 5) General register file (15 hardware registers);
- 6) Register I/O and three interrupts;
- 7) Operator console;
- 8) Rack-mountable enclosure and power supplies;
- 9) Hardware fill;
- 10) Multiply/divide;
- 11) Floating-point hardware;
- 12) Power fail-safe/automatic start;
- 13) Memory parity;
- 14) Director memory processor (DMP).

In addition to the above features, the development processor model II/26-E1 offers:

- 1) 32,768 words of core memory,
- 2) 5.2-megabyte dual-cartridge moving head disc;
- 3) 9-track 45-ips magnetic tape;
- 4) 50 to 150 lpm printer;
- 5) CRT operator console;
- 6) ASR-33 teletype console.

g. HAC Capabilities - Our HAC will provide:

- 1) Immediate response to MCS commands;
- 2) Fail-safe control of up to 128 heliostats per HAC;
- 3) 1-Hz service to each heliostat;
- 4) Control of up to six array controllers in five zones;
- 5) Easy access to heliostat position data for input and modification purposes;
- 6) Retention of standby position for each heliostat;
- 7) Immediate availability of station information on any heliostat;
- 8) MCS interface to each HAC via 9600-baud asynchronous RS-232-C line and UAR/T computer coupling.

3. Software Design Concepts

Our software system will meet or exceed the requirements for response to the MCS, provide fail-safe control of up to 128 heliostats per HAC, perform all required computations, and be easily modified. Through its interdevice communication concept it will

minimize both operational and physical requirements. It will maximize use of off-the-shelf vendor software thereby minimizing development effort and risk.

Our software will be modular and use high-order language in the development phase. Modular software greatly reduces maintenance and modification costs and allows parallel and simultaneous group programming through careful module interface definition.

a. *Software Planning* - The phases and documentation of Figure II-C-6 will provide systematic development of the software subsystem. The documentation will provide easily understood system definition and user

instruction *before* system delivery. Our software system plan will assure the orderly hardware/software event relationship of Figure II-C-7 that shows how we will coordinate HAACS development.

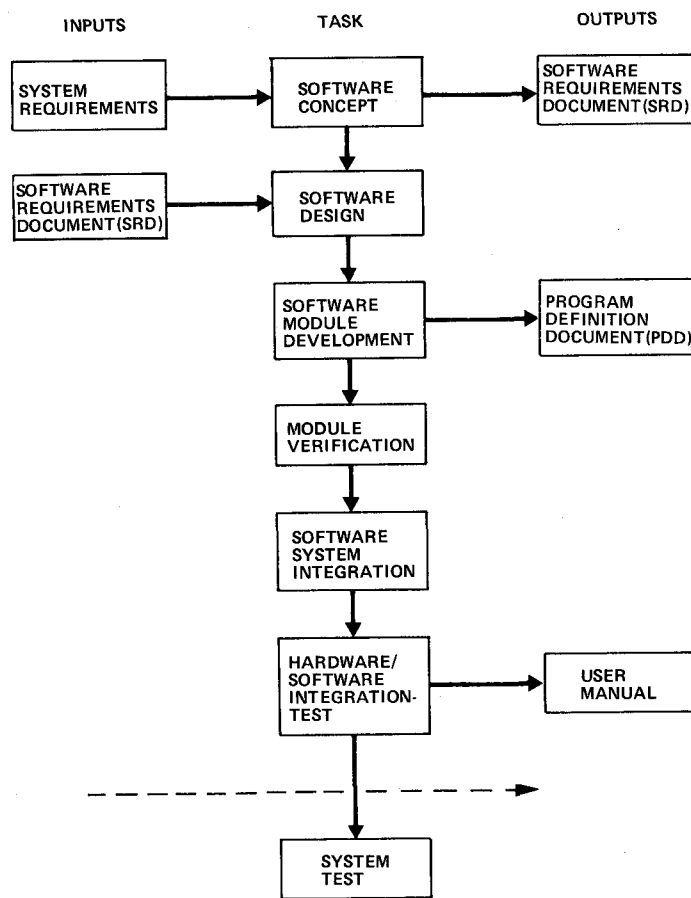


Figure II-C-6 Software Planning Guide

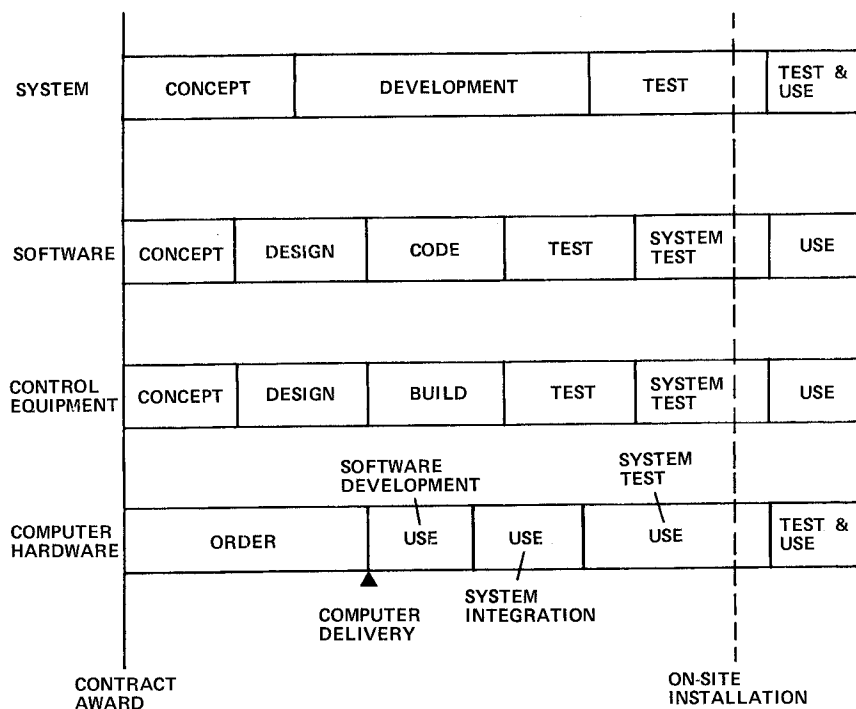


Figure II-C-7 Hardware/Software Event Relationship

b. *Software Requirements Document* - Software requirements will be developed and published in the Software Requirements Document (SRD). Volume IV, Addendum IV is a preliminary version of the SRD. The SRD will be a comprehensive definition of total software requirements and will be presented to the customer for review.

Technical information exchange will be provided through the SRD. As shown in Figure II-C-6, the SRD is one of three documents we will provide. We will also provide the Program Definition Document (PDD) and the User's Manual. All three will be used regularly to discuss our design.

c. *Software Categories* - We have identified the following five software categories:

- 1) On-line heliostat control;
- 2) Off-line heliostat control;
- 3) Heliostat communication control;
- 4) System communication control;
- 5) Heliostat encoder offset correction.

In the design phase, we will group these five categories into three units:

- 1) Heliostat control algorithms;
- 2) Communication control;
- 3) Calibrate update.

The first unit, heliostat control algorithms, will contain the logic to position the heliostats (categories 1 and 2). The second unit, communication control, will contain the logic to control data and message interchange between MCS and HAC and between HAC and heliostats (categories 3 and 4). The third unit, calibration update, will incorporate encoder offset data from MCS or through a development processor console (category 5).

The design of the three software units will be based on the SRD. This design will include the development of detailed flow charts as a part of the PDD. Derived from the SRD, the flow charts consist of the exact (not functional) programming requirements in the form of detailed flow diagrams and equations. The PDD will guide actual coding activity.

The PDD will also provide the basis for our verification program (see Section I) which describes the necessary tests to assure that the coded program is in exact "one-for-one" correspondence with the program requirements. After the program is coded and verified, the validation or system test phase will be entered. At completion of validation, the software will be certified for operational use.

d. Software Discipline - Our software discipline will assure that the program specifications have a logical modular structure and that standards are developed and rigorously enforced. Specifications will be precisely satisfied--no deviations will be allowed without a specification change. Consistent nomenclature will be used throughout and programmer comments will be mandatory to make the code readable. Program module test plans will be documented before coding starts.

A vital part of our software discipline is configuration control to prevent deviations between code and specifications. Configuration control problems that may be discovered during software testing are of two types:

- 1) Program errors that require coding changes for compliance with the specification;
- 2) Specification errors that require a specification change before recoding.

Modular programming techniques facilitate configuration control. As modules are completed, testing will demonstrate specification compliance. Testing will consist of verification and validation phases. The verification phase will show that:

- 1) The code complies with the SRD;
- 2) The code is error free;
- 3) The code is complete.

Manual verification will be performed before software system integration by extensive desk checking, visual code review, and correlation with the SRD.

Each module will be validated using open-loop checks of function code paths. Once the functional operation of each module has been shown, the modules will be integrated and system validation will be performed to show:

- 1) Functional operation of all of the modules working together as an integrated software system;
- 2) That functional performance of the integrated software system complies with the SRD.

Following system integration, but before delivery, extensive system simulations using HCEs and HACs will prove the integrity of the integrated system.

e. Minimum Software Development Costs - All of the software development, verification, and validation will be done in Denver and will use the computational facilities and experience of Martin Marietta. Preliminary hardware/software integration and

test activities will also be done in Denver. All hardware/software interfaces will be fully developed and tested before delivery to insure the operational integrity of the total HACSS. By using currently available Modcomp computers, we can initiate software development immediately on award of contract. Furthermore, we will benefit from Modcomp computer interprocessor communication and digital control software developed by Martin Marietta for the Bureau of Reclamation Central Valley hydroelectric control project.

f. System Usability - Before system delivery, all user documentation will be developed and used. The user manuals will be submitted for customer review. All system operation procedures will be fully defined. Modular system generation procedures will be fully documented. After system delivery, software can be easily modified because of the use of modular programming and a higher order language such as Fortran.

g. Software Development Schedule Integrity - To ensure schedule maintenance, we will conduct weekly status meetings that will show total contract performance to management. Our past success in maintaining schedules in similar software tasks demonstrates our effective management.

Martin Marietta leads in the design and operation of computer-controlled control, automatic checkout, and status monitoring systems. Some of these systems are itemized in Table II-C-2.

We are currently using modular programming and our described disciplines in three other similar projects: the Central Valley hydroelectric control system, programmable automatic checkout equipment (PACE), and a launch checkout and control monitor subsystem (LPS).

4. Software Details

Our software will use the data flow scheme of Figure II-C-8 to provide maximum flexibility in heliostat operation. The MCS/HACSS interface via UAR/T will use the highest priority of the HAC computer interrupt circuits for the fastest response possible to MCS commands, yet maintain 1-second service of each heliostat. A user at an MCS keyboard will be able to elicit HAC response. HAC software will respond to all errors that software can recognize or intercept. It will either correct such errors or alert personnel for action.

a. HAC Console Capability - Every production HAC will be able to communicate bidirectionally with either console attached to the development processor. Two consoles will be provided--one a CRT and the other a standard teletype. The CRT will allow source program data to be input and edited, while the teletype will be used primarily for operator control of the production HACs. Each production HAC will load rapidly from the development processor disc, thereby avoiding individual loading devices.

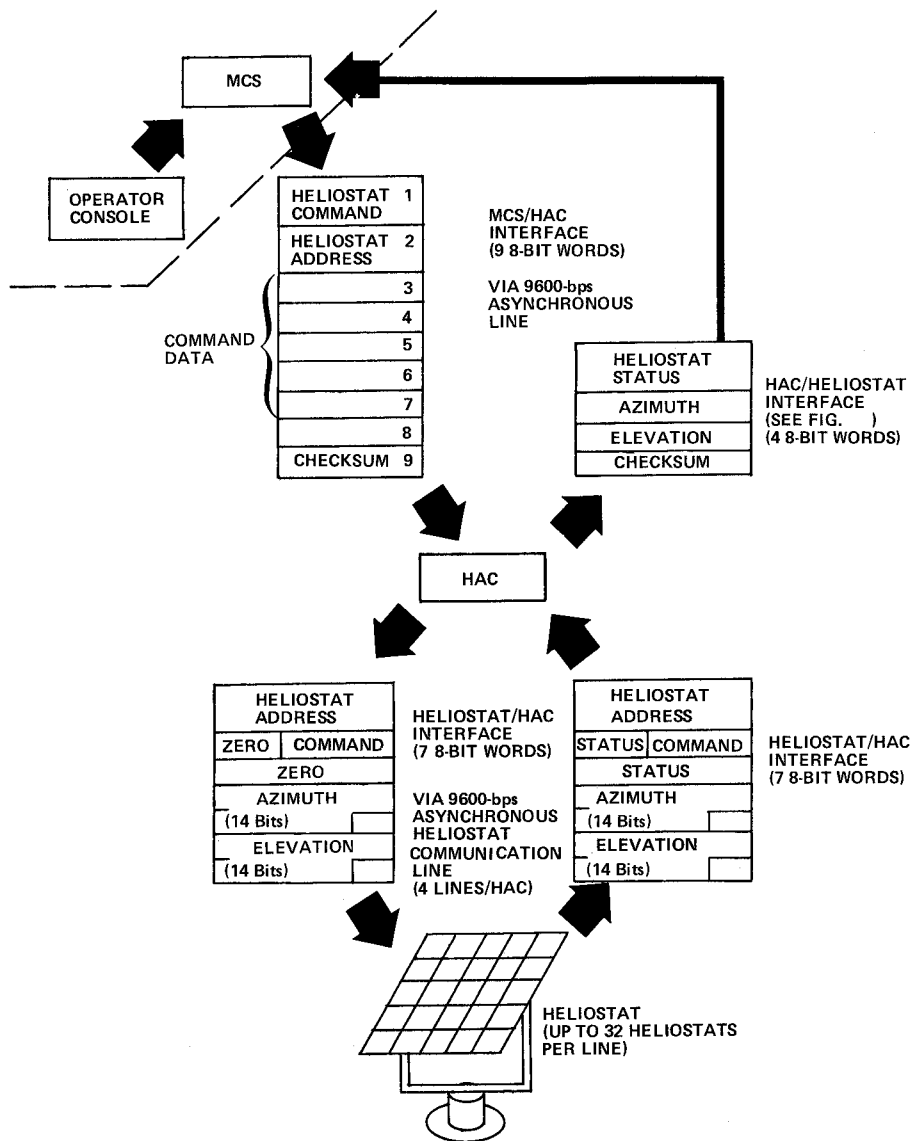


Figure II-C-8 System Data Flow

Our system will allow keyboard insertion of heliostat encoder zero offset data from the HAC and easy user operational control of the software system. If MCS is off-line, heliostats can be controlled through a development processor console. Our software will provide console responses to user keyboard requests for commanded or actual azimuth, elevation, or status.

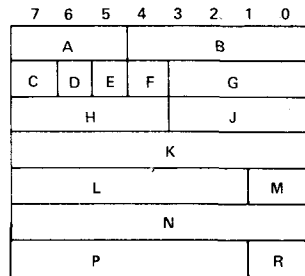
b. *MCS-HAC-HCE Communication* - Except for the MCS EMERGENCY STOW command that will apply to all the HAC-assigned heliostats, MCS heliostat commands address a particular heliostat. For an MCS heliostat command to be acceptable to a HAC, it must be immediately preceded by a CLEAR command addressed to the same heliostat.

Every HAC, as it starts up, will come on line transmitting CLEAR commands to every assigned heliostat at 1-second intervals, using the heliostat interface command (HIC) format of Figure II-C-9. Every HAC will continue thus until instructed otherwise by acceptable MCS commands. At the addressed heliostat, CLEAR will stop the motors and clear the HCE status registers.

When energized, every HCE will come on line with cleared mode registers and motors off by means of a CLEAR command from an internal power turn-on initialization (PTOI) circuit. Therefore the HAC-HCE turn-on sequence is designed to be safety oriented.

Every HCE will reply (using the HIC format) with status, azimuth, and elevation data in response to any HAC command. Thus HAC will be fully informed on all assigned heliostats 1 second after it comes on line and at 1-second intervals thereafter. A heliostat with power turned off or experiencing a power failure will identify itself with a missing reply.

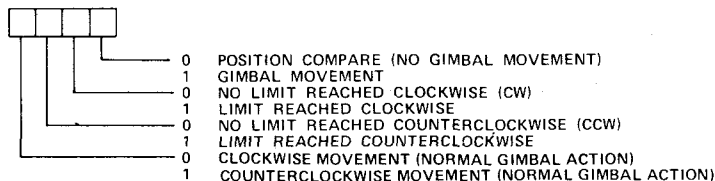
Heliostat commands are defined in Figure II-C-9. HAC will relay every acceptable MCS command to the addressed heliostat within 1 second after receipt and continue to transmit these commands at 1-second intervals until new commands are issued by the MCS. Thus a data error from transmission problems will be corrected 1 second later.



HELIOSTAT INTERFACE COMMAND

- A = LINE DESIGNATOR PORTION OF HELIOSTAT ADDRESS
- B = 5-BIT HELIOSTAT ADDRESS (32 DEVICES PER LINE)
- C = 0 SUN AVAILABLE
1 SUN NOT AVAILABLE
- D = 0 HELIOSTAT UNDER MCS CONTROL
1 HELIOSTAT IN MANUAL CONTROL (WILL NOT RESPOND TO ANY COMMAND)
- E = HELIOSTAT ELECTRONICS RECEIVER ERROR CONDITION
0 IS NO ERROR
1 INDICATES ANY OR ALL OF THE FOLLOWING:
 - 1) LOSS OF LINE SYNCHRONIZATION
 - 2) PARITY ERROR
 - 3) FRAMING ERROR (LOSS OF PROPER STOP BIT)
 - 4) OVERRUN (TOO MANY DATA BITS BEFORE STOP BIT)
- F = SPARE (1 BIT ZERO)
- G = HELIOSTAT COMMAND (SEE TABULATION)
- *H = AZIMUTH GIMBAL STATUS (SEE BELOW)
- *J = ELEVATION GIMBAL STATUS (SEE BELOW)
- †K = AZIMUTH POSITION (UPPER 8 BITS)
- †L = AZIMUTH POSITION (LOWER 6 BITS)
- M = SPARE (2 BITS ZERO)
- †N = ELEVATION POSITION (UPPER 8 BITS)
- †P = ELEVATION POSITION (LOWER 6 BITS)
- R = SPARE (2 BITS ZERO)

GIMBAL STATUS (FIELDS H AND J)



*HAC WILL ISSUE ALL ZEROES IN THIS FIELD AND
HCE WILL INSERT REQUIRED STATUS VALUES
†HAC WILL ISSUE POSITION COMMAND AND
HCE WILL INSERT ACTUAL POSITION

HELIOSTAT COMMAND TABLE

FIELD G OF HIC BINARY VALUE	COMMAND	HELIOSTAT RESPONSE
0000	STATUS	NO PHYSICAL ACTION BY HELIOSTAT. THE ENTIRE CONTENTS OF THE HELIOSTAT CONTROL ELECTRONICS (HCE) REGISTERS ARE RETURNED TO HAC.
0001	CLEAR	ALL HCE MODE REGISTERS ARE CLEARED AND ALL MOTORS ARE STOPPED.
0010 0011	SPARE † SPARE †	RESERVED FOR FUTURE USE.
0100	COARSE TRACK AZIMUTH	AZIMUTH SLEW MOTOR IS ACTIVATED IN CLOSED-LOOP OPERATION. DEADBAND OF AZIMUTH COMPARATOR IS CHANGED TO 0.012 RADIAN.
0101	COARSE TRACK ELEVATION	ELEVATION SLEW MOTOR IS ACTIVATED IN CLOSED-LOOP OPERATION. DEADBAND OF ELEVATION COMPARATOR IS CHANGED TO 0.012 RADIAN.
0110	FINE TRACK AZIMUTH	AZIMUTH TRACK MOTOR IS ACTIVATED IN CLOSED-LOOP OPERATION WITH FULL 14-BIT COMPARATOR.
0111	FINE TRACK ELEVATION	ELEVATION TRACK MOTOR IS ACTIVATED IN CLOSED-LOOP OPERATION WITH FULL 14 BIT COMPARATOR.
1000 1001 1010 1011	DIRECT SLOW AZIMUTH CW DIRECT SLOW AZIMUTH CCW DIRECT SLOW ELEVATION CW DIRECT SLOW ELEVATION CCW	THESE COMMANDS TURN ON RELATED AXIS TRACK MOTOR. ONLY LIMIT SWITCHES OR CLEAR COMMAND WILL TURN MOTOR OFF.
1100 1101 1110 1111	DIRECT SLEW AZIMUTH CW DIRECT SLEW AZIMUTH CCW DIRECT SLEW ELEVATION CW DIRECT SLEW ELEVATION CCW	THESE COMMANDS TURN ON RELATED AXIS SLEW MOTOR. ONLY LIMIT SWITCHES OR CLEAR COMMAND WILL TURN MOTOR OFF.

Figure II-C-9 HelioStat Interface Command (HIC) Definition

Heliostat motion will not occur if the actual and commanded angles are equal. The absolute encoders on both heliostat axes assure nonvolatile position feedback sources. Heliostat movement in 1 second will not exceed 0.4315 mrad in the fine-track mode. Up to three erroneous data transmissions to any given heliostat can be tolerated without exceeding minimum pointing requirements (1.5 mrad). The heliostat movement status bit will be monitored to detect runaway.

c. Encoder Offset Correction and Standby Position Storage -

Our software will have two zero offsets and standby position associated with its attribute table as shown in Figure II-C-10. The offsets may be manually input via the HAC console or transferred from the MCS. They will be used to correct the commands before issuance. The de-

sired heliostat positions will be calculated using the heliostat control algorithm and the sun position issued by the MCS every second.

d. Heliostat Movement Control - On-target pointing will be to within 1.5 mrad (see K93681, para 3.1.4.3.b) and the position will be updated on

HELIOSTAT ATTRIBUTE TABLE REQUIRES 2048 WORDS CONSISTING OF 128 ENTRIES OF 16 16-BIT WORDS EACH WITH EACH ENTRY CONTAINING THE FOLLOWING:

WD 0	C1, 1	}	CURRENT POSITION DATA
1	C1, 2		
2	C2, 1		
3	C2, 2		
4	C3, 1		
5	C3, 2		
6	X STDBY	}	STANDBY COORDINATES
7	Y STDBY		
8	Z STDBY		
9	X LIB	}	HELIOSTAT INITIAL COORDINATES
10	Y LIB		
11	Z LIB		
12	AZIMUTH	}	SAFE STOW COMMAND
13	ELEVATION		
14	AZIMUTH	}	ENCODER OFFSET CORRECTION
15	ELEVATION		

Figure II-C-10 Heliostat Attribute Table (HAT)

a 1-second basis. Large standby and on-target movements will result in a coarse commands (K93681, para 3.1.4.3.a) until fine tracking limits have been achieved. HAC software will insure stowed to standby and standby to on-target positioning well within the required 15-minute limit (K93681, para 3.1.4.4.a and 3.1.4.4.c). HAC software will be able to stow any assigned heliostat autonomously or by MCS command. Stowing will require less than 15 minutes in accordance to K93681, paragraph 3.1.4.4.f. In all cases, unsafe target zones will be avoided to prohibit possible harm to facilities and personnel. For emergency stowing, our software will command for each heliostat the quickest safe path based on its current position. Safe zones will be determined at heliostat installation and their position data will be input to each controlling HAC and maintained in the heliostat attribute table.

e. Sun Obscuration - Our system will provide a sun-present sensor (SPS) for at least every 10 heliostats in each zone. This sensor will provide control of the sun-availability bit in field C of the HIC as shown in Figure II-C-9. If this bit is set, the assigned heliostats will be told to stand by. This includes the heliostat with the sensor (K93681, para 3.1.4.4.c). An alarm message "2" (Fig. II-C-11) will be transmitted from the HAC to MCS for each obscured heliostat and each will remain in standby until commanded otherwise by the MCS.

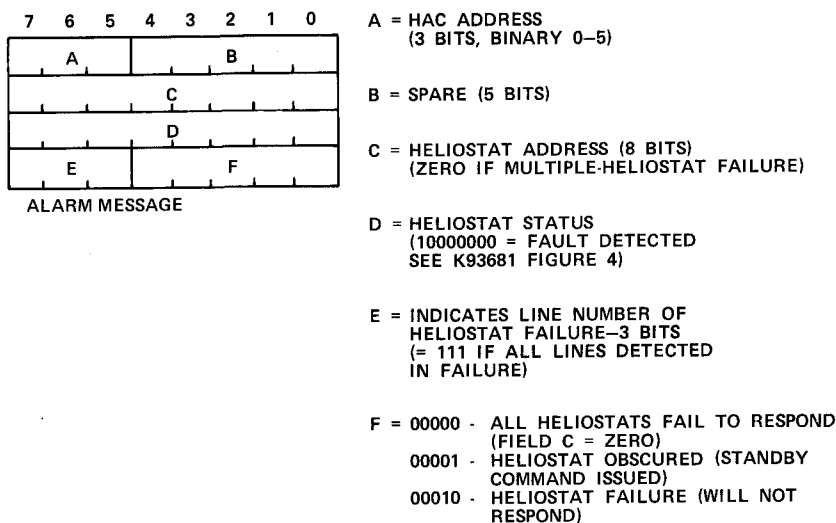


Figure II-C-11 HAC/MCS Alarm Message

f. *Total Versatility* - Our proposed system will support simultaneous operation of up to five heliostat zones using six HACSS. This system will provide adequate computation, communication and control for up to 128 heliostats per HACSS and service each heliostat once a second. Although this configuration will meet or exceed operational requirements, it will provide an easy expansion capability without affecting current system design and operation. Our system will provide maximum versatility and reliability.

g. *Minimum Overall Costs* - This HAC will minimize cost for the life of the project. By using as many off-the-shelf units as possible, development expense will be minimized. Hardware floating point will significantly reduce software development costs. Sufficient storage and timing margins will prevent outgrowing hardware. A multiple-interrupt capability provides top priority to the MCS, assuring fail-safe system response.

5. Manufacturing

Manufacture of the HACSS will consist of building HIM chassis and assembling these into the HIM rack, building cables that connect the computers with the HIM rack, connect to facility power, and distribute data. The computers and their peripherals, including the interconnecting wiring, will be bought from the supplier as an integrated assembly.

The HIM will contain integrated circuits and discrete components mounted on printed circuit (PC) boards. These PC boards will be assembled, and then tested in our Denver facility. This existing facility has the capability, in both equipment and personnel, to build and deliver HACSS hardware on schedule and at minimum cost. Close coordination will be maintained with the designers to promote use of proven available techniques and processes developed in other ground equipment contracts.

Cable assemblies will be fabricated by experienced personnel using standard soldering/crimping and connector assembly procedures.

Final acceptance testing will use an existing automated test system that has proved to be the fastest and most economical for this type of equipment.

All fabrication operations will be controlled by manufacturing process plans that indicate to fabrication and inspection personnel the fabrication operations, mandatory inspection points, applicable engineering documents, special handling requirements, and

provisions for indicating completion and acceptance of fabrication operations. The plans will be used to support engineering requirements in the most economical manner. Figure II-C-12 depicts assembly flow for fabrication of the HIM rack.

6. Interfaces - Interfaces between the HACSS and other subsystems are discussed in the following. The electrical interfaces are described in Section G.4.

a. *HACSS/MCS Interfaces* - Communications between MCS and HACSS will be on a full duplex basis. MCS will transmit commands and sun position data to

HACSS. HACSS will return the same

commands and sun position data to HACSS. HACSS will return the same commands and sun position data to MCS. HACSS will transmit heliostat position and status data to MCS on request.

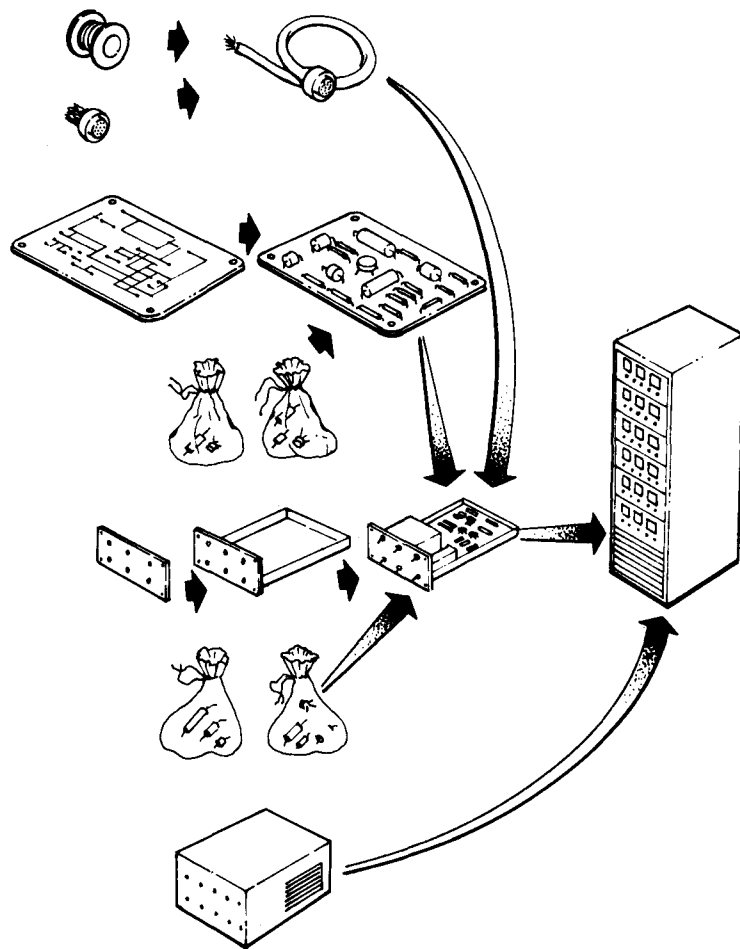


Figure II-C-12 Fabrication of the Heliostat Interface Module

The MCS will transmit to HACSS as follows:

- 1) In format compatible with UAR/T components;
- 2) At a 9600-baud maximum data rate;
- 3) With even parity.

Signal levels and designations will conform to EIA RS-232-C.

Table II-C-5 lists each command, associated parameters, and a description of HACSS action. Each command string is composed of a block of nine 8-bit data words. Parity is determined and transmitted (received) via the UAR/T component. Each communication word will consist of a start bit followed by the eight data bits--least significant data bits first, followed by the parity bit, followed by one stop bit for a total of 11 bits. All binary quantities that can be negative will be represented in two's complement form. The first word of the command string is the command word, as shown in the left-hand column of Table II-C-5. Depending on the command, additional parameters will be transmitted as shown in Table II-C-5. For all binary data words, bit 7 will be the most significant. The last word of the command string will be the checksum word, which is the two's complement of the sum of the previous words (i.e., binary addition of all words in the string produces zero). All data words will be passed as binary counts, each count representing units such as 0.01 m, 0.0001 rad, etc. HACSS will be compatible with the format of Table II-C-5.

Table II-C-5 MCS/HACSS Interface Formats

COMMAND WORD (BINARY CODE, COMPUTER REGISTER)	PARAMETERS TRANSMITTED TO HACSS (BY MCS)	ACTION BY HACSS IN RESPONSE TO COMMAND WORD
CLEAR (00000001)	HELIOSTAT ADDRESS	CANCELS CURRENT COMMAND TO ADDRESSED HELIOSTAT, IF ANY; ENABLES NEW COMMANDS TO BE ACCEPTED. HELIOSTAT STOPS AT CURRENT POSITION.
STANDBY (00000011)	HELIOSTAT ADDRESS AND AIMING POINT	ADDRESSED HELIOSTAT WILL BE MOVED TO SPECIFIED POSITION.
ON-TARGET (00000101)	HELIOSTAT ADDRESS AND AIMING POINT	ADDRESSED HELIOSTAT WILL BE MOVED TO SPECIFIED POSITION.
STOW (00001001)	HELIOSTAT ADDRESS	ADDRESSED HELIOSTAT WILL MOVE TO ITS FIXED STOWAGE POSITION.
EMERGENCY SHUTDOWN (10000001)	NONE	RETURNS ALL HELIOSTATS TO STOWAGE.
STATUS (00010001)	HELIOSTAT ADDRESS, STATUS, AZIMUTH POSITION, ELEVATION POSITION, AND SUN AVAILABILITY	CURRENT STATUS OF ADDRESSED HELIOSTAT WILL BE TRANSMITTED TO MCS
SUN POSITION (00100001)	SUN AZIMUTH AND ELEVATION IN RADIANS	INFORMATION ONLY; NO ACTION REQUIRED. TRANSMITTED FROM MCS AT ONE-SEC INTERVALS. THE SUN POSITION DATA ARE CORRECTED FOR REFRACTION PRIOR TO TRANSMITTAL.
NOTE: ALL INTERFACE SIGNALS DO NOT HAVE TO BE USED AS LONG AS OPERATIONAL MODES CAN BE ACCOMPLISHED.		

The HACSS will transmit to MCS as follows:

- 1) In format compatible with UAR/T components;
- 2) At a 9600-baud maximum data rate;
- 3) With even parity.

Signal levels and designations will conform to EIA RS-232-C.

HACSS will format heliostat status and position data as shown in Table II-C-6 for transmittal to MCS.

Table II-C-6 Heliostat Status and Position Data Format

STATUS TRANSMISSION - HACSS TO MCS	
BIT	7 6 5 4 3 2 1 0
WORD 1	STATUS
WORD 2	AZIMUTH
WORD 3	ELEVATION
WORD 4	CHECKSUM

WORD 1 STATUS: BIT 0 = IN TRANSIT TO CONDITIONS INDICATED BY BITS 1-3
BIT 1 = STOW POSITION
BIT 2 = STANDBY POSITION
BIT 3 = ON-TARGET
BIT 4 = (UNASSIGNED)
BIT 5 = MANUAL CONTROL
BIT 6 = SUN AVAILABLE
BIT 7 = FAULT DETECTED BY HACSS

WORD 2 AZIMUTH: POSITION DATA (8 BITS) BIT 0 = LSB

WORD 3 ELEVATION: POSITION DATA (8 BITS) BIT 0 = LSB

WORD 4 CHECKSUM: SAME FORMAT AS DESCRIBED IN 3.1.1.1(a).

NOTE:	1. CORRESPONDING STATUS BIT IS SET IF CONDITION IS TRUE.
	2. IF STATUS BIT 5 IS SET, OTHER BITS IN STATUS WORD ARE NOT NECESSARILY VALID.

b. *HACSS/HASS (HIM-HCE) Interfaces* - The data interfaces between HACSS and HASS are shown in Figure II-C-13. HAC will output data through an optically coupled isolator to a differential current-mode line driver. The line driver will interface with a twisted shielded pair that runs approximately 600-m (1969 ft)

maximum to the first of 32 heliostats. Differential line receivers will receive the serial data at each heliostat. Each receiver will be isolated from the electronics in each heliostat by optical couplers and isolated power supplies.

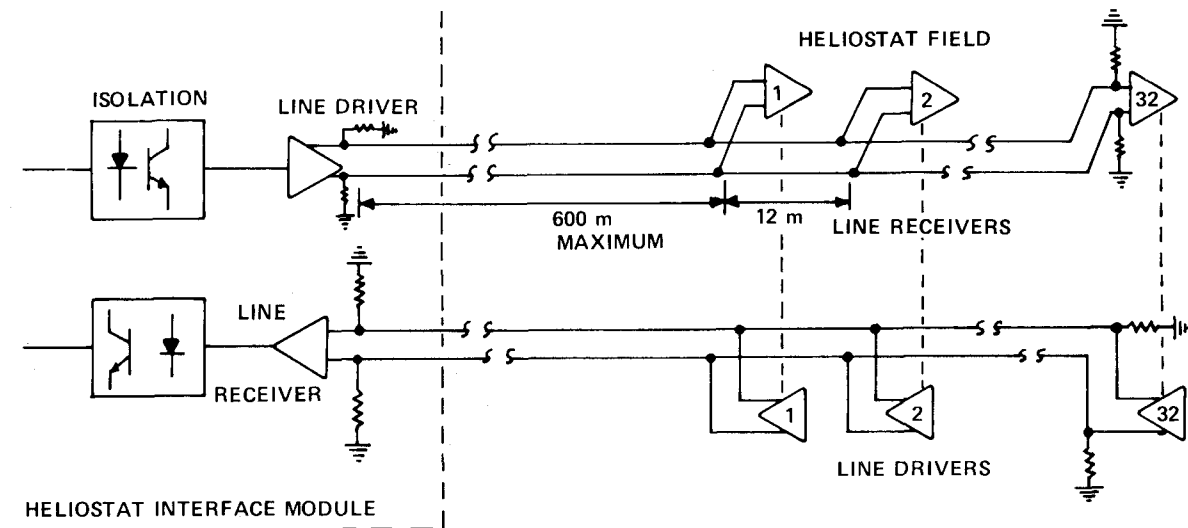


Figure II-C-13 Typical Interface between Heliostat Interface Module and Heliostat Control Electronics

HAC/HIM output will be messages consisting of 7 characters (a character is the basic word made up of 8 bits). A character format will be used that consists of 8 bits of data, 1 parity bit, 1 start bit, and 2 stop bits (refer to Fig. II-B-23). This scheme is being used on other long-line computer/peripheral interfaces at Martin Marietta with excellent results. The first character of the message will consist of 5 address bits, a sync bit, and 2 spare bits. Every heliostat will receive this character. One of the 32 decoders looking at this character will recognize it and open a gate accepting the next 6 characters. Each of these characters will contain 8 bits of data. The data will be marking one for 10 bit times prior to the start of a block of

32 messages (a message is the group of 7 characters), and for 5 bit times between messages. This will synchronize all 32 receiving heliostats to start looking for an address. If the first character of the message does not contain the proper sync bit, the character will be rejected until a character with the proper sync is received.

A block of 32 messages will be sent once a second to all four groups of 32 heliostats.

The return data format will be the same as the received data. A separate line for 32 line drivers will be provided. Only one three-state driver will be active or enabled at one time. Thirty-one drivers will be in a high-impedance output state while one is active. A particular heliostat line driver will go active at acceptance of that heliostat address. It will go inactive at the completion of data transmission from that heliostat. The required data rate between the HAC and the heliostats is computed as follows, assuming an 8-bit data word, 1 start bit, 2 stop bits, and a parity bit:

$$(12 \text{ bit/word}) \times (7 \text{ words/message}) \times (32 \text{ messages}) \div (1 \text{ s} - 170 \text{ bit times}) \\ = 2858 \text{ baud.}$$

The maximum transmission rate capability of the 6-mA current driver in conjunction with our line lengths is calculated by the following:

- 1) 600 m from HAC to field;
12 m x 32, spacing between heliostats;
3 m x 32, stub lengths;
180 m, total line length.

Capacitance per meter of twisted shielded pair (Belden 8227) is approximately 50 pF. Total line capacitance = $50 \times 1080 = 54000$ pF. Driver output current capability - load = $6.5 \text{ mA} - 32 (0.150) = 4.8 \text{ mA}$.

The time to translate through a 0.025 V receiver sensitivity band is

$$t = \frac{54000 \times 10^{-12} (.026)}{.0048} = 0.28 \text{ } \mu\text{S}.$$

Considering that data should be allowed to stabilize for at least 4 times the translation time, this would give an effective data rate of

$$\frac{1}{4(0.28)10^{-6}}$$

or 890 kilobaud. This number agrees with both manufacturers' data regarding the capability of this part and our test results.

In conclusion, the above calculations show the long-line system is capable of data rates far in excess of the 2.858 kilobaud requirements.

c. *HACSS/CSS Interface* - A functional interface will exist between the HACSS and the calibration subsystem (CSS) during the calibration sequence. HACSS will position the heliostat to focus incident solar rays on the target. The MCS will send the necessary pointing commands to HACSS during all phases of calibration, including beam quality checks and determination of beam energy distribution across the face of the target.

The azimuth and elevation encoders will have residual offsets that must be measured and compensated for to point and track accurately. This measurement will be performed during initial calibration operations. Encoder azimuth and elevation offset data will be recorded when the heliostat is pointed on target. The offset data will be stored in HAC memory for subsequent heliostat pointing.

D. Focusing and Alignment Subsystem

D. FOCUSING AND ALIGNMENT SUBSYSTEM

The heliostat focusing and alignment subsystem will include all hardware and instructions necessary for heliostat focusing, alignment, and refocusing. It will be used to focus and align each heliostat after initial installation, and to refocus and realign each heliostat when required. This task will include focusing each mirror on a given heliostat to achieve a best focus (minimum image size) at an aperture located on top of the receiver tower, and aligning the mirrors on each heliostat so the best focus at the aperture is achieved for the entire heliostat. Initial focusing will be done for the single condition defined by the incident solar radiation angle at equinox solar noon in accordance with the requirements of K93681, paragraph 3.1.4.2. Focusing of each mirror will verify the surface contour per the requirement given in paragraph 4.1.2.c of K93681. Table II-D-1 summarizes the major RFQ requirements and our approach to meeting them.

Heliostat focusing and alignment will be performed after each heliostat is installed in the field. This will be done by simulating the condition of solar noon at the equinox. A large collimated white light source will be used to simulate the sunlight incident on each mirror of the heliostat sequentially and reflect the light to a high-efficiency reflective focusing screen located at the receiver aperture position. This approach is

illustrated in Figure II-D-1. This direct simulation technique was selected based on the results of a Martin Marietta internal tradeoff study that considered several other approaches. The results of this study are discussed in subsection 9.

*Table II-D-1
Focusing and Alignment Subsystem Requirements and Approach*

ITEM	KEY RFQ REQUIREMENT	K93681 PARA	PROPOSED APPROACH
1	THE HELIOSTAT MUST DIRECT 90% OF ITS REFLECTED POWER ONTO A CIRCULAR TARGET OF DIAMETER $0.012 \times$ SLANT RANGE FROM HELIOSTAT TO TARGET.	3.1.4.2	THE BEAM QUALITY AT EQUINOX SOLAR NOON OF 90% OF THE HELIOSTAT REFLECTED POWER FALLING ONTO A CIRCULAR TARGET OF DIAMETER 0.012 SR WILL BE ACHIEVED THROUGH THE INITIAL HELIOSTAT FOCUSING AND ALIGNMENT. THIS PROCEDURE WILL INDIVIDUALLY FOCUS AND ALIGN EACH HELIOSTAT MIRROR TO OBTAIN THE SMALLEST POSSIBLE IMAGE AT THE RECEIVER APERTURE AND CENTER MIRROR NOMALS AT EQUINOX SOLAR NOON BY SIMULATING THIS CONDITION WITH AN ARTIFICIAL WHITE LIGHT SOURCE WITH 0.5 DEG COLLIMATION.
2	FOCUSING AND ALIGNMENT SUBSYSTEM SHALL ALLOW ADJUSTMENT OF EACH HELIOSTAT SO POWER DISTRIBUTION AT THE RECEIVER APERTURE WILL BE KNOWN.	3.3	HELIOSTAT ADJUSTMENT AND FOCUSING AND ALIGNMENT SUBSYSTEM. VERIFICATION OF POWER DISTRIBUTION IS PERFORMED USING THE SUBSYSTEM.
3	HELIOSTAT REFOCUSING AND INTERCHANGEABILITY.	3.1.5.f	HELIOSTATS WILL BE CAPABLE OF REFOCUSING PROCEDURE SIMILAR TO THE INITIAL FOCUSING AND ALIGNMENT PROCEDURE. THIS PROCEDURE WILL REQUIRE THE FASS.
4	MIRROR SURFACE VERIFICATION.	4.1.2	THE MIRROR SURFACE CONTOURS WILL BE VERIFIED BY FOCUSING EACH HELIOSTAT MIRROR AS DESCRIBED IN RFQ PARAGRAPH 3.1.4.2 DURING THE INITIAL HELIOSTAT FOCUSING AND ALIGNMENT.

Heliostat focusing and alignment will be performed by first moving the heliostat to its position for equinox solar noon. The light source will be

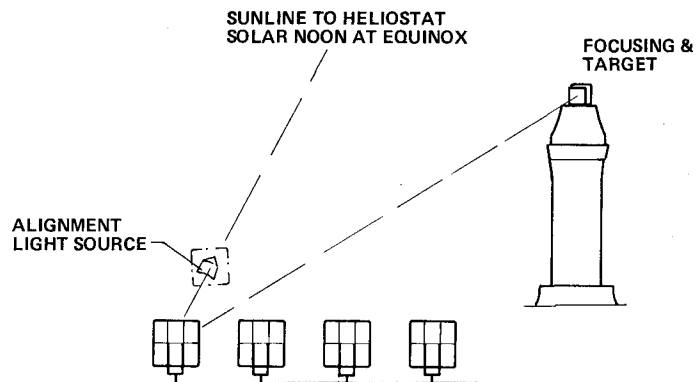


Figure II-D-1 Solar Simulation Focusing and Alignment Geometry

positioned in front of the center mirror in the heliostat so the incident beam will simulate the angle of incidence of solar radiation at equinox solar noon. The mirror will then be adjusted manually so the reflected beam is focused to a minimum spot size at the center of the alignment target near the receiver aperture location. The light source image on the alignment target will be viewed directly by the technician during this adjustment. When the optimum focus is achieved, the collimated light source will be translated to the next mirror of the heliostat. The procedure will then be repeated until the entire heliostat is focused at the aperture. The light translation mechanism will be designed to maintain the same angle of incidence for all mirrors on the heliostat. This focusing and alignment technique will use three alignment subsystems--a heliostat workstand, an alignment target, and a mobile alignment light source.

1. Heliostat Workstand

The heliostat workstand, Figure II-D-2, is a variable-height mobile platform from which the individual heliostat mirrors will be adjusted. This platform will be positioned behind the heliostat being focused to position the focusing technician at the most efficient location.

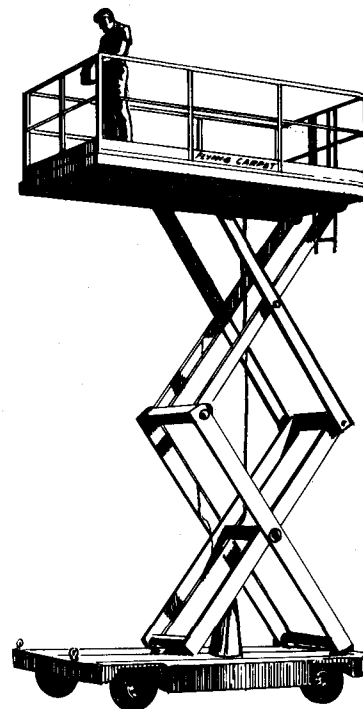


Figure II-D-2
Heliostat Workstand

The workstand is part of the installation and maintenance equipment described in Section F.

2. Alignment Target

The alignment target will consist of a large flat surface of sufficient area to facilitate image location and focusing. The target will be approximately 6.1-m (20-ft) wide and 6.1-m (20-ft) tall. Since dimensions will be optimized based on design tests, they are subject to size modification. The target will be mounted near the top level of the elevating module on the receiver tower with the center as near as feasible to the planned receiver aperture

location. This position is required to optimize the focus at the receiver aperture. The alignment target will be mounted over the face of the calibration target as illustrated in Figure II-D-3. The calibration target is described in detail in Section E. This system provides the capability of positioning the alignment target normal to

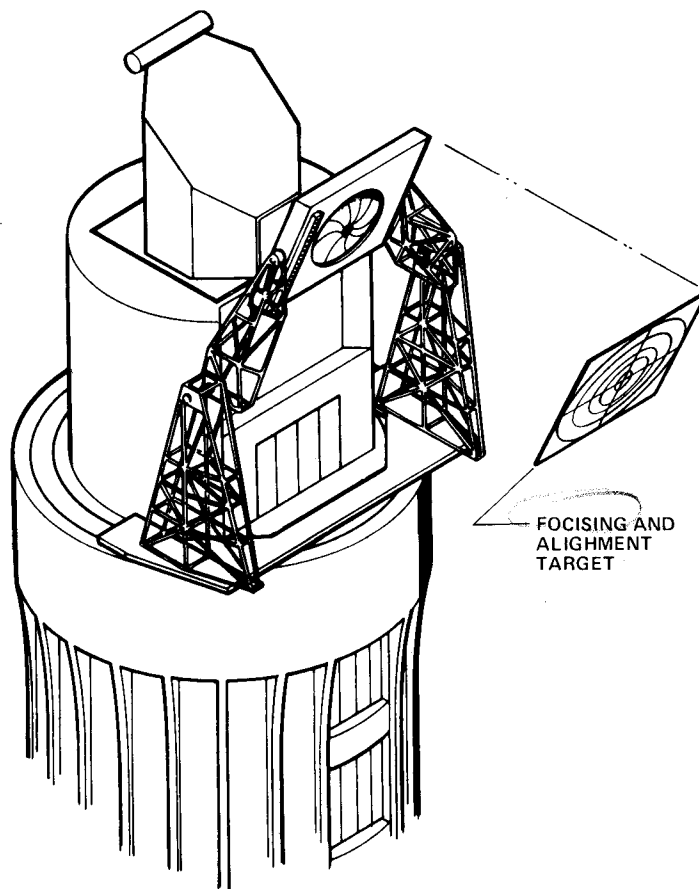


Figure II-D-3 Alignment Target/Calibration Target Interface

the beam reflected from each mirror without a duplication of hardware or additional interface requirements. This positioning is required to obtain maximum reflector efficiency from the alignment target. The alignment target will be designed to be easily positioned on the calibration target to minimize mounting and removal time.

Neither the alignment target nor the calibration system will be mounted on the heliostat calibration ring illustrated on the Black and Veatch drawing, RFQ Figure 8. The illustrated position of the alignment ring is technically unsuitable for focusing, alignment, or calibration because of its separation distance from the equipment apertures. For example, if we consider the Martin Marietta receiver, which gives the minimum receiver aperture-to-calibration ring separation distance and the heliostat closest to the receiver tower, the heliostat-to-calibration ring distance is approximately $3/4$ the heliostat-to-receiver aperture distance. Therefore if the heliostat were focused to a point at the calibration ring, the resultant image at the receiver aperture would be defocused since it is $1/3$ the focal distance beyond the focal point. For a 6.7-m (22-ft) circular heliostat, the image size at the Martin Marietta aperture would be approximately 2.2 m (7.3 ft) in diameter. At the Honeywell receiver aperture, the image would be approximately 3.5 m (10 ft) in diameter. This exploding of the image is unsuitable and shows that the focus, alignment, and calibration target positions must be located as near the aperture location as possible.

The alignment target surface will consist of high-efficiency prismatic reflector materials. The final reflector material will be selected in the early months of this program based on alignment target optimization tests. These tests will be conducted at Martin Marietta's Denver Division. Candidate materials to be tested include 3M high-intensity reflective sheeting, Rowland Development Corporation Reflexite sheeting, and delineator reflectors manufactured for various highway departments. Physical testing will be minimized through material selections based on available data. Focused light image positions will be identified through arrange-

ments of various colors of reflectors to obtain the optimum configuration for visual observation.

The target configuration will be opti-

mized as a part of the reflector tests. A conceptual sample of the alignment target is given in Figure II-D-4.

Selection of the optimum target surface reflective material is required to assure the capability of daylight as well as nighttime focusing operation. Daylight operation will be required to focus and align up to five heliostats per day with a single field alignment light source. This alignment target

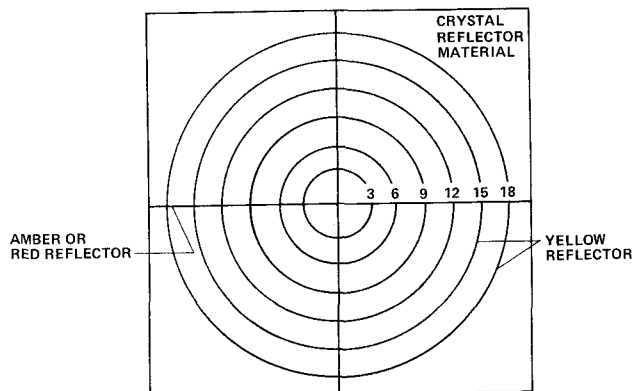


*Figure II-D-4
Sample Alignment Target Configuration*

concept provides the maximum efficiency for image observation at a minimum program cost. Because of the light weight of the reflective sheeting, it also provides a high degree of flexibility for target alteration and movement. Additionally, if alignment schedules require more than one alignment system in the same field, only one alignment target is required since the reflected beam returned from the target is directional and visible only near the mirror creating the image. However, if such simultaneous alignment is required, the heliostats involved should have an angular separation from the target of not more than 15 deg for daylight operation because the reflector efficiency drops off rapidly with increasing angle of incidence.

3. Mobile Alignment Light Source

A critical subsystem in the alignment task is a mobile light source positioning system that will support and position a high-intensity solar simulator in front of each heliostat mirror. The positioning system must be mobile so it can be moved in front of the mirror array, stabilized, and the light platform leveled. The light will then be moved, as a part of the focusing and alignment, to each of 25 positions so each static position maintains the parallel light described.

The solar simulator will consist of a high-intensity xenon arc lamp and reflector system similar to a searchlight. This light will provide a collimated beam of light approximately 1.5 m (5 ft) in diameter. The light beam will be masked to give a square beam approximately 1.28 m (4.2 ft) at the edge.

The beam will illuminate over 96% of the surface of each 1.22 m (4-ft) mirror element in the heliostat. The light beam will be directed downward onto each mirror at an angle of 55 deg and be maintained parallel from position to position with a tolerance of ± 0.1 deg.

The solar-simulating light will also incorporate a side-mounted laser that will be interaligned with the simulator light beam. This laser will be used for system verification and for initial setup and positioning of the mobile positioner prior to starting the main light. This will facilitate accurate light beam positioning and verification.

Because a light-positioning system that maintains proper beam parallelism is essential to the accuracy in this focusing and alignment technique, therefore two design concepts are being considered. These are a "bridge crane" concept that will achieve light positioning by moving the light horizontally in two dimensions above the array of mirrors, and a "mobile tower" concept that will achieve positioning by moving the tower horizontally. The bridge crane concept is illustrated in Figure II-D-5 and the mobile tower concept in Figure II-D-6. Due to the high center of gravity of the mobile tower and the comparatively narrow base, it is possible that the mobile tower could be blown over by high winds. Also, since the tower must be movable during operation, guy-wire tiedowns are feasible only for storage and nonoperational activities. Therefore the bridge crane concept appears preferred. This concept however presents some

structural interference with the reflected light beam from several of the mirrors. Therefore the concept is feasible only if the crane can be a lattice structure that obstructs a minimum amount of light directed through it. The mobile tower, on the other hand, has no light obstruction.

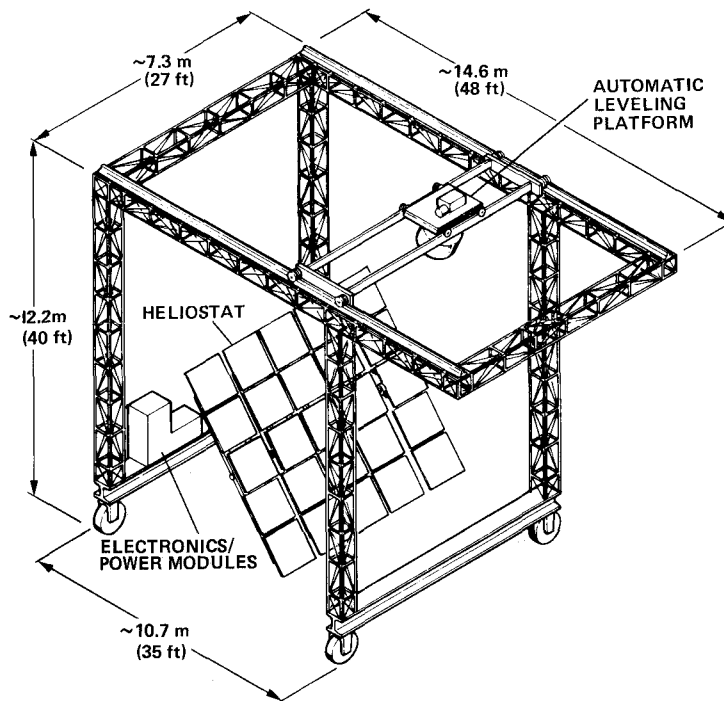


Figure II-D-5 Bridge Crane Concept

Martin Marietta is currently investigating which system approach is optimum based on safety, precision, and cost effectiveness. Preliminary quotes on both systems are included in this proposal. Each system is described.

a. *Bridge Crane Concept Description* - This concept, as illustrated in Figure II-D-5, will provide a bridge structure that will support a two-dimensional horizontal positioning device at the top. The bridge structure will be mobile and may be self-propelled or towed. The bridge structure will be capable of operating on a dry graded dirt, gravel, or macadam surface. Maximum field operating speed will be 8 kmph (5 mph). The bridge support will be capable of spanning each heliostat and will be at least 8.5-m (28-ft) wide with a minimum vertical clearance

of 8.2 m (27 ft). The minimum height of the light source edge of approximately 11.6 m (38 ft) will define the height of the positioning platform. The bridge structure in the area of potential light obstruction will be designed to minimize the visible light obstructed by the structure.

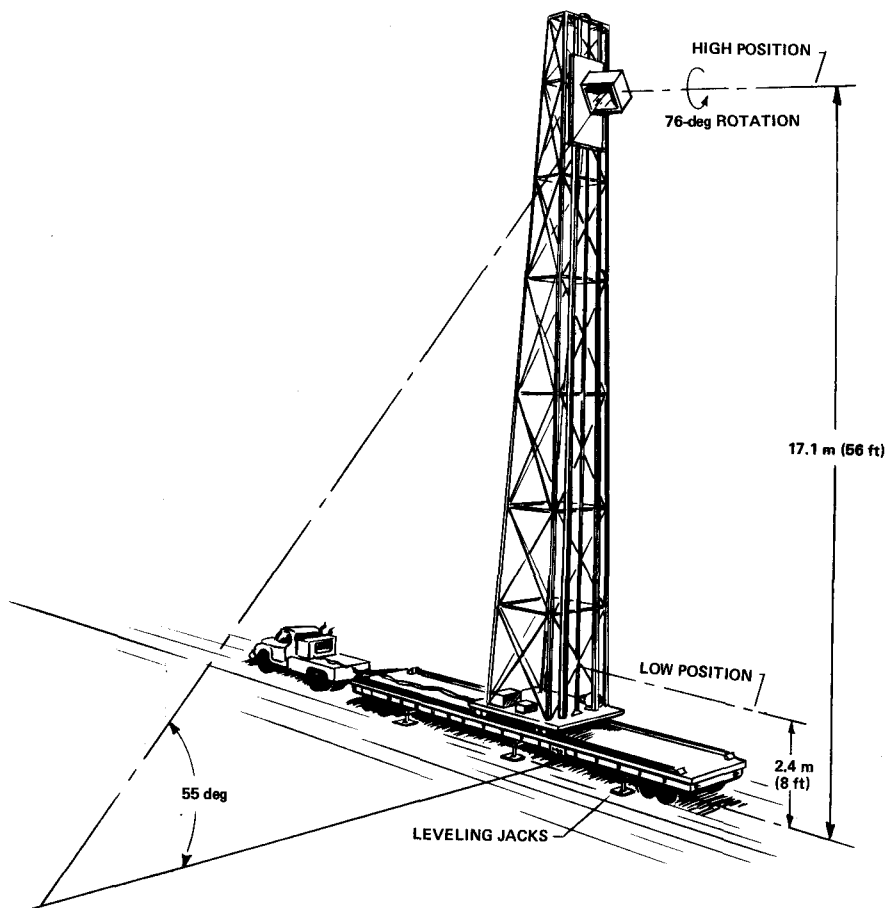


Figure II-D-6 Mobile Tower Concept

The light support platform will provide light-positioning in two orthogonal directions in a horizontal plane with a positioning accuracy of ± 5.1 cm (± 2 in.) in either direction. Length of travel for the center of light beam will be approximately 6.1x12.2 m (20x40 ft). The structure and light transport mechanism will be rigid so the platform rotation about a vertical axis is less than ± 1.7 mrad (± 0.1 deg). The platform will be self-leveling to provide a level at any position to within ± 0.8 mrad (± 0.05 deg).

Electrical transmission line supports for the platform control and light source powerlines will be provided so these lines will not interfere with platform or system moving operations. The positioning platform will also provide provisions for a hoist for lifting the light source from the ground to its permanent operating position.

b. Mobile Tower Description - The mobile tower consists of a tractor system, tower support trailer, and tower assembly. The tractor system will provide transportation of the mobile tower. Field transportation of the mobile tower will be limited to 8 kmph (5 mph).

The tower support trailer will provide support for the tower assembly and the capability to move the tower assembly horizontally on the trailer a distance of at least 6.1 m (20 ft). This motion will be motorized and provide positioning capability of ± 7.6 cm (± 3 in.) at any point within the 6.1-m (20-ft) area. The trailer will have a leveling jack to provide stability and proper

setting of the light beam angle. Light-positioning controls will be mounted on both sides of the trailer and located approximately 0.61 m (2 ft) forward of the center of travel of the light beam.

The tower assembly will be capable of moving the center point of the light source vertically from 2.4 m (8 ft) to 17.1 m (56 ft) above ground level selectable to any position to ± 7.6 cm (± 3 in.) The tower assembly will include an interface plate for mounting the light source external to the tower on the side facing the rear of the tower support trailer. Retractable safety guy-wires will be provided for tower securing during high winds and non-operational storage.

4. FASS Functional Capabilities

The focusing and alignment system will be designed to operate during both daytime and nighttime hours to facilitate alignment of up to five heliostats per day with a single alignment system. This is accomplished by maximizing the intensity of the light source and the efficiency of the alignment target. Initial alignment time is estimated to be approximately 4.5 hours per heliostat using a two-man crew. With experience, this time is expected to be reduced appreciably. Alignment functions will, however, not be attempted in high winds or during rain, snow, or other conditions that restrict visibility or create a potentially hazardous condition.

a. *Alignment Accuracy* - This technique will provide alignment accuracies of image superposition at the alignment target from mirror-to-mirror on a given heliostat of ± 0.13 m (0.43 ft) for the close-in heliostats [SR = 76.2 m (250 ft) to ± 0.51 m (1.67 ft)] for the distant heliostats [SR = 289.6 m (950 ft)].

b. *Focusing Accuracy* - The focusing technique just described provides optimum conditions for focusing a single mirror and is limited only by the target resolution. For reflective sheeting, this value is approximately 0.15 mm (0.006 in.) Total heliostat focusing accuracies are the same as the mirror-to-mirror alignment accuracies given in the previous paragraph.

c. *Pointing Accuracy* - The heliostat pointing angle will not be accurately set during the focusing and alignment previously described because of the uncertainty of the absolute position of the illuminating collimated light. Pointing accuracies from heliostat-to-heliostat will be approximately ± 17.5 mrad (± 1 deg) after focusing and alignment. Each heliostat will be fine-pointed later using the calibration system and the sun. This procedure is discussed in Section II.E.

5. Safety Features

The safety aspects of this subsystem will be evaluated in accordance with the safety plan in Volume II. The design and operation of the subsystem will meet the requirements of 29CFR, Chapter XVII, Part 1910, *Occupational Safety and Health Standards*. Specific safety considerations already considered include:

- 1) Grounding of mobile light source tower and trailer;
- 2) Lightning protection of light source tower;
- 3) Electrical interlock on light source housing;
- 4) Protective clothing for handling xenon lamps;
- 5) Protective equipment for operators.

6. Maintainability Features

The focusing and alignment subsystem will be designed, as far as possible, using standard components requiring standard maintenance. Operating and maintenance manuals will be provided for all components of the focusing and alignment subsystem. These manuals will identify recommended maintenance cycles, critical maintenance components, limited-life components, and recommended replacement cycles. Special maintenance or replacement tools, fixtures, or protective garments will be provided as a part of this subsystem, with instructions for use.

7. Reliability

To provide reliability, spares of key components, long lead items, and special manufactured items will be provided. Spare focusing and alignment parts to be provided will include, but are not limited to:

- 1) Replacement lamps - 10 each;
- 2) Collimating light fixture - 1 each;
- 3) Positioning drive motor - 1 each;
- 4) Lamp cooling fan and motor - 2 each;
- 5) Platform level sensor - 1 each;
- 6) Reflector replacement material - 8.5 m² (200 ft²).

Additional replacement components for the mobile alignment light system and alignment target will be identified as detailed design and component reliability data are available.

8. Interfaces

The focusing and alignment subsystem is designed to minimize facility interface requirements. The mobile alignment light system will require electric power at each heliostat location and the alignment target will have both an electrical and mechanical interface with the receiver tower.

a. Electrical Requirements - Power for the focusing and alignment subsystem will be obtained from two receptacles at each heliostat. One receptacle will provide 117-Vac standard commercial power for the FASS fans, laser, and facility lights. The other receptacle is a 208-Vac 3-phase 18-kVA minimum outlet for operation of the lamps and lamp-positioning motors. These two receptacles will be located adjacent to the heliostat power and data electrical outlets. The FASS does not require any additional control interfaces with the heliostat or HAC beyond the manual control box.

The alignment target electrical interface is defined by the calibration system requirements since the alignment target will be mounted on the front of the calibration target. These interface requirements are given in Section II.E.

Mechanical Interfaces - The focusing and alignment target will have a mechanical interface with the receiver tower elevating module. Since the alignment target must be located as close as possible to the planned receiver aperture location, it will be fastened to the front of the calibration module during focusing and alignment. The mechanical interfaces with the receiver tower are defined in Section E.

The mobile light-positioning system mechanical interface requires a 11.6-m (38-ft) wide roadway access to the heliostat field.

9. Focusing and Alignment Subsystem Tradeoff Study

The definition of an optimum technique for focusing and aligning multiple mirror systems for solar power concentration is a critical problem for large solar power heliostat arrays. This problem is further complicated when adjustable-focus mirrors are used. In an effort to define an optimum technique, Martin Marietta evaluated several approaches to this problem. A brief discussion of the most promising methods, their advantages and disadvantages, and the rationale for rejecting each for this proposed program is discussed.

a. Laser Techniques - The invention of lasers has provided a most powerful tool for the alignment of optical systems. Several laser techniques were evaluated during the study. The major disadvantage of using lasers in this application is that the narrow laser beams illuminate only a small portion of the total mirror surface. Therefore the reflected beam represents

only the optical properties of this small area. If prefocused well-figured mirrors were used, this surface sampling would be adequate. However, focusable mirrors of the type we will use do not provide a consistent precision figure for which a single or even several small-area elements will represent the correct focal point or total mirror performance. Therefore both individual mirror focusing and intermirror alignment require that a large percentage of the focusable mirror surface be illuminated with collimated light, and optimally, the entire mirror. Such illumination provides both an optimum focusing and alignment image and the actual image produced by the full mirror. The requirement for a knowledge of both of these factors in the 5-MW receiver performance caused the eventual elimination of all laser techniques that employed tightly collimated small-area laser beams.

Single Laser Approach - This approach uses a single laser positioned at the receiver aperture location (the point at which the solar beam will be focused by the mirror). The laser beam is then directed sequentially to several premasked points (5 minimum) on each heliostat mirror and the reflected beam displayed on a target. The target is placed at the simulated solar angle. When the mirror is properly focused, the laser images at the target should be spaced identically to the masked points on the mirror indicating parallel light. However, in addition to illuminating only a very small percentage of the mirror surface, this technique suffers from geometric insensitivity

since the laser-to-mirror distance is much larger than the mirror-to-target distance. Therefore, the relative image locations on the target must be precisely adjusted. Such adjustment is complicated because the laser beam is Gaussian and is diffused by this geometry. Locating this image with the precision required for focusing and alignment therefore becomes impractical if not impossible. This is further complicated by the precise pointing requirement placed on the laser. Therefore, focusing using this approach is not considered achievable.

Multiple-Laser Approach - This approach inverts the geometry of the single laser approach described above by positioning several (5 minimum) intercollimated lasers in front of each mirror so their angle of incidence simulates the equinox noon position of the sun. The mirror is then adjusted until the five images are superimposed at the receiver aperture. The prime reason for eliminating this technique was the irregularity of the focusable mirror figure discussed above. This leads to a high probability that the five-point or multiple-point focus will not be the true focal points of the entire mirror. Additionally, no data are generated on the energy distribution from the total mirror surface. This technique also requires the same precise collimation of the incident laser beam from one mirror to the next that is required for the recommended approach. The laser technique does, however, have a much stricter requirement for reflected beam interference, which eliminates positioning devices such as the bridge crane concept.

b. *Collimated White Light Techniques* - The results just discussed point out that the optimum light source for heliostat focusing was a collimated beam of light that would flood the heliostat. Since the heliostat is approximately 6.7-m (22-ft) square, a collimated light source of that size is impractical both to manufacture and position. Therefore, a collimated white light source that floods a single mirror and is sequentially positioned in front of each mirror so the collimation is preserved becomes an achievable solar simulator.

Although, simulation of the solar noon equinox position of the sun, illustrated in Figure II-D-1, is the most straightforward technical approach, accurate positioning of the light source is a difficult problem. This requires that the light source be located on a mobile positioning device that could be moved in front of each heliostat in the field. The light would then have to move to 25 positions and retain collimation from position to position.

In an attempt to avoid this mechanical problem and a tower in the heliostat field, four other techniques that were not direct simulations of the solar geometry were evaluated. Two of these techniques called for locating both the collimated light source and the focusing target on the receiver tower as illustrated in Figure II-D-7. The focusing target would be located near the receiver aperture location and the light source at another location on the tower. Using this configuration, the light source would still have to be moved in front of each mirror

to maintain collima-
tion but the position
would be known very
accurately and ade-
quate collimation
would be more easily

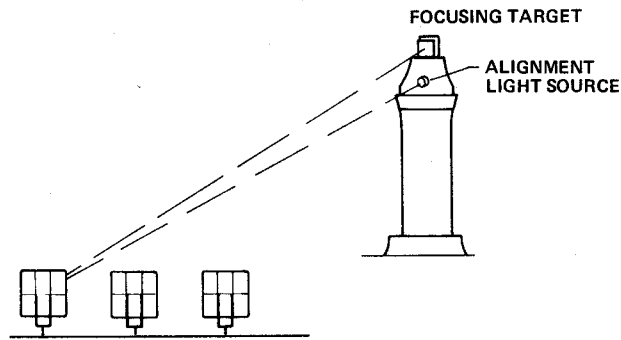


Figure II-D-7 Alignment Light and Alignment Target on the Receiver Tower Geometry

achieved. Since the
off-axis position of

the sun was not being simulated, the Martin Marietta Solar PAGOS computer program was used to calculate the off-axis image correction required. This was done by performing a ray trace analysis for each mirror on the heliostat as a segment of a single mirror representing the entire heliostat. Based on the ray trace information with the heliostat as a theoretical spherical surface, an ideal heliostat figure that gave a minimum image size at the receiver aperture was derived. This perfect surface was then segmented into zones representing each of the heliostat mirrors. The heliostat position was then changed to the geometry of both the light source and alignment target on the receiver tower. The ray trace program was then run for this condition to define both the image positions and shape the ideal mirror would produce for this geometry for each heliostat mirror. This results in each mirror having a displaced image location from that of the center mirror.

To illustrate this approach, several examples of the computer ray trace were done on a sampling basis for a solar heliostat array. The resultant ray trace image distributions are given in Figures II-D-8 and II-D-9. These figures show the images predicted using the center point of the sun for an ideal off-axis mirror in the solar simulation position (Fig. II-D-1) and in the light and target on the tower configuration (Fig. II-D-7). Figure II-D-8 for a mirror located in zone A, six rows north and five rows west of the receiver tower. Figure II-D-9 represents a mirror in zone D, 11 rows south and 6 rows west of the receiver tower. Both figures illustrate the image location required to obtain the ideal focus for the equinox solar noon conditions for several of the 25 heliostat mirrors when the ideal mirror is turned to the light and target on the receiver tower.

Under the first of the two methods of applying this concept, the image displacement would be fed to the heliostat array controller, which would drive the heliostat to the new position predicted by the controller for each mirror. The mirror would then be focused at the center of the alignment target and the process repeated for the next mirror. This would require 25 different heliostat positions for each heliostat focusing and alignment. However, an error analysis showed that the accumulated heliostat positioning error was too large, making this approach unacceptable.

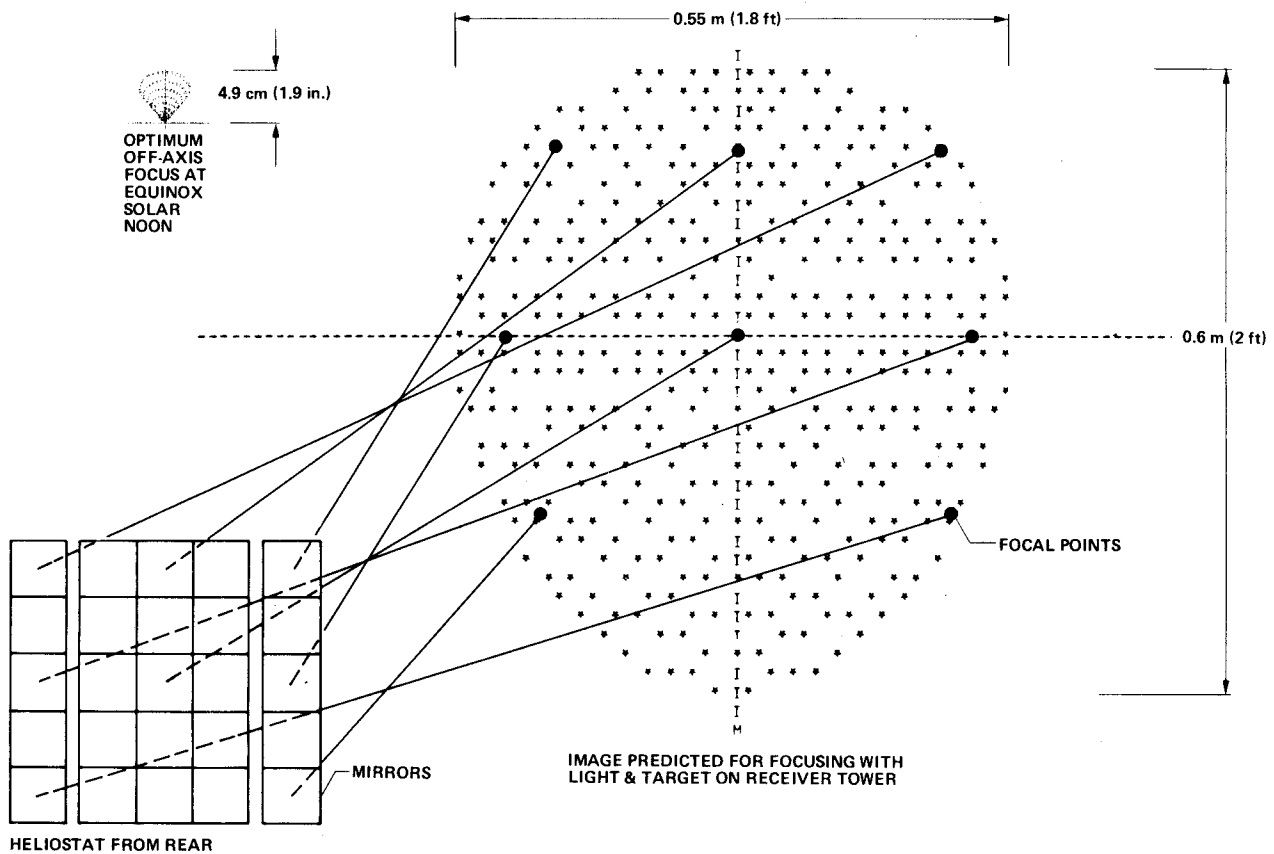


Figure II-D-8 Computer Ray Trace of Focus Offset Positions for Light and Target on Receiver Tower Concept - Sample 1

The second method, using the light and the alignment target on the tower, is identical to the first except the image displacement and shape for optimum focus of each mirror would be computed in advance and provided to the focusing and alignment technician. The focusing would then be done by focusing the the center mirror of the heliostat at the center of the alignment target and each of the other mirrors at the precalculated offset position. This technique is both feasible and within our capability. However, the technique requires a more elaborate alignment target with a position readout capability, installation and operational interface of a large light-positioning

system with the receiver tower, and a logistics and identification system that identifies approximately 13,500 individual pointing positions and image shapes to the technician performing the mirror alignment. The system also requires total reliance on the computer prediction with no demonstration of performance under simulated conditions. Based on these factors, the technique was judged to be inferior to the direct simulation approach.

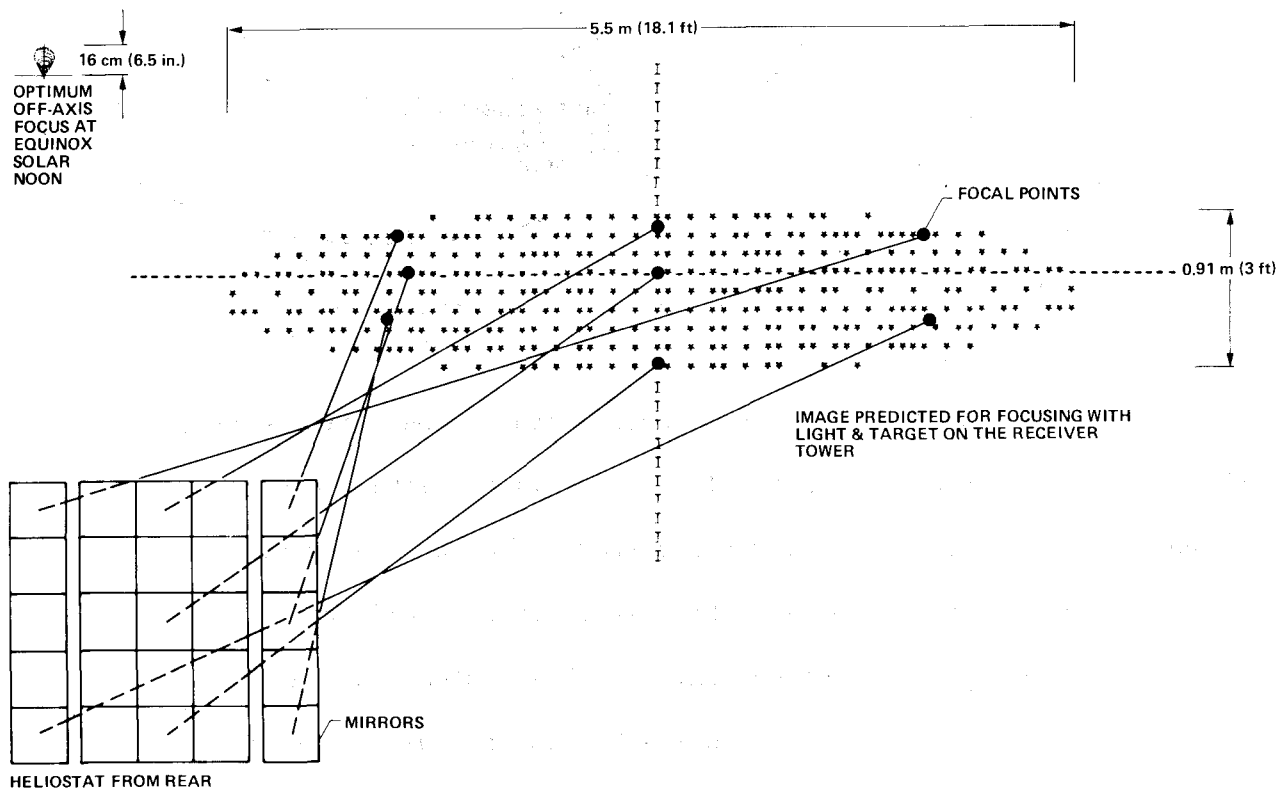


Figure II-D-9 Computer Ray Trace of Focus Offset Positions for Light and Target on Receiver Tower Concept - Sample 2

c. *Off-Site Alignment Techniques* - The two additional techniques that eliminated the direct simulation light-positioning fixture in the heliostat field were based on off-site heliostat focusing and alignment. These techniques would be

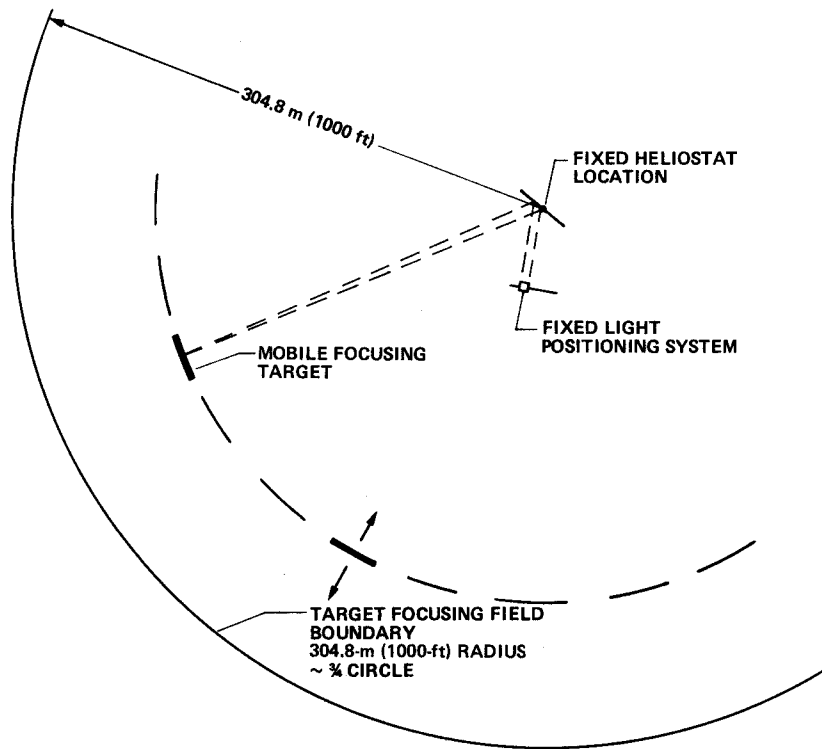
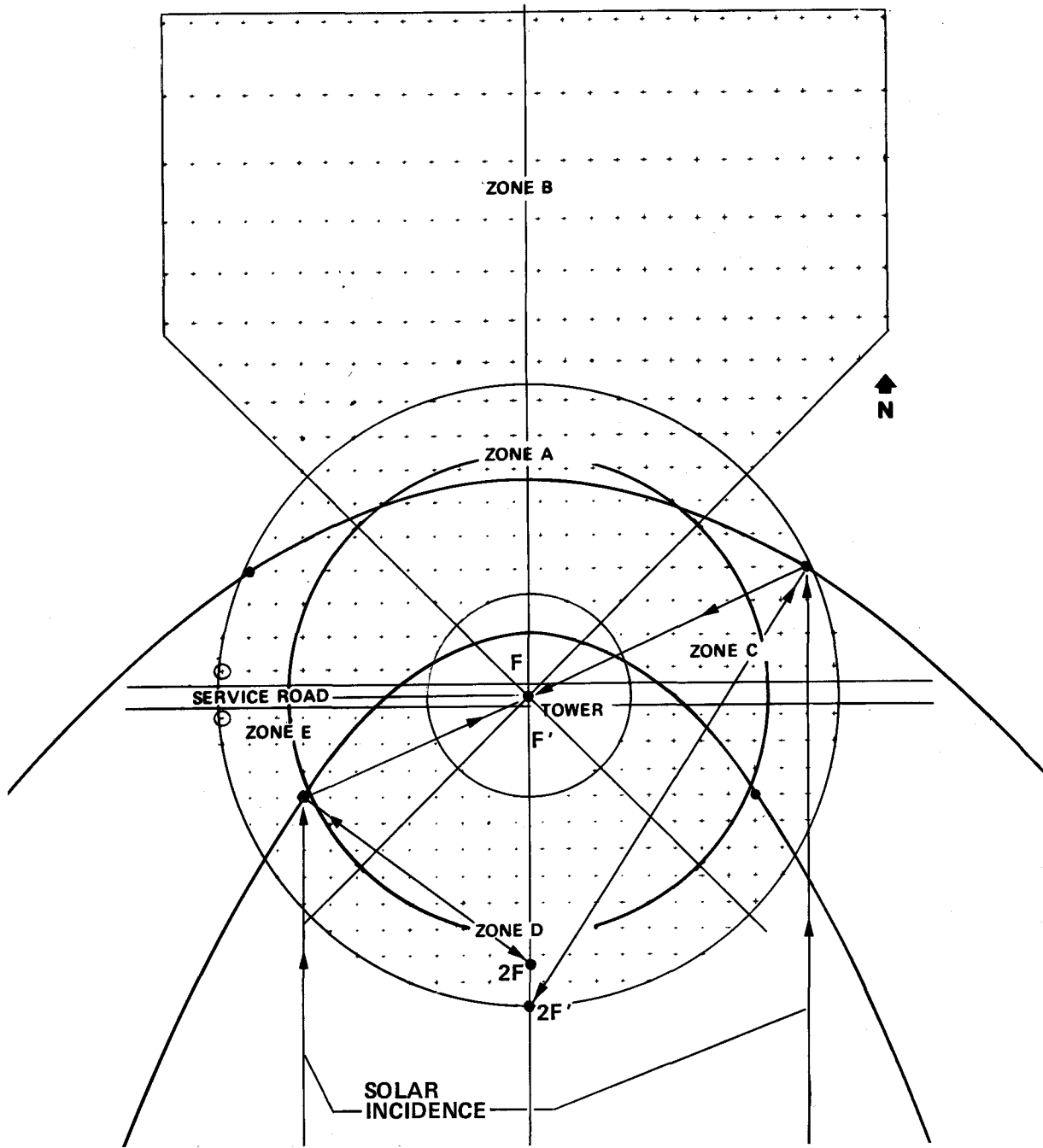


Figure II-D-10 Off-Site Heliostat Focusing Using Off-Axis Angle Simulation

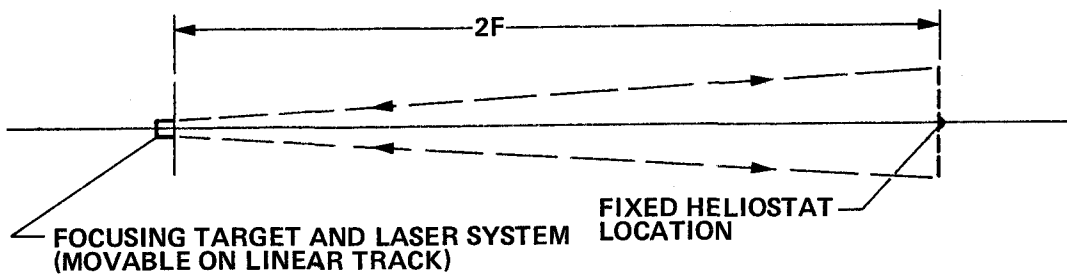
performed at ground level in a horizontal plane. The first technique, as illustrated in Figure II-D-10, is an off-site reconstruction of the solar geometry and mirror-to-target distances in the horizontal plane for each heliostat using a collimated light source and positioning system. In this system the light-positioning system would not be mobile but the alignment target position would vary for each heliostat. This technique provides an acceptable off-site simulation but complicates refocusing since any heliostat would have to be taken to the off-site location for refocusing. This was considered to be unacceptable based on the refocusing requirement given in paragraph 3.1.5.f of K93681.

The other off-site technique considered the geometry of the total heliostat field relative to the incident solar radiation at solar noon at the equinox. At this time each heliostat, F, in the field falls on a theoretical parabola as illustrated in Figure II-D-11. The parabola focal length is defined by the receiver tower aperture. Therefore, in theory, there is a 2F position on the axis of each parabola from which emitted light is focused on itself from any point on the parabola. This 2F-to-heliostat distance could be computed and then set up on a straight horizontal track to test the focus of each heliostat. However, the instantaneous focal length varies with the position on the parabola. This gives rise to the optical aberration known as coma. If this technique were used, the off-axis coma would have to be removed on a mirror-by-mirror basis through a computer ray trace analysis similar to that described above. For this reason and because of the refocusing requirement discussed in the previous paragraph, this technique was also unacceptable.

Several mechanical focusing and alignment techniques were also considered as part of this study. All such techniques were, however, determined to be impractical due to the dimensional accuracies required vs the heliostat size and the nonperfect figure of focusable mirros.



(a) HELIOSTAT FIELD PARABOLIC FOCUSING AT EQUINOX SOLAR NOON



(b) OFF-SITE FOCUSING GEOMETRY

Figure II-D-11 Parabolic $2F$ Focusing and Alignment Geometry

E. Calibration Subsystem

E. CALIBRATION SUBSYSTEM

This section presents Martin Marietta's proposed design and implementation of the calibration subsystem (CSS). Our selected approach satisfies all CSS requirements identified in K93681.

Table II-E-1 lists the key requirements related to the CSS and summarizes Martin Marietta's proposed approach to meet these requirements. The basic requirements of the calibration subsystem can be grouped into two categories. One involves the requirement to determine the relative beam characteristics, including size, shape, and power density centroid of the beam. The other requires the calibration of specific thermal power available at a predetermined size of target. To meet these criteria, we propose the use of photovoltaic (solar) cells and a water calorimeter, respectively. The following paragraphs describe the major design considerations and tradeoffs, with rationale for selection, the selected subsystem design and implementation plan. Addendum VI of Volume IV is a preliminary requirements specification for the CSS; Addendum VII is the preliminary CSS interface requirements specification.

Table II-E-1 Summary of Major Calibration Subsystem Requirements and Proposed Approach

ITEM	KEY RFQ REQUIREMENTS	RFQ PARA	PROPOSED APPROACH
1	CALIBRATE THE ORIENTATION OF THE REFLECTIVE SURFACE.	3.2	DETERMINE POWER DENSITY CENTROID AND BEAM PATTERN AT THREE TIME POINTS BETWEEN 10 am TO 2 pm WHILE THE HASS IS PLACED ON AUTOMATIC TRACKING MODE, USING SILICON SOLAR CELLS AS SENSORS.
2	DETERMINE BEAM QUALITY 0.9 P _R AT CIRCULAR TARGET OF DIAMETER 0.012 SR AT EQUINOX NOON. CALIBRATION TARGET ORIENTED NORMAL TO BEAM. MIRROR SPECULAR REFLECTION MEASUREMENT WITH 5 deg EPPLER PYRHELIOMETER OR EQUIVALENT.	3.2 3.1.4.1 3.1.4.1 3.1.4.1	USE OF WATER CALORIMETER WITH ADJUSTABLE MECHANICAL IRIS TO PROVIDE NEAR-CIRCULAR TARGET OF DIAMETER 0.012 SR, AND ANALYTICALLY VERIFY PERFORMANCE AT EQUINOX. ORIENTATION OF TARGET PLANE TO THE BEAM ACCOMPLISHED BY TWO-AXIS CONTROL CAPABILITY (CSS MODULE AZIMUTH AND TARGET ELEVATION CONTROL). TWO PYRHELIOMETERS USED.
3	SATISFY 1 AND 2 FROM ANY ONE HELIOSTAT LOCATED IN ANY OF THE HELIOSTAT ZONES.	3.2	CALIBRATION TARGET, SENSORS, AND PERIPHERAL EQUIPMENT MOUNTED ON AN ASSEMBLY TEST ROTATES 2π RADIANS AROUND THE TOWER. TWO-AXIS ORIENTATION CAPABILITY OF THE CALIBRATION TARGET PROVIDES COVERAGE OF THE CLOSEST AND FARTHEST HELIOSTAT IN ANY ZONE.
4	PROVIDE SENSOR OUTPUT INTERFACE WITH THE MCS COMPUTER.	3.2	DIGITAL INTERFACE UNIT PROVIDED TO ALLOW SERIAL DATA TRANSFER TO MCS COMPUTER.
5	PROVIDE SUFFICIENT RESOLUTION AND DYNAMIC RANGE IN THE SENSORS TO DETERMINE BEAM QUALITY AND ENERGY CENTROID OF BEAM FROM ANY HELIOSTAT.	3.2	WATER CALORIMETER AND SOLAR CELLS (USING NEUTRAL DENSITY FILTERS) HAVE CAPABILITY TO MEASURE UP TO 58-sun INTENSITY, WHICH IS THE MAXIMUM POSSIBLE PERFORMANCE OF THE CLOSEST HELIOSTAT UNDER BEST SUNLIGHT CONDITIONS. SOLAR CELL OUTPUT MEASUREMENTS (64 CELLS) HORIZONTALLY ACROSS THE TARGET PLANE WILL PROVIDE DATA OVER 5.18x5.18-m AREA.
6	DETERMINE SIZE AND SHAPE OF REFLECTED SOLAR IMAGE FROM ANY HELIOSTAT WITHIN ±0.1 METER.	3.2	SOLAR CELLS, 1x2 cm, (0.39x0.79 in.) LOCATED 8.09 cm (3.19 in.) APART ON A VERTICAL BEAM 5.18 m (17 ft) IN LENGTH WILL PROVIDE ADEQUATE COVERAGE INCLUDING MAXIMUM ABERRATION.

The major design tradeoffs were as follows:

- 1) Size of the calibration target;
- 2) Location of the calibration target (calibration ring vs top of elevator vs platform);
- 3) Beam quality test approach (calorimeter vs pyrhelimeter vs pyranometer vs solar cell);
- 4) Beam size, shape, and power density centroid determination approach.

1. Size of the Calibration Target

A 6.1x6.1-m (20x20-ft) target size was selected. This was dictated by four main factors:

- 1) The RFQ requirement of a circular target of diameter equal to 0.012 times the slant range (SR) at solar noon on the equinoxes for beam quality specification;
- 2) The SR of the farthest heliostat;
- 3) The beam size and pattern;
- 4) Accommodation of the target for the heliostat focusing and alignment subsystem.

Based on the maximum SR of 291.57 m (956.58 ft) in heliostat zone B, the maximum target diameter (d_{\max}) to satisfy the beam quality requirement at solar noon on the equinoxes is

$$\begin{aligned} [1] \quad d_{\max} &= 0.012 (291.57 \text{ m}) \\ &= 3.5 \text{ m (11.48 ft)}. \end{aligned}$$

To allow for the aberration, a factor of 0.015 was used to determine the maximum diameter of the iris to be designed, which is $(0.015) (291.57 \text{ m}) = 4.37 \text{ m (14.35 ft)}$.

The worst-case solar image size would occur for a heliostat at the most distant point in zone B and when mirror aberrations are at maximum values. The degree of aberration depends on the position of the heliostat in the collector field and the time of day and the day of year. At solar noon on the equinoxes, the aberrations of the mirrors are at a minimum since the mirrors will be focused onto the target for those times. For the proposed Martin Marietta warped-mirror heliostat, the maximum solar image size d_s , including off-axis aberrations, can be approximated by the relationship

$$[2] \quad d_s = SR \sin \theta + d_a$$

where θ = angle subtended by the sun's rays on a point on the mirror,

d_a = length of solar image on the target due to optical aberration.

Using the maximum possible aberration of any heliostat, which is 2.44 m (8 ft), the maximum solar image on the target plane for the farthest heliostat is

$$[3] \quad d_s = 291.57 (\sin 0.00931 \text{ rad}) + 2.44$$

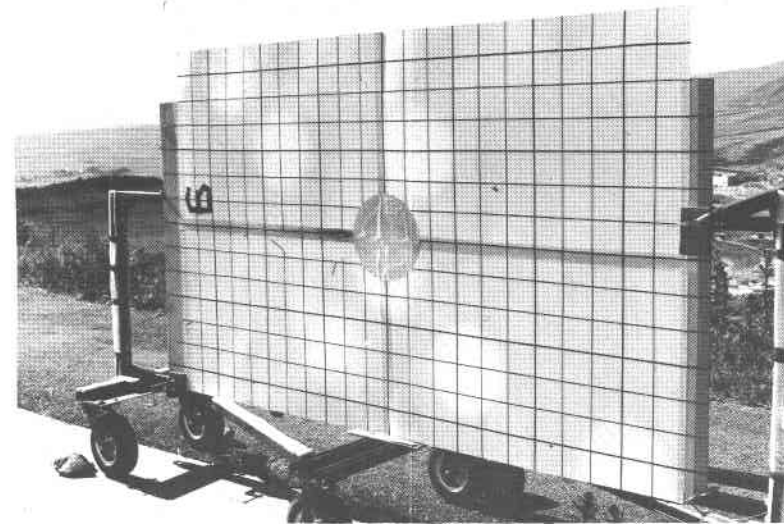
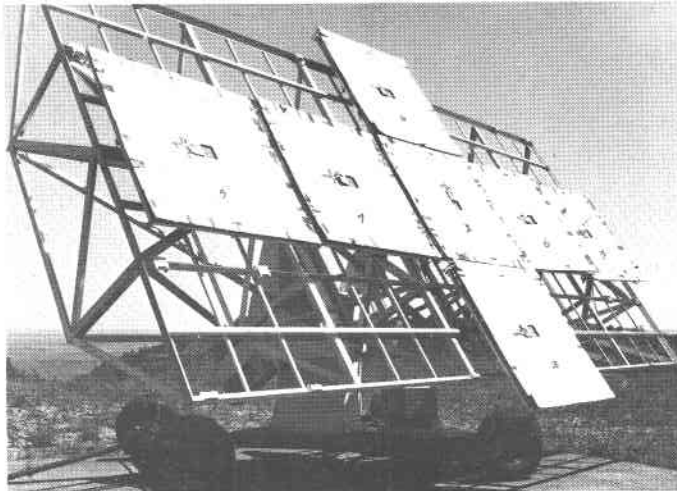
$$d_s = 5.15 \text{ m (16.91 ft).}$$

Figures II-E-1 and II-E-2 show the computer-derived and empirical beam pattern at various times of a given day for a seven-mirror (warped-glass) heliostat. Each mirror was focused (i.e., aberrations minimized) for noon mountain daylight time (11 am true solar noon). These results are shown to illustrate that:

- 1) Reflected beam pattern and size on a fixed target will vary significantly as a function of time of day and date of year;
- 2) The centroid of the actual beam power will remain approximately (not exactly) at the center of the target with time.

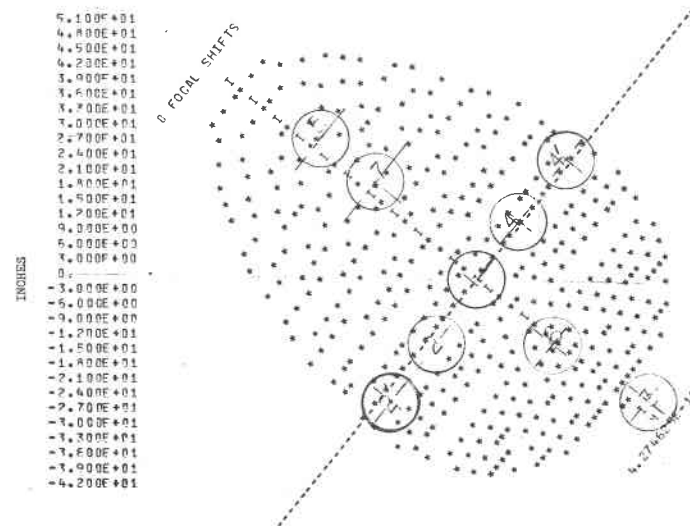
•Item 2) is due to several factors, the key ones being the aberration from off-axis pointing, manufacturing tolerances of the mirror, and imperfect warping of the mirror. The shape of the reflected beam on the target is expected to vary from an elongated ellipse or pear shape to a near circle at solar noon.

Figure II-E-1



(A) OPTICAL TARGET PHOTOGRAPH

SEVEN-MIRROR CONCENTRATING HELIOSTAT
 MASKED FOR CENTER RAY REFLECTION
 OPTICAL PATTERN TESTING TO STUDY
 EFFECTIVE SPHERICAL ABERRATION
 (MARTIN MARIETTA RESEARCH PROGRAM)

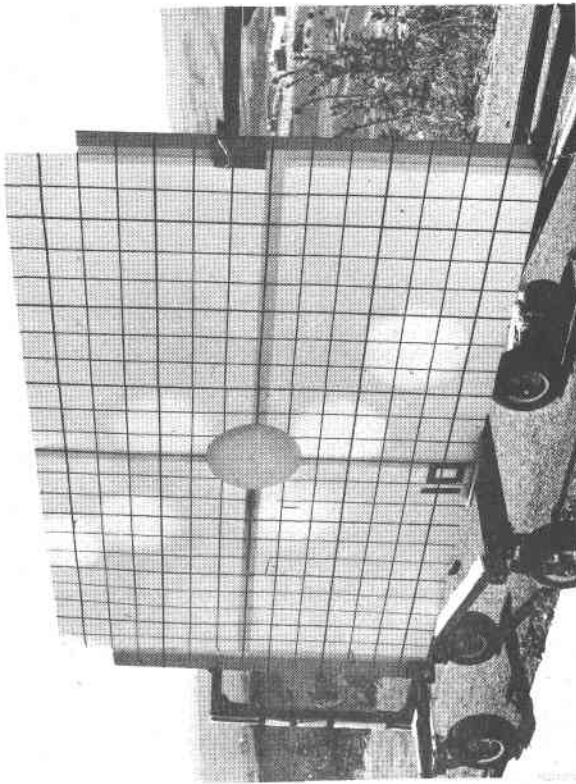


(B) OVERLAY

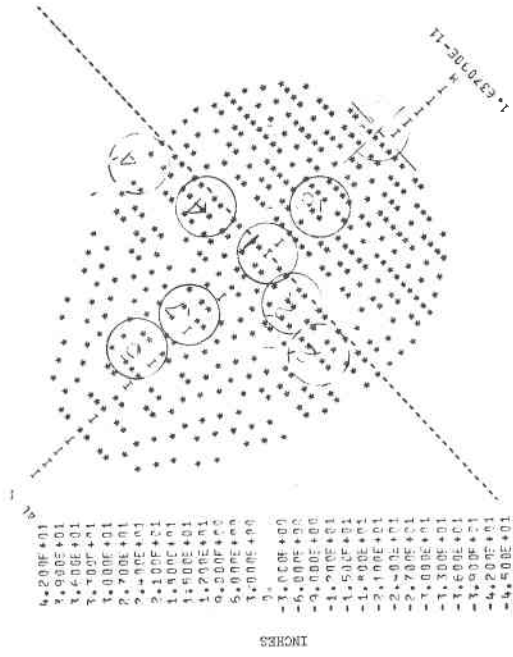
9 am MDT

Figure II-E-1 Optical Target Photograph and Overlay of Test Observation
 Images on Computer Pattern between 9 and 11 am MDT, May 29, 1974

II-E-5

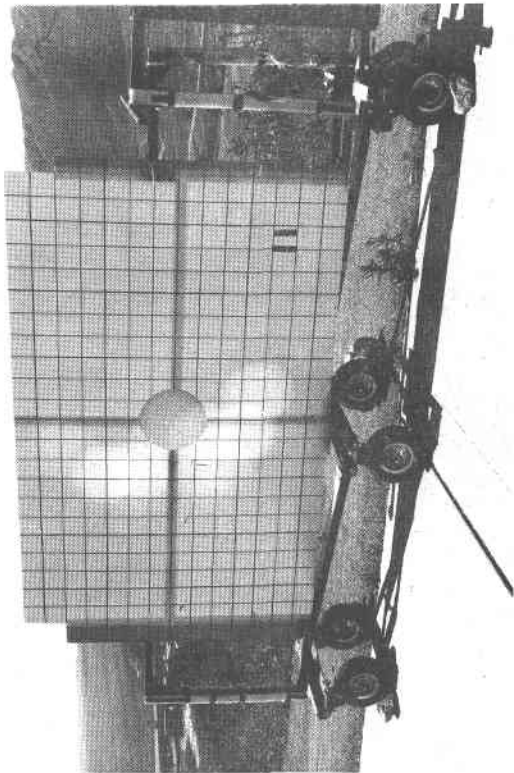


(A) OPTICAL TARGET PHOTOGRAPH

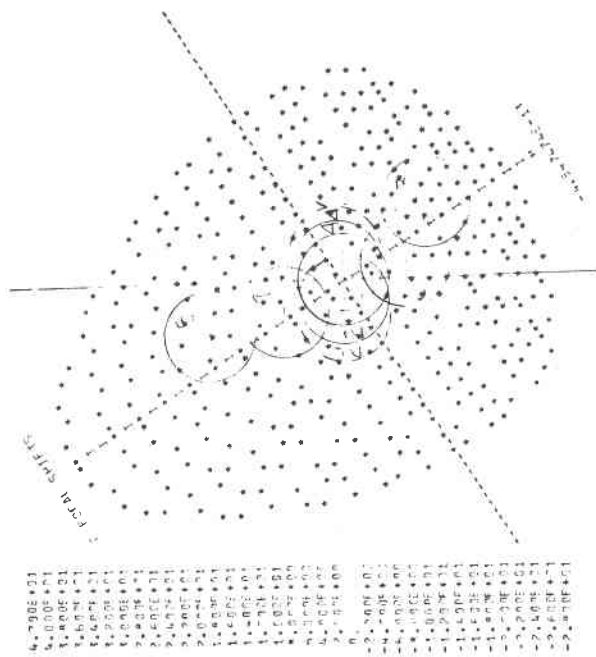


(B) OVERLAY

Figure II-E-1 (Concl)

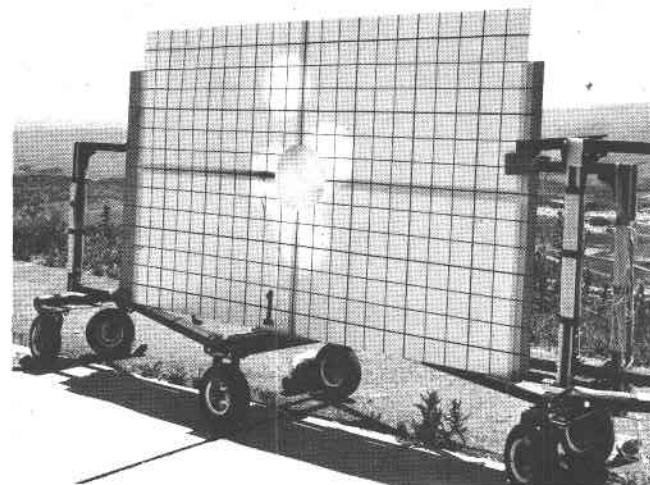
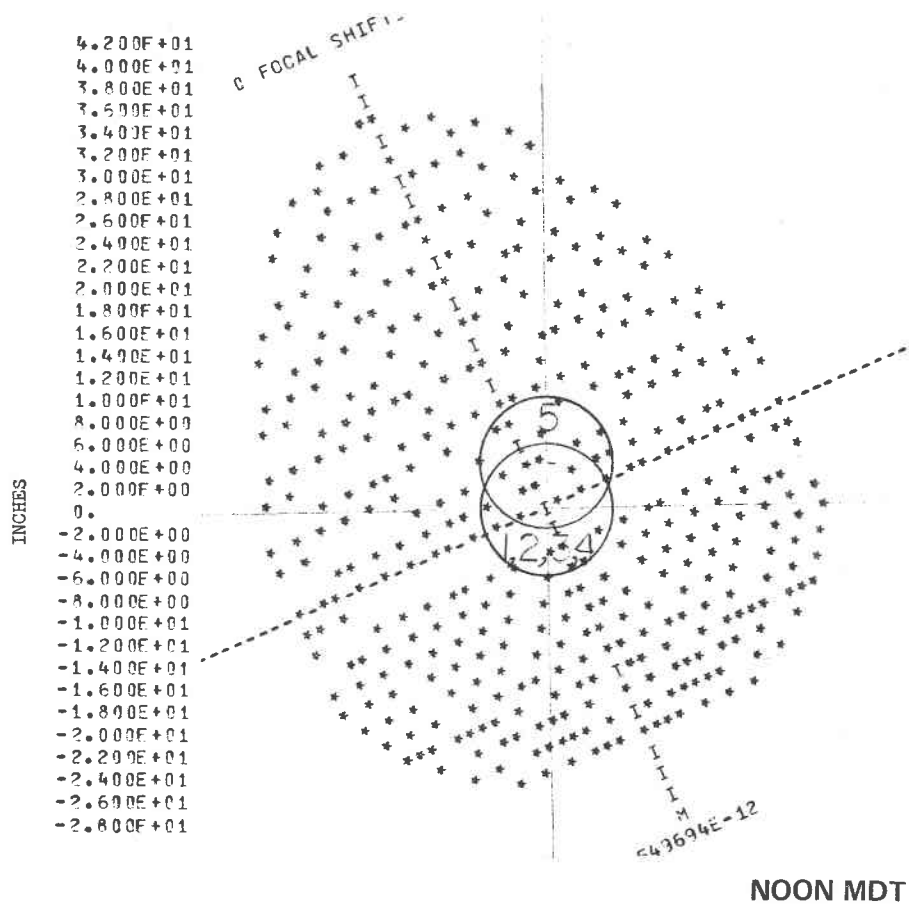


(A) OPTICAL TARGET PHOTOGRAPH

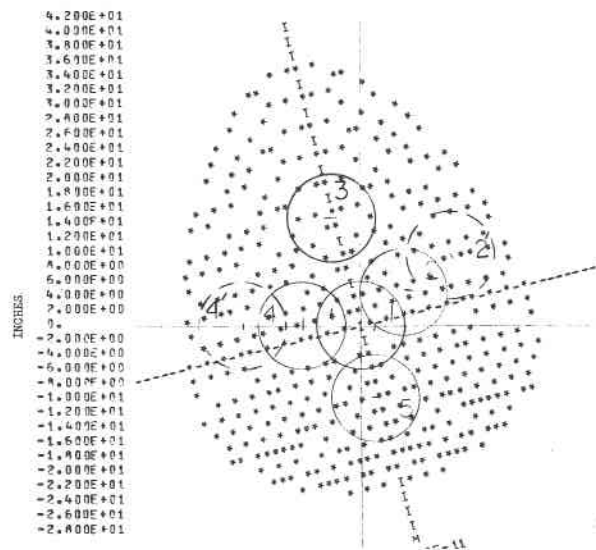


(B) OVERLAY

Figure II-E-2



(A) OPTICAL TARGET PHOTOGRAPH



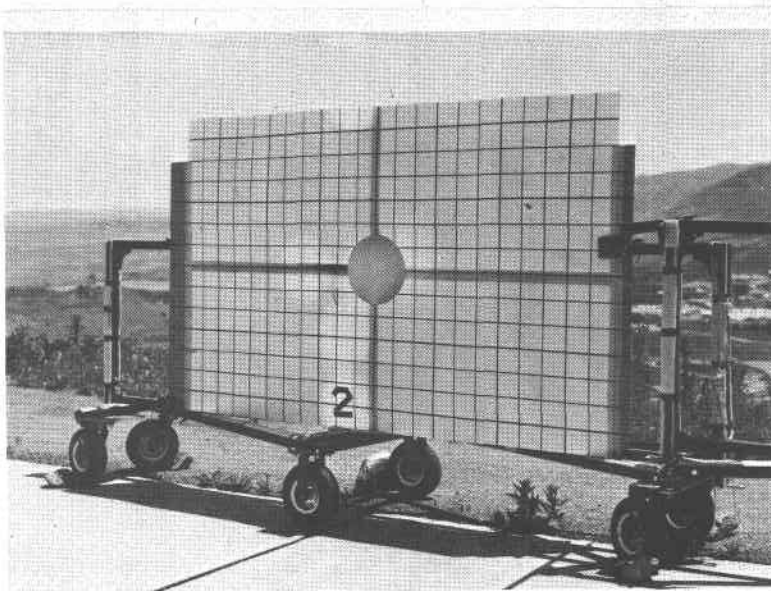
(B) OVERLAY

1 pm MDT

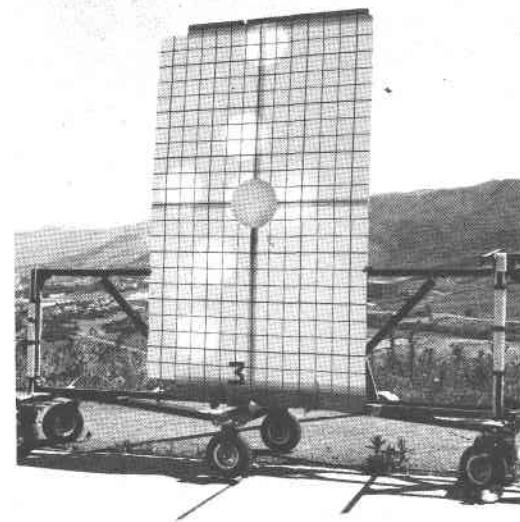
Figure II-E-2 Optical Target Photograph and Overlay of Test Observation
Images on Computer Pattern between Noon and 3 pm MDT, May 29, 1975

II-E-7

Figure II-E-2



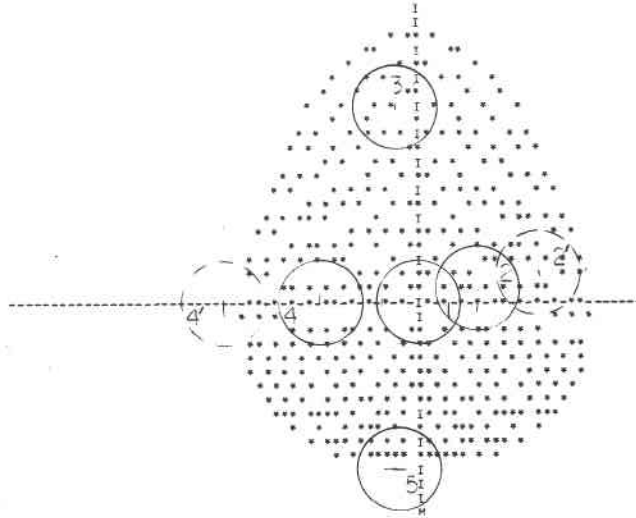
(A) OPTICAL TARGET PHOTOGRAPH



(A) OPTICAL TARGET PHOTOGRAPH

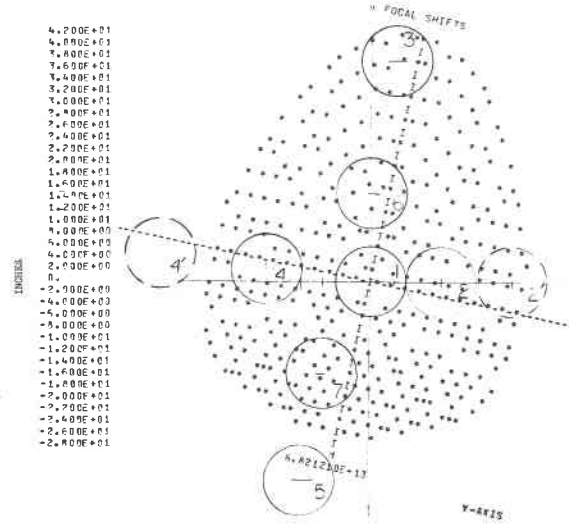
INCHES

4.200E+01
4.000E+01
3.800E+01
3.600E+01
3.400E+01
3.200E+01
3.000E+01
2.800E+01
2.600E+01
2.400E+01
2.200E+01
2.000E+01
1.800E+01
1.600E+01
1.400E+01
1.200E+01
1.000E+01
8.000E+00
6.000E+00
4.000E+00
2.000E+00
0.
-2.000E+00
-4.000E+00
-6.000E+00
-8.000E+00
-1.000E+01
-1.200E+01
-1.400E+01
-1.600E+01
-1.800E+01
-2.000E+01
-2.200E+01
-2.400E+01
-2.600E+01
-2.800E+01



(B) OVERLAY

2 pm MDT



(B) OVERLAY

3 pm MDT

Figure II-E-2 (Concl)

As discussed earlier, length of the image should not exceed 5.15 m (16.91 ft). For this reason, the solar cell sensors will be located on a vertical beam covering a linear distance of 5.18 m (17.0 ft). The beam will be driven across the target plane via a motorized drive system to allow the determination of beam size and shape over a 5.18x5.18-m (17.0x17.0-ft) area.

We have analyzed the requirements and approaches for the mirror alignment and focusing subsystem relative to its target. The alignment target requirement was established as 6.1x6.1 m (20x20 ft), which was considered adequate to satisfy the focusing requirements (see Section D).

Based on the above discussions, the pacing factors influencing the actual target size was the structure required to support a circular target of 4.37-m (14.3-ft) diameter and the need to characterize the beam size up to 5.18 m (17 ft). A 6.1x6.1-m (20x20-ft) target was therefore considered adequate to meet all criteria.

2. Location of Calibration Target

Three basic approaches were considered relative to tower features shown in the Black and Veatch report, *5-Megawatt Solar Thermal Test Facility* dated 20 October 1975.

The first approach (Fig. II-E-3) involved the use of the calibration ring. In the second method (Fig. II-E-4), the calibration target and its mechanical structure is mounted on a platform that could be rolled onto the elevator and moved into the position occupied by a receiver experiment. The third approach (Fig. II-E-5) makes use of the platform on the tower at elevation 57.3 m (188 ft). In all cases, a 5.18x5.18-m (17x17-ft) target is provided and the target is capable of being oriented to any heliostat at any zone. Table II-E-2 compares the three approaches. The elevation module-mounted approach definitely appeared to be the most cost effective. However, to do the calibration, the experiment must be physically removed and replaced with the CSS target; this is unacceptable. On the other hand, the calibration ring location is technically unacceptable for mirror focusing or calibration of the heliostats closest to the tower because of its separation distance from the receiver apertures and the resulting defocusing of the reflected image. For example, if the heliostat mirrors were focused at the receiver aperture, the resulting image at the calibration target would be larger than that at the receiver aperture. Thus, the focus, alignment, and calibration target positions must be located as close to the receiver aperture as possible. The calibration target is mounted on a mobile support tower that elevates the target to the receiver aperture. This tower was located at the 51.21-m (168-ft) platform elevation based on the preceding criteria.

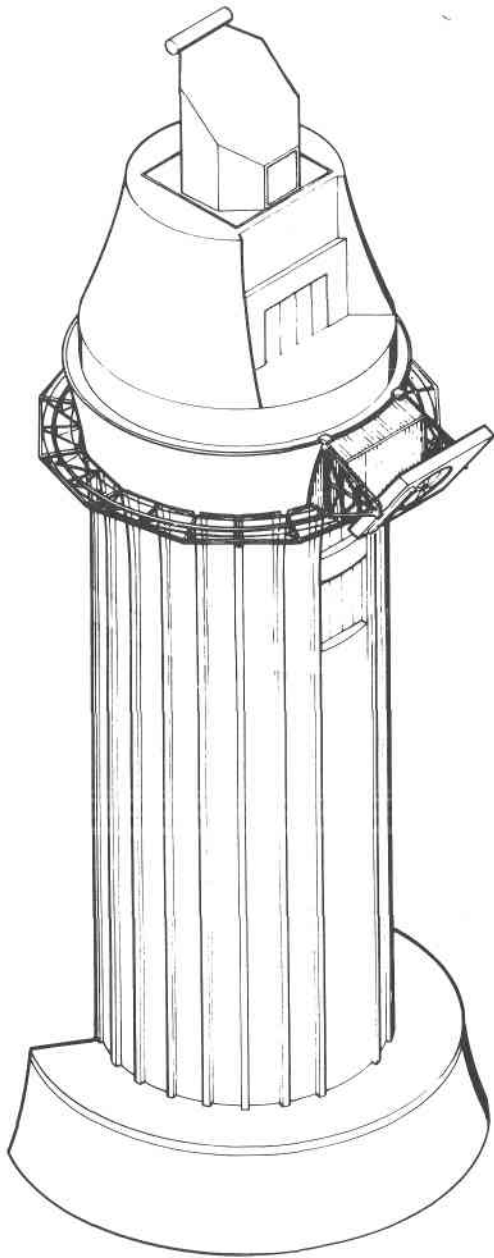


Figure II-E-3 Calibration Target on the Calibration Ring

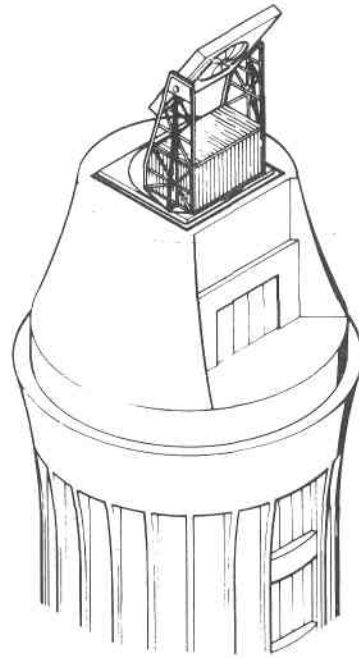


Figure II-E-4 Calibration Target on the Elevation Module

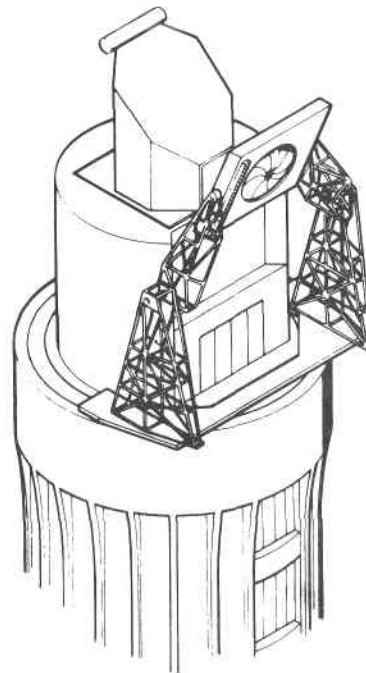


Figure II-E-5 Calibration Target on the Platform below the Receiver

Table II-E-2 Comparison of Three Approaches for the CSS Target Location

APPROACH	ADVANTAGES	DISADVANTAGES
CALIBRATION RING-MOUNTED	TARGET IN PERMANENT LOCATION. CALIBRATION OF HELIOSTATS POSSIBLE WITH RECEIVER EXPERIMENT OPERATING.	BEAM EXTREMELY OUT OF FOCUS ON CLOSEST HELIOSTATS. POOR ACCESS TO SOLAR CELLS AND TARGET FACE FOR MAINTENANCE. MOST EXPENSIVE AND DIFFICULT TO IMPLEMENT.
ELEVATION MODULE-MOUNTED	EASIEST TO IMPLEMENT AND MAINTAIN. MOST COST EFFECTIVE. BEAM CLOSE TO FOCAL POINT.	TECHNICALLY UNDESIRABLE TO OPERATE IN EXPERIMENT OR CALIBRATION MODE (ONE OR THE OTHER). TAKES TIME AND EFFORT IN MOVING EXPERIMENT AND CSS.
PLATFORM-MOUNTED	CALIBRATION POSSIBLE WITHOUT MOVING THE RECEIVER. NEXT BEST CHOICE TO IMPLEMENT. TARGET IN PERMANENT LOCATION. BEAM CLOSE TO FOCAL POINT.	SECOND MOST EXPENSIVE AND DIFFICULT TO IMPLEMENT.

3. Beam Quality Verification Approach

The beam quality requirement specifies that the heliostat be capable of directing at least 90% of the reflected power P_R onto a circular target of diameter 0.012 SR at equinox noon. The reflected power is

[4] $P_R = I\rho A \cos \theta$

where

I = intensity from 5-deg Epply normal-incidence pyrheliometer in kWm^{-2} ,

ρ = Specular reflectivity of mirror,

A = mirror area,

θ = angle between mirror normal and sun vector at equinox noon.

There are several possible approaches of satisfying this requirement. The four approaches we considered are use of the normal-incidence pyrheliometer, pyranometer, silicon solar cell, and calorimeter. The two basic problems common to all these

approaches are (1) how to make the required measurements to determine P_R at any given time and day, and (2) how to extrapolate them to the equinox solar noon conditions. To determine the number and type of the solar flux sensors, the basic properties of the reflected beam at the target plane must be understood. The beam from our heliostat design has the following characteristics:

- 1) Reflected rays are uncollimated;
- 2) Solar intensity can range from 2.9 to 58 solar constants;
- 3) Beam size can occupy an area of diameter from 0.91 m (3 ft) to 5.18 m (17 ft);
- 4) Beam pattern can be circular, pear shape, elliptical, or elongated ellipse;
- 5) Beam intensity can vary in a matter of several seconds.

a. *Pyrheliometer Approach* - The use of the Eppley normal-incidence pyrheliometer (Fig. II-E-6) involves a number of constraints. It has a 0.10-rad deg field of view in its collimated tube and its sensor requires at least 1 second to stabilize before a valid measurement can be made. The sensor, made of platinum, has a flat response from 0.3 to 2.8 μm . The electrical output (in mV) is linear up to two solar constants.

The required measurements over a 4.37-m (14.35-ft) diameter area must be made within several seconds. To do this, one cost effective approach is to mount an array of pyrheliometers about 12.7-cm (5-in.) apart on a 5.18-m (17-ft) vertical support structure. This structure would then be scanned across the target plane horizontally. Because of the 1-second dwell time in making



Figure II-E-6 Pyrheliometer

a stable measurement, the vertical support structure would have to be programmed to stop at least a full second at predetermined lengths. If it stops every 15.24 cm (6 in.), the total measurement time would take about 34 seconds.

Based on the measurements obtained, the reflected power can be determined for a given circular area by calculating the average power over the total area illuminated. Because calibration activities would normally be done on days other than the equinoxes, the circular area equivalent to that of the equinox solar noon must be determined. To do this, the existing Martin Marietta computer program would be used.

The key features of the pyrliometer that are desirable for beam quality determination are:

- 1) Direct electrical measurement;
- 2) No radiation loss (from the sensor);
- 3) Good spectral match with the receiver thermal collector surface (0.3 to 2.8- μ m wavelength).

There are several technical problems. One is measurement accuracy. Since pyrliometer is designed for sensing a collimated beam of light, uncollimated rays from a given heliostat may cause only a small percentage of the energy flux to be intercepted by the pyrliometer sensor. This may present a significant contribution to the measurement error. Another technical problem arises from the extremely high insolation levels. Our preliminary analysis has shown that under the best sunlight condition, the true beam from one heliostat at the target plane can reach 58 solar constants and a steady-state temperature as high as 538°C (1000°F). Because the pyrliometer is limited to two-sun intensity, a neutral density filter is necessary to allow the pyrliometer sensor to operate within its region of linearity.

b. Pyranometer Approach - The main difference between the pyrliometer and pyranometer is that the latter looks at π steradian. Thus, the pyranometer has two features more suited

for the requirement--(1) it is not affected by the uncollimated light and (2) it is less sensitive to pointing errors. However, the pyranometer would be subject to some error due to the diffuse or scatter radiation it sees.

c. Solar Cell Approach - The use of photovoltaic cells presents very similar problems and a similar approach to the pyr-heliometer. For cost and maintenance reasons, the solar cells would also be mounted on a vertical beam that would be scanned across the target (rather than an extensive array of cells on the entire target area). The primary differences between the pyr-heliometer and the solar cells are:

- 1) The solar cells have an instantaneous response. Therefore they can be scanned across the full target as fast as the data acquisition system permits;
- 2) The solar cells are responsive to a 0.4- to 1.1- μm wavelength. This means they are not a good spectral match with the solar thermal collector;
- 3) Assuming 10- to 12-grid solar cells with 2 ohm-cm base resistivity, the solar cell output (i.e., the short-circuit current) is linear with intensity only up to about three solar constants. Use of a neutral density filter is thus required for testing any heliostat that provides an intensity greater than three suns;
- 4) The solar cells do not need a collimating tube. Thus, this approach does not require the pointing accuracy of the pyr-heliometer;

5) Calibration of the solar cells to a given solar intensity is done with a secondary standard solar cell. The secondary standard cell is calibrated to the balloon-flown cells.

d. Calorimetry Approach - The calorimetry approach developed and presently in use at Martin Marietta in the central receiver solar thermal power system project basically involves measurement of the temperature rise of a given amount of water. Figure II-E-7 shows the prototype calorimeter in operation at Martin Marietta. This calorimeter uses a focal plane area of approximately 1.7 m² (18.1 ft²). The focal plane consists of three strips of Olin brass roll-bond (type FS-7610-SW) solar panels, each strip 0.43-m (17-in.) wide and 1.32-m (52-in.) long. The strips are treated with the Martin Marietta optical black surface (MMOBS), which is a form of anodizing that provides an absorptance of greater than 99.0%.

During a test, the heliostat focuses the sun's image on the focal plane receiver of the calorimeter. Water is circulated through the roll bond panels and the inlet and outlet temperature are recorded. By measuring the time required for a preset mass of water to flow, data are obtained from which the heat flux is obtained. This heat flux, extrapolated to the solar noon on the equinoxes, can then be compared with the value determined from equation [4].

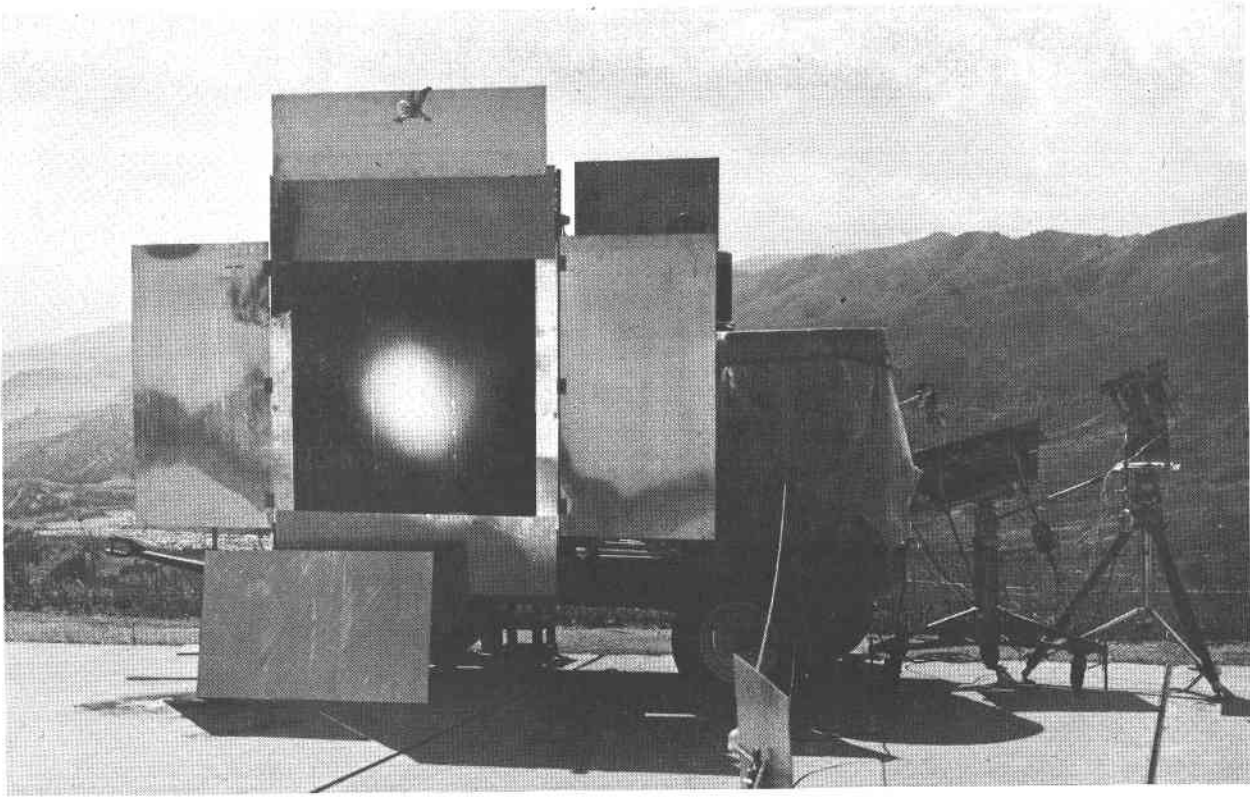


Figure II-E-7 Prototype Calorimeter Being Used for Heliostat Tests at Martin Marietta

e. Selection of Technical Approach - The primary advantages of the sensors (pyrheliometer, pyranometer, and solar cells) over the calorimeter for beam quality verification are:

- 1) System is much simpler and quicker to implement;
- 2) Radiation losses are negligible;
- 3) Direct electrical measurements are possible;
- 4) Overall cost is substantially lower.

Their disadvantages are the following:

- 1) They all require various neutral density filters for different heliostat distances (which cause varying intensity conditions);
- 2) Computer-aided calculations are required;

- 3) A potentially large error in the measurement can occur, especially for the pyrliometer due to uncollimated light beam.

One single advantage of the calorimeter is that it is capable of handling the full range of heat flux from 2.9 to 58.0 solar constants. The other sensors may be able to perform adequately. However, even with careful selection of a neutral density filter at very high intensities, the measurement accuracy that can be achieved with either solar cells or the pyrliometer is uncertain. Based on these technical considerations and the fact that a working calorimeter prototype has been demonstrated by Martin Marietta, we have selected the calorimeter for the beam quality verification.

There are good indications that the silicon solar cells that will be used for beam characterization (shape, size, centroid) may be used to acquire the data for beam quality verification. A detailed analysis, however, is required to determine the effects of spectral differences between the solar cell (0.4 to 1.1 μm) and the pyrliometer (0.3 to 2.8 μm) on the electrical output. The total spectral energy of the sun at the earth's surface between 1.1 and 2.8 μm is 20 to 30% when solar intensity is at least 0.8 kWm^{-2} . During the early contract phase, we will empirically correlate the solar cell and pyrliometer outputs to determine the error band. If the error is found to be acceptable, we will use the solar cell sensors as a backup to the calorimeter for beam quality test.

4. Beam Size, Shape, and Power Density Centroid Determination Approach

To characterize the beam size and shape, and to determine the centroid of the power density, the solar cells were the clear choice. No other sensors are capable of providing accurate intensity measurements. To acquire the data, an array of solar cell sensors mounted on a vertical beam assembly will be scanned across the target as previously described.

The centroid of the beam power density will be determined using the solar cell measurements. Software will be defined for the MCS computer to calculate the centroid of the beam power density. An example of the algorithm for this computation is:

- 1) Acquire solar cell data;
- 2) Divide solar cell data into discrete data points defined relative to the CSS target coordinates;
- 3) Calculate the centroid using the equations

$$[5] \quad \bar{x} = \frac{\sum_{i=1}^n \sum_{j=1}^m (P_{jA_j})_i x_i}{\sum_{j=1}^m (P_{jA_j})}$$

$$[6] \quad \bar{y} = \frac{\sum_{i=1}^n \sum_{j=1}^m (P_{jA_j})_i y_i}{\sum_{j=1}^m (P_{jA_j})}$$

where

\bar{x} and \bar{y} = points on the target coordinates defining the centroid,
 A_j = incremental unit area on the target defined for each discrete
solar cell datum,
 P_j = solar intensity data at each unit area A_j as measured by the
solar cell.

5. Detailed Calibration Subsystem Description

Figure II-E-8 shows the block diagram of the proposed CSS.

It consists of the following subassemblies:

- 1) CSS module - Mechanical components and the structure that houses the CSS target and subsystem elements;
- 2) Solar cell sensor assembly - Electrical and mechanical components required to provide the capability to characterize the reflected beam pattern, intensity distribution, and beam centroid of any heliostat in any zone;
- 3) Calorimeter subsystem - Electrical and mechanical components required to provide capability to determine the beam quality of any heliostat in any zone;
- 4) Interface electronics and cabling - Electronics required to interface solar cell calorimetry and position information with the MCS and all electrical harness related to the CSS;
- 5) Control and display panel - Electrical and mechanical components required to manually control all drive mechanisms, set up calorimeter subsystem, and aid in making calorimetry measurements.

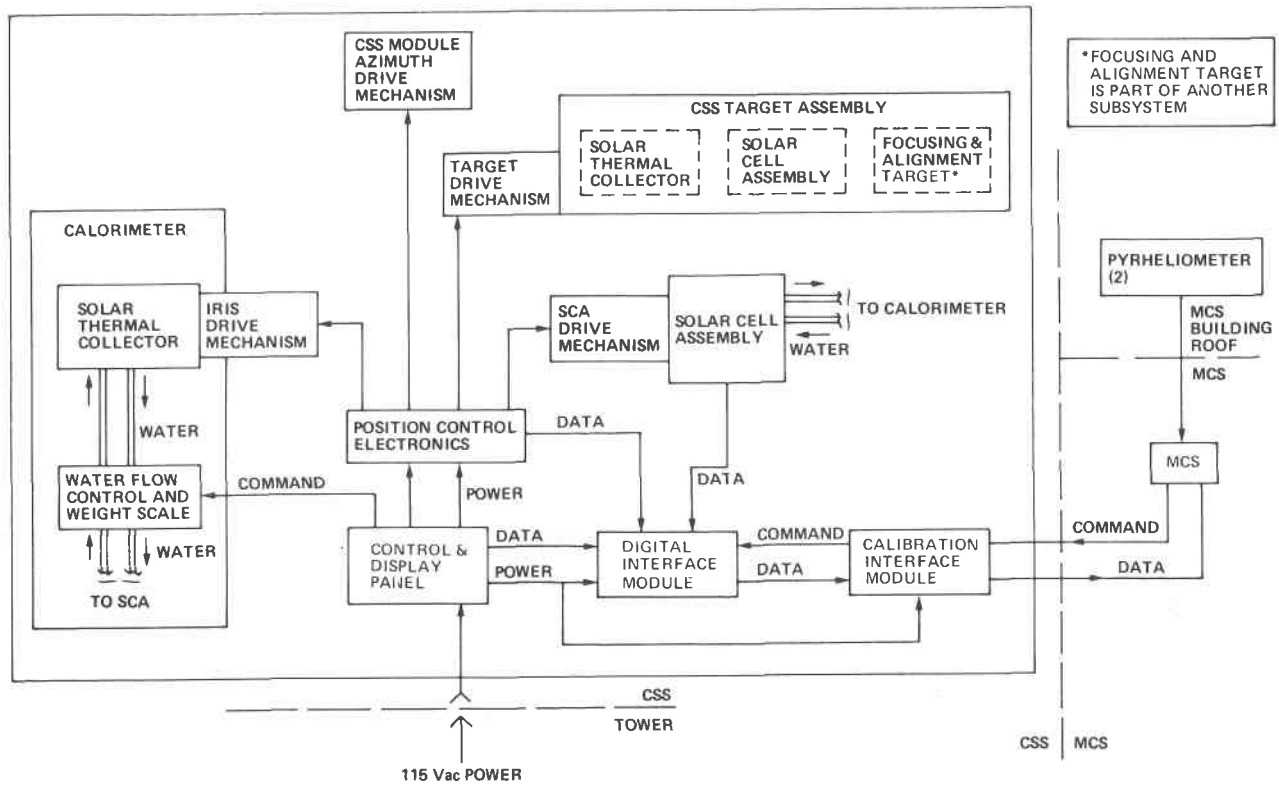


Figure II-E-8 Calibration Subsystem Block Diagram

The following paragraphs summarize both design and functional performance of each of these subsystem components. Safety, reliability, maintainability, manufacturing, and interface features are also discussed.

a. *CSS Module* - To accommodate the functional and performance requirements established for the proposed CSS module, special structural and mechanical features are introduced. The calibration target must be located near the receiver aperture and be able to view the entire heliostat field without interference from tower structures. Our approach, illustrated in Figure II-E-9, uses a platform located at the 51.2-m (168-ft) elevation level. The base of the calibration module support tower is mounted on a rigid

C-shaped support platform. This platform is in turn fixed to three 4-wheel bogies that rotate 2π radians on two ASCE 27.2-kg (60-lb) monorails. The rails are centered about a 7.62-m (25-ft) radius at the 51.2-m (168-ft) elevation level. The drive mechanism to rotate the C-shaped support platform is located in one bogie.

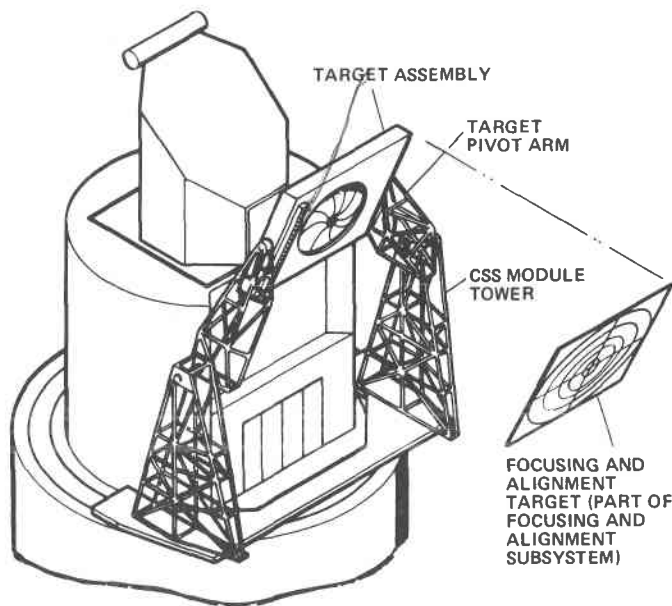


Figure II-E-9 Calibration Subsystem Module

The target support structure consists of two towers and two pivot arms attached to the towers. The target assembly is suspended between the two pivot arms. It has a single degree of freedom to provide an orientation capability (elevation adjustment). An independent drive mechanism provides this rotation control. The pivot arms consist of a trussed frame structure that can rotate approximately π radians on the centerline between the two support towers. This feature is required to move the target

assembly from the stowed position to the operating elevations.

The pivot arm also contains a mechanical locking feature that provides a positive stop at each extreme of travel.

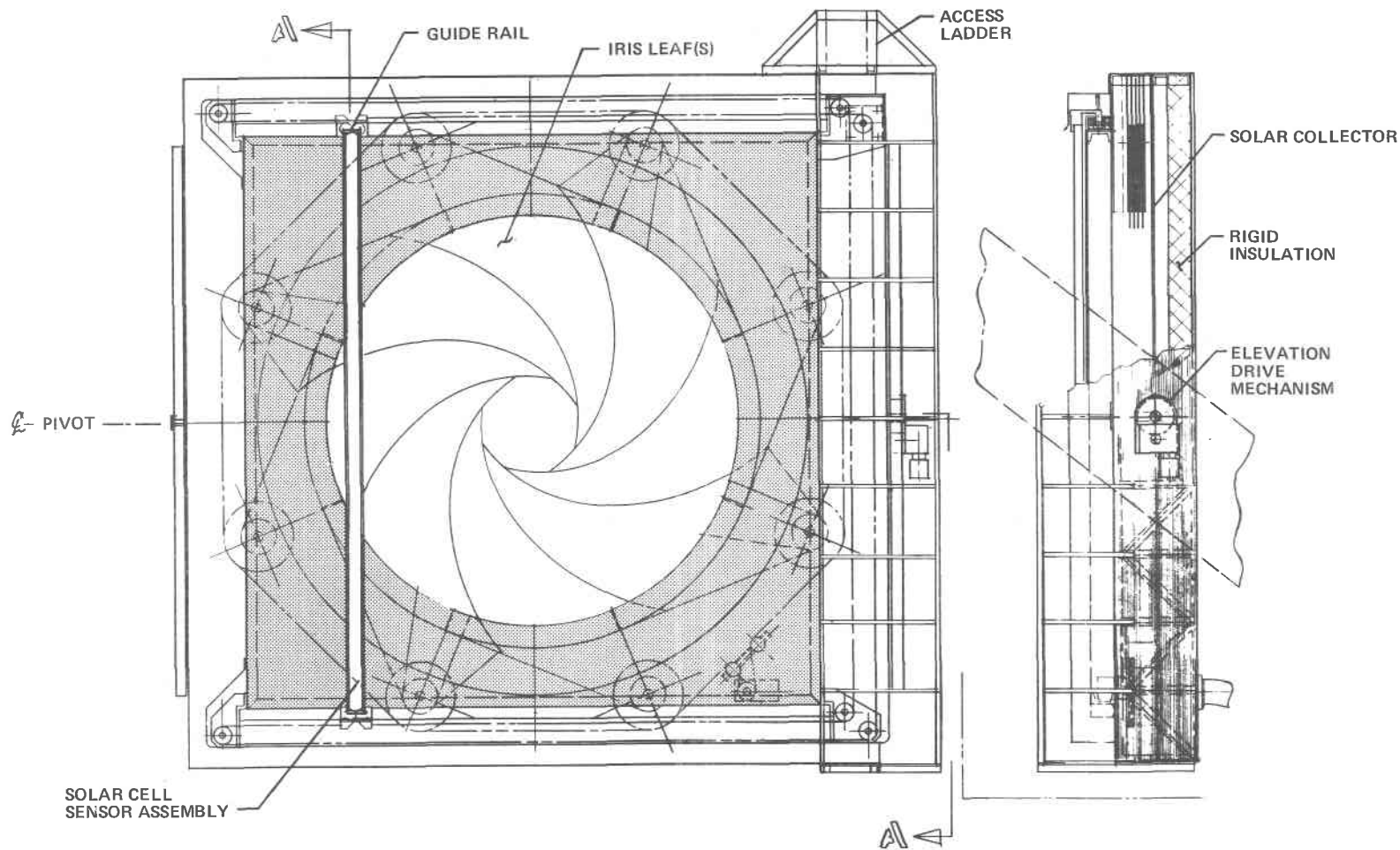
The elevated support structure is a trussed framework composed of 36 steel angle and channel sections. All sections will be joined by welding. This tower is considered fixed at the base to the tiedown platform and must be able to support the suspended CSS module under the influence of relatively high operational winds without deflection.

The lower part of the tower structure is boxed-in to provide an environmental enclosure for the water storage tanks and control systems. An independent floor system of checker-plate aluminum supported on 15.2-cm deep Z-sections provides mounting of special equipment. The roof and wall panels consist of corrugated aluminum panels supported by metal studs.

The mechanism that rotates the pivot arm to the appropriate orientation consists of a large, fixed bull gear about which a driver pinion gear rotates. Torque is applied to the pinion gear through a worm gear reducer. Power is supplied by an ac motor.

The target assembly shown in Figure II-E-10 houses the solar thermal collector and the iris assembly. In addition the forward section of the module provides for the mounting of a rectangular beam with solar cell sensors. This solar cell support structure is approximately 5.18-m (17-ft) high. A chain and sprocket drive system powered by an ac gear motor permits a horizontal translation of the beam assembly. Limit switches are

Figure II-E-10



II-E-25

Figure II-E-10 Calibration Target Assembly

provided to terminate motion at the end points. The support structure is fabricated from a lightweight aluminum tube section with end bracketry to mount 4-wheel bogies. A channel frame provides mounting for the sensor guide rails, the sprocket shaft bearing housings, and the drive gear motor.

The structural enclosure for the iris assembly and the calorimetry assembly and its insulation layer consists of a truss structure approximately 0.71-m (2.33-ft) deep. This truss is heavily reinforced at the center on each side to accommodate a pivot fixture for the elevation drive mechanism. Corrugated aluminum panels used for the siding and rear closure are attached directly to the truss chord members. Subpurlines or girts provide support for the large area of the rear closure panel. The iris assembly is similar in principle to a camera shutter but on a much larger scale. This configuration is based on 12 shutter leafs equally spaced on a circle concentric with the center of the target. The degree of shutter closure defines the size of opening, which varies from 0.71 m (2.33 ft) to 4.37 m (14.35 ft) in diameter. Each individual leaf rotates about its pivot point by a continuous chain and sprocket drive system powered by a motor through a gear reduction unit. Each shutter leaf will be fabricated from 0.3-cm (0.12-in.) thick, 6061-T6 aluminum sheet with a reflective finish. The leafs are stacked in four tiers of two leafs each so overlapping occurs. The effects of high temperature from the reflected beam will be evaluated to optimize the leaf design.

A flat solar thermal collector is placed behind the iris assembly. An aluminum plate, finished with MMOBS provides the exposed surface for this thermal collector. Approximately 20.3 cm (8.0 in.) of rigid thermal insulation is provided behind the calorimetry assembly.

The elevation drive mechanism consists of an external gear set plus a worm gear reducer and drive motor gear reducer and drive motor. This drive mechanism is attached to the main side trusses of the target module. The large spur gear of the external gear set is rigidly attached to the support tower superstructure.

b. Solar Cell Sensor Assembly (SCSA) - This assembly consists of a rectangular mechanical support structure, solar cell units, and temperature control piping (Fig. II-E-11). The mechanical structure interfaces with the SCSA drive assembly and water circulating system in the calorimetry subsystem. The major requirement of the structure is to provide mounting of the solar cell units and solar cell temperature control at $28 \pm 2^\circ\text{C}$ ($82.4 \pm 3.6^\circ\text{F}$) while scanning across the target plane.

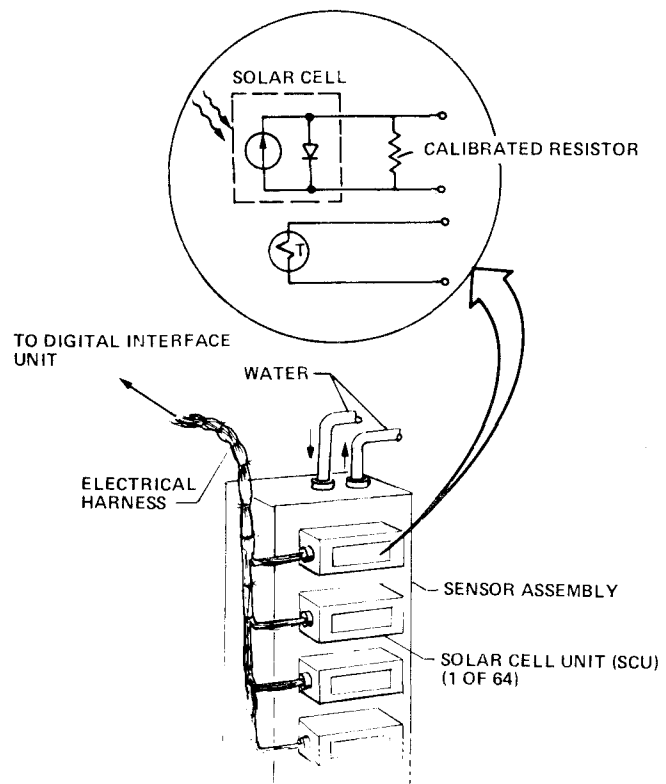


Figure II-E-11 Solar Cell Sensor Assembly

Under certain operational conditions, the solar cell temperature of up to 70°C (158°F) can be permitted. The mounting surface of the solar cell units will be parallel to the calibration target plane.

The solar cell unit consists of a housing, a silicon solar cell, a resistor, and a thermistor. The key characteristics and performance capability of the solar cell unit and its components are:

- 1) Provide sufficient seal and protection to the internal components from the environments (rain, dust, etc);
- 2) Provide capability to clean and/or replace the protective glass cover and the solar cell;
- 3) Provide capability to remove the solar cell unit for periodic calibration of the solar cells in sunlight or under a solar simulator;
- 4) Provide an easily removable plug for the electrical terminations;
- 5) Provide capability to mount a neutral density filter;
- 6) Solar cell may be a 1x2-cm (0.4x0.8-in.) or 2x2-cm (0.8x0.8-in.) N/P-type silicon cell with a base resistivity of 2 ohm-cm. The electrical output of the cell across the shunt resistor without the neutral density filter will be proportional to the solar intensity up to three solar constants;

- 7) Solar cell will be calibrated under prescribed conditions of sun or under a solar simulator such as Spectrolab X-25. The intensity of the light source will be determined using a secondary standard solar cell;
- 8) Solar cell unit with appropriate neutral density filter will be capable of measuring solar intensity up to 58 solar constants (78.47 kWm^{-2}).

c. Calorimeter Subsystem - The primary objectives of the beam quality verification is to demonstrate the capability of each heliostat to direct 90% of its reflected power into a circular area of diameter equal to 0.012 times the slant range of the selected heliostat at solar noon on the equinoxes.

The proposed calorimeter as shown in Figure II-E-12 consists of three major components or assemblies--(1) the solar collector, (2) water storage and flow control, and (3) the data acquisition system.

The solar collector will be fabricated from aluminum tubes manifolded at both the top and bottom so the water flow distance will be identical in each element. The tubes will be anodized using a Martin Marietta black process (MMOBS) that provides an absorptance of greater than 98.2%. The back sides of the tube will be insulated to minimize heat losses. The solar collector will have physical dimensions of 5.18x5.18 m (17x17 ft). This dimension was derived from a formula that calculates the total solar image size including off-axis aberrations for any day or time of the calendar year.

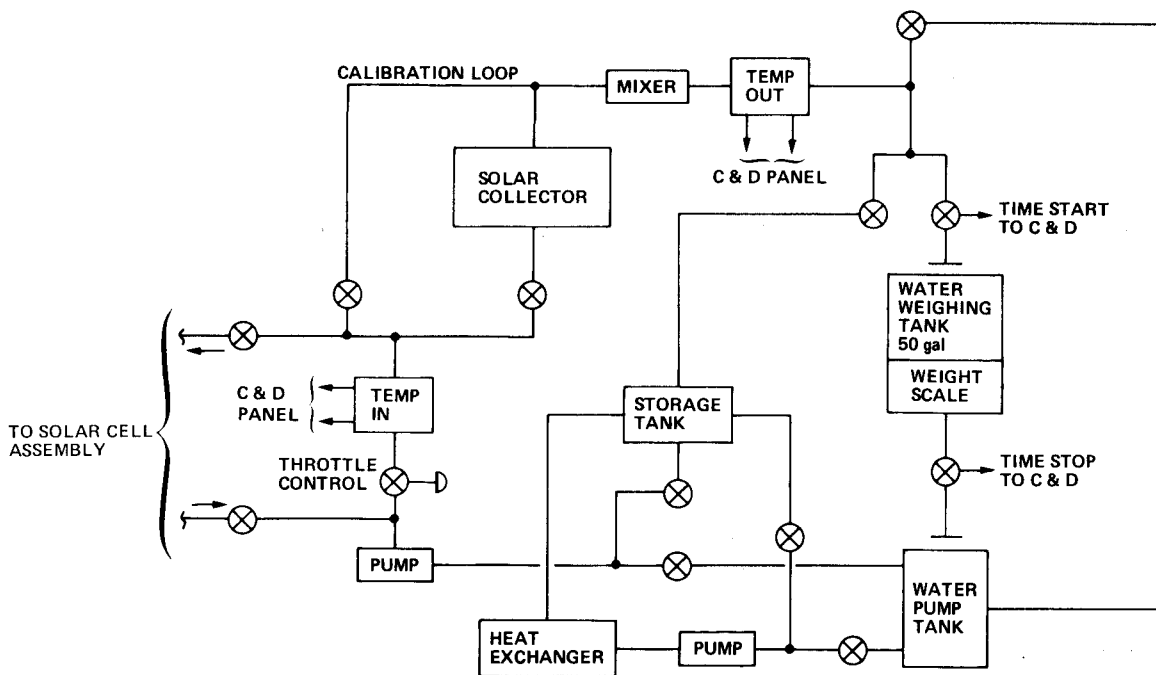


Figure II-E-12 Calorimeter Subsystem

A mechanical iris will be provided to control the size of beam exposure on the collector surface. The iris will have a circular opening with its diameter adjustable to 0.015 SR. The side of the iris exposed to the beam will have a reflective surface. To provide temperature control, the water storage and flow control subsystem will consist of pumping, plumbing, water storage, water collection and weighing, flow control, and a heat exchange device.

The data acquisition subsystem will provide such measurements as (1) water temperature into and out of the solar collector, (2) weight of water collected during test run, and (3) elapsed time during test run.

The water weight measurement will be accomplished by a precision scale or strain gage load cell integrated into the water collection system. Initiation of the control valve to start

test water flow and the output of the water weighing device will be fed to elapsed time electronics for establishing calorimetric testing elapsed time.

The measurements obtained will be transmitted to the control and display console on a real-time basis and to the digital interface unit for input to the facility master control system (MCS).

The accuracy of the calorimetry tests is determined primarily by the temperature and convection loss measurements. These parameters are functions of thermal load and environmental conditions in the vicinity of the solar collector. The following paragraphs describe our approach in assuring accurate measurements of the temperature and convection losses.

The temperature measurement instrumentation consists of precision platinum resistance thermometers and linear bridge amplifiers. The probes and amplifiers used in this system will be installed as matched sets. Before installation in the system, the probe and amplifier will be characterized to provide temperature versus resistance curves for each set. These curves can then be used to establish on-line calibration techniques that will be incorporated in normal operational procedures. The total operational temperature span of the calorimeter appears to be approximately 38°C (100°F). Since the probe/amplifier combination will be selected to have this same operational span, from the temperature versus resistance curves, low, high, and midpoint temperature resistance values can be selected from curves. These values

will then be simulated by a series of precision decade resistors and inserted into the system in place of probes, providing the capability to calibrate and/or adjust the span, linearity, and zero of the temperature measurement system on a daily or individual test basis.

The convection losses for a given iris opening will be determined before and after each test activity by utilizing the calorimeter subsystem without the presence of the solar beam. The data collected during this activity will be used as a correction factor during determination of total energy collected. The determination of convection losses involves (1) measurement of input/output temperature, (2) measurement of thermal losses across the solar collector, and (3) posttest measurements.

Input/output temperature baselines will be established by diverting the calorimeter water flow around the solar collector via the calibration loop to establish stabilization between input and output temperature measurements. Measurement of thermal convection losses is then accomplished by using the same water source flowing through the solar collector and measuring the actual temperature losses between the input water and the output water. This temperature difference will be used to correct the data obtained during the actual beam quality test runs. The third step will be accomplished in the same manner as the preceding two steps except that the water source will be supplied from the test

water used during the beam quality test. This source of water will provide a second set of data points related to water with an elevated temperature point.

After completion of calorimeter alignment and self-calibration, water will be circulated in the solar collector at a rate of 22.68 kg (50 lb) per minute. The source of water during this activity will be closed-loop between the water storage tank and the solar collector. The configuration of the solar collector at this time will be such that the entire solar collector surface will be exposed to the solar beam. The selected heliostat under test will then be directed to point at the calorimeter solar collector. This condition will be maintained until a stable ΔT is attained between the input/output temperature measurement. When stabilization occurs, the output water flow will be diverted from the water storage tank to the water weighing tank until 43.56 kg (100 lb) is collected, at which time the output flow will be returned to the water storage tank. During water weighing, the precise time to obtain 43.56 kg (100 lb) shall be measured. The temperature, mass, and time data will then be used in the following formula to obtain the total energy collected:

$$\text{Thermal Power Received at Calorimeter} = \frac{\text{Mass of H}_2\text{O}}{\text{Flow Time of H}_2\text{O}} \times \text{Average } \Delta T.$$

This procedure is accomplished with a fully opened iris (i.e., total beam inside the iris). This sequence will then be repeated at three other iris openings to obtain four-point data on a thermal power obtained versus iris diameter. The resulting data will

then be analyzed to verify the beam quality requirement. This verification requires that the diameter of the circular target corresponding to 0.012 SR at solar noon on equinox be determined by computer analysis.

To determine the power reflected by the heliostat at the plane of the mirrors for a given time, the following data are required:

- 1) Cosine of solar angle for time and date of test (available at MCS);
- 2) Average pyrliometer reading during the period in which calorimeter measurements are made (available at MCS);
- 3) Total mirror area;
- 4) Specular reflectivity of the mirrors.

In addition to verification of beam quality for purposes of acceptance of the heliostats, we propose to use the calorimeter periodically to measure heliostat power collection efficiency for determination of heliostat degradation using the following formula:

$$\text{Efficiency} = \frac{\text{Btu/hr Received at Calorimeter.}}{\text{Correct Btu/hr at Mirror}}$$

d. Interface Electronics and Cabling - A functional block diagram of the electronics required for the CSS is shown in Figure II-E-13. The electronics consists of six major elements: (1) calibration interface module (CIM), (2) azimuth position electronics, (3) elevation position electronics, (4) solar cell position electronics, (5) iris position electronics, and (6) digital interface unit (DIU).

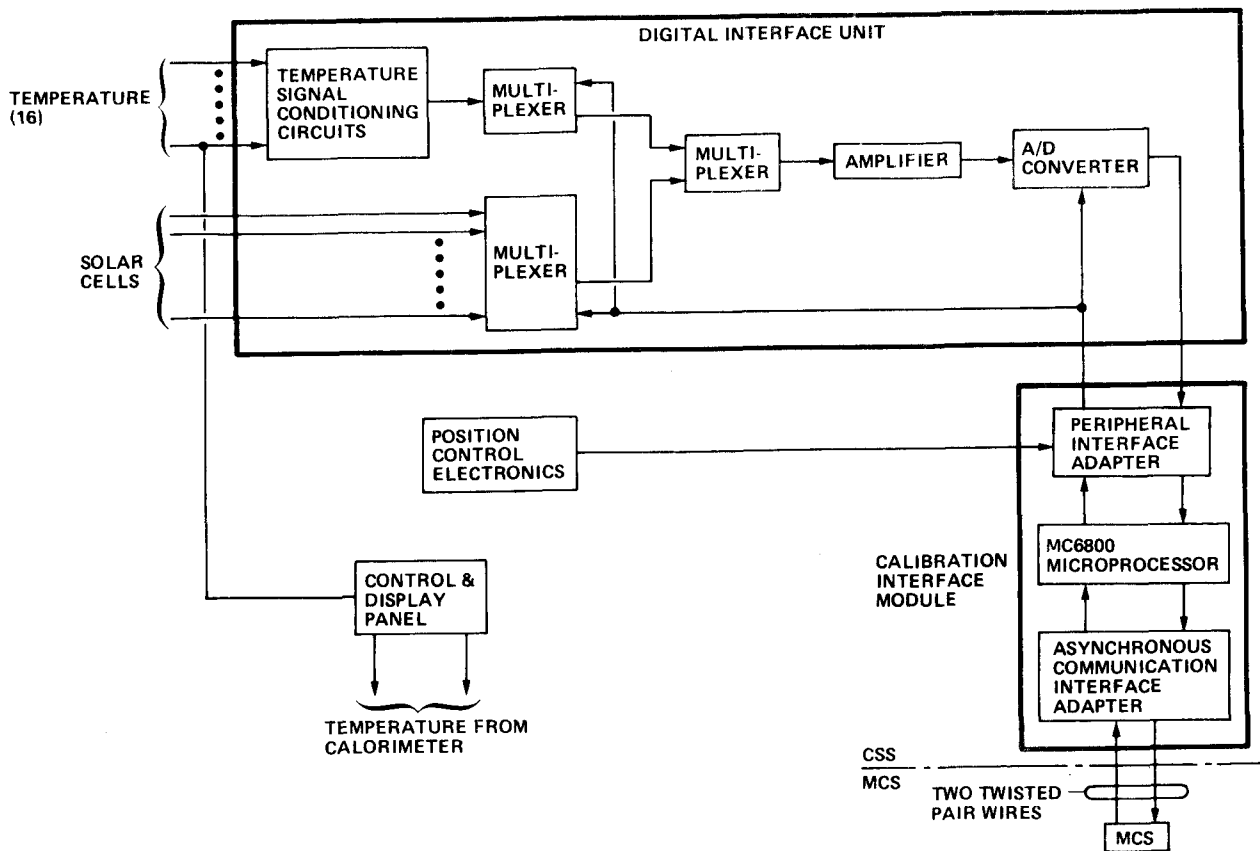


Figure II-E-13 Calibration Subsystem Electronics Block Diagram

Calibration Interface Module - The calibration interface module (CIM) will contain the electronics required to interface the CSS with the MCS. All information provided across the interface will be in the asynchronous NRZ format. The calibration interface module will decode and encode information transmitted between the MCS and the calibration subsystem using a MC6800 microprocessor and its associated peripheral equipment. The use of a microprocessor will provide a cost effective method of interfacing with the MCS while allowing a greater amount of flexibility to changing requirements that will occur as the program

evolves. By going to the microprocessor and serial data transfer, then parallel data transfer, we have reduced the number of wire interfaces with the MCS from 116 to 4.

The major function of the CIM will be to decode the serially transmitted command words into a parallel format that can be used by the subsystem electronics. This will be accomplished using synchronous communications and peripheral interface adapters in conjunction with the microprocessor. As the command is acted on, data will be transmitted back to the MCS. The microprocessor will be used to format the subsystem parallel data into a serial format compatible with the MCS. The command from the MCS to the calibration subsystem will consist of two 8-bit words containing identity and command information. The command will result in some action being performed and also in five 8-bit data words being transmitted back to the MCS containing the required information.

Digital Interface Unit - The digital interface unit will contain the electronics required to characterize and determine heliostat beam pattern and quality by collecting and transmitting the necessary measurements to MCS. It will be mounted on the solar cell assembly to minimize interface wiring between the solar cells and calibration interface module. One digital interface unit will be used for the calibration subsystem.

The unit will provide the capability to monitor 64 solar cell voltages, eight solar cell temperatures, four calorimeter temperatures, and four other temperature measurements at the calibration target. The quantity of measurements can easily be increased

if required later by adding multiplexer units. The digital interface unit can accept a total of 256 different 8-bit commands to provide the required outputs.

Position Control Units - The position control units contain the electronics required to inform the MCS of the azimuth of the CSS module, elevation of the target plane, size of the iris opening, and solar cell sensor assembly position. The electronics is contained in four units: (1) azimuth control electronics, (2) solar cell assembly electronics, (3) iris control electronics, and (4) elevation control electronics. Each unit is mounted on the respective housing for which it is measuring position. The design selected in each case utilizes a photosensing technique to provide position information. This technique requires that phototransistors and a light source be mounted for each housing position to be measured. Hole patterns will be drilled on a controlled surface through which the light will shine to provide the position information. The light source and phototransistors will be stationary while the hole pattern revolves for the azimuth and elevation monitors. The hole pattern will be stationary while the light source and phototransistors move for the solar cell position monitor. The digital gray code will be utilized to provide position information. Position information can be obtained within the following resolution:

- 1) CSS module azimuth, ± 3.14 mrad;
- 2) Target elevation, ± 7.5 mrad;
- 3) Solar cell assembly, ± 1.0 cm.

Harness and Cabling - The calibration subsystem requires power and signal interfaces at the receiver tower. Five electrical power 117 Vac, 15-A outlets are required for: (1) control of the iris, azimuth, elevation and solar assembly drive motors, the command and display console for manual control, and the calorimetry pumps and valves, (2) lighting, (3) maintenance equipment, and (4) air conditioning. Each of these outlets requires its own circuit breaker and will be enclosed in a weatherproof service entrance. A control interface with the MCS consisting of three circular multicontact connectors is also required at the elevator. The polyurethane jacketed cable will be used. Many of the cable harnesses will be required to fold and unfold while the calibration system rotates.

Control and Display Panel - The control and display panel will contain the electronics and equipment required to manually control all calibration subsystem motors and calorimetry valves and pumps. The capability will be provided to move the target in elevation or azimuth independently of the MCS. The calorimeter will be controlled and maintained from this panel. In addition to the functions described above, the control and display panel will calibrate the calorimetry temperature amplifiers, monitor iris position, monitor calorimetry time intervals, and

permanently record all required information on a data logger. The control and display panel will contain all required interfaces with the MCS to perform calorimetry calculations.

Safety Features - The safety aspects of this subsystem will be evaluated in accordance with the Safety Plan, Chapter VI of Volume II. The design and operation of the subsystem will meet the requirements of 29 CFR Chapter XVII part 1910 - *Occupational Safety and Health Standards*. Specific safety considerations already considered include:

- 1) Proper grounding of all electronic hardware;
- 2) Lightning protection of CSS module;
- 3) Protective equipment and garmets for operators.

Maintainability Features - The calibration subsystem will incorporate a modular design concept. This will enable critical hardware and electronics to be removed from the system with minimum effort and will provide for the shortest possible system downtime. Where practical, complete spare units will be built to insure expedient repair of the system. Each unit will be designed using packaging and manufacturing techniques that will ensure easy maintainability of the unit.

The subsystem components will be designed, as far as possible, using standard components requiring standard maintenance. Operating and maintenance instructions will be provided for all major subsystem assemblies. These instructions will identify recommended maintenance cycles, critical maintenance components, limited-life components, and recommended replacement cycles. Special maintenance

or replacement tools, fixtures, or protective garmets and equipment will be provided as a part of the applicable subsystem, including instructions for their use. Special maintenance and calibration requirements, such as for the solar cell units, will be defined and related instructions provided.

Reliability - To ensure a highly reliable design of the calibration subsystem, analyses and tests will be performed during the development phase. The design will take into account worst-case conditions and piece parts and hardware will be derated to ensure reliable operation. A structural analysis will be performed to verify integrity of the calibration subsystem structure.

Spare focus and alignment parts to be provided will include, but are not limited to:

- 1) Solar cell units - 10 each;
- 2) Drive motor - 4 each;
- 3) Photosensors - 50 each;
- 4) Solar thermal collector - 3 each.

Additional replacement components will be identified as detailed design and components reliability data are available.

Manufacturing - The CSS and all associated items will be fabricated and assembled in accordance with the best modern engineering, shop, and field practices and consistent with the standards of the American Institute of Steel Construction, National Electrical Manufacturers Association guidelines, and the Uniform Building Code.

The mechanical assemblies will be designed and built at the Engineering Laboratory in Denver. The system will be fabricated in five major subassemblies in accordance with the applicable ASME practices: (1) solar collector/calorimeter assembly; (2) elevator boom assembly, (3) base structure/trolley assembly, (4) equipment housing, and (5) track assembly. Each of these subassemblies will undergo fit and functional checks. After satisfactory completion of the subassembly checkouts, the entire calibration system will be assembled in Denver and functionally checked for system operation. The mechanical hardware will then be broken into the major subassemblies listed and transported by surface vehicles to Sandia for installation and final checkout. All of the facilities, equipment, and skills required for construction of the calibration subsystem are available in our Engineering Laboratory.

All electronic components, including the solar cell units, will be assembled and checked out at the power sources laboratory in Denver. Existing manufacturing methods will be used where possible to minimize program costs. To provide the most cost effective build of the hardware, the units will be built in our power sources laboratory using certified well-trained, and experienced technicians. The units will be inspected for quality of workmanship during various phases of the build and test of each unit.

Interface - The calibration subsystem will require electrical mechanical interfaces, both power and signal interfaces, at the facility tower. The signal harness requires two command and two data wires to interface the CSS with the MCS. Two 117-Vac power outlets are required on the tower, one for lights and the other for the calibration drive motors.

The mechanical interface of the CSS module will be on the mobile support tower, which is located on a platform at elevation 51.2 m (168 ft). Necessary details of the attachment and CSS module base assembly interface with the platform will be defined during the early months of the contract.

**F. Installation and
Maintenance
Equipment**

F. INSTALLATION AND MAINTENANCE EQUIPMENT

This equipment would include the following:

- 1) Mirror cleaning tool - A tank truck with two 3217-liter (850-gal) tanks, pumps, plumbing, and high-pressure nozzles. The truck will be equipped with a lift device capable of carrying two men to a height of 7.62 m (25 feet). Each tank will be approximately 1.22 m (4 ft) in diameter and 3.04 m (10 ft) long. One tank will contain a mixture of soft water and detergent for initial cleaning and the other will contain soft water for rinsing. Figure II-F-1 illustrates this concept;

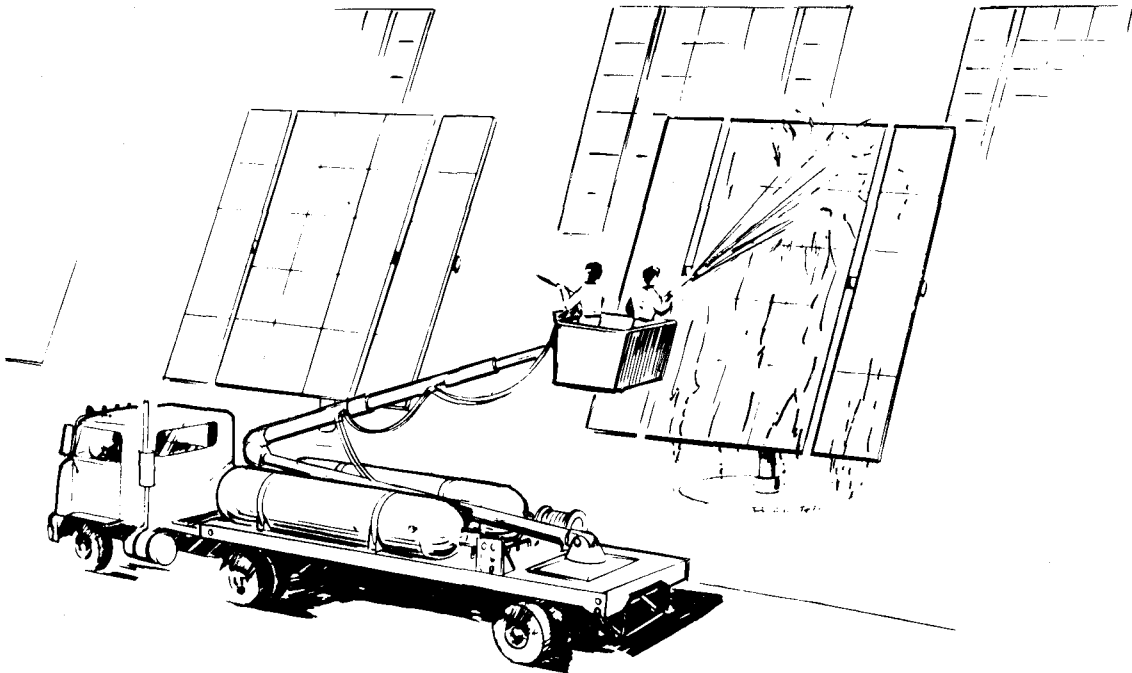


Figure II-F-1 Mirror Cleaning Equipment

2) Heliostat workstand - A 2.13x3.66 m (7x12-ft) commercially produced, self-propelled, adjustable-height platform with service height of up to 7.62 m (25 ft). This stand will be used for installation and initial alignment and focusing as well as any subsequent mirror replacement. Figure II-F-2 illustrates the stand;

3) Motor-generator - A portable 200-W motor-generator for emergency power for moving the heliostat in the fail-safe mode;

4) Spreader bar slings - Slings for handling the yoke module and the mirror module;

5) Mirror module transporter - A 2.4x7.3-m (8x24-ft) low-profile flatbed gooseneck trailer with a transport frame for three mirror modules. The prime mover would be a 1-ton pickup (Fig. II-F-3 illustrates this concept);

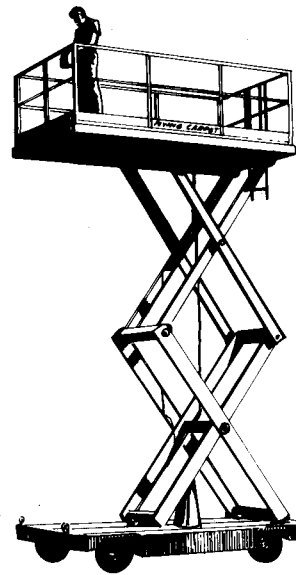


Figure II-F-2 Heliostat Workstand

6) Yoke assembly transporter - A 2.44x7.31-m (8x24-ft) low-profile flatbed gooseneck trailer with a transport frame for four yoke assemblies. Prime mover would be a 1-ton pickup.

7) Lubrication servicing equipment for lubricating worm reducers, gear motors, and bearings. The equipment would consist of a commercial pressurized lubrication set used in conjunction with the mirror servicing tool.

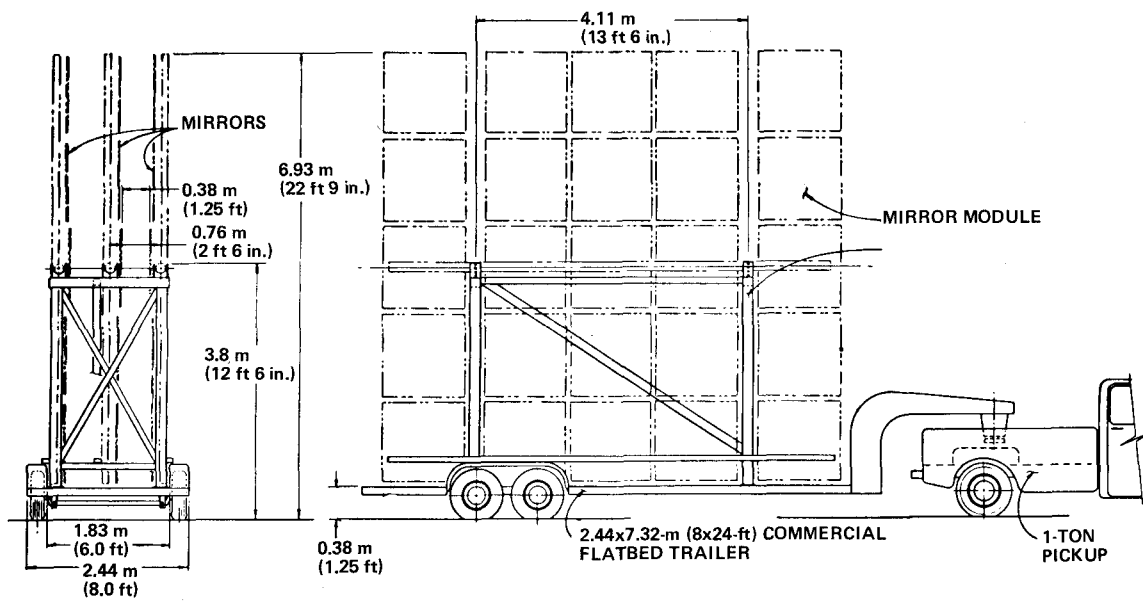


Figure II-F-3 Mirror Module Transporter

G. Key System-Level Considerations

G. KEY SYSTEM-LEVEL CONSIDERATIONS

To satisfy all the requirements delineated in K93681, it was necessary to identify and evaluate considerations affecting the system-level operation. These considerations are presented in the following paragraphs.

Fail-Safe Operations

The heliostat and control system designs provide fail-safe features to meet the requirement of paragraph 3.1.4.1.g of K93681.

a. Loss of Power - During noncritical tests, the test facility will be supplied from commercial power; the facility-supplied diesel generator will be down but will start up and come on-line within 10 seconds of commercial power loss. During critical tests, the diesel generator will be running and will assume the full load within less than a second after commercial power loss.

A power transfer switch that senses commercial power presence, and in its absence transfers to the diesel generator bus, will be a part of the heliostat array control subsystem.

Loss of Commercial Power during Noncritical Tests - If commercial power is lost when the diesel generator is down, the transfer switch will sense the loss and cause the diesel generator to start up and come on-line within 10 seconds. During the 10-second power-off period, the heliostats will remain in the position last commanded and the HAC memory will be automatically saved. Tracking will resume within one second after restoration

of power from the diesel generator. The heliostat beams should not have moved sufficiently off target to affect testing.

Loss of Commercial Power during Critical Tests - The diesel generator will be on line during critical tests. If commercial power is lost, the transfer switch will sense it and immediately transfer the entire load to diesel generator power. Normal system operation will continue during the transfer.

Loss of Commercial Power to Several Heliostats - If power is disrupted to an entire zone of heliostats, the beams will move off target slowly, dispersing somewhat. This could quickly become extremely hazardous. Power at the main bus, either from the commercial source or the diesel generator, would be available. Our design will use power from this source, controlled at a switch panel in the control room, to transfer elevation slew motor inputs and stow the heliostat elevation axes using limit switches.

b. *Loss of Control* - Control data flow continuously from HACs to HIMs to heliostats. Status data flow continuously from heliostats to HIMs to HACs. Bilateral communication between HAC and HIM will include a 1-Hz recognition signal designated a handshake. HAC will continuously monitor the HIM handshake and HIM will continuously monitor the HAC handshake. Absence of the handshake for several cycles will cause remedial action by HAC or HIM. Similarly, if HAC detects loss of MCS control, it will take remedial action.

HAC-to-HIM Control Loss - If the handshake discontinues, HIM will wait 5 seconds. If the handshake is restored in that time, normal operation will resume. If the handshake is not restored, HIM will stow all assigned heliostats.

HAC Detects Heliostat Position Error - The HAC will continuously compare all indicated and commanded positions. If HAC detects a position error, it will warn the MCS. If a single heliostat error continues for 5 seconds, HAC will stow that heliostat. If several heliostats indicate position errors, the warning to MCS will so designate; at this time the user should decide whether to stow.

MCS-to-HAC Communication Lost - If HAC detects missing MCS data, it will warn MCS. The user should then decide whether to stow the affected heliostats.

2. Reliability and Maintainability

The heliostat array and control system design will maximize the availability of the heliostat field for Sandia test operations. The reliability and maintainability design will:

- 1) Maximize life through reduced stresses or increased margin;
- 2) Use parts with proven reliability.
- 3) Eliminate infant mortality failures before installation;
- 4) Provide easy access for maintenance;
- 5) Break the system into replaceable modules to the maximum practical extent;
- 6) Develop alignment techniques that will minimize restoration time after a failure.

Specific subsystem reliability and maintainability achievements are covered in the subsequent subsystem discussions. Some of the major reliability achievements are:

- 1) Life characteristics of the drive mechanism have been enhanced by totally enclosing all mechanism and providing efficient means of lubrication to virtually eliminate gear and bearing wear. Adequate margins in structural and bearing loading and low gear tooth stress levels result in a very rugged unit;
- 2) The slewing and tracking motors will use neither centrifugal switches nor brushes, which are prominent failure causes. The motor control will be all solid state, and the drive will use neither clutches nor brakes;
- 3) The control computer will be subjected to a minimum of 720 hours of operating time prior to acceptance to detect and correct any infant mortality failures prior to field installation.

3. Lightning and Electrical Transient Protection

The HAACS will be protected from electrical transients on an overall system basis. Our design will be immune to transients generated within the test facility by other loads such as arc welders or electric heating equipment.

Without proper design, a lightning strike at or near the test facility could cause computer memory loss, with possibly catastrophic results. A lightning strike on a heliostat or on the

tower-mounted CSS could result in severe damage. There are three lightning protection methods:

- 1) Dissipate the lightning so it will not strike;
- 2) Direct the lightning current away from the equipment;
- 3) Design the equipment so it will survive a lightning strike.

Method 1) creates an ion umbrella above the protected area so the lightning step leader will not penetrate. This method of protection reduces but does not eliminate the risk. It is, however, the least expensive. It would require lightning dissipation arrays on some of the heliostats and at various facility locations. The exact arrangement would be determined through model testing in a high-voltage facility.

Method 2) would require lightning rods on the facility tower and ridge wires or catenary wires from the facility tower over the heliostat and administration and control building where the computers are located to some grounding point on the perimeter of the test facility. The rods or wires would be arranged so they would protect the equipment underneath by attracting the lightning and directing its current to ground, thus preventing it from directly striking the equipment. The several configurations of this system would have to be analyzed to determine the most cost effective.

Method 3) would require that the heliostats, computers, and interconnecting wiring be designed to survive lightning strikes. This would involve stringent control of bonding, grounding, and

shielding all system components. This method is probably the most expensive but it is also the surest method of preventing lightning damage.

Method 2) described above is considered to be the preferred approach. The Black and Veatch report, *5-Megawatt Solar Thermal Test Facility, Preliminary Site and Facility Requirements Definition* dated October 20, 1975 indicates that lightning rods will be placed atop the facility experiment tower. However, the additional protection for heliostats in zone B will be required by the addition of at least two catenary wires across the facility.

In conclusion it is assumed that the lightning protection design will be a cooperative approach by Sandia, Martin Marietta, and the facility A&E contractor.

HAACS/Facility Electrical Interfaces

The electrical interfaces for the 5-MW solar thermal test facility are shown in block diagram form in Figure II-G-1. Each zone has its own electric power branch protected by a circuit breaker and a power transfer switch. The power transfer switch allows power to be manually switched on and off to each zone. The transfer switch also senses the loss of commercial power at each zone, at which time the HACSS goes into the "loss of commercial power" operating mode described in subsection 1.

Figure II-G-2 also shows the power distribution for the calibration subsystem on the tower, the focusing and alignment subsystem at each heliostat foundation, and the assembly and storage areas.

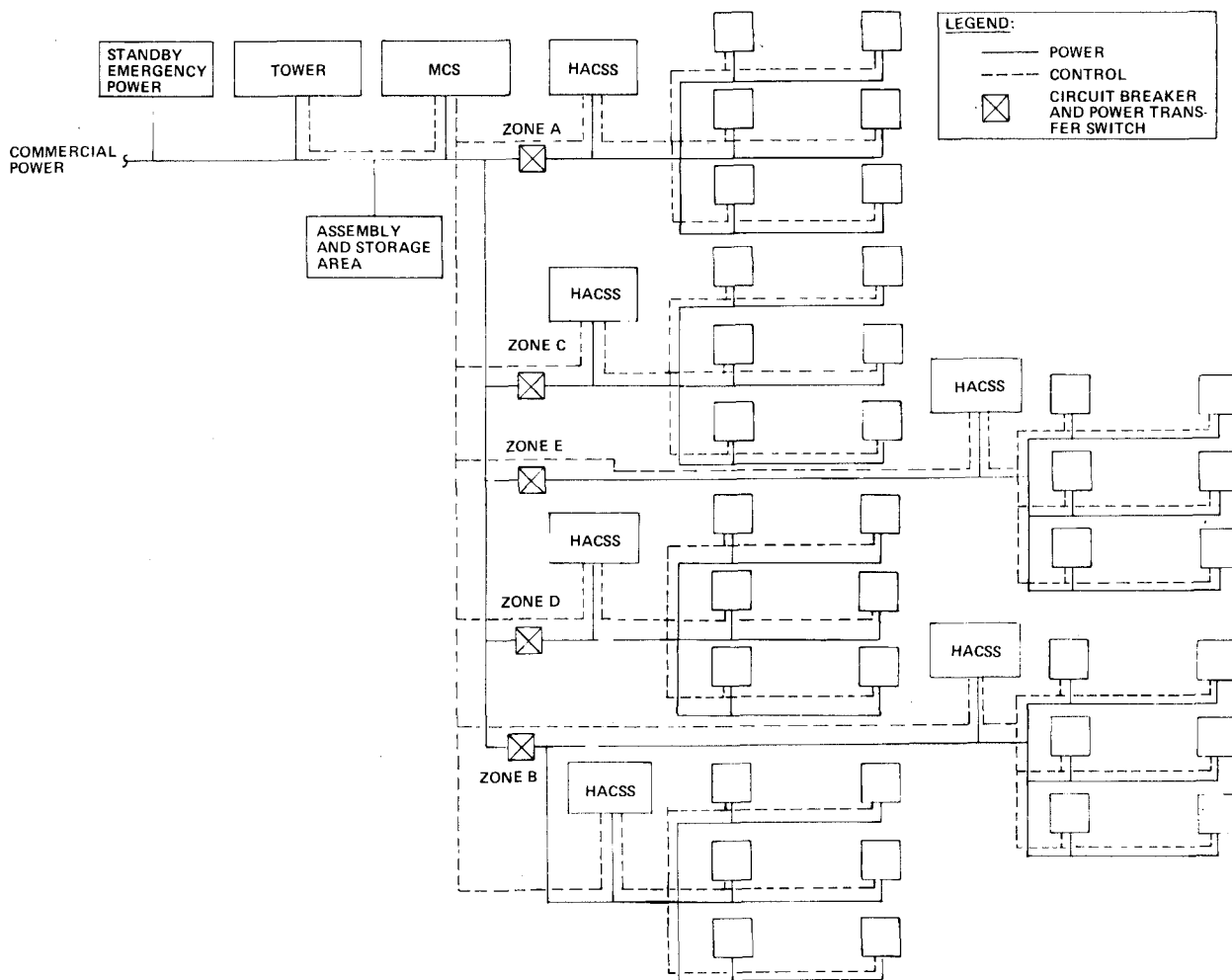


Figure II-G-1 Power and Control Wiring Block Diagram

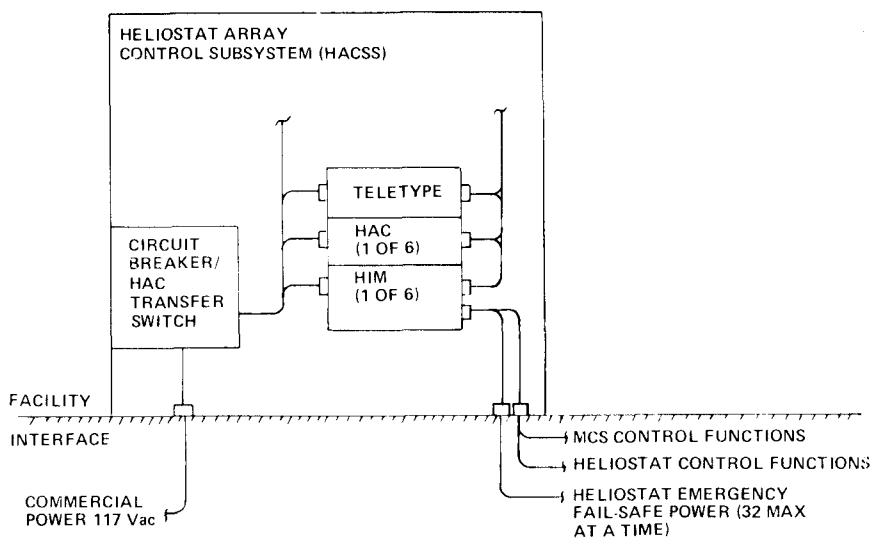


Figure II-G-2 HACSS Electrical Interfaces

The specific electrical interfaces for one zone of the HACSS are shown in Figure II-G-2. The facility power comes through the circuit breaker/ power transfer switch described above to the specific HACSS equipment. The quality of the commercial power required for the HAACS (both the HACSS and the heliostats) is reflected in Table II-G-1.

Table II-G-1 Power Quality

PARAMETER	DESCRIPTION
VOLTAGE	117 Vac SINGLE-PHASE, 2 WIRES, PLUS GROUND WIRE INPUT RANGE: 112 TO 126 V
FREQUENCY	60 ± 0.3 Hz
FREQUENCY RATE OF CHANGE	1 HZ/s MAXIMUM
HARMONIC DISTORTION	5% MAXIMUM
VOLTAGE TRANSIENTS	10% FROM THE QUIESCENT LEVEL
TRANSIENT RECOVERY TIME	1 s MAXIMUM

The power budget for the HACSS is shown in Table II-G-2. It reflects the normal power usage of the HACSS for an average day, as shown under cycle time, and an average month of 25 days. The total HAACS power budget is shown for each zone and various combinations of zones in Table II-G-3. The total operating power for the entire HAACS is 96.4 kW.

Table II-G-2 Total HACSS Power Budget

ITEM	QUANTITY	EQUIPMENT	POWER REQUIRED, EACH, W	POWER REQUIRED, TOTAL, W	CYCLE TIME, hr/day	TOTAL ENERGY, kW-h/day
1	6	HELIOSTAT INTERFACE MODULE (HIM) (INCLUDES UAR/T)	25	150	11.5	1.7
2	1	TELETYPE	234	234	1	0.2
3	7	COMPUTER (INCLUDES PERIPHERAL EQUIPMENT)	1755	12,285	11.5	141.3
TOTAL				12,669		143.2

Table II-G-3 Total Power Budget

POWER USER	POWER, kW		ENERGY, kWh	
	NOMINAL	MAXIMUM	DAILY REQUIREMENT	MONTHLY REQUIREMENT
ZONE A HELIOSTATS (78) HAC (1)	3.5 2.0	11.7 3.8	24.3 42.3	610 1,057
TOTAL	5.5	15.5	66.6	1,667
ZONES A & B HELIOSTATS (294) HACs (3)	13.2 5.5	44.0 7.3	91.6 107.5	2,290 2,686
TOTAL	18.7	51.3	199.1	1,976
ZONES A, C, D, & E HELIOSTATS (344) HACs (4)	15.4 7.3	51.4 9.1	107.3 169.2	2,690 4,228
TOTAL	22.7	60.5	276.5	6,918
ZONES A, B, C, D, & E HELIOSTATS (560) HACs (6)	25.1 10.9	83.7 12.7	174.6 234.4	4,370 5,857
TOTAL	36.0	96.4	408.0	10,227
ZONE B HELIOSTATS (216) HACs (7)	9.7 3.8	32.3 5.5	67.3 67.2	1,680 1,629
TOTAL	13.5	37.8	132.5	3,309
ZONE C HELIOSTATS (83) HAC (1)	3.7 2.0	12.4 3.8	25.9 42.3	650 1,057
TOTAL	5.7	16.2	68.2	1,707
ZONE D HELIOSTATS (100) HAC (1)	4.5 2.0	14.9 3.8	31.2 42.3	780 1,057
TOTAL	6.5	18.5	73.5	1,837
ZONE E HELIOSTATS (83) HAC (1)	3.7 2.0	12.4 3.8	25.9 42.3	650 1,057
TOTAL	5.7	16.2	68.2	1,707

The electrical control functions and distribution through the test facility are also depicted in Figure II-G-1. Each zone has its own independent control distribution system emanating from the HIM rack of the HACSS, as shown in Figure II-G-2.

As reflected in this figure, the HIM has a control interface internally with the HAC and externally with the MCS and each heliostat in its zone. There is another auxiliary power interface with each heliostat for heliostat emergency fail-safe power to operate groups of up to 32 heliostats to the elevation stow position (described in Section F.1).

Cable harnesses are provided inside the HACSS with commercial plugs/receptacles in accordance with applicable building codes. Power will be supplied to each rack and separate piece or peripheral equipment and will be routed to reduce noise coupling into the control cables. The cable harnesses will be designed for easy replacement of the interconnecting harnesses and the electronics.

The heliostat array control subsystem power interface with the facility consists of eight 117-Vac power outlets. Seven are 50 ampere for the HACs and one is 15 ampere for the HIMs. The control interface consists of two twisted/shielded pairs of 20 AWG wires (4 wires total) to each set of no more than 32 heliostats (16 wires maximum for each HIM to the maximum of 128 heliostats). One twisted/shielded pair will provide the data link information to the heliostats and the other twisted/shielded pair will provide the encoder data from each heliostat to the HACSS. Shielding will be tied to ground on the receiving end of the cable and floated at the source end of the cable. There are also twisted/shielded pairs of 20 AWG wires going from the HACSS to the MCS through the same HACSS/facility interface connector. One twisted pair of 20 AWG wires go to each group of 32 heliostats for the heliostat emergency fail-safe power interfaces.

H. Maintenance
Requirements

H. MAINTENANCE REQUIREMENTS

The heliostat array and control system (HAACS) design features facilitate both preventive and failure-type maintenance operations. This is achieved without compromising inherent protection against the environments. After contract award, we will continually monitor the system design as it is finalized to incorporate maximum maintainability. Maintenance instructions will be prepared and delivered in accordance with paragraph 3.1.1.j of K93681.

Heliostat Array Control Subsystem Computer Racks/Teletype

The standard configuration computer racks containing CPUs, memories, disc storage units, and power supplies will undergo functional maintenance on a weekly (approximately) basis. A diagnostic routine will be used to fully exercise all the computer functions and check for proper responses. The diagnostic program will be loaded into the computer, the program started, and a hardcopy of the results obtained from the teletype. An operator can also manually input selected tests via the teletype keyboard. During these maintenance tests, normal "all-up system" operations will not be interrupted since the spare/development HAC can be used in place of the HAC under test.

Physical maintenance of this equipment will be accomplished per the manufacturer's recommendations, e.g., equipment filter cleaning.

2. Heliostat Array Subsystem (HASS)

a. *HASS Structure* - The steel HASS structure will require no maintenance. Each structure will be visually inspected after installation and a functional check (including focusing, alignment, calibration and operational sequencing) will be conducted to verify structural integrity, e.g., no stress cracks. This inspection will be repeated on a regular basis as well as an operation in which fasteners at the following locations are retorqued: (1) foundation/leveling plate/HASS attachments, (2) yoke module attachment to azimuth drive pivot shaft, and (3) elevation drive tube-to-yoke attachment.

b. *Mirror Assembly* - Normal maintenance of the mirror assembly will consist of periodic cleaning as indicated by visual inspection or as required by performance degradation, e.g., indicated by analysis of calibration data. The ability to perform this operation will be provided in the form of a tank truck. This truck will be equipped with two 850-gallon tanks, one for containing a wash solution of soft water and detergent and the other containing soft water for rinsing. The truck will have a lift device capable of carrying two men to a height of 25 feet from which the wash and rinse fluids can be applied using hoses with high-pressure nozzles.

Although frequent replacement of mirror assemblies will not be required, when necessary they will be replaced using two heliostat workstands with adjustable platforms capable of lifting men to a height of 25 ft. One workstand will be placed in front and one

in back of the mirror assembly. A mirror handling device attached to the workstand will allow easy, safe replacement of the assembly. Replacement of individual mirrors has been facilitated--the removal of three nuts is all that is required. A similar workstand will also be used during the focusing and alignment operations.

c. *Sun-Present Sensor* - Maintenance of the sun-present sensor will consist of occasional cleaning of its surface, accomplished during the overall mirror assembly cleaning, its infrequent replacement in case of failure, and possibly its readjustment of its threshold light intensity setting (compensation for seasonal sun incidence variation).

d. *Drive Mechanisms* - The azimuth and elevation drive mechanisms on the heliostat have been designed for ease of maintenance. Component stress and wear due to normal operations should not be as severe as that caused by the environments (e.g., temperature, sand, and dust). Therefore environmental protection has been stressed--enclosures have been installed around the lower part of the main shaft and around the worm gear reducer/motor assemblies. These enclosures are easily removed when required. For example, the enclosure will be removed when performing periodic lubrication of the reducer and the motors. Motors and reducers can be easily replaced in place at the site. The thrust bearings and external gearing will be lubricated by grease nipples that are accessible without removing covers. Periodic preventive maintenance will also include inspection of shaft bearing seals for leakage. In case of failure, replacement seals can be installed without removing the entire heliostat assembly.

e. *Shaft Encoders* - After initial heliostat installation when "zeroing" and alignment of the encoder disc and pickup is performed, maintenance will consist of realignment and zeroing, or replacement if faulty operation is detected by the MCS (via the HAC). On the azimuth drive, the cap from the encoder housing will be removed to give unobstructed access to the disc and the pickup for maintenance. On the elevation drive two encoder positions are being considered. In the worst case the outer row of mirrors on the side nearest the elevation drive must be removed to gain access to the encoder. For the other positions the same procedure can be followed as that for the azimuth drive. At no time must the entire heliostat be removed from its foundation for encoder maintenance, replacement, or adjustment.

f. *Limit Switches* - The azimuth and elevation shaft limit switches, both the travel limit and emergency shutdown switches, require no maintenance. These switches are rated for 10,000,000 cycles and mechanical failures will be infrequent. Replacement due to switch contact contamination giving intermittent operation is easily accomplished since they are installed in unobstructed areas.

g. *Control Electronics Assembly* - This environmentally sealed assembly containing the electronics for interfacing the heliostat with the MCS needs no normal maintenance. In case of failure, the unit will be removed from the heliostat yoke (approximately four screws) and replaced as an assembly. Since these units are interchangeable, no adjustments after installation will be required except for possible readjustment of the sun-present sensor threshold

adjustment potentiometer. Bench repair is easily accomplished. The two printed circuit boards, four power supplies, and internal harness can be removed as an integral subassembly from the housing for testing and component replacement. The PC boards will be replaced by cutting interconnect wires and soldering the new boards into the harness. Sufficient harness length will be incorporated in the subassembly to allow such repair operations. The reliability of the PC board circuitry versus the unreliability of commercial-grade PC board connectors dictated this approach.

h. Heliostat Manual Control Unit - The only normal maintenance required for this "suitcase-type" unit will be replacement of the operator's light on its face. Removing the front face by taking out six screws allows access to the circuitry and internal harness, and allows replacement of switches when required.

3. Focusing and Alignment Subsystem (FASS)

Maintenance requirements for the FASS will be identified in the focusing and alignment instructions supplied in accordance with paragraph 3.1.2.h of K93681. This document will be prepared and provided as a part of the FASS. These requirements will be minimized by the selection of standard components requiring standard maintenance. Specific scheduled maintenance requirements, maintenance cycles, and replacement requirements will be delineated in this manual. All special equipment, tools, etc will be identified in the instructions.

The FASS components requiring maintenance are:

- 1) Heliostat workstand - Maintenance requirements are minimal as this system is all electric. Batteries are charged through a built-in battery charger. Greasing will be required on a periodic basis;
- 2) Mobile alignment light source - This device will require maintenance to the light source, which is a high-intensity xenon arc lamp. The light-positioning system will require daily maintenance in the form of greasing and safety checks;
- 3) Electrical cables - All cables and connectors will require safety inspections before using the FASS.

4. Calibration Subsystem (CSS)

Maintenance requirements of the CSS are summarized in Table II-H-1. The CSS has been designed to facilitate these maintenance requirements. The system is constructed in modules wherever possible so individual components can be replaced without disassembly of large main assemblies. For example, each one of the 64 solar cell assemblies can be removed independently from the assembly beam for repair or replacement.

Table II-H-1 Calibration Subsystem Maintenance Requirements

CALIBRATION SUBSYSTEMS	PERIODIC LUB (6 MO MINIMUM)	CLEAN OPTICAL SURFACE	LIGHT OUTPUT CALIBRATION (6 MO MINIMUM)	PART REPLACEMENT (UNSCHEDULED MAINTENANCE)	INSPECT MATERIAL EXPOSED TO BEAM (REPLACE AS REQUIRED)
1. CALORIMETER SUBSYSTEM WATER TANK PIPING SYSTEM FLOWMETERS TEMPERATURE SENSORS SOLENOID SWITCHES				X X X X X	
2. SOLAR CELL SENSOR SUBSYSTEM MICROSWITCHES MECHANICAL TRACK SENSOR ASSEMBLY	X	X	X *	X X	X X
3. CSS STRUCTURE TARGET ASSEMBLY (MOVING JOINTS) CSS (HOUSING) MICROSWITCHES	X X			X	X
4. CALIBRATION INTERFACE UNIT C&D PANEL DATA INTERFACE UNIT				X	
*REMOVE AND TEST UNDER PRESCRIBED SUN CONDITION NEAR TOWER.					

I. Verification Program

I. VERIFICATION PROGRAM

Martin Marietta's verification program is based on the concept of proving performance integrity with adequate margin and assuring that reliable hardware, fully capable of meeting Sandia specification K93681, is delivered, installed, and checked out.

The heliostat array and control system verification program is shown in Table II-I-1 and is an integrated blend of testing, assessment (including inspection and design review), and analysis. Our test plans will be designed to utilize the subsystem research experiment (SRE) ERDA contract E(04-3)1110 facilities located at Martin Marietta/Waterton to the fullest extent possible on a noninterference basis. For example, we will use one of the heliostat foundations now being installed for system testing. The possibility of using an SRE heliostat for focusing, alignment, and calibration development testing is also being considered.

Table II-I-2 illustrates how, with component testing, major objectives were met by using off-the-shelf in-production electrical-electronic components. The verification program will use assessment and analysis instead of test to reduce program costs wherever confidence would not be degraded.

Table II-I-1 HelioStat Array and Control System Verification Requirements Matrix

K93681 PARAGRAPH NO.	TITLE	ASSESSMENT/ INSPECTION	ANALYSIS	TEST	OTHER
1.	GENERAL				INFORMATION
2.	DOCUMENTS		X		
3.	REQUIREMENTS				NA
3.1	COLLECTOR SYSTEM (DEFINITION)				
3.1.1	DELIVERABLE ITEMS	X	X	WHERE REQUIRED	
3.1.2	DELIVERABLE SPECIFICATION AND DOCUMENTS	X			
3.1.3	INTERFACES				NA
3.1.3.1	SUN MOVEMENT/COLLECTOR POSITIONING/ RECEIVER			X	
3.1.3.2	MASTER CONTROL/HELIOSTAT ARRAY CONTROLLER			X	
3.1.3.3	COLLECTOR FOUNDATION SITE		X		SOIL DATA BY SANDIA
3.1.4	PERFORMANCE		X	X	
3.1.4.1	APERTURE POWER FROM HELIOSTAT ARRAY		X	BY SANDIA	
3.1.4.2	BEAM QUALITY		X	X	
3.1.4.3	HELIOSTAT AIMING REQUIREMENTS		X	X	
3.1.4.4	MODES OF OPERATION		X	X	
3.1.4.5	LOCAL CONTROLS		X	X	
3.1.4.6	FOUNDATIONS		X	BY SANDIA	
3.1.4.8	POWER AND CONTROL WIRING		X	BY SANDIA	
3.1.5	PHYSICAL CHARACTERISTICS	X	X		
3.1.6	RELIABILITY	X	X		
3.1.7	MAINTENANCE	X	X		
3.1.8	ENVIRONMENTAL CONDITIONS		X	X	
3.1.9	TRANSPORTABILITY	X			
3.1.10	INSTALLATION	X		X	
3.1.11	DESIGN AND CONSTRUCTION	X			
3.1.11.1	MATERIALS, PROCESSES, AND PARTS	X	X		
3.1.11.2	ELECTRICAL TRANSIENTS	X	X		
3.1.11.3	NAMEPLATES AND PRODUCT MARKING	X			
3.1.11.4	WORKMANSHIP	X			
3.1.11.5	INTERCHANGEABILITY	X			
3.1.11.6	SAFETY	X	X		
3.1.12	DOCUMENTATION				NA
3.1.12.1	CHARACTERISTICS	X			
3.1.12.2	INSTRUCTIONS	X			
3.1.12.3	CONSTRUCTION	X			
3.2	CALIBRATION SYSTEM		X	X	
3.3	HELIOSTAT FOCUSING AND ALIGNMENT		X	X	

Table II-I-2 Component Design Verification Test Matrix

COMPONENTS/ASSEMBLIES	DESIGN STATUS	ENVIRONMENT TEST									
		FUNCTIONAL*	TEMPERATURE CYCLING	HUMIDITY	RAIN	SNOW AND ICE	SAND AND DUST	LIGHTNING	EARTHQUAKE	VIBRATION	LIFE
HELIOSTAT ARRAY CONTROLLER											
COMPUTER	↑ O F F T H E S H E L F ↓	1, 2	-	-	-	-	-	-	-	-	S
I/O INTERFACE		2	-	-	-	-	-	-	-	-	S
ASYNCHRONOUS CONTROLLER (TTY)		2	-	-	-	-	-	-	-	-	S
FOUR-LINE ASYNCHRONOUS MULTIPLEXER		2	-	-	-	-	-	-	-	-	S
COMMUNICATIONS CONNECTOR PANEL		2	-	-	-	-	-	-	-	-	-
9600-baud ASYNCHRONOUS LINE CONTROLLER		2	-	-	-	-	-	-	-	-	S
DISC STORAGE UNIT		2	-	-	-	-	-	-	-	-	S
CABINET		-	-	-	-	-	-	-	-	-	-
TELETYPE		2	-	-	-	-	-	-	-	-	S
LINE DRIVER FOR 914-m (3000 ft) LINE		D	X	-	-	-	-	-	-	-	-
HELIOSTAT ASSEMBLY											
MANUAL CONTROL PANEL (PLUG-IN)	D	X	A	X	X	A	-	-	-	-	A
MOTOR GEAR SET	D, 3	X	-	-	X	-	X	-	A	A	A
TRACKING MOTOR	OS	S	S	S	X	A	X	A	S	-	-
SLEW MOTOR	OS	S	S	S	X	A	X	A	S	-	S
TRACKING GEAR BOX	OS	S	S	S	X	A	X	-	A	A	S
SLEW GEAR BOX	OS	S	S	S	X	A	X	-	A	A	S
ENCODERS	OS	S	S	S	X	A	X	A	-	A	S
LIMIT SWITCHES	OS	S	S	S	X	-	X	A	-	X	S
POWER SUPPLIES	D, 4	X	S	S	X	A	X	A	-	A	A
HELIOSTAT CONTROL ELECTRONICS ASSEMBLY	D	X	S	S	X	A	X	A	-	A	A
MIRROR ASSEMBLY AND HOLDER	D	X	X	A	A	X	X	-	A	A	-
HELIOSTAT SUPPORT FRAME	D	X	A	-	-	-	-	-	A	-	-
YOKE MODULE	D	X	A	-	-	-	-	-	A	-	-

LEGEND/NOTES:

- X TEST
- NOT REQUIRED
- S SIMILARITY
- A ANALYSIS
- * FUNCTIONAL INCLUDES MECHANICAL INTEGRITY, ESPECIALLY STIFFNESS IN CASE OF HELIOSTAT STRUCTURE.
- D DESIGN REQUIRED
- OS OFF-THE-SHELF
- 1. SOFTWARE VERIFICATION/VALIDATION TESTS
- 2. SOFTWARE/HARDWARE INTERFACE TEST
- 3. MOTOR GEAR SETS ASSEMBLED FROM OFF-THE-SHELF COMPONENTS
- 4. ENCLOSURE DESIGN ONLY; FUNCTIONAL ELECTRONICS PURCHASED
- 5. ENVIRONMENTAL TESTS WILL BE PERFORMED IN ACCORDANCE WITH MARTIN MARIETTA SPECIFICATION M-67-45, TEST METHODS AND CONTROLS.

1. Analysis

Verification of many specification requirements will be satisfied by analysis as displayed in Table II-I-1. The performance analyses will be verified by test. Analyses not verified by test will be performed using standard industry techniques Martin Marietta is very familiar with and has applied to a broad spectrum of products.

An example of special analysis for terrestrial solar power systems is that required for beam characteristics at the receiver. The CRSTPS computer program has been used to analyze beam quality, spot size, and variation at the receiver depending on beam alignment and focus. It has also been useful in arriving at an initial design for an aligning tool for use in verifying heliostat performance. The computer program will analyze each heliostat array to verify directed radiation power levels from each zone through the apertures listed in Table 2 of K93681. The results will be used to obtain early estimates of total HAACS performance.

2. Component Tests

As shown in the component design verification test matrix, Table II-I-2, most of the components are off-the shelf, i.e., designed and in production. These are marked "S" for similarity even though they are identical and will, for overall test cost effectiveness, receive no additional environmental testing except in the case of motor-gear sets and encoders that must operate while exposed to the outdoor environment. Comprehensive component test plans and test instructions will be developed concurrently with design of new-development components.

Because of low stresses, it is expected that integrity or performance tests be nondestructive and that the component will ultimately be used in the operational system.

3. Test Program Control

All testing will be conducted in accordance with detailed plans and instructions. The instructions will include objectives, limits and tolerances, fail/success criteria, and backout provisions for hazardous operations. All instructions will be reviewed by engineering, quality, and safety personnel. The tests will be conducted by qualified test engineers and technicians. All test results will be documented and appropriate data included in a test report.

4. Assessment/Inspection

Engineering drawings, test plans, and test instructions will be reviewed prior to release to verify that they meet the requirements of the HAACS specification.

Purchased components and fabricated assemblies will be inspected in accordance with a sampling plan covered in Chapter II.B.

a. *Mirror Performance Verification* - The mirror surface consists of second-surface glass with a minimum reflectance of 85% when measured by collimated specular reflectivity measuring techniques (equivalent to Eppley normal-incidence pyrhelimeter).

The specular reflectivity can be demonstrated with the test rig shown in Figures II-I-1 and II-I-2. The reflected beam from the test mirror is monitored by the reverse-mounted

pyrheliometer. To avoid shadowing, the mirror sample is tested with a 10-deg tilt ($\cos(10) = 0.98481$). The reference insolation input to the mirror is monitored by the pair of independently tracked pyrheliometers shown in Figure II-I-2.



Figure II-I-1 Specular Reflectivity Test Rig Using Normal-Incidence Pyrheliometers, Profile View

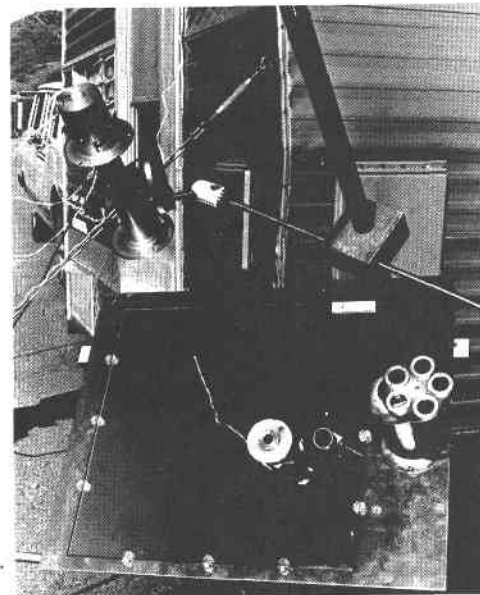


Figure II-I-2 Specular Reflectivity Test Rig Using Normal-Incidence Pyrheliometers, Front View

b. Heliostat Mechanical Integrity - The approach to verifying mechanical integrity requires two test sequences--the first to corroborate analyses developed during the design phase by comparison of heliostat structural deflections resulting from an idealized test loading and analytical predictions for the same idealized loadings, and the second a test of the yoke assembly with horizontal and azimuth drives installed to demonstrate that these mechanisms will function under load.

The testing will be conducted at the Denver Division's structures laboratory. The heliostat base will be affixed to a stiff base fixture. Test loads for an idealized load case (perhaps loading only one quadrant of the assembly) will be applied to the back side of the heliostat with dead weight and a cable and pulley arrangement. Deflections and movement of the base of the heliostat will be measured to provide base fixture movement data that will be used to modify measured deflections at the mirror surface. All deflections will be measured with electrical deflection transducers with resolutions no greater than 0.001 inch or with dial gages. The deflection transducers will be mounted on a structure that is structurally independent of the base fixture or test loading apparatus.

The second test will be conducted with the heliostat yoke assembly, with drive systems installed, mounted on the base fixture as in the first test. A dummy rack assembly will be installed on the horizontal axis. Time interface of the dummy back with the yoke will duplicate that of the deliverable hardware rack. Test loads simulating critical design conditions will be applied to the dummy back and the drive mechanisms activated to demonstrate operation. A few degrees of movement is anticipated to be adequate proof of operation, specifically to prove that the slew motor-gear sets will operate under worst-case winds to bring the heliostat to a safe position.

c. *Acceptance Testing* - Acceptance testing will be performed as delineated in Table II-I-3 and will verify that production hardware is free of defects and complies with specification requirements. All testing will be performed in accordance with approved test instructions and the results included in the inspection records. In most cases, the functional tests specified will satisfy the requirements of component verification (Table II-I-2). The subsystem and system tests are described in the following sections. The inspections and functional tests, as specified, will each be peculiar to the type of hardware being tested. Coupons will be used to sample characteristics of the mirrors rather than testing each mirror. The computer burn-in test will be of 100-hour duration.

Table II-I-3 *Acceptance Test Program Matrix*

ITEM	INSPECTION	FUNCTIONAL TEST	LOT SAMPLE	COUPON TESTS	BURN IN	SUBSYSTEM TEST	SYSTEM TEST
HAC						X	X
UART	X	X					
DISC STORAGE UNIT	X	X					
COMPUTER	X	X			X		
I/O CIRCUITS	X	X					
TELETYPE	X	X					
TTY	X	X					
MULTIPLEXER	X	X					
CABINET	X						
COMMUNICATION PANEL	X						
LINE CONTROLLER	X	X					
LINE DRIVER	X	X					
HELIOSTAT ASSEMBLY						X	X
MANUAL CONTROL PANEL	X	X					
GEARMOTORS	X	X	X				
ENCODERS	X	X	X				
POWER SUPPLIES	X	X					
HCEA	X	X					
MIRRORS	X			X			
STRUCTURAL ITEMS	X					X	
PIECE PARTS	X		X				
RAW MATERIALS	X		X				
CALIBRATION SUBSYSTEM						X	X

Where lot sampling is specified, an AQL level will be selected from MIL-STD-105D for the applicable item and submitted to Sandia for approval.

5. Subsystem Tests

After installation is completed, each subsystem will be tested as described here. The tests will be conducted in conformance with approved operating instructions with all data and results properly documented and reported.

a. Heliostat and HAC Power Verification - To assure compliance with the electric power requirements, the performance of two heliostats in each zone and at the HAC will be verified by test. The verification will consist of voltage and power quantity tests. Power quality will be the facility responsibility.

b. Heliostat Array Subsystem (HASS) Tests - After each heliostat of the HASS is installed, checked out, and calibrated, each heliostat will be subjected to a series of tests to verify that it meets the tracking, focusing, and energy collection specification requirements. The test configuration will consist of the completed collector installation, including the calibration subsystem. The tests will be conducted in conformance with detailed test, operating, calibration, and alignment and focusing instructions. Testing will be conducted during periods when environmental conditions permit.

Beam Quality - The size, shape, and point of center of energy concentration of the beam from each heliostat will be measured by solar cells. Measurements will ascertain if the heliostats are capable of directing 90% of the reflected power on a calorimeter target at the specified slant range using two heliostats per zone.

Tracking Performance - The tracking test will verify the ability to command the heliostats to the standby and on-target positions within specification limits as to orientation and time limits, tolerances, and slew rates. The sun sensors will be covered/uncovered to verify standby orientation and ability to command to on-target position by master control.

Stow - The heliostats will be moved from the standby position to the stowage position to verify the position change within the time requirement.

Emergency Shutdown - In this mode, measurements will verify the specification requirements of moving the beams away from the target receiver and moving the heliostats to the stowage position.

c. Heliostat Performance - A field test tool will be used to exercise the command/response capability of each heliostat's control system. This tool will simulate the HAC's serial data inputs; a read-only memory will be interrogated during field checkout of the heliostat. The checkout sequence will take about 60 minutes in which time the track, slew, direct, and data readout modes will be checked. A typical operating

sequence will be commanded and compared against specification response times and position accuracies.

d. *HACSS Performance* - Compatibility tests with MCS interfaces and the heliostat control electronics will be performed in Denver. Our computer configuration will allow us to simulate a MCS interface driver in our development configuration and drive the HCE through a production HAC.

Individual functions will be tested to verify that the specified data rates can be achieved in the interface, that interface data formats are not violated, and that responses are within specified times. These functions will also be tested to verify that failure situations are properly handled and proper alarms issued.

The three specific interfaces will be tested extensively to verify that each interface has the proper response and that the specified data rates are achieved. Each test format will be established and a test sequence will be developed to incrementally step through the interfaces. After each interface is verified, the interfaces will be tested as an integrated system. The integrated system test is described in Subsection 7.

e. *Calibration Subsystem (CSS) Performance* - The CSS tests will be conducted at the subassembly level before and after installation, and at the integrated subsystem level.

The following tests will be performed at the subassembly level.

- 1) The drive mechanisms for the calorimeter and solar cell sensor arm will be verified. Starting and running currents and voltages, steady-state performance, motor vibration, control capability and positioning, and subassembly interfaces will be checked;
- 2) The solar cell sensor will be tested to verify that the installed solar cell response is equivalent to the response obtained at the component level. Subassembly operations will be verified;
- 3) The calorimeter subassembly will be calibrated after installation. The platinum resistance thermometer and associated amplifiers will be tested to confirm that the installed calibration is the same as the component calibration. Flow tests will be conducted to establish the initial baseline, measure the convection losses across the solar collector, and perform the posttest measurements. The controls and operations for the iris positioning system will be checked. Each iris operation will be checked;
- 4) Interface electronics and cabling will be tested end-to-end after installation. All wiring will be checked for continuity, insulation resistance, and proper terminations. The electronics will be calibrated;

- 5) Operation of the control and display panel will be verified. Switch positioning, indicators, displays, and amplifiers will be checked for proper installation, terminations, operations, and calibration.

The CSS integrated tests will be conducted in two parts; solar cell sensor and calorimeter checks.

- 1) The solar cell sensor tests will consist of a series of test runs using one heliostat and a computer prediction of mirror pattern shape and energy centroid. The solar cell sensor subassembly will be driven across the heliostat beam at approximately 10:00 am, 12:00 noon, and 2:00 pm. The pattern image and energy centroid obtained will be compared with the predicted data for the selected heliostat at the appropriate times. This test will demonstrate the resolution and dynamic range of the solar cell sensor. The CSS module, interface electronics and cabling, and control and display panel subassemblies will be used to support these tests as required;
- 2) The calorimeter tests will be used to determine beam quality. One heliostat will be selected to provide the solar input to the calorimeter surface. The sequence will be as described in Chapter II.E. This test sequence will obtain a minimum of five data points. The first and last runs will not use the iris. The other runs will use the iris set for approximately 0.009 SR, 0.012 SR, and 0.015 SR based on the time of

year, time of day, and heliostat selected. The beam quality will be calculated. The other subassemblies will support these tests as required.

f. Focusing and Alignment Performance - FASS verification will be performed at both the system and subsystem levels. Subsystems will be verified to operate according to performance specification as a part of the subsystem acceptance tests to be performed by the manufacturing subcontractor. The following subsystem tests will be performed:

- 1) High-intensity light source,
 - a) Functional verification test,
 - b) Optical collimation/beam quality test,
 - c) Laser interalignment test,
 - d) Lamp replacement test;
- 2) Alignment light-positioning subsystem,
 - a) Functional verification test,
 - b) Platform leveling test,
 - c) Position accuracy test,
 - d) Beam collimation test,
- 3) Alignment target - Reflector visibility verification.

After delivery of the complete FASS, a verification test will be performed to verify total subsystem performance. These tests will include:

- 1) Electrical interface verification;
- 2) Mechanical interface verification;
- 3) Light pointing/positioning test;

4) Functional alignment verification.

6. Software Tests To Be Used for Verification and Validation

The test phase is divided into two separate types of testing usually referred to as verification and validation. These two types of testing have different objectives; use different tools, techniques, and disciplines; and it is cost effective to perform one before the other (see Table II-I-4).

Table II-I-4 Software Verification and Validation

	VERIFICATION	VALIDATION
OBJECTIVES	A. PROVE THE CODING MATCHES THE DESIGN SPECIFICATION B. PROVIDE A FORMAL CHECK ON THE SOFTWARE BUILD PROCESS C. PROVE THE ELIMINATION OF CODING ERRORS	A. PROVE THE FUNCTIONAL REQUIREMENTS ARE MET B. PROVIDE A FORMAL CHECK FOR THE DESIGN PROCESSES USING END ITEM SOFTWARE C. PROVE THE PERFORMANCE REQUIREMENTS
TOOLS AND TECHNIQUES	A. PATH ANALYSIS B. CODING TO SPECIFICATION CORRELATION C. DIMENSIONAL ANALYSIS D. ACCURACY ANALYSIS E. TIMING ANALYSIS F. USAGE ANALYSIS G. CODING RULES COMPLIANCE	A. HELIOSTAT RESPONSE SIMULATORS B. PROTOTYPE COMPUTERS AND ELECTRONICS C. PERFORMANCE ANALYZERS
DISCIPLINES	SOFTWARE SYSTEM ENGINEERING	SYSTEM ANALYSIS

It is important to note that these test activities should follow the informal testing and debugging performed by the coders during software development. The validations performed during system test prove performance requirements only.

7. System Tests

System tests will be conducted after installation of the system at the Sandia test facility.

a. *Integrated System Test* - The integrated system test of interfaces will consist of timing tests and maximum load tests

to verify proper time response and system capability to handle 128 heliostats per HAC, in addition to 49 MCS-type commands per second.

The HAC response test will verify (1) the HCE adherence to specification, (2) the HCE response to given axis movement command (one axes per test), and (3) capability to relay HCE status correctly.

The HCE will also be tested in two closed-loop environments. The first test will consist of laboratory verification of HCE performance. The second test will involve two phases: (1) the ability of the HCE to respond over the maximum length of line, and (2) the ability of two HCEs to respond to minimum-length and maximum-length line environment. HAC operation will be extensively tested. All algorithm computation phases will be verified. Timing analysis of each operation phase will be made to verify conformance to specification and results will be closely checked to verify accuracy.

After all identified test phases have been verified, the system will be subjected to exhaustive closed-loop testing:

- 1) Tracking system performance will be tested under operating conditions specified in paragraph 4.1.2.a of K93681;
- 2) All failure modes will be tested to verify proper responses.

b. Fail-Safe System Verification Test - Fail safe operation

will be verified by the following steps:

- 1) Power will be shut down to one HAC and it will be verified that the I/O (HIM) sends a signal to stow its heliostats (up to 128) after 15 seconds of power loss;
- 2) Power will be shut down to one I/O of the HAC system and verification will be same as in 1) above;
- 3) The digital interface from the HAC to the HIM will be disconnected at a connector and it will be verified that after TBD seconds, all 128 heliostats are commanded to their stowed position;
- 4) A heliostat motor cable will be disconnected to simulate a faulty heliostat. It will be verified that after TBD seconds, the stow command will be sent to that heliostat;
- 5) The "red fail-safe button" on the HAC will be pushed, the HAC/HIM will be off (power and control), and it will be verified that the heliostats are moved to the stow position;
- 6) Commercial power will be turned off and the transfer switch will be verified to start the facility motor-generator set;
- 7) The motor-generator set will be verified to operate when each HAC/HIM circuit breaker is thrown open to simulate HAC/HIM loss of power.

Appendices

Appendix A—Wind Tunnel
Tests from
CRSTPS

APPENDIX A—WIND TUNNEL TESTS FROM CRSTPS

Wind tunnel tests were required to determine the wind loads imposed on the Martin Marietta configuration of the collector (heliostat) in the central receiver solar thermal power system program. Five 1/10th scale collector models were tested in the Colorado State University Industrial Aerodynamics Wind Tunnel at Fort Collins, Colorado. The models comprised simulated metal-backed and sandwich-backed mirrors in a 25-mirror and a 9-mirror configuration as well as a large rectangular single-mirror configuration.

Sufficient results were obtained to define critical loads on the baseline configuration and on configurations similar to the tested configurations. Particular emphasis was made to obtain data that could be used to verify and/or modify existing methods of load analyses. This was accomplished and the result of the modified analysis are presented.

At the time of this test the Martin Marietta baseline configuration for the collector for the central receiver solar thermal power system was essentially a "billboard" consisting of an array of 25 mirrors. These mirrors were arranged in a rectangular pattern with axes of rotation about the horizontal and vertical centerlines of the rectangle. Since "billboard" is exposed to

the environment and, in particular, wind loads, determination of realistic wind loading was important for a cost effective design for the collector.

The collector extends 6.8 m (22.5 ft) above the ground and in the operational mode may experience wind up to 22.35 m/s (50 mph), measured at 9.06 m (30 ft) above the ground. This wind velocity may occur with the collector rotated to any combination of elevation and/or azimuth angles relative to the wind.

Maximum base loads such as base shear and base bending may be conservatively calculated by assuming a uniform wind normal to the plane of the mirrors. This is not true, however, of other important wind loads. Base or azimuth torque, elevation torque, and lift require knowledge of the resultant normal force and center of pressure of this force on the mirror assembly. The effect of a nonuniform vertical wind profile on elevation torque may also be significant.

The most appropriate method of load analysis available, prior to this test, was to treat the mirror array as a low-aspect-ratio rectangular wing. The analysis is empirical based on the results of wind tunnel testing that had been done as far back as 1930. Results of the analysis are coefficients of lift, drag, and normal force, and the center of pressure at which the normal force acts. From these could be determined the required load on the collector structure; however, the analysis required an assumption of the angle of attack at which flow separation occurred. This assumption has a significant effect on the resulting loads as illustrated

in Figure A-1. Varying the separation angle from 0 to 30 deg in increments of 10 deg increases the torque 41, 193, and 339%, respectively. These loads directly affect the design of the collector drive mechanisms. Therefore it became necessary to experimentally determine the correct separation angle for the proposed mirror array.

The wind tunnel test was conducted to determine the answer to the question concerning separation angle. In detail, the objectives of the wind tunnel tests were to:

- 1) Establish the correct separation angle for the collector configuration;
- 2) Evaluate the Reynolds number effect, if any, on the collector configuration;
- 3) Obtain data to verify and/or modify the existing method of load analyses;
- 4) Evaluate the effects of minor changes to the baseline mirror array such as different size mirrors, varying the space between mirrors, etc.

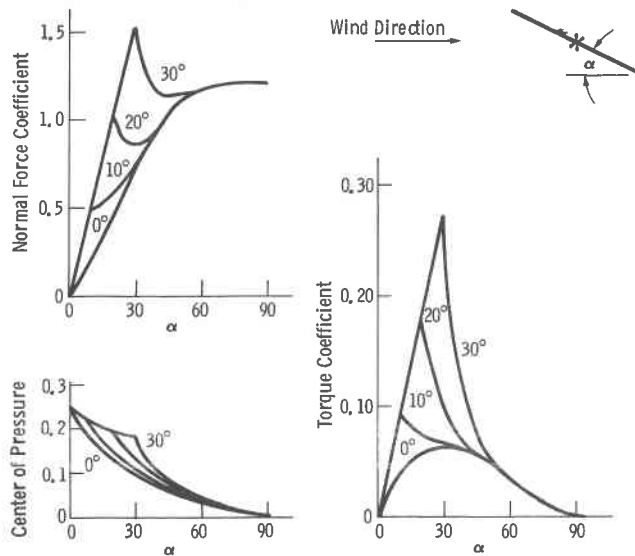


Figure A-1 Analytical Wind Load Predictions

A. TEST FACILITY

The test facility used was the Industrial Aerodynamic Wind Tunnel at the Fluid Dynamics Laboratory at Colorado State University in Fort Collins, Colorado. The wind tunnel provided a 1.8x1.8-m (6x6-ft) test section. Vertical velocity profiles in the test section were thoroughly surveyed and modified by the addition of roughness of the floor of the tunnel in front of the model. The profile selected for this series of test is illustrated in Figure A-2. This figure also shows the standard wind profile predictions for desert ($V = V_{36} (Z/36)^{.14}$) and suburban ($V = V_{36} (Z/36)^{0.233}$) locations. The test profile falls between these two profiles. Since smooth floor profile approaches a uniform wind, it was felt it would have a conservative and undesirable effect on elevation torque.

Velocity measurements in the tunnel were provided through a pitot tube mounted 121.9 cm (49 in.) above the tunnel floor and immediately above the model. Scale-wise, the velocity measurement should have been at 91.4 cm (36 in.) so corresponding adjustments of test velocities on the models were required.

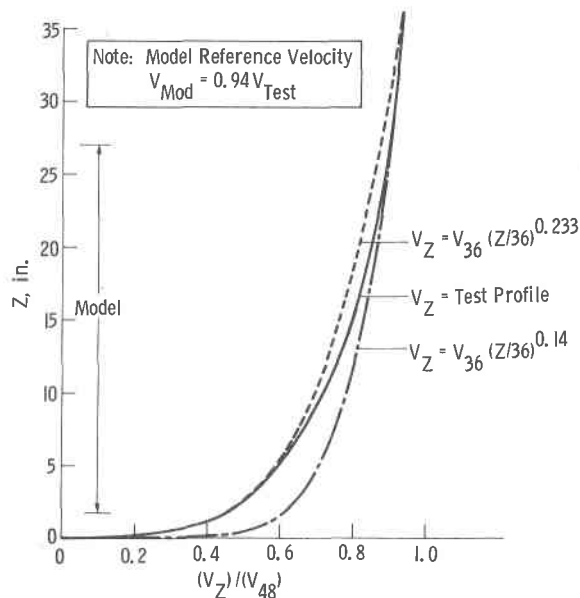


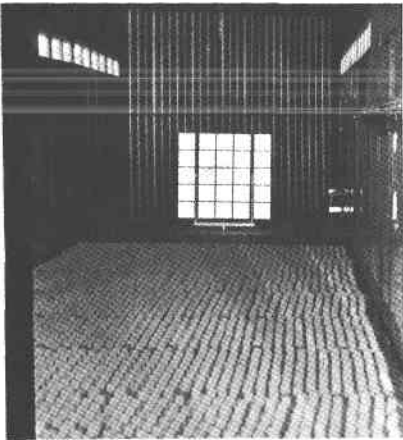
Figure A-2 Wind Tunnel Testing - Test Velocity Profile

A turntable was provided in the floor of the tunnel. The model was mounted at the center of the turntable allowing a 360-deg azimuth rotation if desired. Instrumentation wires were fed out through the base of the turntable.

B. MODEL DESCRIPTION

The base model was a 1/10 scale model of the 25-mirror configuration collector (Fig. A-3). The primary structure was made of solid steel round or rectangular bars, made as closely as possible to 1/10 scale, from material readily available.

Test Setup



9-Mirror Model

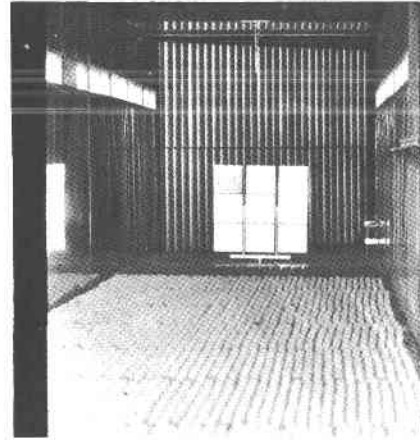


Figure A-3 Wind Tunnel Model and Test Setup

The mirrors were sheared from 0.15-cm (0.060-in.) steel sheet stock. Rings were soldered to the backs of the mirrors and wooden diagonals bonded to the backs to simulate actual structure. The mirrors were attached to the primary structure by screws through the center of the mirrors. The collector yoke was attached to

a six-component Task balance and, in turn, to the turntable in the tunnel floor. The six-component balance was oriented so the N-forces were normal to the plane of the mirrors.

In addition to the base model, four modifications of the base model were tested. The first modification consisted of replacing the 25 metal mirrors with 25 thick mirrors. The mirrors were made from 3/16 fiberboard and simulated proposed sandwich-backed mirrors. Modifications 2 and 3 were 9-mirror configurations. The vertical arms of the collector yoke were each moved in 7.62 cm (3.0 in.). Two mirror support arms were removed and the remaining arms were used to support the mirrors through center screws. Two mirror configurations were used--metal mirrors constructed as described for the 25 metal mirror configurations and 1/4-inch fiberboard mirrors. The last configuration consisted of 60.9x60.9-cm (24x24-in.) piece of 1/4-in. plywood. The plywood was attached to the five mirror support arms of the base configuration.

C. TEST SETUP

The test setup consisted of mounting the model on the turntable in the floor of the wind tunnel. Instrumentation wires ran from the Task balance through the bottom of the turntable mechanism to an eight-brush recorder adjacent to the wind tunnel.

Zero azimuth angle was established utilizing a laser beam. The laser was positioned at a reference point at the far end of the tunnel test section. The beam was reflected off a mirror on the elevation axis of the model back to a target at the laser.

Zero elevation angle was established utilizing an adjustable combination level-square. Each arm was checked for zero elevation angle and attached rigidly to the elevation axis. All elevation rotation subsequent to this was accomplished by rotating the entire mirror assembly as a unit.

The task balance was calibrated by applying loads to the model and adjusting the recorder response to the scale desired. Reactions N_A and N_F were calibrated by applying a force parallel to N_A and N_F at the center of the elevation axis. Reactions Y_A and Y_F were calibrated by applying a force parallel to Y_A and Y_F at the end of the elevation axis. Base torque (R) was calibrated by applying two loads to the upper ends of the model yoke. The loads were applied normal to the plane of the yoke and in opposite directions, resulting in a torque without lateral load in the balance. Lift (X) was calibrated by applying a downward force at the center of the model yoke.

The baseline model was mounted on the wind tunnel turntable with the six-component Task balance in place. The model was positioned at zero azimuth and elevation angle and the tunnel started. The tunnel wind velocity was stabilized at a reference velocity of approximately 13.5 m/s (30 mph) and the wind velocity recorded on the stripchart. The model was then rotated in azimuth

to the angles 0, 20, 40, 50, 60, 70, 80, 90, 100, 110, 120, 130, 140, 160, and 180 deg. At each azimuth angle (α) there was a pause in azimuth rotation and the angle was recorded on the strip-chart. Rotation in azimuth continued to an angle of $\alpha = 180$ deg. At this point, the model was rotated continuously back to $\alpha = 0$ deg. During this rotation, the recorder remained on and the azimuth angles were indicated on the stripchart. There was no pause at the various azimuth angles, but a second "check" reading was made available in this manner.

After the above azimuth survey, the tunnel was stopped and the model positioned to a new elevation angle. This required entering the tunnel and manually positioning the model to the desired elevation angle. The tunnel was then started, stabilized, and the model rotated in azimuth as described above.

The above procedure continued until elevation angles (β) of 0, 20, 40, 60, 70, 80, 90, 200, 220, 230, 240, 250, 260, and 270 deg were tested. The entire series was conducted at a reference velocity of approximately 13.5 m/s (44 fps). Tunnel velocities and temperatures were recorded for each β setting and are reflected in the reduced data.

The above β angles actually encompass the entire range of β angles, including those from 90 to 200 and 270 to 360 deg. Testing at $\beta = 20$ deg gives the results for $\beta = 160$ deg with essentially a reverse shift in α . That is, the results of $\alpha = 0$ and $\beta = 20$ are the same as $\alpha = 150$, $\beta = 160$ deg. Since each of the β angles tested has a "mirror" angle, the entire range was tested.

A test was then conducted to evaluate the Reynolds number effect on the base model. The model was returned to the original position ($\alpha = \beta = 0$ deg). The tunnel velocity was increased to approximately 17.7 m/s (40 mph). This represented an upper load limit on the six-component balance because of the manner in which it was mounted and calibrated. After tunnel stabilization, the model was rotated in azimuth as in the original survey with the corresponding stripchart recordings.

Four modifications of the base model were then introduced and each was tested to this procedure. As before, reference velocity and tunnel temperature were recorded on the stripchart for each β setting.

D. TEST RESULTS

Test results are given in Figure A-4. Results have been scaled up to a full-size collector as well as corrected to a wind velocity of 22.4 m/s (50 mph) at 9.2 m (30 ft) above the ground. The lift curve shown in Figure A-4 indicates that the separation angle must be equal to, or fairly close to, zero. A nonzero separation angle would show a spike in the data on either side of $\alpha = 90$ and 270 deg. Lack of this spike was apparent as the data were being recorded. The N_A , N_F , Y_A , Y_F , and R readings from the six-component balance would have shown this type of response but none were evident.

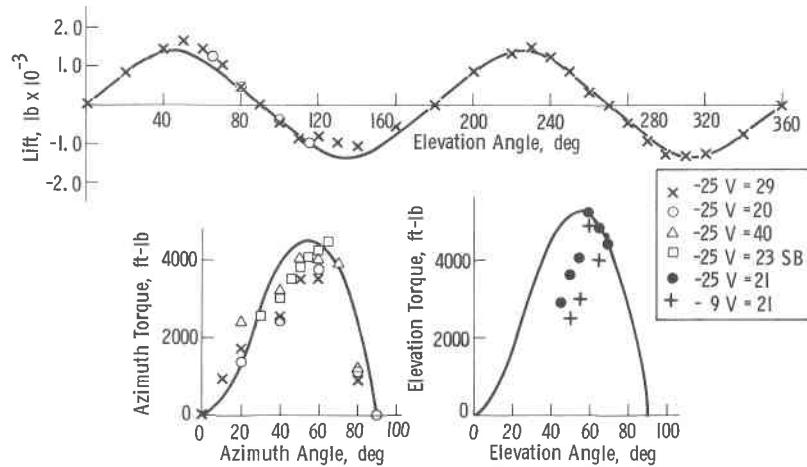


Figure A-4 Wind Tunnel Test Results - 50-mph Wind

Although azimuth torque curve (Fig. A-4) could be interpreted to show a peaking of the data at $\alpha = 80$ deg and thus a separation angle of 20 deg, this is inconsistent with the lateral and vertical force data and the high level of data between 30 and 60 deg on this plot. Continuing the assumption of a separation angle = 0 deg appears to give an analytical prediction curve that best fits the available data.

E. LOAD ANALYSIS PROGRAM MODIFICATION

The original computer program was written to determine force coefficients for a low-aspect-ratio rectangular wing. The initial modification was to include the capability of calculating the desired forces and torques on the collector for a nonuniform velocity profile. The nonuniform velocity was handled by using an integrated average velocity based on the elevation angle. Since the wind tunnel test established the separation angle to be 0 deg, the load curve shapes indicated in Figure A-4 were established.

The final program modification was to add multiplying factors to the elevation and azimuth torque calculations. These multiplying factors were 0.9528 and 0.9189 for azimuth and elevation, respectively. This reduced the calculated torques to the test values shown in Figure A-4.

The modified analysis program was used to calculate loads for various collector configurations and for various velocity profiles. The results for the baseline are given in Figures A-5 and A-6.

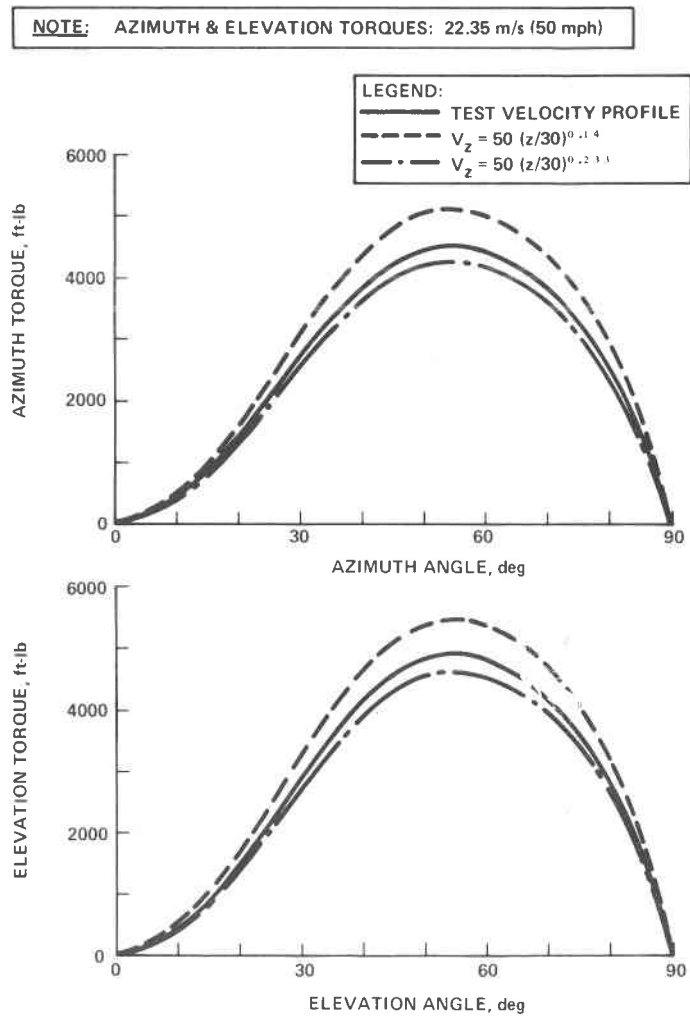
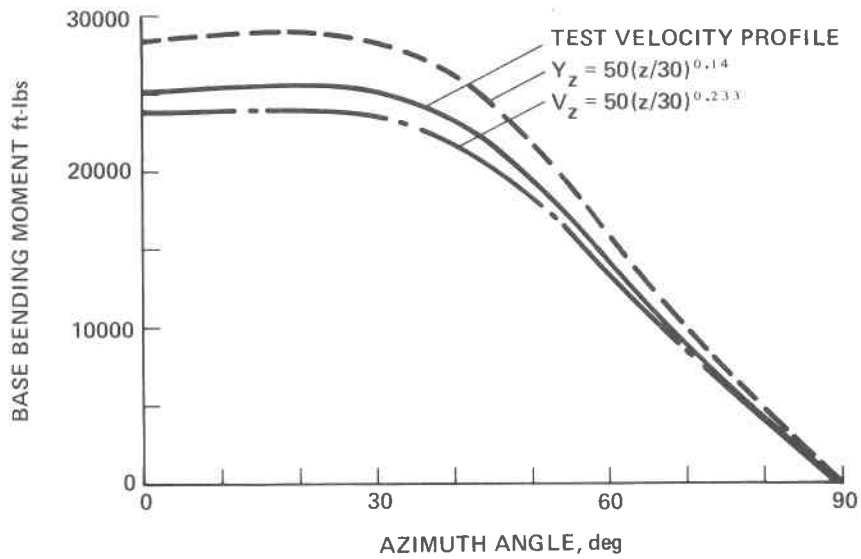


Figure A-5 Design Loads, 25-Mirror Configuration

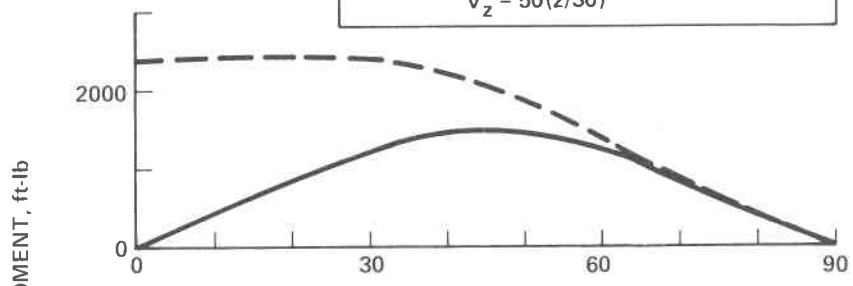
NOTE: BASE BENDING MOMENT: 50 mph
25 MIRROR CONFIGURATION



NOTE: LIFT & BASE SHEAR - 50 mph

LEGEND:
 - - - BASE SHEAR lbs
 ——— LIFT, lbs

NOTE: 25-MIRROR CONFIGURATION,
 $V_z = 50(z/30)^{0.14}$



NOTE: 25-MIRROR CONFIGURATION,
 $V_z = 50(z/30)^{0.233}$

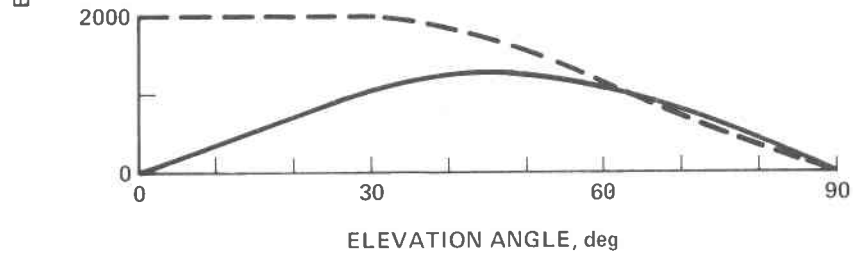


Figure A-6 Design Loads

F. CONCLUSIONS

The wind tunnel tests demonstrated that the configurations tested had a separation angle of 0 deg and that there was no discernable Reynolds number effect. The modified load program may be used to predict loads for similar collector configurations. Important factors in using this program are to include the entire frontal area of the collector and to use a similar mirror spacing. The mirror spacing tested was a scaled 7.62 cm (3.0 in.). The one test conducted to evaluate mirror spacing was inconclusive but did indicate an area of concern. If it is necessary to increase mirror spacing appreciably, care should be taken in applying the predicted loads. If possible, additional testing would be desirable.

Appendix B—Subsystem
Research
Experiment
Tradeoff
Studies

APPENDIX B—SUBSYSTEM RESEARCH EXPERIMENT TRADEOFF STUDIES

In our proposal preparation effort we have reviewed all the related tradeoff studies and testing previously accomplished in the CRSTPS program. In particular we directed our review at studies and tests concerning the subsystem research experiment (SRE) for the collector design as they might be applicable to the heliostat array and control system. These studies included mirror module configuration, heliostat mirror arrangement, zone layout, mirror reflectivity, mirror focusing techniques, and cost reduction projections.

We also reviewed other studies and testing that included analyses to identify error allocations to various subsystem components, wind tunnel testing, mirror support structure, collector efficiency to demonstrate feasibility of collector design, and definition of configuration and operating constraints of both executive and fine-tracking control systems. The following sections present some results and conclusions.

A. DESIGN MECHANISM TRADEOFF STUDY

The many possible design solutions for the drive mechanisms fall into two basic categories characterized by the type of tracking error they introduce:

- 1) Backlash error systems - Where a tooth mesh involves backlash but negligible elasticity;

2) Elastic error systems - Where a roller chain, ball screw, cable, flex spline, or volume of hydraulic fluid involves elastic deflection. The results of this tradeoff study are summarized in Table B-1.

The "direct gear drive" was shown to be the most cost effective solution. The primary reason for this was the high cost involved in beefing-up the elastic members of competitive designs to achieve acceptable detection characteristics.

A previously undefined advantage of the direct gear drive is that from a dynamics viewpoint, the involvement of backlash, which is normally nullified by aerodynamic torque, is preferable to the involvement of elastic elements.

Table B-1 Comparison of Attributes of Various Drive Systems

Type of Tracking Error	Backlash		Elastic Deflection					
Drive Method Attribute	Direct Gear Drive	Gearbox Mounted	Chain and Sprocket	Wire Rope	Harmonic Drive	Linear (Preloaded) Ballscrew	Hydraulic: Rotary Vane Actuator with Metering Pumps	Hydraulic: Dual Cylinder
Hardware Development Effort	Minimal	Zero	Medium	Medium/High	Medium/Low	Minimal	High	High
Potential Problem Areas	None Anticipated	None Anticipated	Tensioning Mechanisms to Code with Tracking Accuracy, Bidirection Operation, & Veering Winds		Compliance of Flex Spine	Difficult to Apply to 3.84 rad (220 deg) Angular Motion	Requires Constant Pressurization & Low Operating Pressure for Tracking Accuracy Due to Oil Compressibility	
Adaptability to Elevation Drive	Excellent	Poor	Acceptable	Poor	Poor	Good	Good	Medium
Size	Excellent	Ok for Azimuth	Satisfactory	Cumbersomely Large	Requires 2 ft Extra Height	Excellent	Excellent	Satisfactory
Size of Work Reducer, CD	8.89 cm (3 1/2 in.)	20.32 cm (8 in.)	8.89 cm (3 1/2 in.)	7.6 to 8.89 cm	5.08 cm (2 in.)	Included in Actuator	N/A	N/A
Maintenance Effort	Minimal	Minimal	Medium	High	Minimal	Minimal	?	?
Tracking Capability, arc-min	1 1/4 Backlash	1.6	2 to 7 at 13.5 cm (30 mph)	3 to 5 1/2 at 13.5 cm (30 mph)	Flexspline Elasticity, TBS	Very Low ~1	Depends on Actuator Size, ~2	Depends on Actuator Size ~ 2
Cost Factor	1	2.0	1.25 to 1.6	1.3 to 1.4	2.0	1.7	?	?

1. Design Requirements

The wind tunnel testing reported in Appendix A established the following tabulated performance requirements.

Base Bending Moment (Azimuth) at 22.3 m/s (50 mph)		456.39 kg-m (39,600-lb)
Aerodynamic Torque at 22.3 m/s (50 mph)(Slew Only)		673.06 kg-m (58,400 in. -lb)
Aerodynamic Torque at 13.5 m/s (30 mph)(Max Tracking Torques)		242.02 kg-m (21,000 in. -lb)
Aerodynamic Lift at 22.3 m/s (50 mph)	Positive	634.2 kg (1400 lb)
	Negative	634.2 kg (1400 lb)
Slew Speed		13.4 rad/hr (755 deg/hr)
Tracking Speed, Azimuth		1.5 rad/hr (89 deg/hr)
Angular Displacement of Heliostat, Azimuth		$\pm 1.91 \pm 0.09$ rad ($\pm 110 \pm 5$ deg)
Angular Displacement of Heliostat, Elevation		-4.71 ± 0.09 rad (-270 ± 5 deg)
Tracking Increment		1 arc-min
Weight to be Supported		2718 kg (6000 lb)
Drive Must Be Irreversible (Cannot Be Back-Driven)		

Figure B-1 illustrates those torque requirements in the form of tangential load versus radius. The supplementary abscissa scales relate worm reducer capability. The right-hand ordinant defines the amount of circumferential motion at a given radius equal to 1 arc-minute and thus gives an immediate idea of the extent of backlash or elasticity that can be tolerated at a given radius.

The chain pull abscissa indicates the considerable increase of tooth load capability using a hollow shaft reducer (providing rated torque is not exceeded).

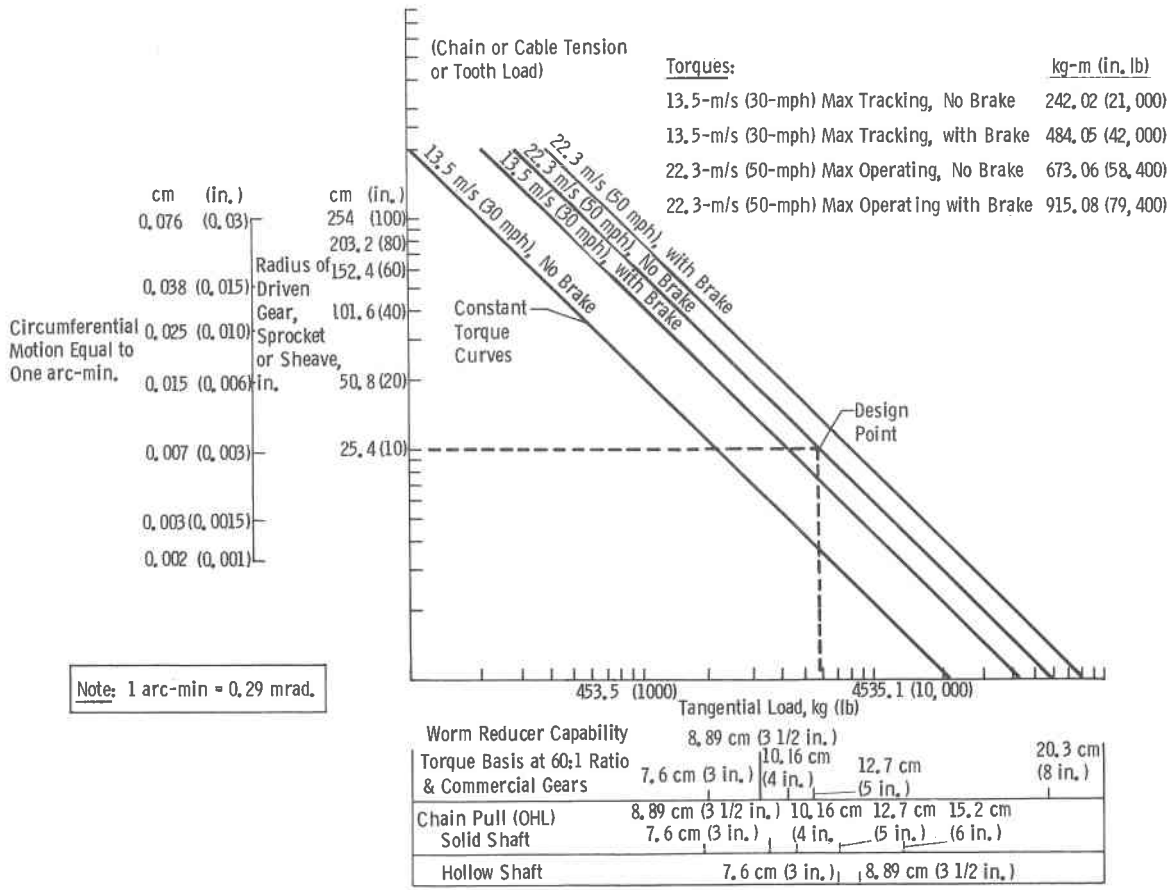


Figure B-1 Tangential Load vs Radius

Figure B-2 applies strictly to a geared final drive system, illustrating the degree of tracking error at a 13.41 m/s (30 mph) wind velocity that could be introduced by gear mesh clearance. This error would be realized only during the limited periods when wind veering in conjunction with heliostat angle would cause a reversal of aerodynamic torque.

The design operating points given for the various sizes of gear reducer are based on the use of unheat-treated commercial gears as discussed in the following subsection. The reflected backlash from the worm reducer is also indicated and is additive to that defined in the abscissa.

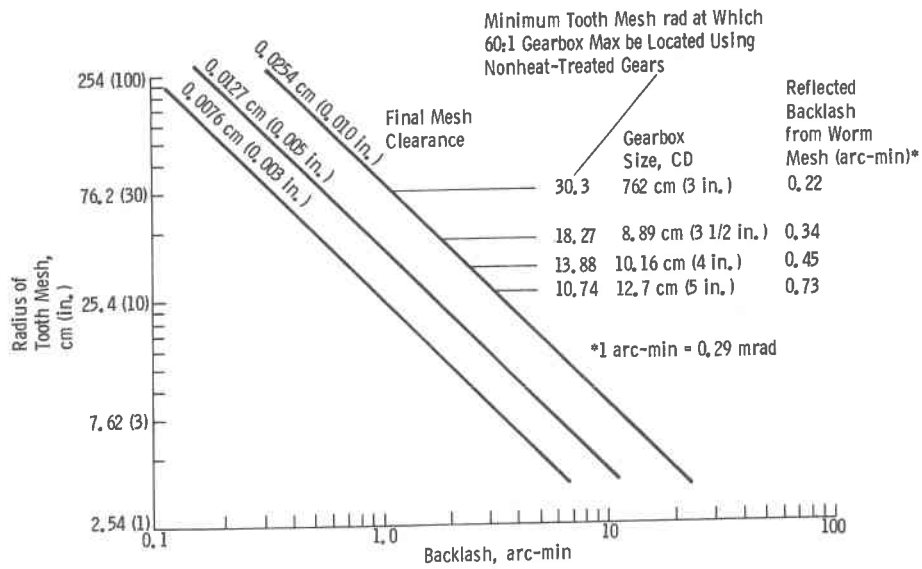


Figure B-2 Backlash vs Pitch Radius

2. Direct Gear Drive Concepts

a. *Direct Gear Drive Concepts using Yoke-Mounted Reducers -*

The design points defined in Figures B-1 and B-2 are exemplified in Figure B-3 using yoke-mounted reducers and stationary unheat-treated gears (pinions heat-treated). The backlash-induced tracking errors delineated assume a maximum tooth clearance of 0.025 cm (0.010 in.), which is probably optimistic for such large commercial gears. Obviously these concepts are adaptable to any form of bearing system.

These particular versions of the direct gear drive, utilizing commercially available gears, pinions, and worm reducers, did not prove cost effective in comparison with the use of turntable-type bearings having integral high-strength gear teeth (Fig. B-4) or the modular approach of Figure B-5.

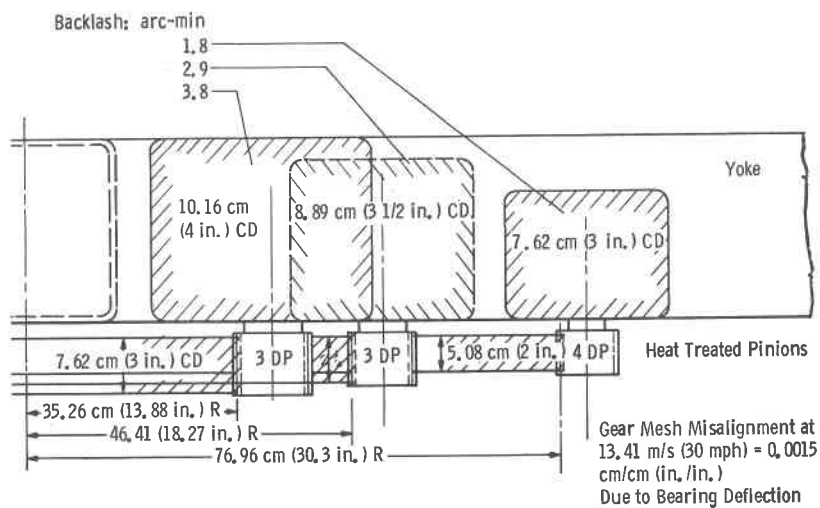


Figure B-3 Direct Gear Drive Concepts Using Yoke Mounted Reducers

b. Direct Gear Drive Using Turntable Bearing - The concept shown in Figure B-4 represents a very conventional approach for precision tracking systems. The turntable-type preloaded bearing, however, is quite expensive and must be mounted without distortion, which is the reason for introducing the stiff machined mounting ring. Similar precision must be maintained on the mounting plate attached to the yoke.

With this arrangement, a mesh clearance of 0.007 cm (0.003 in.) maximum is practical, representing a $1\frac{1}{4}$ arc-minute potential tracking error at a 13.4 m/s (30-mph) wind velocity (when backlash is taken up by reversing aerodynamic torques).

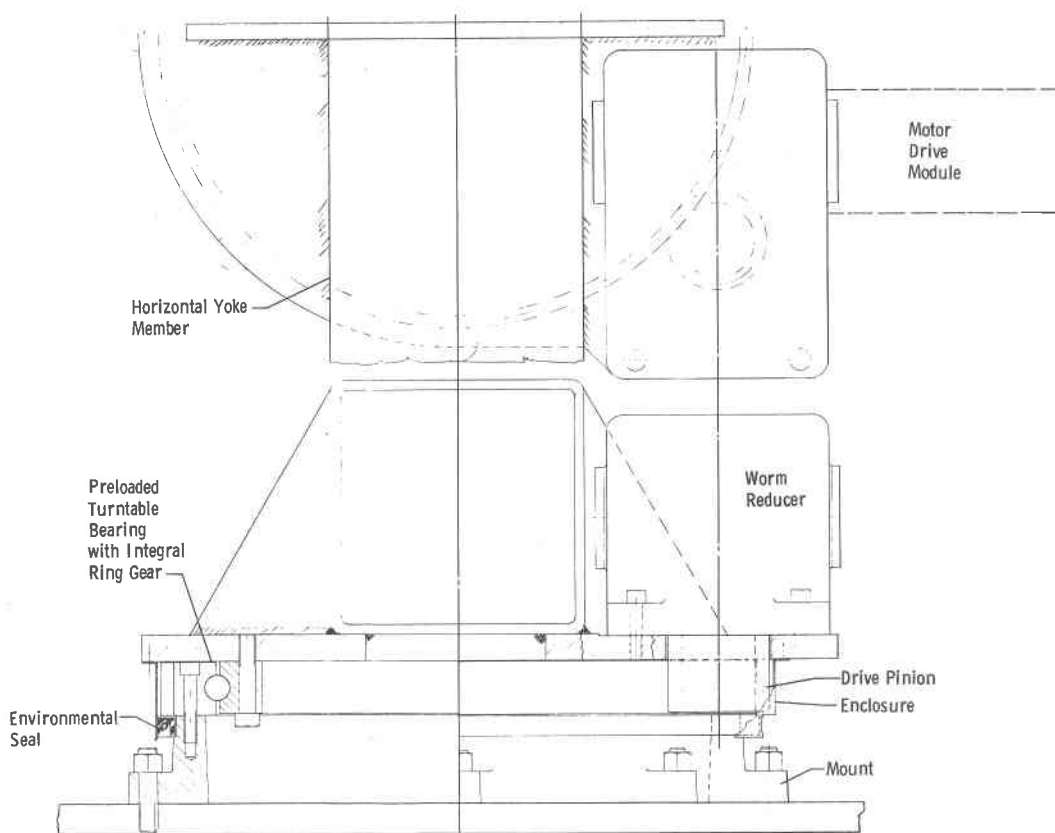


Figure B-4 Direct Gear Drive Using Turntable Bearing

c. *Low Duty Cycle Considerations* - The total number of tooth meshes involved in normal duty plus emergency stowage operations and maintenance amount to approximately 26,100. Bearing in mind that tooth load is proportional to (wind velocity)², the following tabulation defines load distribution based on the most severe wind velocity history of any recorded site in the southwest desert terrain of the U.S.

Wind Velocity	Gear Meshes
14% at Winds Reaching 1.78 m/s (4 mph)	3,645
58% at Winds Reaching 7.15 m/s (16 mph)	15,066
23% at Winds Reaching 14.3 m/s (32 mph)	5,589
7% at Winds Between 14.3 m/s (32 mph) and 22.35 m/s (50 mph)	1,800

In the light of these statistics it is unnecessary to utilize the fatigue stress values normally associated with AGMA tooth strength calculations. Instead, values approaching the normal yield may be used, e.g., 65% of yield.

d. Direct Gear Drive Using Preloaded Taper Roller Bearings -

This concept, which is shown in Figure B-5 utilizes a nodular iron casting (ductile iron) to AGMA grade NI5 and tooth strength equated to 65% of yield as previously discussed. It provides a very rigid combination mounting and final drive of utmost simplicity. The same casting also houses two preloaded tapered roller bearings. The bearings cost 1/7 of the turntable bearing previously illustrated (because they are a high-production item) and incur less deflection. For the cost balance, the remainder of the drive can be provided in a configuration readily adaptable to the elevation drive. The nodular iron casting is heat-treated to 255 BHN and the steel pinion to 300 BHN, leaving an optimum hardness differential. An accurate gear geometry and pitch line concentricity will be assured by precision gear finishing techniques.

An important advantage of this concept compared to chain and cable systems is that it comprises an independent interchangeable functional module. Eight bolts attach it to the foundation and it is then operational-no time-consuming on-site assembly operations are involved. The drive will be enclosed and completely sealed from the environment. Lubrication nipples will service both bearings and gear mesh.

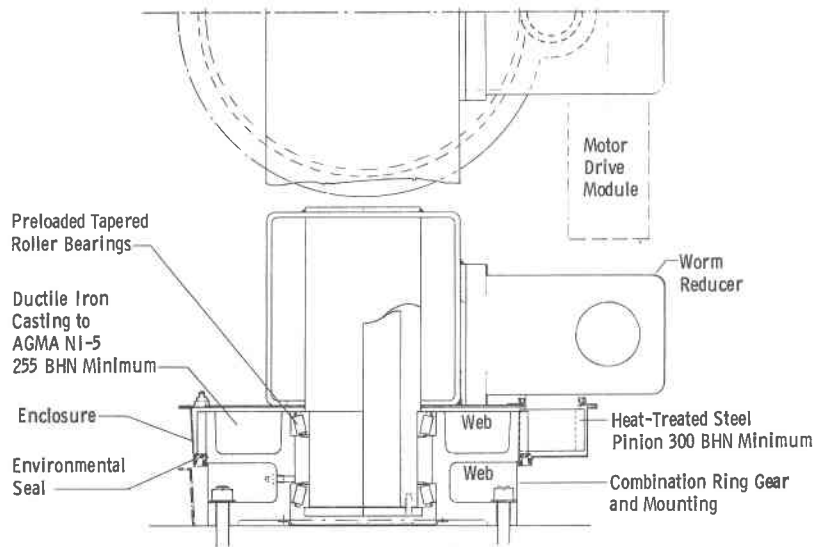


Figure B-5 Direct Gear Drive Using Preloaded Tapered Roller Bearings

3. Chain and Sprocket Drives

The determining criterion for a chain drive system (Fig. B-6) is chain elasticity and strain energy, as is in the case of a cable system. Irreversibility of the drive gearbox is, of course, essential in any case; and the chain represents an elastic linkage to the heliostat that the aerodynamic torque will strain proportionally to (wind velocity)². An increase in wind velocity will create a tracking error by stretching the chain; a reduction in wind velocity reduces chain tension and permits the strain energy of the chain to diminish chain stretch and again effect a tracking error.

The incorporation of a brake is of no advantage in a chain drive system. (In a nonelastic gear-driven system, it would successfully eliminate backlash.) The brake would presumably be set to maximum tracking torque at 13.4 m/s (30 mph). The drive

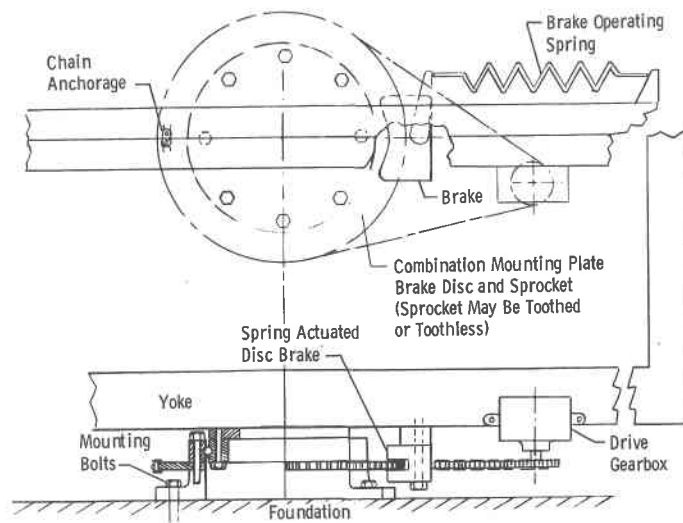


Figure B-6 Typical Chain and Sprocket Drive

mechanism torque would then have to be twice this value and chain strain energy will also be doubled, thus reintroducing the wind velocity sensitivity previously described.

These elasticity-induced errors are merely in proportion to the size of chain selected and size of sprocket. Two examples are given in the cost comparison in subsection 5.

An apparent simplification that could be incorporated would be to use a toothless sprocket. Unfortunately, the additional length of chain now exposed to tension introduces greater elastic stretch and tracking errors. The use of an even larger chain failed to produce a cost effective solution.

These complications, combined with the need for a bidirectional tensioning device, a well-sealed enclosure, and assured lubrication, plus a high cost estimate gave this type of system a low rating.

4. Cable and Capstan

a. *3 Arc-Minute Accuracy* - Figure B-7 schematically illustrates a relatively simple arrangement for tracking control. A virtual sheave comprising nonrotating pulleys is provided on the foundation. The reducer-driven capstan mounts to the yoke and winds itself around the stationary pulleys. The arrangement, however, is particularly inconvenient for adaptation to the elevation axis.

Appreciable slack side tension must be provided to minimize the necessary wraps on the capstan. This is complicated (even in the case of the azimuth drive where tracking accuracy is necessary in only one direction of rotation) due to the reversibility of aerodynamic torques. Cable creep is also liable to prove troublesome (see subsection 5 for cost comparison).

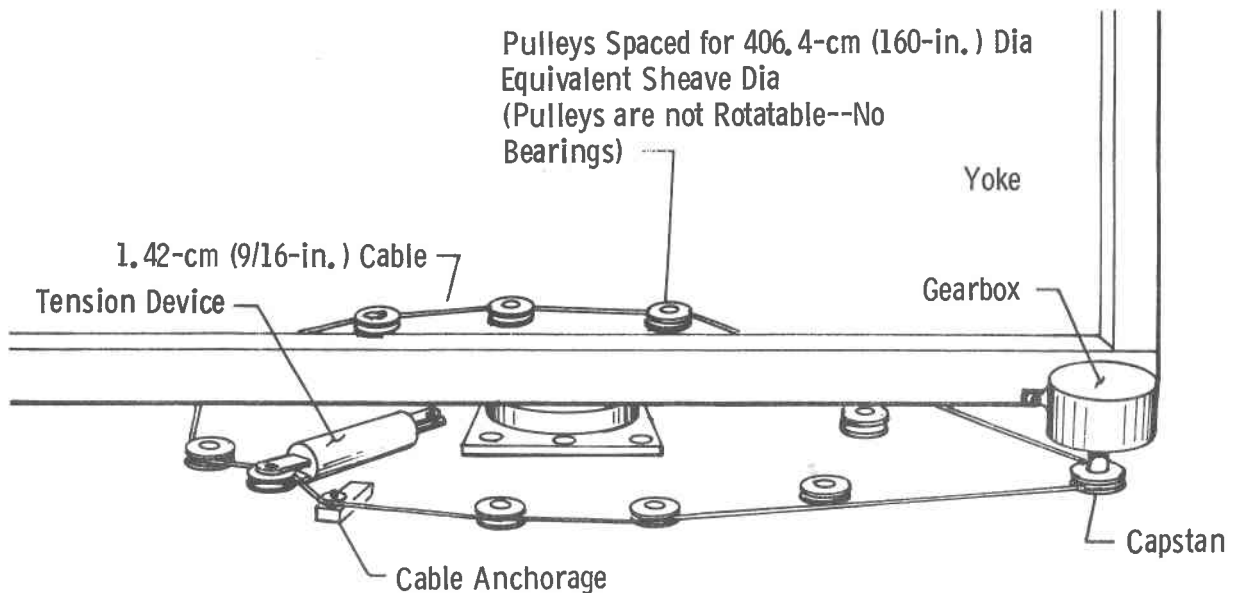


Figure B-7 Cable and Capstan Drive - 3 arc-minute Accuracy

b. *5 Arc-Minute Accuracy* - Figure B-8 schematically illustrates a tensioning arrangement that could satisfy the bidirectional requirement previously discussed. A dual spring-loaded pulley arrangement such as used on ferris wheels might be a satisfactory alternative. This figure also depicts a smaller sheave that could be adaptable to the elevation axis drive. However it would still be clumsy and involve considerable shadowing of mirrors.

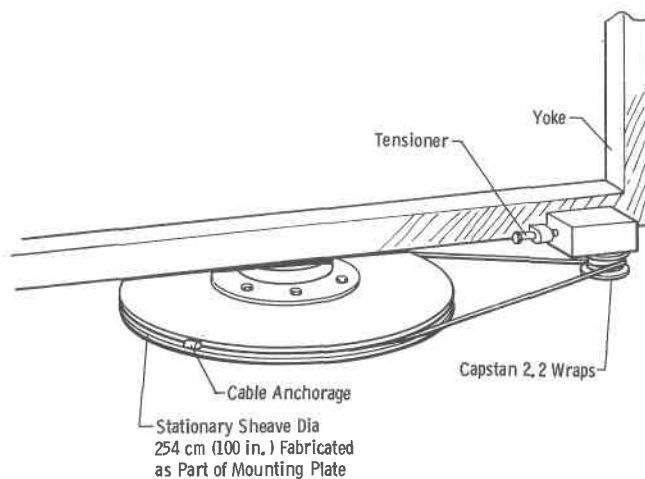


Figure B-8 Cable and Capstan Drive - 5 arc-minute Accuracy

c. *Tracking Error vs Sheave Diameter* - Figure B-9 illustrates the relationship between cable elasticity in terms of arc-minute tracking error and sheave diameter for a 1.42-cm (9/16-in.) diameter unlubricated wire rope. A tension ratio of 5.5 was selected as a compromise between number of capstan wraps and "slack side" tension. Note that it is the deflection (stretch), not strength, of the rope that is important.

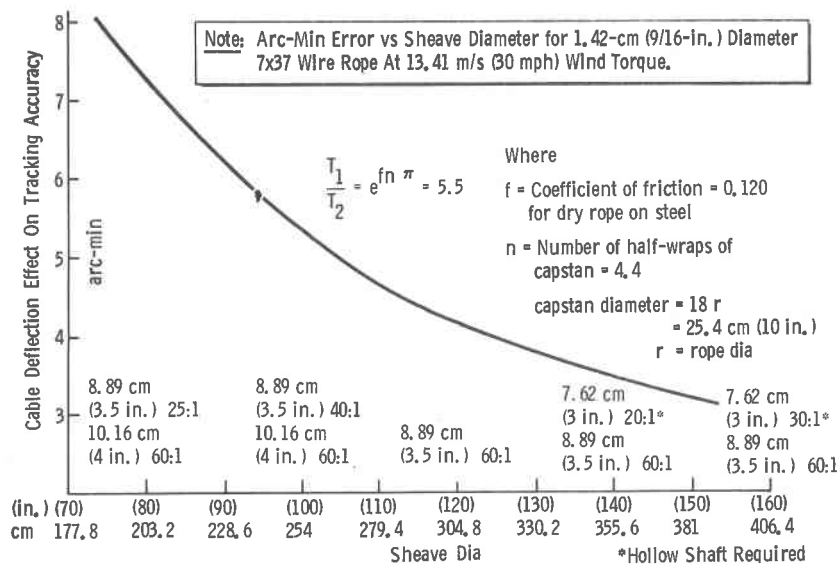


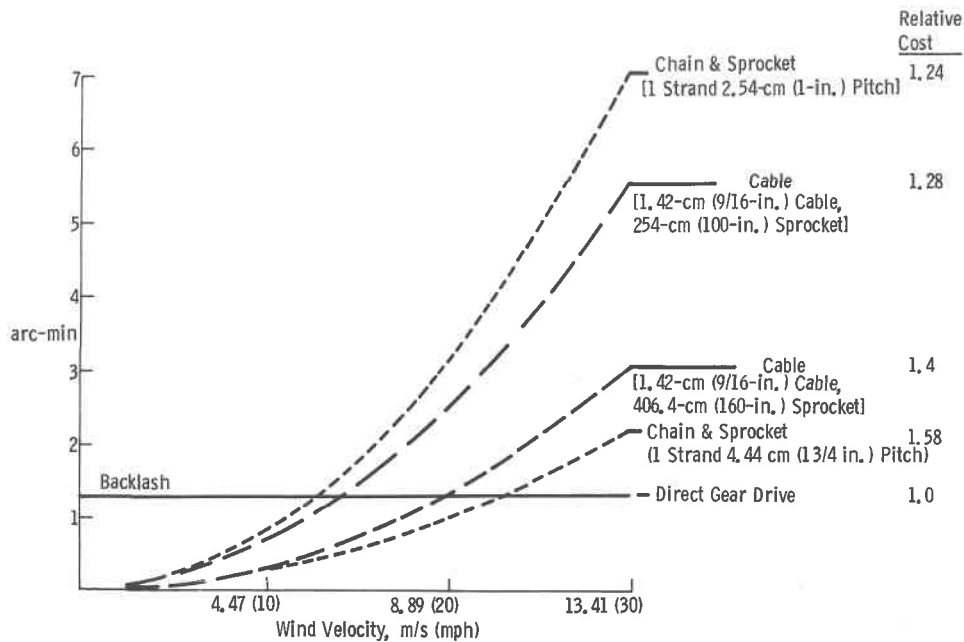
Figure B-9 Tracking Error vs Sheave Diameter for Cable and Capstan Drives

In general, it was concluded that although the tracking error at low wind velocities is less than the potential backlash error of a geared system, the unwieldiness of a cable system, combined with higher cost and its poor adaptability as an elevation drive mechanism eliminates it from serious consideration. Also, the difficulty and expense of enclosing it from the environments renders it a high maintenance risk.

5. Cost vs Tracking Error Comparison

Figure B-10 shows that although the systems subject to elasticity errors, i.e., the chain and cable systems, can yield relative low errors at the lower wind velocities, these are indeed errors.

The nonelastic gear systems are merely subject to potential backlash errors of the magnitude shown. The magnitude shown of $1\frac{1}{4}$ arc-minute cannot be directly compared with the elastic errors



Assuming the Use of the Same Bearings and Control System

Figure B-10 Cost vs Tracking Error, Gear, Cable and Chain and Sprocket Drives

of the other systems since this will only be realized on reversal of aerodynamic torque. As long as the direction of torque remains constant regardless of wind velocity there will be no induced error from the gearing (the elasticity of the teeth being insignificant). However, on reversal of aerodynamic torque, the backlash will introduce a tracking error. The extent, however, is limited to $1\frac{1}{4}$ arc-minute regardless of the magnitude of wind velocity, whereas in the case of the elastic systems the total error could be twice that illustrated. In steady winds, the torque reversal will occur once as the heliostat tracks through the zero angle of attack. Unsteady winds will produce elastically induced tracking errors equal to those given on the graph whereas the geared system is wind-velocity insensitive.

The cost factor points to the direct drive gear system as the most cost effective.

6. Hydraulic System Evaluation

Like the cable and chain drive systems, the hydrostatic design approach suffers from elasticity shortcomings due to oil compressibility. The analysis of Figure B-11 simply shows that because a given tracking accuracy and bulk modulus predetermines the maximum permissible operating pressure, for any particular operating radius the minimum size of operating cylinder is also fixed.

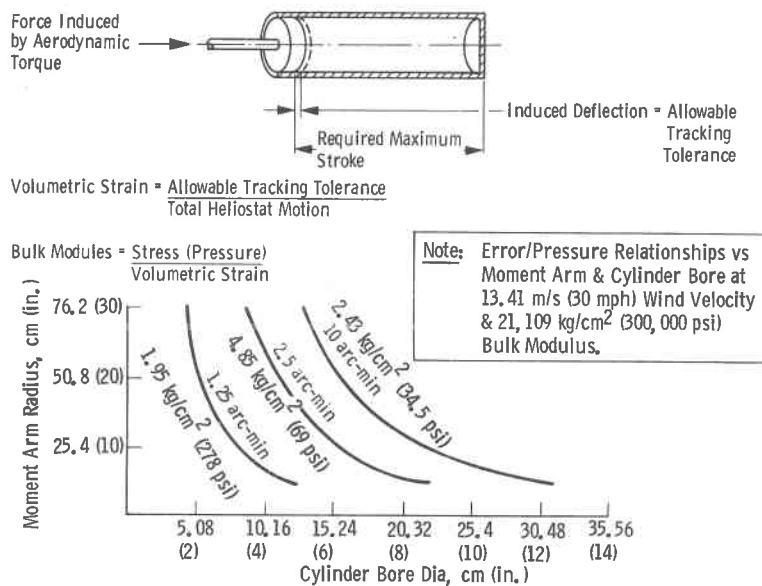


Figure B-11 Hydraulic Compressibility-Induced Errors

If the required motions of the two axes had not exceeded approximately 110 deg, a simple hydraulic cylinder-operated crank would have been a viable solution using a pressurized return and miniature metering pumps operating through check valves into either side of the piston. To accommodate the required 270-deg motion, a dual cylinder arrangement or a vane-type actuator can be used. Both are regarded as sufficiently developmental to preclude serious consideration at the present.

7. Direct Coupled Gearboxes - Comparison With Baseline Design

Probably the simplest drive solution is to mount the heliostat on a large worm reducer with output shaft bearings of sufficient capacity to accept the base bending moment of 5476 kg-m (39,600 ft-lb). This approach, shown in Figure B-12, is compared with a harmonic drive installation and the direct gear drive system, previously described, using back-to-back tapered roller bearings. The harmonic drive will introduce flex spline compliance (of an undetermined amount) and is not irreversible, necessitating a worm reducer to drive it.

The compactness of the direct gear drive system as opposed to the bulkiness of the harmonic drive system is obvious. The costs are also much greater for these two direct coupled arrangements compared to the baseline design.

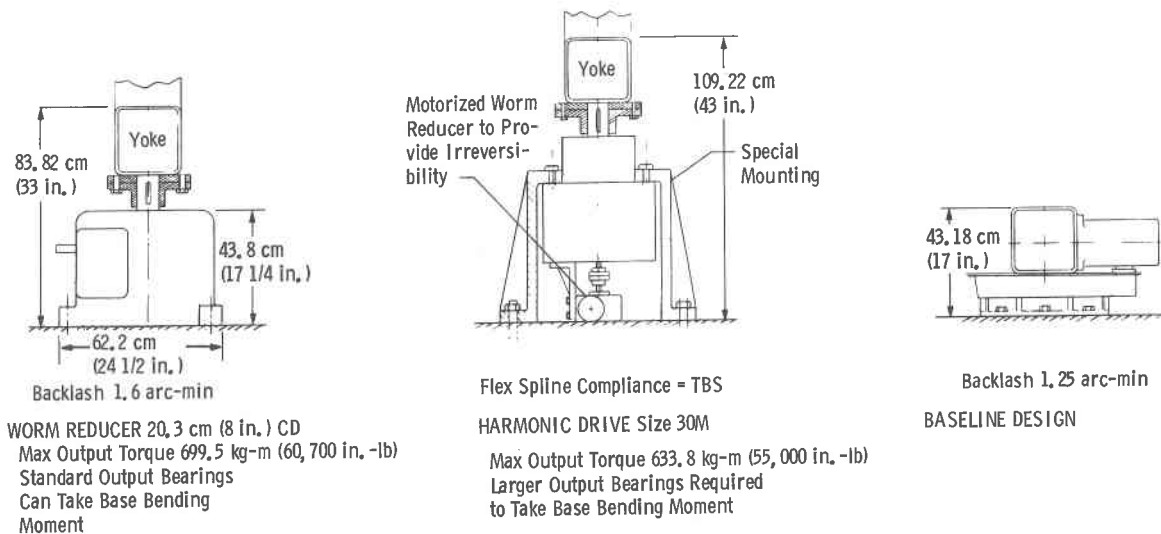


Figure B-12 Direct Coupled Gearboxes in Comparison with Baseline

8. Bearing and Bearing Mount - Elastic Deflection

The bearing deflection data given in Figure B-13 were obtained from the bearing manufacturers. In the case of the tapered roller bearing concepts, the manufacturer ran extensive computer programs to optimize the selection of bearing size, bearing center distance, deflection, and cost. This resulted in the back-to-back arrangement of concept C. In comparison, it will be observed that the considerable structural deflection of concept C has been eliminated.

It is to be noted that azimuth bearing deflections affect elevation tracking accuracy, but the reverse is not true.

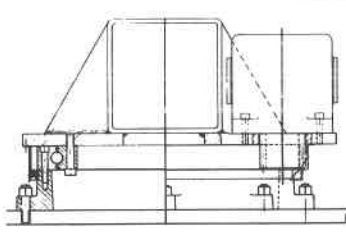
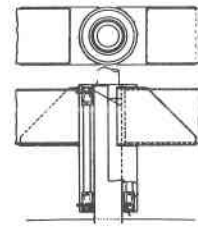
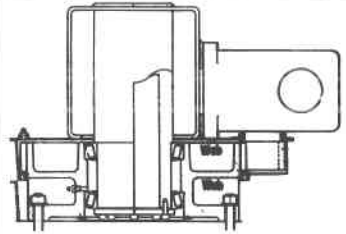
		A.	B.	C.
Bearing Arrangement				
		arc-min	arc-min	arc-min
6.70 m/s (15 mph)	Bearing Deflection Only	0.47	0.28	0.6
	Bearing & Structure Deflection	0.48	1.29	0.61
13.41 m/s (30 mph)	Bearing Deflection Only	13.0	0.66	1.6
	Bearing & Structure Deflection	13.4	4.71	1.7

Figure B-13 Deflections of Bearings and Associated Structure

B. MIRROR WARPING TRADEOFF STUDY

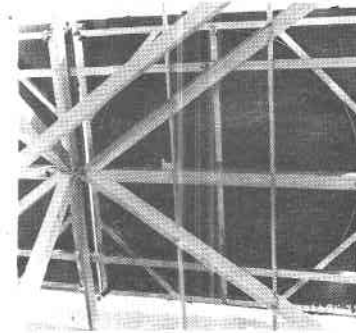
Each of the mirrors in a heliostat assembly requires a separate warping and targeting structure. A series of designs evolved at Martin Marietta since 1973 has finally resulted in a design that provides improved warping and targeting capability and that can be fabricated at reasonable cost.

The first warping design evaluated [Fig. B-14(a)] consisted of a rectangular frame. Eight thrust rods distributed around the perimeter of the frame forced the edges inward. A similar threaded rod bonded to the center of the back surface of the mirror applied tension. The net effect was to produce a surface with circular curvature. While of low cost, this system did not warp the mirror uniformly, resulting in a distorted solar image at the target.

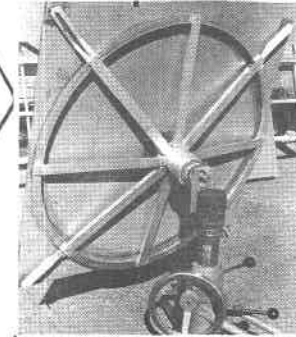
A modified approach was tested [Fig. B-14(b)]. This method utilized a circular ring bonded to the rear surface of the mirror in addition to the square frame. The method of applying force around the edges and in the center was similar to the one used in the previous design. Although this technique provided improved warping capability, the more complex structure significantly increased the unit cost.



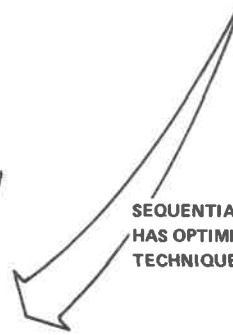
- (a)
- LOWEST COST
 - POOR WARPING



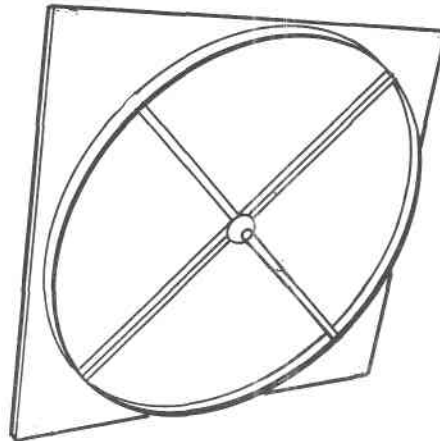
- (b)
- IMPROVED WARPING
 - COMPLEX BACK STRUCTURE



- (c)
- OPTIMUM WARPING
 - OPTIMUM TARGETING
 - SIMPLIFIED BACK STRUCTURE



SEQUENTIAL DEVELOPMENT
HAS OPTIMIZED WARPING
TECHNIQUE



- (d) PROPOSED DESIGN
- SAME TECHNICAL FEATURES AS (c)
 - STRUCTURAL DESIGN SIMPLIFIED TO REDUCE COST
 - VIABLE DESIGN FOR MOLDING, CASTING, AND STAMPING
 - LOWEST COST COMPATIBLE WITH HIGH PERFORMANCE

Figure B-14 Mirror Support and Warping Structure Tradeoffs

While trying to reduce cost and yet increase the warping capability, the design of Figure B-14(c) was evolved. Based on a circular ring bonded to the mirror's rear surface, the design uses struts radiating from a central position to provide warping pressure. Although this design provided the necessary warping accuracy, it resulted in no substantial cost reduction.

A second-generation model [Fig. B-14(d)] with improved warping structure achieved the optimum warping capability, while providing a low-cost, easily fabricated design. Initial discussions with vendors suggest that this design can be inexpensively produced on a large scale and therefore has been selected as the baseline design.

C. MIRROR TRADEOFF STUDY

In an effort to obtain comparative data for several candidate mirror surfaces with specular collimation similar to that of the solar monitoring instrumentation, the reflectivity test rig shown in Figures B-15 and B-16 was assembled. The reflected beam from the test mirror is monitored by the reverse-mounted pyrheliometer. To avoid shadowing, the mirror sample is tested with a 10-deg tilt ($\cos = 0.98481$). The reference insolation input to the mirror is monitored by the pair of independently tracked pyrheliometers shown in Figure B-16.



Figure B-15 Specular Reflectivity Test Rig Using Normal-Incidence Pyrheliometers, Profile View

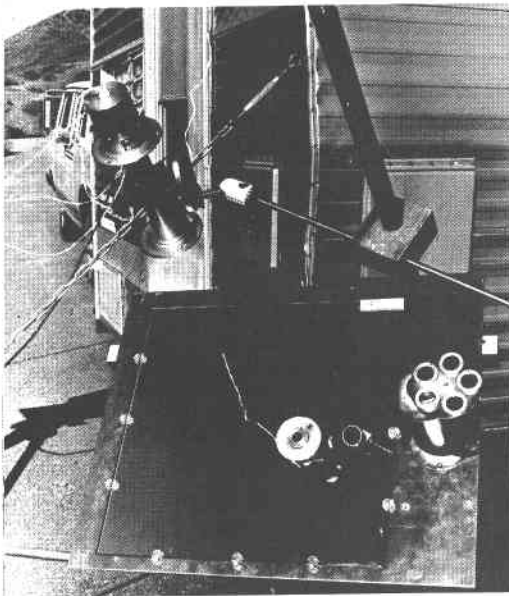


Figure B-16 Specular Reflectivity Test Rig Using Normal Incidence Pyrheliometers, Front View

The baseline design specular reflectivity necessary to be consistent with the design sizing is 85%. For a given flux into the receiver cavity, the field size is approximately inversely proportional to the spectral reflectivity of the mirror. Although the mirror with the highest reflectivity has the highest cost per unit area, the net cost saved by the reduction in number of heliostats required justifies its use.

The results of specular reflectivity tests we have completed are shown in Table B-2. From the samples tested, it is apparent that a specular reflectivity of 85% is only attainable with either first-surface aluminized teflon or with a laminated second-surface mirror with glass of improved transmissivity.

Table B-2 Results of Terrestrial Spectral Reflectivity Tests of Candidate Mirror Surfaces as Compared with Cost

DESCRIPTION OF MIRROR SAMPLE	DATE	SPECULAR REFLECTIVITY (%)			COST (\$/ft ²)
		HIGH	LOW	AVERAGE	
FIRST SURFACE ALUMINIZED TEFLON (REFERENCE SURFACE)	10/01/74	86.5	86.1	86.27	UNKNOWN, BUT IS PROBABLY GREATER THAN \$10.76/m ² (\$1/ft ²)
	10/08/74	86.6	83.5	85.11	
SECOND SURFACE SILVERED COMMERCIAL FLOAT GLASS LAMINATED MIRROR, 3mm FRONT TO MIRROR SURFACE	09/20/74	83.1	82.7	82.90	\$18.84/m ² (\$1.75/ft ²) FROM GARDNER MIRROR
	09/23/74	83.9	83.3	83.56	
	10/08/74	84.1	82.7	83.47	
SECOND SURFACE SILVERED WHITE GLASS LAMINATED MIRROR, 3mm FRONT TO MIRROR SURFACE	03/13/75	89.7	90.0	90.2	ESTIMATED \$18.84/m ² (1.75/ft ²) FROM GARDNER MIRROR AND FORCOUT COMPANY
	03/13/75	90.8	93.9	92.3	
	03/13/75	91.2	94.4	92.8	
SECOND SURFACE SILVERED COMMERCIAL FLOAT GLASS, 6mm THICK	09/20/74	72.2	70.5	71.27	\$10.76/m ² (\$1/ft ²) GARDNER MIRROR
	10/08/74	73.3	72.7	73.05	
SECOND SURFACE SILVER ON ACRYLIC, 3.2mm THICK	09/23/74	79.3	78.3	78.7	UNKNOWN, BUT IS PROBABLY GREATER THAN \$10.76/m ² (\$1/ft ²)

The second-surface silvered white glass laminated mirrors were chosen over the aluminized teflon for reasons of producibility and reliability. First-surface mirrors, such as the aluminized teflon, show a greater surface degradation rate than a second-surface silvered glass mirror. Also, special cleaning

fluids and techniques would probably be necessary to avoid damage of the aluminum surface. Samples of second-surface silver on teflon have not been available to us from the manufacturer although diligent efforts to obtain them have been made over a 13-month period.

The laminated white glass mirrors, which exhibit considerably higher spectral reflectivities than even the aluminized teflon, are available for an estimated $\$18.84/\text{m}^2$ ($\$1.75/\text{ft}^2$) without increased technology. The large-scale production cost and feasibility of the aluminized teflon mirror is not presently known.

The choice of mirror surface also dictates the size of mirror obtainable. At this time, the laminated glass mirror is only available in 1.2x1.2-m (4x4-ft) sheets instead of the 2.1x2.1-m (7x7-ft) sheets in which ordinary mirror glass is available. For the preliminary HAACS baseline, 1.2x1.2-m (4x4-ft) mirrors have been chosen to take advantage of the higher reflectivity.

Although the smaller mirrors increase the heliostat structural cost, they also furnish benefits that potentially offset the increase. Studies and tests indicate that the 1.2x1.2-m (4x4-ft) mirror not only provides better flux targeting and suffers less stress under warping, but that the higher cost is neutralized by the increased optical efficiency that results in reduced field size and a reduced number of heliostats.

An additional characteristic considered in the HASS design was the individual mirror weight. The 1.2x1.2-m (4x4-ft) laminated glass mirrors weigh approximately 18.1 kg (40 lb) each as compared to the 54.4 kg (120-lb) weight of the 2.1x2.1-m (7x7-ft) mirrors.

The smaller mirror provides definite advantages for maintenance reasons since they could be mounted or changed by a two-man crew (one man to hold the mirror).

1. Collector Sizing Tradeoffs

Optimization of an overall solar thermal plant design is closely keyed to the individual mirror configuration on the heliostats. Studies have shown that the proper mirror configuration can result in smaller receiver aperture sizes, which in turn increases receiver efficiency by reducing radiation losses. This increased efficiency permits a reduced number of collectors in the field, thereby lowering costs.

In heliostat design, one of the principal elements to be considered is the overall structural size. Heliostats of various sizes have been built and tested in many places, including Martin Marietta. Martin Marietta performed a series of tradeoff studies using the basic heliostat size of 6.1x6.1 m (20x20 ft). Figure B-17 illustrates the designs compared and Table B-3 presents a summary of the results.

In Table B-3, two factors are immediately apparent. The aberration of the image, which depends on the overall heliostat size and limits of rotation, is constant for all of three designs considered. Likewise the reflected sun image size, a function of the optical transmission distance, is approximately 4.8 m (15.9 ft) for a heliostat located approximately 487.7 m (1600 ft) from the receiver opening. For any design, the resulting projected image is the sum of the projected mirror size, the aberration, and the theoretical size of the sun's image.

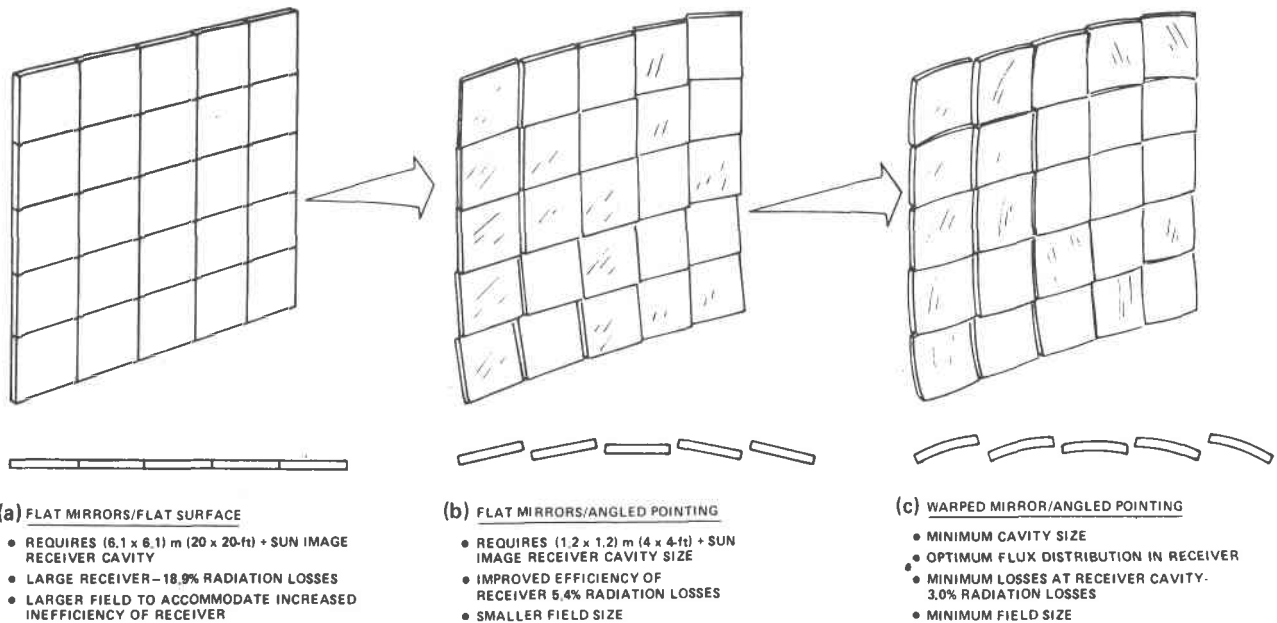


Figure B-17 Mirror Configuration Performance Tradeoff

The design consisting of 25 1.2x1.2-m (4x4-ft) flat mirrors mounted on a common axis [Fig. B-17(a)] requires a cavity aperture of at least 12x2x12.2 m (40x40 ft). A design in which the

25 flat mirrors are individually pointed [Fig. B-17(b)] results in a much reduced cavity opening, i.e., approximately 7.3x7.3 m (24x24 ft).

The smallest projected image size is achieved by using 25 1.2x1.2-m (4x4-ft) mirrors, each individually pointed and focused [Fig. B-17(c)]. The warping is obtained by distorting the flat mirrors with mechanical frames. The maximum flexure

Table B-3 Comparison of Projected Image Sizes of Various Heliostat Designs

HELIOSTAT DESIGN (BASED ON 25 1.2x1.2-m (4x4-ft) MIRRORS PER HELIOSTAT)	PROJECTED IMAGE SIZE*			
	PROJECTED MIRROR WIDTH, m (ft)	ABERRA- TION, m (ft)	THEORETICAL SUN IMAGE SIZE, m (ft)	RESULTANT RE- CEIVER CAVITY OPENING, PER SIDE, m (ft)
FLAT MIRRORS ON SAME AXIS (FIG. 2BC3-1A)	6.1 (20)	1.2 (4)	4.8 (15.9)	12.16 (39.9)
1.2x1.2-m (4x4-ft) FLAT MIRROR ANGLED AND POINTED (FIG. 2BC3-1B)	1.2 (4)	1.2 (4)	4.8 (15.9)	7.28 (23.9)
1.2x1.2-m (4x4-ft) WARPED MIRROR WITH ANGLED POINTING	(0)	1.2 (4)	4.8 (15.9)	6.06 (19.9)

*BASED ON BASIC HELIOSTAT SIZE OF 6.1x6.1 m (20x20 ft) LOCATED APPROXIMATELY 487.68 m (1600 ft) FROM THE RECEIVER.

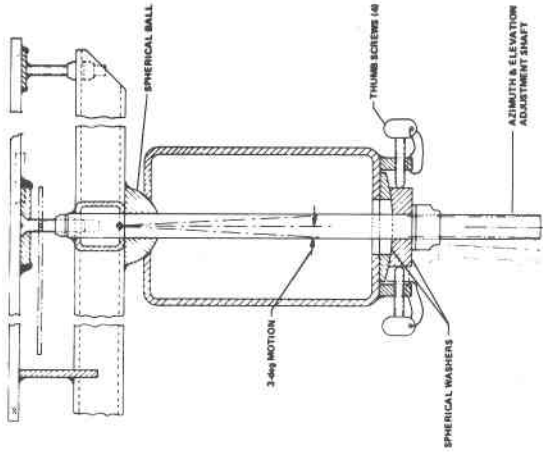
from the corner to the center of each mirror ranges from 0.02 to 0.28 cm (0.008 to 0.110 in.), depending on the distance of the heliostat from the receiver. This technique has proved to be reliable in tests at Martin Marietta.

The warped and angled mirror requires additional heliostat structure and therefore has an inherently high cost per heliostat. However, the reduction in field size, tower height, and number of heliostats as a result of increased efficiency of the boiler is substantial and every indication shows that the warped and angled mirror design provides the lowest cost total system approach.

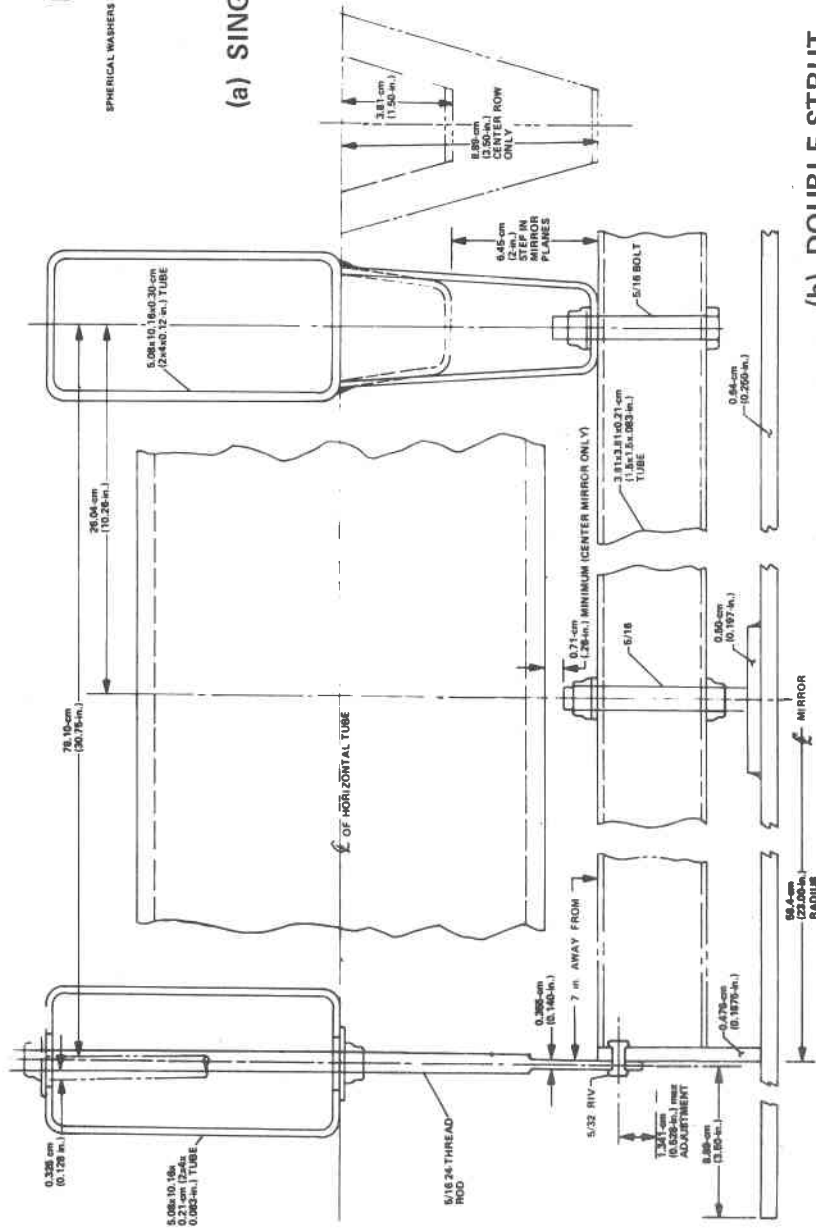
We have therefore selected the warped angled approach because it optimizes efficiency, reduces field size and the size of the power station, and has potentially the least system cost.

D. MIRROR SUPPORT/ALIGNMENT TRADEOFF STUDY

Figure B-18(a) represents the mirror assembly support alignment approach used in our central receiver solar thermal power system proposal. Recent testing has indicated that torsional flutter could occur, especially with the tubular steel mirror holder. The single support tube is therefore quite heavy to accommodate and minimize this torsional flutter. The single-area positioning method is good, but the short-couple adjustment is tedious.



(a) SINGLE-STRUT



(b) DOUBLE-STRUT

Figure B-18 Mirror Support

Figure B-18(b) is our baseline design, using two members instead of one for support of mirror assemblies. This approach is readily adaptable to the tubular steel mirror holder. The two supports resist rotation and reduce the cost and weight below that of the single support in Figure B-18(a). Positioning of the mirror assembly is accomplished with a fixed pivot and two inexpensive adjusting-type studs (vertical and horizontal). The large distance between supports provides the capability for fine adjustment.

E. STRUCTURE TRADEOFF STUDY

1. Support Structure

The heliostat structure has been designed primarily for stiffness because of the requirements for precise aiming of the mirrors. Of the total aiming tolerance budget, 2.04 mrad were allocated to structural deflection. A symmetrical configuration appeared to be the most practical and cost effective solution.

Several configurations were investigated; the primary candidates are illustrated in Figure B-19. These are characterized by the method of pivoting the mirror assembly for elevation control. The configuration of Figure B-19(a) pivots about an axis just below the lower row of mirrors. That of Figure B-19(b) pivots about a central axis with a yoke spanning the complete width of the heliostat. The configuration of Figure B-19(a) uses a shortened yoke but is otherwise the same as Figure B-19(b).

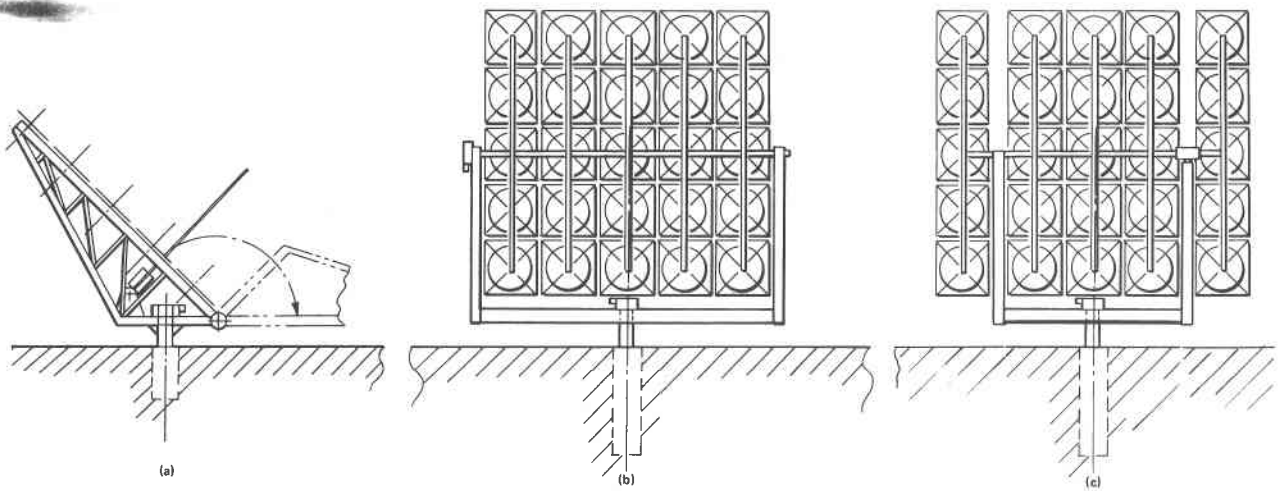


Figure B-19 Structural Design Alternatives

The design of Figure B-19(a) was discarded primarily because of severe pointing errors during elevation adjustment. The sightline actually moves vertically and at a different rate for each mirror. Although it offers a lower overall profile and a lower wind moment acting on the azimuth bearing, its unbalanced design introduced larger actuation mechanisms.

The design of Figure B-19(b) provided the most convenient method of actuating the elevation control. A drive unit attached very simply to the yoke could drive the mirror assembly from one end. Supporting the horizontal member at the end points, however, results in fairly high aiming errors because of deflection of the longer bearing span.

The baseline design of Figure B-19(c) is the result of shortening the yoke. The resultant shorter bearing span reduces deflection of the cross-member to a secondary order. Even when the drive unit is interposed in the horizontal tubular member,

which introduces a discontinuity in stiffness, this configuration provides greater stiffness than that of Figure B-18(b) for the same weight.

Deflection of the horizontal yoke member is a primary contributor to mirror aiming error and the shortening of this member by 1.29 m (51 in.) per side achieves considerable extra stiffness for the same weight.

The stiffness analysis determined that the structure could withstand a wind velocity of approximately 15.6 m/s (70 mph) without exceeding the 50% of yield strength criterion. To withstand the upper-limit 44.7-m/s (100-mph) criterion, the mirror assembly must be rotated to a horizontal stowed position.